Thermodynamic and transport properties of aluminium (Al)-based liquid binary alloys

Ph.D Treatise Submitted

by

Md. Fysol Ibna Abbas

to

The Department of Theoretical Physics

in partial fulfillment of the requirements

for the Degree of

Doctor of Philosophy

in the subject of

Theoretical Condensed Matter Physics.

University of Dhaka

Dhaka-1000

(2013–2018)

Abstract

In this thesis, the thermodynamic and transport properties of Aluminum (Al) based liquid binary alloys ($Al_{1-x}X_x$, here X=Zn, In, Sn, Bi, Cu, and Au) are systematically theoretically investigated. The thermodynamic properties of liquid binary alloys which are named as the free energy (A), the energy of mixing (ΔA), the enthalpy of mixing (ΔH) and the entropy of mixing (ΔS) have been studied.

Atomic transport properties (ATP) such as the coefficients of shear viscosity (η), the diffusion coefficients (D), and the friction coefficients (ζ) are theoretically calculated for Al-based liquid binary systems. On the other hand, for electron transport properties, I have also studied the electrical resistivity (Ω) and conductivity theoretically.

The general microscopic theory (GMT) is employed to describe the inter-ionic and electron-ion interactions of the above metals. The inter-ionic interaction and a reference liquid are the fundamental components of this theory. For understanding the inter-ionic interactions in the high temperature liquid state, the Bretonnet-Silbert (BS) model has been used and extended it for simple metals (Al, In, Sn, Bi). This model treats *sp* and *d* bands separately within the well established pseudopotential mechanism. A liquid of hard spheres (HS) of two different effective diameters and charges is used to describe the reference system. The LWCA thermodynamic perturbative method is used to calculate the effective hard sphere diameter and the partial structure factor, $S_{ij}(q)$.

For studying ATP, the distribution function method has been used which was proposed by Rice-Allnatt (RA) and is very convenient for numerical calculations due to its simple form. More importantly, the physical significances of each term

in the theory are very transparent for understanding various transport mechanisms involved. Besides, studying the ETP for different liquid binary alloys, extended form of Faber and Ziman (1965) formula has been employed to calculate the electrical resistivity. Ziman's theory is based on the Nearly Free Electron (NFE) model and predicting reasonable values for resistivity of liquid metals, and this theory has been extended here for liquid binary systems.

In addition, I have also studied the thermodynamic and transport properties such as the excess entropy, the shear viscosity and the diffusion coefficient using the Universal Scaling Laws (USL) proposed by Dzugutov for single system namely for Al. Excess entropy is the main ingredient in the USL.

Results for both thermodynamic and transport properties of Aluminum (Al) based liquid binary systems agree well with the available experimental data.

Contents

Title Page . . . . . a

Approval Sheet . . . . . b

Abstract c

Acknowledgement . . . . . d

Dedications . . . . . e

List of Published and to be Published Papers . . . . . f

Contents . . . . . (i-v)

List of Tables . . . . . (vi-viii)

List of Figures . . . . . (ix-xiv)

1 Introduction **1**

2 Metals **11**

2.1 Concept of Metals 12

2.2 Classification of Metals 14

2.3 Alkali Metals 14

2.3.1 Properties of Alkali Metal 16

2.4 Alkaline Earth Metals 17

2.4.1 Properties of Alkaline Earth Metals 17

2.5 Transition Metals 19

2.5.1 Properties of Transition Metals 20

2.6 Semi-Metals or Metalloid 21
2.6.1 Properties of Semi-Metals 22
2.7 Metals or Basic Metals 23
2.7.1 Properties of Metals 24
2.8 Lanthanides 25
2.9 Actinides 27
2.10 Properties of Al, Zn, In, Sn, Bi, Cu and Au 29

3 Theories **34**

3.1 Pseudopotential for Inter-Ionic Interaction 34
3.1.1 Pseudopotential Theory 39
3.1.2 Purpose of Pseudopotential 45
3.2 Models of Pseudopotential 45
3.2.1 Bretnot-Silbert Model Pseudopotential (BS) 46
3.2.2 The Empty Core Model Pseudopotential (EMC) 48
3.3 Structural Properties of Liquid Alloys 50
3.3.1 Effective Hard-Sphere Diameter 50
3.3.2 LWCA Theory 51
3.3.3 Partial Pair Correlation Function 54
3.3.4 The Ashcroft-Langreth (AL) Partial Structure Factor 55
3.4 Thermodynamic Properties for Liquid Binary System 57
3.4.1 Energy of Mixing for Liquid Binary Alloys 59
3.4.2 Enthalpy of Mixing for Liquid Binary Alloys 67
3.4.3 Entropy of Mixing for Liquid Binary Alloys 68
3.5 Atomic Transport Theory for Liquid Binary System 69
3.5.1 Atomic Transport Property 69
3.5.2 Shear Viscosity for Liquid 70

3.5.3 Diffusion Coefficient for Liquid 74
3.6 Electron Transport Theory for Liquid Binary System 78
3.6.1 Ziman's Formula for the Electrical Resistivity 81
3.6.2 Corrections to Ziman's Expression 84
3.6.3 Scaling Laws for Transport Coefficients 84

4 Results, Discussions, & Conclusions 87
4.1 Effective Values of Parameters 88
4.2 Thermodynamic Properties for $Al_{1-x}Zn_x$ Liquid Binary System . . . 90
4.2.1 The Effective Partial Pair Potentials (V_{ij}) 90
4.2.2 The Pair Correlation Functions (g_{ij}) for the Reference Hard Sphere Liquids and Hard Sphere Diameters (σ_{ij}): 92
4.2.3 A, ΔA, ΔH and ΔS for $Al_{1-x}Zn_x$ Liquid Binary System . . . 94
4.2.4 Conclusion 98
4.3 Thermodynamic Properties for $Al_{1-x}In_x$ Liquid Binary System 100
4.3.1 The Effective Partial Pair Potentials (V_{ij}) 100
4.3.2 The Pair Correlation Functions (g_{ij}) for the Reference Hard Sphere Liquids and Hard Sphere Diameters (σ_{ij}): 101
4.3.3 A, ΔA, ΔH and ΔS for $Al_{1-x}In_x$ liquid Binary System 103
4.3.4 Conclusion 106
4.4 Thermodynamic Properties for $Al_{1-x}Sn_x$ Liquid Binary System . . . 108
4.4.1 The Effective Partial Pair Potentials (V_{ij}) 109
4.4.2 The Pair Correlation Functions (g_{ij}) for the Reference Hard Sphere Liquids and the Hard Sphere Diameters (σ_{ij}): 112
4.4.3 A, ΔA, ΔH and ΔS for $Al_{1-x}Sn_x$ liquid Binary System 114
4.4.4 Conclusion 118
4.5 Thermodynamic Properties for $Al_{1-x}Bi_x$ Liquid Binary System 120

4.5.1 The Effective Partial Pair Potentials (V_{ij}) 121
4.5.2 The Pair Correlation Functions (g_{ij}) for the Reference Hard Sphere Liquids and the Hard Sphere Diameters (σ_{ij}): 123
4.5.3 Systematic Study of Segregation for $Al_{1-x}Bi_x$ liquid Binary System 125
4.5.4 Conclusion 129
4.6 Thermodynamic Properties for $Al_{1-x}Cu_x$ Liquid Binary System . . . 130
4.6.1 The Effective Partial Pair Potentials (V_{ij}) 130
4.6.2 The Pair Correlation Functions (g_{ij}) for the Reference Hard Sphere Liquids and the Hard Sphere Diameters (σ_{ij}): 132
4.6.3 A, ΔA, ΔH and ΔS for $Al_{1-x}Cu_x$ liquid Binary System 134
4.6.4 Conclusion 138
4.7 Thermodynamic Properties for $Al_{1-x}Au_x$ Liquid Binary System . . . 139
4.7.1 Conclusion 142
4.8 Comparative Study for ΔA, ΔH and ΔS for Al-based Alloys 143
4.9 Results & Discussions for Atomic Transport (ATP) Properties 146
4.9.1 The First and Second Derivatives of the Partial Potential Curve for Different Binary Systems 148
4.9.2 The Partial Integrand (X_{ij}) for Different Binary Systems . . . 153
4.9.3 Table for Atomic Transport Coefficients for Al-based Systems 156
4.9.4 Conclusion 170
4.10 Comparative Study for Viscosity and Diffusion Coefficients for Al-based Alloys 171
4.11 Results, Discussion, & Conclusions for Electron Transport Properties for Al-based Liquid Binary Systems 176
4.11.1 Form-factor for Different Al-Based Binary Systems 178

4.11.2 Table for Electrical Resistivity (Ω) 181
4.11.3 Conclusion 183

A Origin of Local Minimum in Potentials of Polyvalent Metals 185
A.1 Introduction 185
A.2 Result 187
A.3 Conclusion 195

B Effects of Local Minimum appeared in Inter-atomic Potential on Atomic Transport of Liquid Aluminium 197
B.1 Introduction 197
B.2 Theory 200
B.2.1 Scaling Laws for Transport Coefficients 200
B.2.2 The Empty Core Model Potential(EMC) 202
B.2.3 VMHNC Integral Equation Theory 204
B.3 Results and Discussion 205
B.4 Conclusion 214

C Some Relevant Theories for Liquids 215
C.1 Pair Distribution Function for Liquids 215
C.2 Gibbs-Bogoliubov Variational Scheme 220
C.3 Derivative form for Entropy 222

D Phase Diagram 225

Bibliography (228-247)

List of Tables

2.1 Physical and Atomic Properties of Aluminium(Al) 33

4.1 BS Pseudopotential Parameters for Different Liquid Binary Systems. 89

4.2 The soft and hard core parts of the friction coefficients, $\zeta(\times 10^{-12} * kgs^{-1})$ and partial diffusion coefficients, $D_{Al,Zn}(\times 10^{-9} * m^2 s^{-1})$ for both constituents and mutual diffusion coefficients, $D_{Al-Zn}(\times 10^{-9} * m^2 s^{-1})$ are listed for $Al_{1-x}Zn_x$ alloys. 157

4.3 Different contributions to the viscosity (η) for $Al_{1-x}Zn_x$ liquid binary alloys. Units are in cP. 159

4.4 The soft and hard core parts of the friction coefficients, $\zeta(\times 10^{-12} * kgs^{-1})$ and partial diffusion coefficients, $D_{Al,In}(\times 10^{-9} * m^2 s^{-1})$ for both constituents and mutual diffusion coefficients, $D_{Al-In}(\times 10^{-9} * m^2 s^{-1})$ are listed for $Al_{1-x}In_x$ liquid binary alloys. 160

4.5 Different contributions to the viscosity (η) for $Al_{1-x}In_x$ liquid binary alloys. Units are in cP. 161

4.6 The soft and hard core parts of the friction coefficients, $\zeta(\times 10^{-12} * kgs^{-1})$ and partial diffusion coefficients, $D_{Al,Cu}(\times 10^{-9} * m^2 s^{-1})$ for both constituents and mutual diffusion coefficients, $D_{Al-Cu}(\times 10^{-9} * m^2 s^{-1})$ are listed for $Al_{1-x}Cu_x$ alloys. 163

4.7 Different contributions to the viscosity (η) for $Al_{1-x}Cu_x$ liquid binary alloys. Units are in cP. 164

4.8 The soft and hard core parts of the friction coefficients, $\zeta(\times 10^{-12} * kgs^{-1})$ and partial diffusion coefficients, $D_{Al,Au}(\times 10^{-9} * m^2 s^{-1})$ for both constituents and mutual diffusion coefficients, $D_{Al-Au}(\times 10^{-9} * m^2 s^{-1})$ are listed for $Al_{1-x}Au_x$ liquid binary alloys. 165

4.9 Different contributions to the viscosity for $Al_{1-x}Au_x$ liquid binary alloys. Units are in cP. 166

4.10 Mutual diffusion coefficients, $D_{Al-Bi}(\times 10^{-9} * m^2 s^{-1})$ for $Al_{1-x}Bi_x$ liquid binary segregating alloys at different temperatures. 168

4.11 Different contributions to the total viscosity for $Al_{1-x}Bi_x$ liquid binary segregating alloys at different temperatures. Units are in cP. 169

4.12 Comparison among the calculated resistivity at different concentrations for Al-based liquid binary alloys. Units are in Ω-m 182

B.1 Temperature dependent number density (ρ), hard sphere diameters (σ) and excess entropy (S_E) for our concerned liquid. 204

B.2 Presents viscosities of liquid polyvalent Al metal. Calc.1 present calculated viscosities by Empty Core model with core radius r_c=0.90 a.u, 1.092 a.u and 1.20 a.u respectively. Similarly, Calc.2 present calculated viscosities by Rosenfeld model with core radius r_c=0.90 a.u, 1.092 a.u and 1.20 a.u respectively. Calculated viscosities are compared with Experimental, Theoretical and Simulated results. 208

B.3 Diffusion coefficients of liquid polyvalent Al metal. Calc.1 present calculated diffusion coefficients by Empty Core model with core radius r_c=0.90 a.u, 1.092 a.u and 1.20 a.u respectively. Similarly, Calc.2 present calculated diffusion coefficients by Rosenfeld model with core radius r_c=0.90 a.u, 1.092 a.u and 1.20 a.u respectively. Calculated diffusion coefficients are compared with Experimental, Theoretical and Simulated results. 210

B.4 Verification of Stokes-Einstein Law. 213

List of Figures

2.1 P-V-T phase diagram [4]. 13

2.2 Position of Alkali Metals, Alkaline Earth Metals, Transition Metals, Semi Metals, Basic Metals, Lanthanide, and Actinides in the periodic table. 15

4.1 Partial pair potential (V_{ij}) for $Al_{1-x}Zn_x$ liquid binary system for concentrations x=0.1 and 0.5. 90

4.2 Partial pair potential (V_{ij}) for $Al_{1-x}Zn_x$ liquid binary system for concentration x=0.9. 91

4.3 Partial pair correlation function for $Al_{1-x}Zn_x$ liquid binary system for concentrations x=0.1, 0.5, and 0.9, respectively. 92

4.4 Hard sphere diameter for $Al_{1-x}Zn_x$ liquid binary alloys. 93

4.5 Free energy for $Al_{1-x}Zn_x$ liquid binary system. 96

4.6 Energy of mixing (ΔA) for $Al_{1-x}Zn_x$ liquid binary alloys. 97

4.7 Enthalpy of mixing (ΔH) and Entropy of mixing (ΔS) for $Al_{1-x}Zn_x$ liquid binary system. 98

4.8 Partial pair potential for $Al_{1-x}In_x$ liquid binary alloys. 100

4.9 Partial pair potentials for $Al_{1-x}In_x$ liquid binary alloys. 101

4.10 Partial pair correlation functions for concentration x=0.1, 0.5, and 0.9, respectively for $Al_{1-x}In_x$ liquid binary alloys. 102

4.11 Hard sphere diameter for $Al_{1-x}In_x$ liquid binary system. 103

4.12 Free energy for $Al_{1-x}In_x$ liquid binary alloys. 104

4.13 Energy of mixing (ΔA) for $Al_{1-x}In_x$ liquid binary alloys. 105

4.14 Enthalpy of mixing (ΔH) and Entropy of mixing (ΔS) for $Al_{1-x}In_x$ liquid binary system. 106

4.15 Partial pair potential for $Al_{1-x}Sn_x$ liquid binary alloys. 110

4.16 Static structure factors for liquid Al element for different core raduis R_c. 111

4.17 Partial pair correlation function. 112

4.18 Partial pair correlation function. 113

4.19 Hard sphere diameter for $Al_{1-x}Sn_x$ liquid binary system. 113

4.20 Free energy for $Al_{1-x}Sn_x$ liquid binary alloys. 114

4.21 Energy of mixing (ΔA) for $Al_{1-x}Sn_x$ liquid binary alloys. 115

4.22 Enthalpy of mixing (ΔH) and Entropy of mixing (ΔS) for $Al_{1-x}Sn_x$ liquid binary system. 117

4.23 Partial pair potential for concentrations x=0.1, 0.5 and 0.9 for $Al_{1-x}Bi_x$ liquid binary alloy at T=1173 K. 122

4.24 Static structure factors for liquid Al and Bi for different core radius R_c. 123

4.25 Partial pair correlation function for $Al_{1-x}Bi_x$liquid binary alloys. . . . 124

4.26 Hard sphere diameter for $Al_{1-x}Bi_x$ liquid binary alloys. 125

4.27 Energy of mixing as a function of concentration for $Al_{1-x}Bi_x$ liquid binary alloys at 1173 K. 126

4.28 Energy of mixing as a function of concentration for $Al_{1-x}Bi_x$ liquid binary alloys at different temperatures. 127

4.29 Enthalpy of mixing (ΔH) and Entropy of mixing (ΔS) for $Al_{1-x}Bi_x$ liquid binary system. 128

4.30 Partial pair potential for concentration x=0.1 for $Al_{1-x}Cu_x$ liquid binary alloy. 130

4.31 Partial pair potential for concentrations x=0.5 and 0.9 for $Al_{1-x}Cu_x$ liquid binary alloy. 131

4.32 Partial pair correlation function for $Al_{1-x}Cu_x$ liquid binary alloys for concentration x=0.1. 132

4.33 Partial pair correlation functions for $Al_{1-x}Cu_x$ liquid binary alloys for concentrations x=0.5 and 0.9, respectively. 133

4.34 Hard sphere diameter for $Al_{1-x}Cu_x$ liquid binary system. 134

4.35 Free energy for $Al_{1-x}Cu_x$ liquid binary alloys. 135

4.36 Energy of mixing (ΔA) for $Al_{1-x}Cu_x$ liquid binary system. 136

4.37 Entropy of mixing (ΔS) for $Al_{1-x}Cu_x$ liquid binary system. 137

4.38 Hard sphere diameter for $Al_{1-x}Au_x$ liquid binary system. 140

4.39 Energy of mixing (ΔA) for $Al_{1-x}Au_x$ liquid binary system. 141

4.40 Entropy of mixing (ΔS) for $Al_{1-x}Au_x$ liquid binary system. 142

4.41 Comparing the results of ΔA for Al based liquid binary systems, $Al_{1-x}X_x$; here, X= Zn, In, Sn, and Bi. 143

4.42 Comparing the results of ΔH for Al based liquid binary systems, $Al_{1-x}X_x$; here, X= Zn, In, Sn, and Bi. 144

4.43 Comparing the results of ΔS for Al based liquid binary systems, $Al_{1-x}X_x$; here, X= Zn, In, Sn, and Bi. 145

4.44 Partial pair potential V_{ij} and their derivatives for $Al_{1-x}Zn_x$ liquid binary system for concentration x=0.1 for temperature 1000 K, respectively. 149

4.45 Partial pair potential V_{ij} and their derivatives for $Al_{1-x}In_x$ liquid binary system for concentration x=0.1 for temperature 1173 K, respectively. 150

4.46 Partial pair potential V_{ij} and their derivatives for $Al_{1-x}Sn_x$ liquid binary system for concentration x=0.1 for temperature 973 K, respectively. 151

4.47 Partial pair potential V_{ij} and their derivatives for $Al_{1-x}Cu_x$ liquid binary system for concentration x=0.1 for temperature 1373 K, respectively. 152

4.48 Partial pair potential V_{ij} and their derivatives for $Al_{1-x}Au_x$ liquid binary system for concentration x=0.1 for temperature 1338 K, respectively. 153

4.49 Partial integrand X_{ij} as a function of r for $Al_{1-x}X_x$ liquid binary systems for concentration x=0.5; here, X=Zn, In, and Sn respectively. 154

4.50 Partial integrand X_{ij} as a function of r for $Al_{1-x}X_x$ liquid binary systems for concentration x=0.5; here, X=Cu, Au, and Bi respectively. 155

4.51 Comparison of Mutual Diffusion Coefficients for Al-based alloys at different thermodynamic states 171

4.52 Comparison of total Viscosity for Al-based liquid binary alloys at different thermodynamic states 172

4.53 Comparison of Mutual Diffusion Coefficients for $Al_{1-x}Bi_x$ liquid binary alloys at different thermodynamic states 173

4.54 Comparison of the total Viscosity for $Al_{1-x}Bi_x$ liquid binary alloys at different thermodynamic states 174

4.55 Variation of Form-factor, $F(q)$ as a function of q for $Al_{1-x}Zn_x$ liquid binary system for concentration, x=0.1, 0.5, and 0.9, respectively. . . 178

4.56 Variation of Form-factor, $F(q)$ as a function of q for $Al_{1-x}In_x$ liquid binary system for concentration, x=0.1, 0.5, and 0.9, respectively. . . 179

4.57 Variation of Form-factor, $F(q)$ as a function of q for $Al_{1-x}Cu_x$ liquid binary system for concentration, x=0.1, 0.5, and 0.9, respectively. . . 180

4.58 Variation of Form-factor, $F(q)$ as a function of q for $Al_{1-x}Au_x$ liquid binary system for concentration, x=0.1, 0.5, and 0.9, respectively. . . 181

4.59 Comparison of resistivity, Ω, for $Al_{1-x}Zn_x$, $Al_{1-x}In_x$, $Al_{1-x}Cu_x$, and $Al_{1-x}Au_x$ liquid binary alloys. 183

A.1 Effective partial pair potential for liquid Na and Zn from core radius r_c=0.15 a.u to 2.0 and 0.90 a.u respectively. 188

A.2 Effective partial pair potential for liquid Al from core radius r_c=0.15 a.u to 0.90 a.u. 189

A.3 Effective partial pair potential for liquid Sn and Bi from core radius r_c=0.15 a.u to 0.90 a.u respectively. 190

A.4 (a) Position of minimum of the 1^{st} well of V_{eff}(r) as a function of R_c. (b) Energy level of the 1^{st} well of V_{eff}(r) as a function of R_c. 191

A.5 Efective partial pair potential for liquid Na and Zn for fixed core radius r_c=0.15 a.u, but for different electron number density, ρ(=nZ). 193

A.6 Efective partial pair potential for liquid Al, Sn and Bi for fixed core radius r_c=0.15 a.u, but for different electron number density, ρ(=nZ). 194

B.1 (a) Hard sphere diameter for core radius, r_c= 0.90 a.u, 1.092 a.u and 1.20 a.u respectively for liquid Al. (b) Excess entropy for core radius, r_c= 0.90 a.u, 1.092 a.u and 1.20 a.u respectively for liquid Al. 205

B.2 Pair correlation function for liquid Al with EMC model for core radius, r_c= 0.90 a.u, 1.092 a.u and 1.20 a.u respectively. The red circles are corresponding experimental data [29]. 207

B.3 Figure: (a) and (b) representing the potential well for r_c=0.90 a.u. for two different range. Similarly, Figure: (c) and (d), Figure: (e) and (f) representing the potential well for r_c=1.092 a.u. and 1.20 a.u, respectively. 209

B.4 (a) Black circle, dashed line and black-white circle representing the pair correlation function with temperature 950 K for core radius r_c=1.20 a.u, 1.092 a.u and 0.90 a.u respectively (b) Triangle and dashed line representing the pair correlation function with different temperatures for T= 950 K and 1150 K respectively with core radius, r_c= 1.092 a.u. 212

B.5 Verification of Stokes-Einstein Law. 212

D.1 Phase diagram for $Al_{1-x}Zn_x$ liquid binary system. 225

D.2 Phase diagram for $Al_{1-x}In_x$ system for liquid state at 1173 K. 226

D.3 Phase diagram for $Al_{1-x}Sn_x$ system for liquid state at 1173 K. 226

D.4 Phase diagram for $Al_{1-x}Bi_x$ system for liquid state at 1373 K. 227

D.5 Phase diagram for $Al_{1-x}Bi_x$ system for liquid state at 1338 K. 227

Chapter 1

Introduction

The main purpose of the present research work is to study the 'Thermodynamic and Transport Properties of Al-Based Liquid Binary Alloys, $Al_{1-x}X_x$; here, X=Zn, In, Sn, Bi, Cu, and Au'. Thermodynamic properties such as Helmholtz free energy (A), the energy of mixing (ΔA), the enthalpy of mixing (ΔH), the entropy of mixing (ΔS), and transport properties (both Atomic Transport Property (ATP) and Electrical Transport Property (ETP)) namely, the shear viscosity (η), the diffusion coefficients (D), the friction coefficients (ζ), the electrical resistivity (Ω), and the electrical conductivity are of utmost interest [1–3] for several reasons. Aluminium and its alloys are used in many facets of our daily lives and are produced in huge amounts every year. Aluminium based liquid binary alloys have always been the key aspect of industrial development.

Therefore, physicists, chemists, and metallurgists are finding ways to have a better understanding of the thermodynamic and transport properties of liquid Al metal and its various alloys. The experimental studies of atomic transport properties and electron transport properties [1–3] are not always auspicious and sometimes are very costly. In addition, they are very difficult to manage properly as well.

A, ΔA, ΔH and ΔS play the important roles to understand the properties like the

segregation of alloys, phase transition of alloys, compound formation and stability of liquid metals and their alloys at different thermodynamic states [1–3]. Besides, the X-ray diffraction [4–6] for the measurements of the total and partial structure factor raises further attention to calculate the mixing behavior theoretically, and to compare it with the experimental data [4–6]. Viscosity (η) of different fluids inside the human body control a great number of [1, 5, 6] physiological activities. Similarly, diffusion (D) is another basic and important factor that helps to design and understand [2, 4] many important phenomena, such as precipitation, homogenization of alloys, recrystallization, grain boundary migration, creep, solidification, protective coatings and also controls many industrially important reactions. The protein synthesis and transportation of necessary biochemicals can only be possible with the help of diffusion. Among the various diffusion coefficients (self-diffusion, impurity diffusion, intrinsic diffusion, and chemical diffusion coefficients), the impurity diffusion coefficient is of the greatest importance. It is defined as the diffusion of a solute in a solvent at an extremely small concentration.

In the modeling of microstructure and the micro-segregation in multicomponent commercial use of Al-based alloys, Xie et.al [7] and Yan et.al [8] had shown the presence of back-diffusion in the solid by using impurity diffusion coefficients of various elements and their alloys. Electron transport is another important concept for describing various physical quantities of alloys such as the electrical resistivity (ρ), thermoelectric power and thermal conductivity (σ) of materials. Further study of electrical resistivity (ρ) of liquid metal alloys is being spread out day by day [9–28].

The reasons for choosing to study the Al-based alloys are fourfold. First, the alloy forming elements Al, In, Sn and Bi are heavy polyvalent metals and Zn, Cu, Au are transition metals and are sometimes difficult to handle theoretically, particularly, in the framework of pseudopotentials. Second, $Al_{1-x}X_x$, (here, X=Zn, In, Sn, Bi,

Cu, Au) liquid binary alloys have not been studied yet, from any microscopic theory to our knowledge, although some attempts are made from the empirical or semi-empirical models. Third, experimental data for static structure factors for elemental liquid Al, Zn, In, Sn, Bi, Cu, and Au are available in the literature [29] at the thermodynamic state in question. Fourth, the physical properties that we are interested in to investigate theoretically are already measured by different experimentalists. The above aspects and prospects motivate us to study the Al-based liquid binary alloys theoretically.

On a molecular level, A, ΔA, ΔH and ΔS are of great interest [1,5,6,8,29] because these macroscopic variables provide information about molecular properties. In ideal materials, intermolecular forces are the same between every pair of molecular kinds, so that a molecule feels no difference between itself and its molecular neighbors.

Consequently, there might be different in between the intermolecular forces [1, 6] or specific molecular effects between various species despite being chemically non-reacting. The mixing behaviors (ΔA, ΔH, ΔS) provide the information about different intermolecular forces or specific molecular effects in the materials. The energy of mixing (ΔA), the enthalpy of mixing (ΔH), the entropy of mixing (ΔS) are not independent of each other and rather related by the following thermodynamic relation [4, 29],

$$\Delta G = \Delta H - T\Delta S \tag{1.1}$$

where ΔG denotes the Gibbs free energy of mixing. Note that at one atmospheric pressure [4, 29] (p), $\Delta G \simeq \Delta A$ and $\Delta H \simeq \Delta E$, where ΔA and ΔE are Helmholtz free energy of mixing and internal energy of mixing; and at zero pressure the above relations become equal. However, evaluation of energy of mixing directly involves the full profile of the inter-ionic pair potentials (V_{ij}) whereas the entropy of mixing is related directly to the derivative of free energy with respect to temperature. So, it

is always a challenging task to calculate them theoretically. The statistical concept of randomness is used for statistical mechanical explanation of ΔA, ΔH, and ΔS. Mixing of ideal materials is regarded as random at a molecular level and correspondingly mixing of non-ideal materials may be non-random. So far, several theories have been used to advance to study A, ΔA, ΔH and ΔS for liquid binary alloys, these are mentioned below,

(i). The Quasi-Lattice Theory (QLT) [30, 31],

(ii). The General Microscopic Theory (GMT) [32],

(iii). The Computer Simulation (CS) [33], and

(iv). The Empirical Linear Free Energy Theory (ELT) [34].

In QLT the activity is expressed in terms of average inter-ionic interaction energy and the formation of mixing via the Gibbs free energy. The energy of formation is determined by fitting to the experimental data of the activity [4, 15]. The ELT is empirical and is applicable only when the solute concentration is very low [15]. The GMT is based on the electronic theory of metals, the static structure factor obtainable from the knowledge of inter-ionic pair interaction through the statistical mechanics and the perturbation or variational theory [31]. The first principle perturbation approach uses the full profile of the potential. Each term in GMT is clearly understandable from the physical point of view. Moreover, the GMT is relatively simple to handle numerically and has proven to be successful for some liquid binary alloys [35–58]. It is to be noted here that, the advent of sophisticated theories of

metals for transition and less simple metals in the last two decades have opened a new window of interest to revisit old approaches like the GMT for better predictions. The present research work also justifies this statement.

Several theories have advanced to study the ATP of (namely, η, D and ζ) liquid metals and their alloys [41–44]. Among them, we can especially mention mode-mode coupling (MCM) and the distribution function method. These two theories are based on two different ideas and consequently have their own limitations for success. The dynamic structure factor $S(q,\omega)$ lies at the heart of the MCM approach. In the limit $q \to 0$ and $\omega \to 0$ the dynamic structure factor $S(q,\omega)$ gives the shear viscosity. Anyway, the calculation of the dynamic structure factor itself is a difficult problem computationally. On the other hand, the distribution function method as developed by Rice and Allnatt (RA) [59–64] is very convenient due to its simplicity of numerical calculations. More importantly, the physical significance of each term in the theory is very transparent for understanding various transport mechanisms involved. Another advantage of the RA theory is that it has already been extended for the liquid binary alloys [41–44]. Moreover, the RA theory proved to be successful for some liquid simple metals [37–40] and their binary alloys [41–44,50]. The RA theory divides the effective inter-ionic pair potential into a long-range called soft part and a short-range called hardcore part. This division is made possible by considering the statistical events due to the strong repulsive core of the pair potential at short inter-ionic distances. It can conveniently be separated from the remaining statistical events considered which justifies the division of the potential for our concerned system.

From the distribution function method [59–64], we can write the total viscosity as a sum of three separate contributions. The first contribution arises from the kinetic part, which was derived using the singlet reduced distribution function in the statistical mechanics. The second contribution comes from the momentum transfer

that occurs during the hardcore collisions. This term is evaluated by using the doublet reduced distribution function. Finally, the third contribution comes from the region $r > \sigma$(σ is the effective hard sphere diameter) is obtained by using the small step theory involving the doublet reduced distribution function. These terms are denoted by η_k, $\eta_v(\sigma)$ and $\eta_v(r > \sigma)$ respectively. The RA theory for viscosity then has the final form of,

$$\eta = \eta_k + \eta_v(\sigma) + \eta_v(r > \sigma) \tag{1.2}$$

For full numerical calculation of viscosity, the RA theory also needs the pair distribution function of the hard spheres and the first and second derivatives of the partial pair potentials. For some systems, reports say $\eta_v(r > \sigma)$ evolves as the dominating part [4, 29], while for some systems $\eta_v(\sigma)$ dominates over the other terms [59–64]. Due to the comparison, it is established that the soft part contribution plays the significant role in viscosity calculation. The soft term consists of an integration whose upper limit is infinity. But for potentials with long-range Friedel oscillations (for example, pseudopotentials) the integrand diverges although the pair correlation function and the potentials and their derivatives converge. In a work, Bhuiyan *et. al* [41–44] has given the proper prescription to truncate the upper limit of the integration. So, we consider the way shown in Bhuiyan *et al* [41–44] to determine the proper value of the soft part contribution. It can also be addressed that for RA theory, the correlation between the hard and soft part (sometimes referred to as cross term) is negligibly small relative to the others. Now, the calculation of ATP involves the first and second order derivatives of the pair potential in RA theory. This makes the potential a delicate candidate, whose involvement greatly affect the calculation of shear viscosity and diffusion coefficient. Thus, it is most important to determine appropriate potentials for our concerned alloys.

One widely used theory for the electrical resistivity (Ω) is Ziman's formula based

on single-site scattering [9]. Its starting point rests on first-order time-dependent perturbation theory [4]. For the present research work, the electrical resistivity (Ω) is calculated with the extended Ziman's theory [9,15,65–68]. Ziman's theory is based on the long Mean Free Path (MFP) approximation. But, practically, the MFP of conduction electrons in liquid metals has a finite range. This finiteness of the MFP, following the Heisenberg uncertainty principle results in a blurred Fermi surface instead of a sharp one which is assumed in Ziman's theory [9]. In some papers [9, 15] the extended Ziman's theory is found to be in very good agreement with corresponding data calculated for the electrical resistivity. Anyway, most of these papers are somewhat accountable to the question of the internal uniformity of the calculations. In the present work, internal consistency is retained. By consistency we mean the following: Static structure and pair correlation function are intimately connected with inter-ionic interaction [65–68]. In addition, the static structure profile is very sensitive for the electrical resistivity. An inconsistency arises when the structural data and the potential are chosen independently. Thereupon, the reliability of the resistivity results reduces remarkably.

To estimate the inter-ionic interactions for a real metallic system, many pseudopotential theories have been proposed over the years [16–58]. Among them, the Bretonnet and Silbert model [44] is a promising candidate due to its successful application. In 1992, Bretonnet and Silbert [44] proposed a local pseudopotential model to describe the inter-ionic potential of simple liquid metals and binary alloys. This model combined the *d*-band effect and the *sp*-band contribution within the pseudopotential formalism. The *sp*-band effect is described by the empty core potential while the *d*-band effect is derived from the *d*-band phase shift by an inverse scattering approach. Our concerned alloys namely $Al_{1-x}Zn_x$, $Al_{1-x}In_x$, $Al_{1-x}Sn_x$, $Al_{1-x}Bi_x$, $Al_{1-x}Cu_x$ and $Al_{1-x}Au_x$ consist of transition elements Zn, Cu and Au which show

a fair amount of hybridization effect. In principle, BS model is easy to calculate pseudopotential numerically. Besides, this model can account adequately for the hybridization effects. BS model is also used for the calculations of atomic transport properties of elemental system [37–40], binary alloys [41–44], electronic transport and thermodynamic properties of binary alloys [45–58]. Considering this success, we intend to employ the BS model for our present study. We note here that the pseudopotential can be local or non-local in character. We have chosen the local pseudopotential instead of a non-local one. The *sd*-hybridization effect is accounted for approximately by changing the relative occupancy of the s and d bands. In doing this, there is no restriction to use the suitable values for the effective valency, Z. For example, Will-Harrison [48,49] used Z=1.5 for all elements of the $3d$, $4d$ and $5d$ series except for Au for which they used Z=2.

The pair correlation function, $g_{ij}(r)$ for hard spheres of reference liquid is a very important ingredient to describe the thermodynamics of mixing and transport properties for liquid binary systems. In order to evaluate g(r), the different approximation methods are used. These are classified into three groups. First, the perturbation and variational [4, 29] theories. Second, the integral equation theories and third, computer simulation methods. A reference system is required in thermodynamic perturbation theory. Hard sphere (HS) reference system is used in the present work. Among the various perturbation theories available for liquid systems we have used Weeks-Chandler-Anderson (WCA) [69–72] and Linearized Weeks-Chandler-Anderson (LWCA) [71,72] theories along with Percus-Yevick (PY_{HS}) theory for pair correlation function.

The main objective of the structural theories of the liquids or dense fluid is to find the appropriate form for pair correlation function g(r) and its counterpart in momentum space S(q) at some specified state point for a given pair potential. For

simple liquid, this task is done by the so called 'reference system' approach in light of physical basis that the structure of dense fluid is mostly determined by the inter-atomic repulsive forces, which gives rise to the volume effect [70]. As a consequence, a fluid explained by pair potential leads to the consideration of infinitely strong HS system. Structural properties of such a system can be calculated approximately [71, 72]. The actual fluid of concern is then investigated by variational method after getting the appropriate reference system by determining the specific form of the remaining non-repulsive part of interaction as well as their influence on the structure of the reference systems [70]. Using these reference systems particularly the HS one in our case, the treatment of thermodynamic perturbation theory is discussed in chapter 3. Development of the WCA perturbation theory [71, 72] and its simplified model LWCA [69] are explained in details there. The WCA theory starts with dividing the effective inter-ionic interaction into a soft core repulsive part and a perturbation tail part. The LWCA is capable to produce $S(\mathrm{q})$ that is almost produced by the full WCA, except a disagreement for small q. It is worth mentioning that, σ_{12} evaluated from the LWCA is close enough (within 0.01%) to the mean value of $(\sigma_{11} + \sigma_{22})/2$. Therefore, we can take the average of these two values instead of calculating σ_{12}.

Besides, we have also systematically investigated for the first time the effect of the core size of the ion and the role of conduction electron density [73–75] on the inter-ionic pair interactions of monovalent and polyvalent metals. The effective inter-ionic interaction [73–75] is described by the Ashcroft empty core model [4] and Ichimaru-Utsumi theory for dielectric function [76, 77]. Here, the combined effect of the core size and the conduction electron density plays the role. More interestingly, for smaller core size [73] conduction electron density plays the major role [74] and for larger core size the core [75] radius plays the major role in determining the local minimum. Details are given in Appendix A.

This research dissertation has been organized in the following way. In chapter 2 we have described the classification of metals and properties of the constituent elements of Al-based liquid binary alloys in brief. Chapter 3 is devoted to a brief discussion of related theories and models used in this study. I have presented the results, discussions, and conclusions for Al-based alloys in Chapter 4. Appendix B, C, and D are organized for the transport properties of liquid Al, some relevant theories, and phase diagrams of the studied Al-based liquid binary alloys, respectively.

Chapter 2

Metals

Most elements of the modern periodic table are found in their metallic state in nature (see Figure 2.2). Many scientists, chemists, and physicists consider the electronic configuration, and band structure for classifying these fundamental elements. There are different groups of these elements, such as the Alkali metals, Alkaline earth metals, Transition metals, Lanthanide (rare earth elements), Actinides, etc. Although separate position on the periodic table, the Lanthanide and Actinides are really specific types of transition metals. According to the rearrangement of the elements in the periodic table, we can classify the elements as given below:

(i). Alkali Metals,

(ii). Alkaline Earth Metals,

(iii). Transition Metals,

(iv). Semi-metals or Metalloid,

(v). Nonmetals,

(vi). Basic Metals,

(vii). Halogens,

(viii). Noble Gases or Inert Gases,

(ix). Lanthanide, and

(x). Actinides.

In this Chapter, we have focused on discussing the classification and a brief discussion of Metals.

2.1 Concept of Metals

To understand the insight features of metals, one needs a clear concept about Electronic Band Structure [4, 29], Fermi Surfaces [32] and Density State Theory [4]. The electrons of a single isolated atom occupy atomic orbitals which set a discrete energy level, but in a molecule, atomic orbitals separate into molecular orbitals at different energies, which are very small and they form molecular bands.

With the help of the Schrödinger equation, we can calculate the band structure, which describes the energy as a function of wave number k. Besides, a filled band cannot conduct electricity but partially filled bands can, as they have available unoccupied states of scattered electrons. The Fermi level is the highest filled level at $T = 0$, in which the band energy is called Fermi energy. The energy surface in k-space corresponding to Fermi energy is called Fermi surface. In a filled band there is no Fermi surface between occupied and unoccupied states. The behavior of metals can be thoroughly described using the Fermi surface.

Materials in nature exist in different states, for example, solid, liquid, and gas at a certain thermodynamic condition. Besides this, there are two other states; the Plasma and the Liquid crystal, which are potential candidates for the position of the fourth state of matter [4, 29]. But, unfortunately, none of them has yet been able to occupy this position firmly. Any preferred state among these three depends on the temperature (T), pressure (P), and volume (V), which can be depicted in a single $P - V - T$ phase diagram as shown in Figure 2.1. At the triple point, all the three states of the matter remain in equilibrium. Above the critical point, we can not

distinguish between liquid and vapor, because this is the state of fluid with uniform density. The phenomenon of supercooling of liquid exists at the temperature below the triple point.

Liquid, one of the three commonly recognized states in which matter occurs, is, the state, as distinguished from solid and gas, in which a substance has a definite volume but no definite shape. The concept of the idealized model is the key to the study of properties of matter. If we look at the progress of these studies from ancient times to the present days, it becomes clear that a tremendous amount of progress has been made for the solids and liquids both in experiment and theory. It is very unfortunate that, there is still no idealized model for liquid systems. Therefore, it is more difficult to analyze the behavior of the liquid. Evidently, available scientific literature tells us that, the liquid has intermediate properties of solid and gas, but in reality, we cannot merely average between those properties [4, 29].

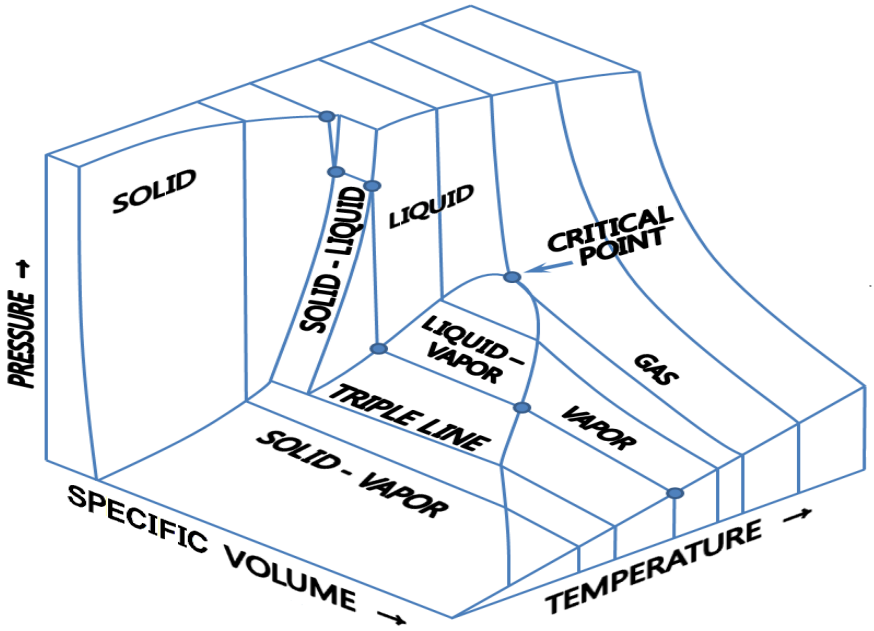

Figure 2.1: P-V-T phase diagram [4].

Most of the solids around us are nonmetals. In spite of that, if we look at the periodic table as shown in Fig. 2.2, we find that almost two third of the elements are metals. The most striking characteristics of metals are their high electrical and thermal conductivity. Metals have temperature independent carrier concentrations. They have high optical absorption coefficient, which remains almost constant in the visible spectrum, causing the high reflexivity. The total energy of metal consists of two parts. One is the structure-independent energy which determines largely by the high binding energy of metals and which depends only on the volume. Another part is the structure dependent energy (coming from the effective pair potential) [4, 29], which depends on the detailed configuration of the respective ions.

2.2 Classification of Metals

According to electronic configuration and band structure, we may classify metals into seven categories which are as follows:

(i). Alkali Metals,

(ii). Alkaline Earth Metals,

(iii). Transition Metals,

(iv). Semi-metals or Metalloid,

(v). Basic Metals,

(vi). Lanthanide, and

(vii). Actinides.

2.3 Alkali Metals

In Alkali metals, all electrons reside at the Fermi surface [4], and they are named as s-electrons and p-electrons. The Fermi surface is spherical and the conduction

Figure 2.2: Position of Alkali Metals, Alkaline Earth Metals, Transition Metals, Semi Metals, Basic Metals, Lanthanide, and Actinides in the periodic table.

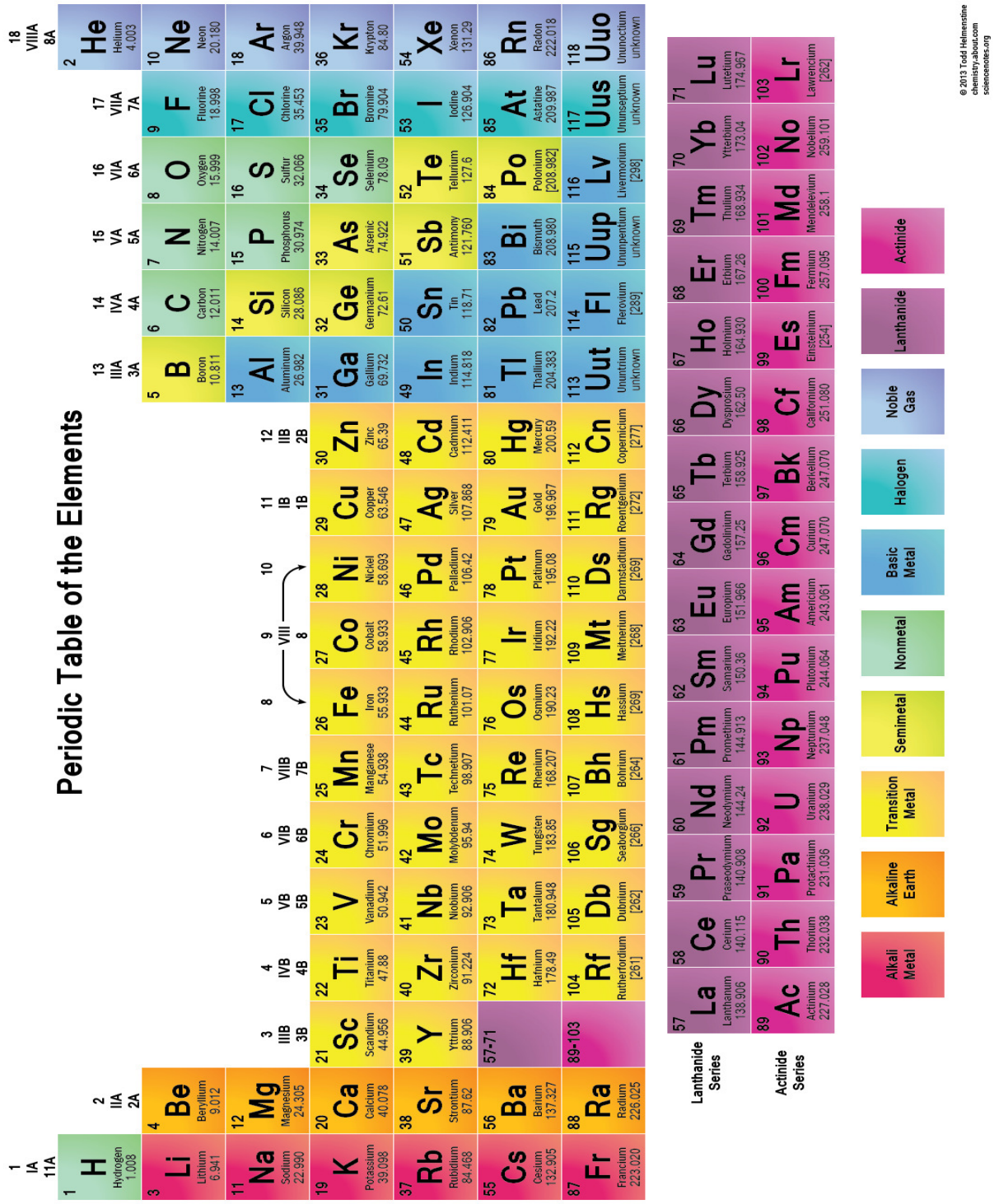

electrons are nearly free. But the valence band is separated from the next core-level bands. Properties of these kinds of metals can be explained by the nearly free electron model. In this model, it is assumed that the crystal potential is so weak that, the electrons behave essentially like free particles. The metals whose physical properties are explained by this model are known as simple metals. Specifically, the potential energy in the liquid simple metals can be presented by the pairwise additive approach and their structure mostly by the hard sphere theory.

The Alkali metals are the elements located in Group IA of the periodic table. The alkali metals are Lithium (Li), Sodium (Na), Potassium (Ca), Rubidium (Ru), Cesium (Cs), and Francium (Fr).

2.3.1 Properties of Alkali Metal

The alkali metals exhibit many of the physical properties common to metals, although their densities are lower than those of other metals. Alkali metals have one electron in their outer shell, which is loosely bound. This gives them the largest atomic radii of the elements in their respective periods. Their low ionization energies result in their metallic properties and high reactivities. An alkali metal can easily lose its valence electron to form the univalent cation. Alkali metals have low electronegativities. They react readily with nonmetals, particularly halogens.

Common Properties:

The common properties for Alkali metals are discussed below:

(i). Lower densities than other metals,

(ii). One loosely bound valence electron,

(iii). Largest atomic radii in their periods,

(iv). Low ionization energies,

(v). Low electro-negativities, and

(vi). Highly reactive.

2.4 Alkaline Earth Metals

The Alkaline earth metals are the elements located in Group IIA of the periodic table. This is the second column of the table. The list of elements that are alkaline earth metals is small. In order of increasing atomic number, the six element names and symbols are Beryllium (Be), Magnesium (Mg), Calcium (Ca), Strontium (Sr), Barium (Ba), and Radium (Ra).

If element 120 is produced, it will most likely be a new alkaline earth metal. Presently, Radium is the only one of these elements that is radioactive with no stable isotopes. Element 120 would be radioactive, too. All of the Alkaline earth metals except Magnesium and Strontium have at least one radioisotope that occurs naturally.

2.4.1 Properties of Alkaline Earth Metals

The alkaline earths possess many of the characteristic properties of metals. Alkaline earths have low electron affinities and low electro-negativities. As with the alkali metals, the properties depend on the ease with which electrons are lost. The alkaline earths have two electrons in the outer shell. They have smaller atomic radii than the alkali metals. The two valence electrons are not tightly bound to the nucleus, so the alkaline earths readily lose the electrons to form divalent cations.

Common Properties:

The common properties for Alkaline earth metals are discussed below:

(i). Two electrons in the outer shell and a full outer electron s shell,

(ii). Low electron affinities,

(iii). Low electro-negativities,

(iv). Relatively low densities,

(v). Relatively low melting points and boiling points, as far as metals are concerned,

(vi). Typically malleable and ductile. Relatively soft and strong,

(vii). The elements readily form divalent cations (such as Mg^{2+}, Ca^{2+}),

(viii). The alkaline earth metals are very reactive, although less so than the alkali metals. Because of their high reactivity, the alkaline earths are not found free in nature. However, all of these elements are found naturally. They are common in a wide variety of compounds and minerals,

(ix). These elements are shiny and silver-white as pure metals, although they usually appear dull because they react with air to form oxide layers on the surface,

(x). All the alkaline earths except beryllium form corrosive alkaline hydroxides, and

(xi). All of the alkaline earths react with halogens to form halides. The halides are ionic crystals, except for beryllium chloride, which is a covalent compound.

The Alkaline earth metals get their names from their oxides, which were known to mankind long before the pure elements were isolated. These oxides were called Beryllia, Magnesia, Lime, Strontia, and Baryta. The word "earth" comes from an old term used by chemists to describe a nonmetallic substance that did not dissolve in water and resisted heating. It wasn't until 1780 that Antoine Lavoisier suggested the earths were compounds rather than elements.

2.5 Transition Metals

Of all the groups of elements, the transition metals can be the most confusing to identify because there are different definitions under which elements should be included. According to the IUPAC, a transition metal is any element with a partially filled d-band electron sub-shell. This describes groups 3 through 12 on the periodic table, although the f-band elements (Lanthanide and Actinides, below the main body of the periodic table) are also transition metals. The d-band elements are called transition metals, while the Lanthanide and Actinides are called "inner transition metals". The elements are called "transition" metals because the English chemist Charles Bury used the term in 1921 to describe the transition series of elements, which referred to the transition from an inner electron layer with a stable group of 8 electrons to one with 18 electrons or the transition from 18 electrons to 32.

Transition metals have features of narrow (tight binding) bands and nearly free electron behavior. In the noble metals, the tight binding structure is maintained with minimum energies equal to the highest occupied energy level. In transition metals, the Fermi level lies within the d-band. For transition metals [4, 29], d-band electrons specifically cannot be classified as core or valence electrons. The rare earth elements with incomplete f-band may be sometimes described by the approach similar to that of transition metals.

The transition elements are located in groups IB to VIIIB of the periodic table. In other words, the transition metals are:

(i). 21 (Scandium) through 29 (Copper),

(ii). 39 (Yttrium) through 47 (Silver),

(iii). 57 (Lanthanum) through 79 (Gold), and

(iv). 89 (Actinium) through 112 (Copernicium)- which includes the Lanthanide and Actinides.

Another way to view it is that the transition metals include the *d*-band block elements, also many people consider the *f*-band block elements to be a special subset of transition metals. While Aluminium, Gallium, Indium, Tin, Thallium, Lead, Bismuth, Nihonium, Flerovium, Moscovium, and Livermorium are metals, these "basic metals" have less metallic character than other metals on the periodic table and tend not to be considered as transition metals.

2.5.1 Properties of Transition Metals

Because they possess the properties of metals, the transition elements are also known as the transition metals. These elements are very hard, with high melting points and boiling points. Moving from left to right across the periodic table, the five d orbitals become more filled. The d electrons are loosely bound, which contributes to the high electrical conductivity and malleability of the transition elements. The transition elements have low ionization energies. They exhibit a wide range of oxidation states or positively charged forms. The positive oxidation states allow transition elements to form many different ionic and partially ionic compounds. The formation of complexes causes the d orbitals to split into two energy sublevels, which enables many of the complexes to absorb specific frequencies of light. Thus, the complexes form characteristic colored solutions and compounds. Complexation reactions sometimes enhance the relatively low solubility of some compounds.

Common Properties:

The common properties for Transition metals are discussed below:

(i). Low ionization energies,

(ii). Positive oxidation states,

(iii). Multiple oxidation states, since there is a low energy gap between them,

(iv). Very hard,

(v). Exhibit metallic luster,

(vi). High melting points,

(vii). High boiling points,

(viii). High electrical conductivity,

(ix). High thermal conductivity,

(x). Malleable,

(xi). Form colored compounds, due to $d - d$ electronic transitions,

(xii). Five d orbitals become more filled, from left to right on periodic table,

(xiii).Typically form paramagnetic compounds because of the unpaired *d*-electrons, and

(xiv). Typically exhibit high catalytic activity.

2.6 Semi-Metals or Metalloid

Between the metals and nonmetals is a group of elements known as either the Semi-metals or the Metalloid, which are elements that have properties intermediate between those of the metals and nonmetals. Most Metalloids have a shiny, metallic appearance, but are brittle, unexceptional electrical conductors, and display non-metallic chemical properties. Metalloids are elements that have semiconductor properties and form amphoteric oxides.

The Metalloids or Semi-metals are located along the line between the metals and nonmetals in the periodic table. Because these elements have intermediate properties, it is sort of a judgment call as to whether a particular element is a metalloid or should be assigned to one of the other groups. The name of these elements are Boron (B), Silicon (Si), Germanium (Ge), Arsenic (As), Antimony (Sb), Tellurium (Te), Polonium (usually recognized, sometimes considered a metal), and Astatine

(sometimes recognized, otherwise seen as a halogen).

Element 117, Tennessine, has not been produced in sufficient amounts to verify its properties, but is predicted to be a metalloid. Some scientists consider neighboring elements on the periodic table to either be Metalloids or to have metalloid characteristics. An example is Carbon, which may be considered either a nonmetal or a metalloid, depending on its allotrope. The diamond form of carbon looks and behaves as a nonmetal, while the graphite allotrope has a metallic luster and acts as an electrical semiconductor, so is a metalloid. Phosphorus, and Oxygen are other elements that have both non-metallic and metalloid allotropes. Selenium is considered to be a metalloid in environmental chemistry. Other elements that may behave as Metalloids under certain conditions are hydrogen, nitrogen, sulfur, tin, bismuth, zinc, gallium, iodine, lead, and radon.

2.6.1 Properties of Semi-Metals

The electro-negativities and ionization energies of the Metalloids are between those of the metals and nonmetals, so the Metalloids exhibit characteristics of both classes. Silicon, for example, possesses a metallic luster, yet it is an inefficient conductor and is brittle. The reactivity of the Metalloids depends on the element with which they are reacting. For example, boron acts as a nonmetal when reacting with Sodium (Na), yet as a metal when reacting with fluorine. The boiling points, melting points, and densities of the Metalloids vary widely. The intermediate conductivity of Metalloids suggest that they tend to make good semiconductors.

The most abundant metalloid in the Earth's crust is silicon, which is the second most abundant element overall (oxygen is most abundant). The least abundant natural metalloid is tellurium. Metalloids are valuable in the electronics industry. Silicon, for example, is used to make chips found in phones and computers. Arsenic

and polonium are highly toxic Metalloids. Antimony and tellurium are used primarily in metal alloys to add desirable properties.

Common Properties:

The common properties for Semi-metals are discussed below:

(i). Electro-negativities between those of metals and nonmetals,

(ii). Ionization energies between those of metals and nonmetals,

(iii). Possess some characteristics of metals/some of nonmetals,

(iv). Reactivity depends on properties of other elements in reaction,

(v). Often make good semiconductors,

(vi). Often have a metallic luster, although may have allotropes that appear non-metallic,

(vii). Usually behave as nonmetals in chemical reactions,

(viii). Form alloys with metals,

(ix). Usually brittle, and

(x). Usually solids under ordinary conditions.

2.7 Metals or Basic Metals

Metals are located on the left side and the middle of the periodic table. Group IA and Group IIA (the alkali metals) are the most active metals. The transition elements, groups IB to VIIIB, are also considered metals. The basic metals make up the element to the right of the transition metals. The bottom two rows of elements beneath the body of the periodic table are the lanthanides and actinides, which are also metals.

Most of the elements on the periodic table are metals. In order of increasing atomic number, the name & symbols of the eleven basic elements are:

(i). Aluminum (Al),

(ii). Gallium (Ga),

(iii). Indium (In),

(iv). Tin (Sn),

(v). Thallium (Ti),

(vi). Lead (Pb),

(vii). Bismuth (Bi),

(viii). Nihonium (Nh, Element 113),

(ix). Flerovium (Fl, or Element 114),

(x). Moscovium (Mc, or Element 115), and

(xi). Livermorium (Lv, or Element 116).

2.7.1 Properties of Metals

Metals are shiny solids at room temperature (except mercury, which is a shiny liquid element) with characteristic high melting points and densities. Many of the properties of metals, including large atomic radius, low ionization energy, and low electro-negativity are due to the fact that the electrons in the valence shell of metal atoms can be removed easily. One characteristic of metals is their ability to be deformed without breaking. Malleability is the ability of a metal to be hammered into shapes. Ductility is the ability of a metal to be drawn into wires.

Because the valence electrons can move freely, metals are good heat conductors and electrical conductors.

Common Properties:

The common properties of metals are given below:

(i). Shiny "metallic" appearance,

(ii). Solids at room temperature (except mercury),

(iii). High melting points,

(iv). High densities,

(v). Large atomic radii,

(vi). Low ionization energies,

(vii). Low electro-negativities,

(viii). Usually high deformation,

(ix). Malleable,

(x). Ductile,

(xi). Thermal conductors, and

(xi). Electrical conductors.

2.8 Lanthanides

The Lanthanides or d-block elements are a set of elements of the periodic table. Here is a look at their location and common properties:

The Lanthanides are located in block $5d$ of the periodic table. The first $5d$ transition element is either Lanthanum or Lutetium, depending on the interpretation of the periodic trends of the elements. Sometimes only the Lanthanides, and not the Actinides, are classified as rare earths. The Lanthanides are not as rare as was once thought; even the scarce rare earths (e.g., Europium, Lutetium) are more common than the platinum-group metals. Several of the Lanthanides form during the fission of Uranium, and Plutonium.

The Lanthanides have many scientific and industrial uses. Their compounds are used as catalysts in the production of petroleum and synthetic products. Lanthanides are used in lamps, lasers, magnets, phosphors, motion picture projectors, and X-ray intensifying screens.

Common Properties of the Lanthanides:

Lanthanides share the following common properties:

(i). Silvery-white metals that tarnish when exposed to air, forming their oxides,

(ii). Relatively soft metals. Hardness increases somewhat with higher atomic number,

(iii). Moving from left to right across the period (increasing atomic number), the radius of each lanthanide 3^+ ion steadily decreases. This is referred to as 'lanthanide contraction',

(iv). High melting points and boiling points,

(v). Very reactive,

(vi). React with water to liberate hydrogen (H_2), slowly in cold/quickly upon heating. Lanthanides commonly bind to water,

(vii). React with H^+ (dilute acid) to release (H_2) (rapidly at room temperature),

(viii). React in an exothermic reaction with (H_2),

(ix). Burn easily in air,

(x). They are strong reducing agents,

(xi). Their compounds are generally ionic,

(xii). At elevated temperatures, many rare earths ignite and burn vigorously,

(xiii). Most rare earth compounds are strongly paramagnetic,

(xiv). Many rare earth compounds fluoresce strongly under ultraviolet light,

(xv). Lanthanide ions tend to be pale colors, resulting from weak, narrow, forbidden f x f optical transitions, and

(xvi). The magnetic moments of the lanthanide and iron ions oppose each other.

2.9 Actinides

At the bottom of the periodic table there is a special group of radioactive metallic elements. These elements have interesting properties and play a key role in nuclear chemistry. The Actinides or Actinoids are a set of radioactive elements on the periodic table, ranging from atomic number 89 to atomic number 103. The modern periodic table has two rows of elements below the main body of the table. The actinides are the elements in the bottom row. The top row is the lanthanide series. The reason these two rows of elements are placed below the main table is because they don't fit in the design without making the table confusing and very wide. However, these two rows of elements are metals, sometimes considered a subset of the transition metals group. In fact, the Lanthanides and actinides are sometimes called the inner transition metals, referring to their properties and position on the table. Two ways of including the Lanthanides and actinides within a periodic table are to include those elements in their corresponding rows with the transition metals (making the table wider) or ballooning them out to make a three-dimensional table. The 15 Actinide elements. Actinium (Ac), Thorium (Th), Protactinium (Pa), Uranium (U), Neptunium (Np), Plutonium (Pu), Americium (Am), Curium (Cm), Berkelium (Bk), Californium (Cf), Einsteinium (Es), Fermium (Fm), Mendelevium (Md), Nobelium (No) and Lawrencium (Lr).

Actinide Abundance:

The only two actinides found in appreciable quantities in the Earth's crust are Thorium, and Uranium. Small quantities of Plutonium and Neptunium are present in Uranium orders. Actinium and Protactinium occur as decay products of certain Thorium and Uranium isotopes. The other Actinides are considered synthetic elements. If they occur naturally, it is part of a decay scheme of a heavier element.

Common Properties of the Actinides:

Actinides share the following common properties:

(i). All are radioactive. These elements have no stable isotopes,

(ii). Actinides are highly electro-positive,

(iii). The metals tarnish readily in air. These elements are pyrophoric (spontaneously ignite in air), particularly as finely divided powders,

(iv). Actinides are very dense metals with distinctive structures. Numerous allotropes may be formed (plutonium has at least 6 allotropes!). The exception is Actinium, which has fewer crystalline phases,

(v). They react with boiling water or dilute acid to release Hydrogen gas,

(vi). Actinide metals tend to be fairly soft. Some can be cut with a knife,

(vii). These elements are malleable and ductile, and

(viii). All of the actinides are paramagnetic.

Actinide Uses:

For the most part, we don't encounter these radioactive elements much in daily life. Americium is found in smoke detectors. Thorium is found in gas mantles. Actinium is used in scientific and medical research as a neutron source, indicator, and gamma source. Actinides may be used as dopants to make glass and crystals luminescent.

The bulk of actinide use goes to energy production and defense operations. The primary use of the actinide elements is as nuclear reactor fuel and for the production of nuclear weapons. The actinides are favored for these reactions because they readily undergo nuclear reactions, releasing incredible amounts of energy. If the conditions are right, the nuclear reactions may become chain reactions.

2.10 Properties of Al, Zn, In, Sn, Bi, Cu and Au

In this report, we are interested to study the thermodynamic and transport properties of Al-based liquid binary alloys ($Al_{1-x}X_x$, here X=Zn, In, Sn, Bi, Cu and Au).

Aluminium (Al):

Aluminium is the most widely used non-ferrous metal. The global production of Aluminium in 2017-2018 was 88.03 million metric tons (Daily Mirror, British national daily tabloid newspaper). It exceeded that of any other metal except Iron (Fe, 1231 million metric tons). Aluminium is almost always alloyed, which markedly improves its mechanical properties, especially when tempered. For example, the common Aluminium foils and beverage cans are alloys of 92% to 99% Aluminium. Aluminium is used for transportation (automobiles, aircrafts, trucks, railway cars, marine vessels, bicycles, spacecraft, etc) because of its low density; packaging (cans, foil, frame, etc) because it is non-toxic, non-adsorptive, and splinter-proof; electricity related uses because it is relatively cheap, highly conductive, has adequate mechanical strength and low density, and resists corrosion; machinery and equipment related uses because of its corrosion resistance, non-pyrophoricity, and mechanical strength [4].

Zinc (Zn):

Zinc is most commonly used as Galvanizing (55%), Brass and Bronze (16%), other alloys (21%), and miscellaneous (8%). In 2009, in the United States, 55% or 893 thousand tonnes of the Zinc metal was used for galvanization. Zinc is more reactive than Iron or Steel, and thus will attract almost all local oxidation until it completely corrodes away. Galvanization is used on chain-link fencing, guard rails, suspension bridges, lightposts, metal roofs, heat exchangers, and car bodies. Zinc is also used to cathodically protect metals that are exposed to sea water. A zinc disc attached

to a ship's iron rudder will slowly corrode while the rudder stays intact. Similarly, a zinc plug attached to a propeller or the metal protective guard for the keel of the ship provides temporary protection. Zinc powder is sometimes used as a propellant in model rockets. Zinc sheet metal is used to make zinc bars.

A widely used zinc alloy is brass, in which Copper is alloyed with anywhere from 3% to 45% zinc, depending upon the type of brass. Brass is generally more ductile and stronger than Copper, and has superior corrosion resistance. These properties make it useful for communication equipment, hardware, musical instruments, and water valves. Alloys of zinc with small amounts of copper, Aluminium, and magnesium are useful in die casting as well as spin casting, especially in the automotive, electrical, and hardware industries. These alloys are marketed under the name Zamak. An example of this is zinc Aluminium. The low melting point together with the low viscosity of the alloy makes possible for the production of small and intricate shapes. The low working temperature leads to rapid cooling of the cast products and fast production for assembly. Another alloy, marketed under the brand name Prestal, contains 78% zinc and 22% Aluminium, and is reported to be nearly as strong as steel but as malleable as plastic. This super-plasticity of the alloy allows it to be molded using die casts made of ceramics and cement [4].

Indium (In):

Indium was discovered in 1863 by Ferdinand Reich and Hieronymous Theodor Richter by spectroscopic methods. Indium has no biological role, though its compounds are somewhat toxic when injected into the bloodstream. Indium has no metabolic role in any organism. In a similar way to Aluminium salts, indium(III) ions can be toxic to the kidney when given by injection. The first large-scale application for indium was coating bearings in high-performance aircraft engines during World

War II, to protect against damage and corrosion; this is no longer a major use of the element. Indium has many semiconductor-related applications. Some indium compounds, such as indium antimonide and indium phosphide, are semiconductors with useful properties. Indium wire is used as a vacuum seal and a thermal conductor in cryogenics and ultra-high-vacuum applications, in such manufacturing applications as gaskets that deform to fill gaps [4].

Tin (Sn):

The first Tin (Sn) alloy used on a large scale was bronze, made of Tin and Copper, from as early as 3000 BC. After 600 BC, pure metallic Tin (Sn) was produced. Tin (Sn) has long been used in alloys with Lead (Pb) as solder, in amounts 5 to 70% w/w. Tin (Sn) bonds readily to Iron and is used for coating Lead, Zinc, and Steel to prevent corrosion. Tin (Sn)-plated steel containers are widely used for food preservation, and this forms a large part of the market for metallic Tin. Tin (Sn) in combination with other elements forms a wide variety of useful alloys like $Al_{1-x}Sn_x$ liquid binary alloy. This metal alloy is referred to as spotted metal. Major advantages of using Tin (Sn) alloys for pipes include its appearance, its workability, and resistance to corrosion [4].

Bismuth (Bi):

Bismuth metal has been known since ancient times, although it was often confused with Pb and Sn, which share same physical properties. Bismuth was long considered the element with the highest atomic mass that is stable. Bismuth appears in the 1660s, from obsolete German Bismuth, Wismut, Wissmuth (early 16th century); perhaps related to Old High German hwiz ("white"). Bismuth has few commercial applications, and those applications that use it generally require small quantities relative to other raw materials. In the United States, for example, 884 tonnes of

Bismuth were consumed in 2010, of which 63% went into chemicals (including pharmaceuticals, pigments, and cosmetics); 26% into metallurgical additives for casting and galvanizing; 7% into Bismuth alloys, solders and ammunition; and 4% into research and other uses. Bismuth is an ingredient in some pharmaceuticals, for example subsalicylate is used as an antidiarrheal. Bibrocathol is an organic Bismuth containing compound used to treat eye infections. Bismuth-Subgallate the active ingredient in Devrom, and it is used as an internal deodorant to treat malodor from flatulence, and feces [4].

Copper (Cu):

Cu is one of the few metals that occur naturally in directly usable metallic form. The major applications of copper are electrical wire (60%), roofing and plumbing (20%), and industrial machinery (15%). Cu is used mostly as a pure metal, but when greater hardness is required, it is put into such alloys as brass and bronze (5% of total use). For more than two centuries, copper paint has been used on boat hulls to control the growth of plants and shellfish. A small part of the copper supply is used for nutritional supplements and fungicides in agriculture. Machining of copper is possible, although alloys are preferred for good machinability in creating intricate parts [4].

Gold (Au):

Gold is the most malleable of all metals. Gold has been widely used throughout the world as money, for efficient indirect exchange (versus barter), and to store wealth in hoards. For exchange purposes, mints produce standardized gold bullion coins, bars and other units of fixed weight and purity. [4]

The properties for heavy polyvalent Al element is given below in a table.

Table 2.1: Physical and Atomic Properties of Aluminium(Al)

Properties	Details
Period	3
Group	13
Block	p
Atomic Number	13
Atomic Mass	26.98
Group Name	Simple Element
Electronic Configuration	$[Ne]3s^2 3p^1$
Electrons per shell	2, 8, 3
Phase	Solid
Liquid Density	2.3758 $gm.cm^{-3}$
Melting Point	933.47K
Boiling Point	2792K
Heat of fusion	10.71 kJ/mol
Heat of vaporization	284 kJ/mol
Molar heat capacity	24.20 $J/(molK)$
Crystal Structure	fcc
Atomic radius	143 pm
Thermal conductivity	237 $W/(mK)$
Electrical resistivity	28.2 nm
Magnetic susceptibility	+16.5*10^6 cm^3/mol
Oxidation Number	+3

Similar results for Zn, In, Sn, Bi, Cu and Au can be found in [4, 29].

Chapter 3

Theories

3.1 Pseudopotential for Inter-Ionic Interaction

In physics, a pseudopotential or effective potential is used as an approximation for the simplified description of complex systems. This is an attempt to replace the complicated effect of the motion of the conduction electrons and the positive ions with an effective potential. The Schrödinger equation [4,29] thus contains a modified effective potential term instead of the bare Coulomb potential term for core electrons, but provide the same energy eigenvalue. The pseudopotential approximation [4,5,29] was first introduced by Harris in 1934 [5]. According to this, the valence wave function generated is to be orthogonal to all core states.

The pseudopotential is constructed to replace the atomic "all electron" potential in the way that, the core states are eliminated and the valence electrons are described by node less pseudo-wave function. Here, only the chemically active valence electrons are dealt with explicitly, and the core electrons are 'frozen', being considered together with the nuclei as rigid non-polarized ion cores. Norm-conserving pseudopotentials are derived from an atomic reference state requiring that the pseudo eigenstates, and all electron eigenstates have the same energies and amplitude outside a chosen core

radius, r_c. Pseudopotentials with larger cutoff radius are said to be softer, that is more rapidly convergent. There are different types of pseudopotentials such as the model pseudopotentials, and "ab initio" pseudopotential etc. Again the "ab initio" pseudopotential is constructed by using different methods.

But for all instances, the pseudopotential [4, 5, 29] is based on these following assumptions:

(i). There exist a self-consistent "one electron Hamiltonian" in metals [4, 5, 29]. The interaction between electrons can be replaced by a potential, which depends upon the states, and is occupied by electrons.

(ii). The conduction band is the range of electron energies enough to free an electron from binding with its atom to move freely within the atomic lattice of the material as a delocalized electron state or valence level unless this state include filled $d-shell$ as core levels. Both the valence, and core levels are separable, and the later is assumed to be small, and the same eigenstates in metals as in the free atoms.

(iii). The pseudopotential is sufficiently weak, and the corresponding pseudo wave function is sufficiently smooth. For one particle time independent Schrödinger equation for the conduction electrons, we can write the following approximation:

$$\left[-\frac{\hbar^2}{2m}\nabla^2 + V(r) \right] |\Psi^\gamma\rangle = E|\Psi^\gamma\rangle. \tag{3.1}$$

The Schrödinger equation for the core electron is

$$\left[-\frac{\hbar^2}{2m}\nabla^2 + V(r) \right] \Psi^c(r) = E\Psi^c(r). \tag{3.2}$$

Where V(r) is the one electron self-consistent real potential, $\psi(r)$ defines the state function, and the superscript γ and c indicate the valence, and the core states, respectively.

By knowing the core states, the conduction electron states could be obtained. A useful approach to this problem is to expand the conduction electron in the plane waves which have been modified so as to be automatically orthogonal to the core states. This is known as the method of orthogonal plane waves or OPW. Now the orthogonalized plane wave may be written as

$$|OPW\rangle = |k\rangle + \sum b_c |\Psi^c\rangle, \tag{3.3}$$

and this will be orthogonal to the core states. Such as,

$$\langle \Psi^{c'} | OPW \rangle = 0 \tag{3.4}$$

or,

$$\langle \Psi^{c'} | k \rangle + \sum_c b_c \langle \Psi^{c'} | \Psi^c \rangle = 0 \tag{3.5}$$

or,

$$\langle \Psi^{c'} | k \rangle = -\sum_c b_c \delta_{cc'} \tag{3.6}$$

$$= -b_{c'}. \tag{3.7}$$

Equation (3.7) can be written in the form also

$$b_c = -\langle \Psi^c | k \rangle. \tag{3.8}$$

So we get,

$$|OPW\rangle_k = |k\rangle - \sum_c |\Psi^c\rangle \langle \Psi^c | k \rangle. \tag{3.9}$$

Where,

$$|k\rangle = \exp(i\vec{k}.\vec{r}). \tag{3.10}$$

The OPW is orthogonal to all the states as to say,

$$\begin{aligned} \langle \Psi^c | OPW \rangle_k &= \langle \Psi^c | k \rangle - \sum_c \langle \Psi^c | \Psi^c \rangle \langle \Psi^c | k \rangle \\ &= \langle \Psi^c | k \rangle - \langle \Psi^c | k \rangle \\ &= 0. \end{aligned} \tag{3.11}$$

Let us define the projection operator as

$$p = \sum_c |\Psi^c\rangle\langle\Psi^c|. \tag{3.12}$$

From equation (3.9) we have,

$$|OPW\rangle_k = (1 - P)|k\rangle. \tag{3.13}$$

The band wave function can be expanded in terms of the OPW as

$$\begin{aligned} |\Psi_k\rangle &= \textstyle\sum_k a_k (1 - P)|k\rangle \\ or, |\Psi_k\rangle &= (1 - P) \textstyle\sum_k a_k |k\rangle \\ or, |\Psi_k\rangle &= (1 - P) \textstyle\sum_k |\phi_k\rangle. \end{aligned} \tag{3.14}$$

Here

$$|\phi_k\rangle = \sum_k a_k |k\rangle, \tag{3.15}$$

and a_k's are the coefficient of expansion. Now putting the value of $|\psi\rangle$ in equation (3.2) we find

$$\left(-\frac{\hbar^2}{2m}\nabla^2 + V(r) \right)(1-P)|\phi_k\rangle = E(1-P)|\phi_k\rangle$$

$$or, \left(-\frac{\hbar^2}{2m}\nabla^2 + V(r) \right)|\phi_k\rangle - \left(-\frac{\hbar^2}{2m}\nabla^2 + V(r) \right)|\psi^c\rangle\langle\psi^c|\phi_k\rangle = E|\phi_k\rangle$$

$$or, \left(-\frac{\hbar^2}{2m}\nabla^2 + V(r) - E^c P + EP \right)|\phi_k\rangle = E|\phi_k\rangle. \tag{3.16}$$

Thus we get

$$\left(-\frac{\hbar^2}{2m}\nabla^2 + W(r) \right)|\phi_k\rangle = E|\phi_k\rangle. \tag{3.17}$$

Where the expression for $W(r)$ can be written as

$$W(r) = V(r) + \sum_c (E - E^c)P. \tag{3.18}$$

Equation (3.18) is the pseudopotential equation. There are two important points in the formulation of the pseudopotential theory.

(i). The pseudopotential, in general, is non-local because of the energy-dependent operator, which is obvious from equation (3.18).

(ii). We have the freedom of choosing pseudopotential for the same energy eigenvalue. The second term of the right-hand side of the equation (3.18) acts as a repulsive potential because of the positive sign of the $(E - E^c)$ and the operator p tends to cancel the strong attractive potential $V(r)$ in the core again. Therefore valence electrons in the metal behave as if they did not interact strongly with ions.

3.1.1 Pseudopotential Theory

The form of pseudopotential [1, 4, 5, 29] is,

$$W(r) = V(r) + \sum_c (E - E^c)|\Psi^c\rangle\langle\Psi^c|. \tag{3.19}$$

Let us assume that

$$|\Psi^c\rangle = |\alpha\rangle. \tag{3.20}$$

Here, $V(r)$ is the strong potential and ψ^c is the core wave function which is defined as,

$$\Psi^c = \alpha(E - E^c). \tag{3.21}$$

So, substitute the value from equation (3.20) and (3.21) into equation (3.19), we get as

$$W(r) \quad = V(r) + \textstyle\sum_\alpha (E(k) - E^\alpha)|\alpha\rangle\langle\alpha|$$

$$or, W(r) \quad = V(r) + \textstyle\sum_\alpha f(k,\alpha)|\alpha\rangle\langle\alpha|. \tag{3.22}$$

Now multiplying both sides from the right with $|k\rangle$ in equation (3.22), then we get

$$W|k\rangle = V|k\rangle + \sum_\alpha f(k,\alpha)|\alpha\rangle\langle\alpha|k\rangle. \tag{3.23}$$

As the potential terms due to the cores also contribute to $V(r)$, we may be able to write it approximately as a sum of potentials associate with the individual ions, and these are spherically symmetric. So,

$$V^{ion} = \sum_j v^{ion}(|\vec{r} - \vec{r_j}|). \tag{3.24}$$

Here, the index j labels the ions. Finally, the core states entering the final term in the pseudopotential may be written as

$$|\alpha\rangle = \Psi_t(|\vec{r} - \vec{r_j}|). \tag{3.25}$$

Where subscript t denotes the energy and the angular momentum numbers for the core state of the ion. Therefore, $f(k, \alpha)$ depend upon through t. Thus we can write as,

$$W = \sum_j w(|\vec{r} - \vec{r_j}|). \tag{3.26}$$

From these above equations we get,

$$\begin{aligned} W(|\vec{r} - \vec{r_j}|)|k\rangle &= V(|\vec{r} - \vec{r_j}|) \\ &+ \frac{\exp(i\vec{k}.\vec{r})}{\Omega^{\frac{1}{2}}} \left[\sum_t f(k,t)\Psi_t(|\vec{r} - \vec{r_j}|) \int d^3r \Psi_t^*(|\vec{r} - \vec{r_j}|) \right]. \end{aligned} \tag{3.27}$$

From the scattering theory we can write,

$$\langle k+q|W(r)|k\rangle = \Omega^{-1}\int \exp\left(-i(\vec{k}+\vec{q}).\vec{r}\right)\sum_j w(|\vec{r}-\vec{r_j}|)\exp\left(i\vec{k}.\vec{r}\right)d^3r \quad (3.28)$$

$$= \Omega^{-1}\times N\times\frac{1}{N}\sum_j \exp(-i\vec{q}.\vec{r_j})\int \exp\left(-i(\vec{k}+\vec{q}).(\vec{r}-\vec{r_j})\right)$$

$$w(|\vec{r}-\vec{r_j}|)\times\exp\left(i\vec{k}.(\vec{r}-\vec{r_j})\right)d^3r$$

$$= \frac{N}{\Omega}\times S(q)\int \exp\left(-i(\vec{k}+\vec{q}).(\vec{r}-\vec{r_j})\right)w(|\vec{r}-\vec{r_j}|)$$

$$\times\exp\left(i\vec{k}.(\vec{r}-\vec{r_j})\right)d^3r$$

$$= S(q)\times\int \exp\left(-i(\vec{k}+\vec{q}).(\vec{r}-\vec{r_j})\right)w(|\vec{r}-\vec{r_j}|)$$

$$\times\exp\left(i\vec{k}.(\vec{r}-\vec{r_j})\right)d^3r.$$

Where we define the static structure factor $S(q)$ as $\frac{1}{N}\sum_j \exp(-i\vec{q}.\vec{r_j})$.

It is convenient to rewrite the matrix element in the form

$$\langle k+q|W(r)|k\rangle = S(q)\langle q+k|w|k\rangle, \quad (3.29)$$

and

$$\langle q+k|W|k\rangle = \Omega^{-1}\int \exp\left(-i(\vec{k}+\vec{q}).\vec{r}\right)\exp\left(i\vec{k}.\vec{r}\right)d\tau. \quad (3.30)$$

Here, Ω_0 is the volume per ion, $\frac{\Omega}{N}$. Since the static structure factor is

$$S(q) = \frac{1}{2}\sum_j \exp(-i\vec{k}.\vec{r})d\tau. \quad (3.31)$$

So, we can write as

$$\begin{aligned}\langle k+q|W(r)|k\rangle &= \frac{N}{\Omega}S(q)\int \exp(-i(\vec{k}\vec{q}).(\vec{r}-\vec{r_j})\\ &\times\ (|\vec{r}-\vec{r_j}|)\exp(-i\vec{k}.(\vec{r}-\vec{r_j}))d\tau\\ &= S(q)\langle q+k|w|k\rangle. \quad (3.32)\end{aligned}$$

We are interested primarily for the matrix elements, in-between states on the Fermi sphere i.e. $\langle k+q|W|k\rangle$ for which the magnitude of k and the magnitude of $k+q$ have the eigenvalue k_F, which is Fermi radius. In the diffraction model, we do not explicitly include any interaction between conduction electron, this has been done with the determination of the potential w. Therefore, in the calculation of the total energy in the diffraction model, we add only the interaction between the electrons and ions, not the interaction between electrons. Now, the total energy of an ion is defined as,

$$E_{el} = \frac{1}{N}\sum_{k<K_F} E(k) = \frac{2\sigma_0}{2\pi^3}\int E(k)d^3k. \tag{3.33}$$

From the second order perturbation theory we get,

$$\begin{aligned} E(k) &= \frac{\hbar k^2}{2m} + \langle k|w|k\rangle + {\sum_q}' \frac{\langle k+q|W|k\rangle\langle k|W|k+q\rangle}{\frac{\hbar^2}{2m}(k^2-|(k+q)^2|)} \\ &= \frac{\hbar k^2}{2m} + \langle k|w|k\rangle + \sum_q S^*(q)S(q)\frac{\langle k+q|W|k\rangle\langle k|W|k+q\rangle}{\frac{\hbar^2}{2m}(k^2-|(k+q)^2|)}, \end{aligned} \tag{3.34}$$

where the prime over the sum indicates that $q \neq 0$.

So, the contribution to the E_{el} from the first term is simply valence Z, and average K.E. of the electrons in the form of

$$\frac{Z\int_0^{k_F} 4\pi k^2\left(\frac{\hbar^2k^2}{2m}\right)dk}{\int_0^{k_F} 4\pi k^2 dk} = \frac{3}{5}Z\left(\frac{\hbar^2k_F^2}{2m}\right). \tag{3.35}$$

Where Z is the number of valence electron per ion.

Now from the contribution of the 2nd term, $\langle k|W|k\rangle$ will be shifted to the total energy by a constant amount.

Considering, the third term we get

$$\sum_q S^*(q)S(q)\frac{2\Omega_0}{(2\pi)^3}\int d^3k\frac{\langle k+q|W|k\rangle\langle k|W|k+q\rangle}{\frac{\hbar^2}{2m}(k^2-|(k+q)^2|)}. \tag{3.36}$$

This is known as the band structure energy [4], and may be written as

$$E_{bs}=\sum_q{}' S^*(q)S(q)F(q). \tag{3.37}$$

In equation (3.37) $F(q)$ is the structure factor, and can be expressed in below

$$F(q)=\frac{2\Omega_0}{(2\pi)^3}\int d^3k\frac{\langle k+q|W|k\rangle\langle k|W|k+q\rangle}{\frac{\hbar^2}{2m}(k^2-|(k+q)^2|)}. \tag{3.38}$$

The first two term together gives the free electron energy,

$$E_g=Z\left(\frac{3}{5}\frac{\hbar^2}{2m}+\langle k|W|k\rangle\right). \tag{3.39}$$

So,

$$E=E_g+ZE_{bs}. \tag{3.40}$$

The peak of $F(q)$ comes at the position where the OPW form factor cross zero, these are the wave numbers for which the repulsive and attractive terms in the effective potential of each ion as seen by the electrons cancel each other. Thus

$$\begin{aligned}E_{bs}&=\sum_q S^*(q)S(q)F(q)\\&=\sum_q\sum_{ij}\frac{1}{N^2}F(q)\exp(-i\vec{q}(\vec{r_i}-\vec{r_j}))\\&=\sum_{i\neq j}\frac{1}{2N}\left(\frac{2}{N}\right)\sum_q\sum_{ij}\frac{1}{N^2}F(q)\exp(-i\vec{q}(\vec{r}-\vec{r_j}))+\sum_q\frac{1}{N}F(q).\end{aligned} \tag{3.41}$$

Where,

$$\sum_{ij} \exp(-i\vec{q}(\vec{r_i} - \vec{r_j})) = N. \tag{3.42}$$

Let us define,

$$\left(\frac{2}{N}\right) \sum_{q} \sum_{ij} \frac{1}{N^2} F(q) \exp(-i\vec{q}(\vec{r} - \vec{r_j})) = V_{ind}(|\vec{r} - \vec{r_j}|). \tag{3.43}$$

Therefore,

$$E_{bs} = \frac{1}{2N} \sum_{i \neq j} V_{ind}(|\vec{r} - \vec{r_j}|) + \sum_{ij} \frac{1}{N} F(q). \tag{3.44}$$

From equation (3.44),

$$\begin{aligned} V_{ind} &= \frac{2\Omega}{(2\pi)^3} \int F(q) \exp(-iqr \sin\theta) q^2 dq \sin\theta d\theta d\phi \\ &= \frac{\Omega_0}{\pi^2} \int_0^\infty F(q) \frac{\sin qr}{qr} q^2. \end{aligned} \tag{3.45}$$

Here V_{ind} is a two bodied central force interaction between ions [4] just as the direct interaction. The two bodies may be added to give a total effective interaction between ions. Screening plays an important role in the behavior of metals, but we are interested in non-screened inter-ionic interaction too.

The final interaction between ions can be written as,

$$V(r) = \frac{Ze^2}{2} + \frac{\Omega_0}{\pi} \int_0^\infty F(q) \frac{\sin qr}{qr} q^2 dq. \tag{3.46}$$

We can use this interaction to determine the pseudopotentials over the elements in the binary alloys.

3.1.2 Purpose of Pseudopotential

The purpose [4], of pseudopotentials hold in our theory is mostly to achieve a smooth potential for core states, which suffice the difficulty faced by the wave function in the core region.

Pseudopotential has more unique features. It is additive and transferable. Additivity can most easily be achieved by building pseudopotentials for atoms in reference states. Whereas by transferable, we mean that, the same pseudopotential should work accurately for an atom in all possible chemical environments. This feature of pseudopotential is quite important as our allocated environment of simulation might differ for different phase transitions due to chemical reaction [21–28].

3.2 Models of Pseudopotential

Norm-conserving and Ultra-soft are the two most common forms of pseudopotential used in modern plane-wave electronic structure calculation. They allow a basis set with a significantly lower cut-off to be used to describe the electron wave functions.

Norm-conserving pseudopotentials are constructed to enforce the condition that, inside the cut-off radius, the norm of each pseudo-wave function is to be identical to its corresponding all-electron wave function. But Ultra-soft pseudopotentials relax the norm-conserving constraint to reduce the necessary basis-set size further at the expense of introducing a generalized eigenvalue problem.

In our present study, we consider a model pseudopotential for simplicity. There are several established model to describe this form of pseudopotential. But in midst of them, Bretonnet-Silbert(BS) model [44,55–58] of pseudopotential is the most reliable candidate. And we have considered another model pseudopotential for finding the core interaction in the elemental system (for liquid Al, Appendix B) namely Empty

Core Model Pseudopotential (EMC) [4, 5, 29].

3.2.1 Bretnot-Silbert Model Pseudopotential (BS)

Bretonet-Silbert (BS) model [44] is based on the modification of already established Pseudopotential model. The BS model makes the pseudopotential function continuous and thus it's quite easy to manipulate. Previously, the local Oli [4, 45, 47] model potential accounts for the '$s-d$' scattering inside the ion core of radius R_c, while outside R_c , the Coulomb ion-electron potential is suggested as,

$$W_0(r) = \begin{cases} \sum_{m=1}^{2} B_m \exp\left(\frac{-r}{mR_c}\right) & : r < R_C, \\ \frac{-Z_s e^2}{r} & : r > R_c, \end{cases}$$

where B_1, and B_2 are the Dirichlet coefficients and Z_s is the effective number of valence electrons per atom. The form inside the core is obtained using an inverse scattering approach, especially using the distorted plane wave method, developed by Swan [4, 45] and improved by Oli [4, 45]. But in the core potential $W_0(r)$ is not continuous at $r = R_c$.

In the Bretonet-Silbert (BS) model pseudopotential [44], an arbitrary parameter, "a" is introduced in place of R_c. This parameter is called the softness parameter. Now the potential can be written as,

$$W_{BS}(r) = \begin{cases} \sum_{m=1}^{2} B_m \exp\left(\frac{-r}{ma}\right) & : r < R_C, \\ \frac{-Z_s e^2}{r} & : r > R_c. \end{cases}$$

This implies that, W_{BS} must be continuous at the core, $r = R_c$. In the BS model, another condition is implied, which states that the derivative is also continuous at the core. We need to apply this condition because, physically the repulsive part should not affect drastically the behavior of the s electrons, while the attractive part

should only slightly depend on the interaction potential so as to counteract the s states making the transition metals more compact, and more tightly bound.

The softness parameter, "a" in this model plays an important role in determining the effective pair interaction, particularly the repulsive part and the depth of the interactive potential well. As the value of "a" increases, the repulsive part becomes softer and the depth of the attractive well decreases and the position of the first minima shift towards larger values of r. Here, in Bretonet-Silbert model, B_1 and B_2 are defined in terms of parameters namely, "a", "R_c", and "Z" to satisfy the approximations written above. Consequently, the form factor is different. These coefficients are written as,

$$B_1 = \frac{Z_s e^2}{R_c}\left(1 - \frac{2a}{R_c}\right)\exp\left(\frac{R_C}{a}\right), \tag{3.47}$$

and

$$B_2 = \frac{2Z_s e^2}{R_c}\left(\frac{a}{R_c} - 1\right)\exp\left(\frac{R_C}{2a}\right). \tag{3.48}$$

The unscreened form factor can be expressed as,

$$W_{BS}(q) = 4\pi n a^3\left[\frac{B_1 J_1}{1 + a^2q^2} + \frac{8B_2 J_2}{(1 + 4a^2q^2)^2}\right] - \frac{4\pi n Z_s e^2 \cos(qR_c)}{q^2}. \tag{3.49}$$

From equation (3.49), n is the ionic number density, and J_m is defined as

$$J_m = 2 - \exp(-\frac{R_c}{ma})\left[\frac{R_c}{ma}(1 + m^2a^2q^2) + (1 - m^2a^2q^2)\right]\frac{\sin(qR_c)}{maq} + \exp(-\frac{R_c}{ma})\left[2 + \frac{R_c}{ma}(1 + m^2a^2q^2)\right]\cos(qR_c). \tag{3.50}$$

Although in this particular form, the term corresponding to the *sd* mixing effects tends to zero when q approaches zero, and for the long-wavelength limit of second form factor $W(r)$ is preserved,

$$\lim_{q \longrightarrow 0} \frac{W_{BS}(q)}{\varepsilon(q)} \longrightarrow -\frac{2}{3} E_F, \tag{3.51}$$

where, $\varepsilon(q)$ is the dielectric function related to the local Field-function $G(q)$.

The effective inter-ionic pair potential(in atomic units) is given by,

$$v(r) = \frac{Z_s e^2}{r}\left[1 - \frac{2}{\pi}\int F_N(q)\frac{\sin(qr)}{q}dq\right], \tag{3.52}$$

where, F_N is the normalized energy wavenumber characteristic in the form of,

$$F_N = \left(\frac{q^2}{4\pi n e^2 Z_s}\right)^2 W_{BS}^2\left[1 - \frac{1}{\varepsilon(q)}\right]\left[\frac{1}{1 - G(q)}\right]. \tag{3.53}$$

Here, $\varepsilon(q)$, and $G(q)$ denotes the dielectric function, and the local field correction respectively. And the dielectric screening function $\varepsilon(q)$ is given by,

$$\varepsilon(q) = 1 - \frac{4\pi e^2}{q^2}[\chi(q) - G(q)] \tag{3.54}$$

These are taken from Ichimaru and Utsumi [48–51,71] because their form satisfies the compressibility sum rule, and the short-range correlation condition in addition to their applicability over a wide range of metallic densities.

3.2.2 The Empty Core Model Pseudopotential (EMC)

The Empty core potential (EM) for one component metallic systems may expressed as [4, 5, 29],

$$E_m(r) = \begin{cases} 0; & \text{if } r < r_c, \\ \\ -Ze^2/r; & \text{if } r > r_c. \end{cases} \tag{3.55}$$

In equation (3.55), r_c, Z, and e are the core radius, the effective s-electron effective valence, and the electronic charge respectively. The partial unscreened form factor [4] from equation (3.49) can be written as,

$$v_{ij}(r) = -\frac{4\pi Z\rho}{q^2}\cos(qr_c), \tag{3.56}$$

where, ρ is the ionic number density, and q is the momentum transfer.

If we observe the equation (3.56), then it could be noticed that the core radius r_c, enters into the form factor of the interaction through the scattering matrix. This form factor finally carries the r_c into the inter-ionic interaction.

Within the pseudopotential formalism, the effective inter-ionic pair interaction can be written as,

$$v_{eff}(r) = \frac{Z^2}{r}\left[1 - \frac{2}{\pi}\int dq I^N \frac{\sin(qr)}{q}\right]. \tag{3.57}$$

Here, the energy wave number characteristic can be defined as,

$$I^N = [\frac{q^2}{\pi n Z}]^2 |V(q)|^2 \left[1 - \frac{1}{\varepsilon(q)}\right] \left[\frac{1}{1 - G(q)}\right], \tag{3.58}$$

where, $V(q)$ denotes the local pseudopotential of the component, and n is the number density of ions. Besides, $\varepsilon(q)$, and $G(q)$ are the dielectric screening function, and the local field factor, respectively. Here, the dielectric function,

$$\varepsilon(q) = 1 - \left[\frac{\frac{4\pi e^2}{q^2}\chi(q)}{1 + \frac{4\pi e^2}{q^2}G(q)\chi(q)}\right], \tag{3.59}$$

where $\chi(q)$ is Lindhard function, and can be written as

$$\chi(q) = -\frac{m k_F}{\pi^2 \hbar^2}\left[\frac{1}{2} + \frac{4k_F^2 - q^2}{8 q k_F} \ln\left|\frac{2k_F + q}{2k_F - q}\right|\right]. \tag{3.60}$$

3.3 Structural Properties of Liquid Alloys

Here, we are interested to study the structure of our concerned alloys. Among all of them, we are most anticipating to learn the behavior of hard-sphere diameter, and the partial pair correlation function. These two are the basic building blocks of our calculation along with the thermodynamic perturbation theory.

3.3.1 Effective Hard-Sphere Diameter

The Weeks-Chandler-Anderson [69–72] theory describes, the static structure factor for a system of particles interacting through a repulsive potential in terms of hard sphere diameter, σ. The Linearized Weeks-Chandler-Anderson [70] (LWCA) perturbation theory, is used to determine the values of hard-sphere diameters.

3.3.2 LWCA Theory

The LWCA theory [69–72] describes, the structure factor, $S(q)$ for a system of particles interacting via a repulsive potential, corresponding to a system of hard-spheres, called hard-sphere potential v_σ. For such a hard-sphere system, there is an associated function $Y_\sigma(r)$. This function is continuous at $r = \sigma$, where σ is the diameter of the hard-sphere is equal to the hard-sphere radial function $g(r)$ for $r > \sigma$.

Simple liquids which are composed of spherical or nearly spherical molecules, the intermolecular structure of them are very similar to a fluid made up of the hard sphere. In a dense liquid, nearest neighbors are packed extremely close to one another. Any displacement of a particle will cause a large change in the energy associated with the inter-particle repulsions. These interactions are not quickly varying functions of the inter-particle separation. As a result, the high density structure is mainly occurs by the repulsive forces.

The diameter of the hard-sphere diameter is determined by the Blip function. This method is used to determine the effects of repulsive forces. The Blip function provides a good relationship between the equilibrium properties of the hard sphere fluid, and the properties of fluids with realistic repulsive forces. In accordance with the LWCA theory, the free energy of a system is expressed in terms of a functional Taylor expansion with a soft repulsive potential $v(r)$ and hard sphere repulsive potential $v_\sigma(r)$ related to the Blip function $B(r)$ given by,

$$B(r) = Y_\sigma\{\exp[-\beta v_\sigma(r)] - \exp[\beta v_\sigma(r)]\}. \tag{3.61}$$

The mathematical terms in equation (3.61) can be expressed

$$\beta = (k_B T)^{-1}, \tag{3.62}$$

and k_B is known as the Boltzmann constant.

By taking the Fourier transform of $B(r)$ we get,

$$B(k) = 4\pi \int_0^\infty B(r) r^2 \frac{\sin(kr)}{kr} dr. \tag{3.63}$$

Now the LWCA structure factor $S(k)$ is formulated as

$$S(k) = S_\sigma(k) + nB(k), \tag{3.64}$$

where $S_\sigma(k)$ is the hard-sphere structure factor. If we consider that

$$h(r) = g(r) - 1, \tag{3.65}$$

where $h(r)$ can be represented in terms of $h_\sigma(r)$, and $B(r)$ in terms of bond density expansion. From Jacobs and Anderson, we get that summing over all chain diagrams [4] in the expansion results in the following expression for the structure factor,

$$S(k) = \frac{S_\sigma(k)}{(1 - nS_\sigma(k)B(k))}, \tag{3.66}$$

which has the advantages of eliminating a spurious bump at $k \approx \frac{\pi}{\sigma}$ which appears when equation (3.66) is used. For this approximation, σ is chosen as such that $B(0) = 0$ which completes the description.

Now another function, $C(r) = r^2 B(r)$ always consists of two sharp teeth, so this is useful to approximate it by triangulation in the fashion indicated above.

Again, $C(r)$ has a short range, so $J_0 \equiv \frac{\sin(kr)}{kr}$ can be extended about $r = \sigma$.

So, equation (3.66) becomes,

$$B(k) = 4\pi \sum_0^\infty \frac{-1^n}{n+2} (k\sigma)^n J_0^n(k\sigma) \left(\sigma \frac{C_-}{K_-^{n=1}} - \sigma \frac{C_+}{K_+^{n=1}} \right). \tag{3.67}$$

From equation (3.67) we can therefore achieve,

$$\sigma C_- = \sigma^3 g_0 \exp[-\beta v(\sigma)], \tag{3.68}$$

$$\sigma C_+ = \sigma^3 g_0 (\exp[-\beta v(\sigma) - 1),$$

$$K_- = -\beta\sigma v(\sigma) + Y + 2,$$

and

$$K_+ = -\beta\sigma v(\sigma)\frac{\exp[-\beta v(\sigma)]}{\exp[-\beta v(\sigma)] - 1} + Y + 2. \tag{3.69}$$

Here, g_0 is the value of the hard sphere radial distribution function at $r = \sigma$, and

$$Y = \left[\frac{\partial \ln g_\sigma(r)}{\partial \ln r}\right]. \tag{3.70}$$

These equations are known with good precession for packing fraction, $\xi = \frac{1}{6}n\sigma^3$.

Any given system which is specified via $v(r)$, and β any choice of σ can be very easily summed and the convergence is fast. In fact the first term vanishes in equation (3.69), and the next step gives a good approximation of the series.

Now we need to attribute the thermodynamic condition in such a way that the hard-sphere diameter vanishes and this will lead to the transcendental equation to,

$$\beta v(\sigma) = \ln\left(\frac{-2\beta\sigma u_{ij}(r) + Y + 2}{-\beta\sigma u_{ij}(r) + Y + 2}\right). \tag{3.71}$$

Solving this equation, we have found the trivial solution for σ. The solution of this transcendental equation gives the hard-sphere diameter of a metal and it can be extended for liquid binary alloys. From the above equation, we get σ_{ij} when $i = j$ i.e. σ_{11} and σ_{22} for constituent metals of the alloys. By using the hard-sphere formulation we obtain σ_{ij} when $i \neq j$ as of the form of

$$\sigma_{12} = \frac{\sigma_{11} + \sigma_{22}}{2} = \sigma_{21}. \tag{3.72}$$

This will be the desirable hard-sphere diameter (equation (3.72)) for liquid binary alloys.

3.3.3 Partial Pair Correlation Function

The Pair Distribution Function (PDF) describes the probability of finding two atoms separated by a short-range distance in the materials. It can be applied to all kinds of amorphous and liquid material systems. Recently it has been applied to the quantitative study of disordered crystalline materials. It is important for two reasons:

(i). If we assume that the total potential energy is pairwise additive i.e.,

$$v(r) = \sum_{j>i} u(r_{ij}). \tag{3.73}$$

Then all thermodynamic quantities can be expressed in terms of the radial distribution functions.

(ii). The pairwise distribution function can be derived from the experiment of diffraction (i.e. X-ray, Neutron, and Electron diffraction) data. So, we can compare the theoretical diffraction with observed value.

The Ashcroft-Langreth (AL) partial structure factors S_{ij} are calculated in line with their original work [50]. In order to calculate the structure factors we need the concentration of two spheres in the alloy, the number of ions per unit volume and the effective hard-sphere diameter. These effective hard-sphere diameters are determined by using the Linearized Weeks-Chandler-Anderson theory [69–72].

3.3.4 The Ashcroft-Langreth (AL) Partial Structure Factor

Ashcroft-Langreth in their work [50] in 1967, proposed the following definition for the partial structure factor $S_{ij}(q)$,

$$S_{ij}(q) = (N_i N_j)^{-\frac{1}{2}} \left\langle \sum_{m=1}^{N_1} \sum_{n=1}^{N_2} \exp[-i\vec{q}.(\vec{r}_{mi} - \vec{r}_{nj})] \right\rangle - (N_i N_j)^{\frac{1}{2}} \delta_{k,\theta}. \tag{3.74}$$

The forward scattering term of the above definition is excluded. Combining equations we obtain an expression for the coherent intensity of a liquid binary alloy (excluding the forward scattering), which may be written as

$$\begin{aligned} I^{coh} &= N \sum_i \sum_j (c_i c_j)^{\frac{1}{2}} f_i(q) f_j(q) S_{ij} \\ &= N_1 f_1^2(q) S_{11}(q) + N_2 f_2^2(q) S_{22} + 2(N_1 N_2)^{\frac{1}{2}} f_1(q) f_2(q) S_{12}(q). \end{aligned} \tag{3.75}$$

We can define the scattering intensity per atom as,

$$I_\alpha^{coh} = \sum_i \sum_j (c_i c_j)^{\frac{1}{2}} f_1(q) f_2(q). \tag{3.76}$$

At large value of q, the atom independently scatter x-rays, and we get

$$\begin{aligned} I_\alpha^{coh} &= c_1 f_1^2(q) + c_2 f_2^2(q) \\ &= \langle f^2(q) \rangle. \end{aligned} \tag{3.77}$$

Using the relation $S_{ij} \longrightarrow \delta_{ij}$, we get the AL total structure factor $S_{AL}(q)$ as,

$$\begin{aligned} S_{AL}(q) &= \frac{I_\alpha^{coh}}{\langle f^2(q) \rangle} \\ &= \sum_i \sum_j (c_i c_j)^{\frac{1}{2}} \frac{f_i(q) f_j(q)}{\langle f^2(q) \rangle} S_{ij}(q). \end{aligned} \tag{3.78}$$

For a two component system in real space, the structure is given by the three partial pair distribution functions. We can introduce, the number density of j-type

atoms found at a radial distance r from an α-type atom at the origin. The formula states,

$$\begin{aligned}\rho_{ij}(r) &= c_j\rho_0 g_{ij}(\vec{r}) \\ &= N_i^{-1}\left\langle \sum_m \sum_n \delta[\vec{r} - (\vec{r}_{mi} - \vec{r}_{nj})] \right\rangle - \delta_{ij}\delta(\vec{r}).\end{aligned} \tag{3.79}$$

We have also used that

$$c_j\rho_{ji}(r) = c_i(r), \tag{3.80}$$

$$N_j\rho_{ij}(r) = N_i\rho_{ij}(r), \tag{3.81}$$

In equation (3.81), we have followed that $g_{ij}(r) = g_{ji}(r)$.

Since $\rho_{ij}(r)$ becomes equal to $\frac{N_j}{V} = c_j\rho_0$ at large value of r, then g_{ij} tends to unity. Using these properties we can rewrite ρ_{ij} as,

$$\rho_{ij}(\vec{r}) = c_j\rho_0\left[g_{ij}(\vec{r}) - 1\right] + c_j\rho_0. \tag{3.82}$$

So we get,

$$N_i^{-1}\left\langle \sum_j \sum_k \delta[\vec{r} - (\vec{r}_{ij} - \vec{r}_{jk})] \right\rangle - c_j\rho_0 = c_j\rho_0\left[g_{ij}(\vec{r}) - 1\right] + \delta_{ij}\delta(\vec{r}). \tag{3.83}$$

Taking the Fourier transform on both sides of equation (3.83) and multiplying by $(N_iN_j)^{-\frac{1}{2}}$ we obtain the relation as,

$$\begin{aligned}(N_iN_j)^{-\frac{1}{2}}\left\langle \sum_j \sum_k \delta[\vec{r} - (\vec{r}_{ij} - \vec{r}_{jk})] \right\rangle - (N_iN_j)^{-\frac{1}{2}}\delta_{Q0} = \\ (c_ic_j)^{\frac{1}{2}}\rho_0 \int \left[g_{ij}(\vec{r}) - 1\right]\exp(-i\vec{q}.\vec{r})d\vec{r} + (\frac{c_i}{c_j})^{\frac{1}{2}}\delta_{ij}.\end{aligned} \tag{3.84}$$

The left hand side of this equation corresponds to the partial structure factor. Thus we can obtain a relation between $S_{ij}(q)$ and g_{ij} such as,

$$S_{ij}(\vec{q}) = \delta_{ij}(\vec{r}) + (c_ic_j)^{\frac{1}{2}}\rho \int \left[g_ij(\vec{r}) - 1\right]\exp(-i\vec{q}.\vec{r})d\vec{r}. \tag{3.85}$$

Now, taking the inverse Fourier transformation to both sides of the above equation and after some further simplification we get,

$$g_{ij} = 1 + \frac{1}{(2\pi)^3\sqrt{c_i c_j}} \int \left(S_{ij} - \delta_{ij} \right) \exp(-i\vec{q}.\vec{r}) d\vec{r}. \tag{3.86}$$

This relation is therefore used to obtain the partial pair correlation in our concerned alloys.

3.4 Thermodynamic Properties for Liquid Binary System

In this section, I will discuss the Thermodynamic Properties namely the energy of mixing (ΔA), the enthalpy of mixing (ΔH), and the entropy of mixing (ΔS). The Free energy (A), the entropy (E) and the enthalpy (H) of a physical system are of great importance in the physical quantities to be clearly understood to predict different behaviors of matters such as segregation of alloys [3,53,54], the Materialistic phase transition in crystalline solids [2], the glass transition temperature [17,18], the nucleation effect [4] and the stability of liquid metals and their alloys at different thermodynamic state.

The study of energy of mixing (ΔA), the enthalpy of mixing (ΔH), and the entropy of mixing (ΔS) for liquid binary alloys are always a challenging task to do theoretically. The entropy is related directly to the derivative of the free energy with respect to the temperature but not directly to the full profile of the inter-ionic potentials as in the case of energy and enthalpy evaluation [5].

That means that, the success of the entropy calculations depends not on the free energy (A) and the value for enthalpy (H), but on the accuracy of the detailed shape of the free energy (A) and the enthalpy (H) profile as a function of temperature for the concerned system. So, the magnitude of the free energy (A) and enthalpy (H)

can be, sometimes, found to be good in agreement with experimental data [92], but the enthalpy of mixing (ΔH), and the entropy of mixing (ΔS) evaluated from the same approach is not found to be even qualitative in agreement.

Moreover, both the enthalpy of mixing (ΔH) and the entropy of mixing (ΔS) are of very small quantity relative to the total enthalpy (H) and entropy (S), so any small change in the free energy (A) profile may cause a very large discrepancy. We believe that, these are the root causes of not finding many works on this subject in the literature.

The energy of mixing (ΔA), enthalpy of mixing (ΔH) and entropy of mixing (ΔS) are not independent to each other, these are rather related by the following thermodynamic relation [4],

$$\Delta G = \Delta H - T\Delta S, \tag{3.87}$$

where ΔG denote the Gibbs free energy of mixing. We note that, at one atmospheric pressure (p), $\Delta G \simeq \Delta A$ and $\Delta H \simeq \Delta E$, where ΔA and ΔE are Helmholtz free energy of mixing and internal energy of mixing; and at zero pressure the above relations become exactly equal. Here, we are interested to study the structure of our concerned alloys. Among all of them, we are most anticipating to learn the behavior of hard-sphere diameter and the partial pair correlation function. These two are the basic building blocks of our calculation among with the thermodynamic perturbation theory.

3.4.1 Energy of Mixing for Liquid Binary Alloys

Within the first order perturbation theory, the Helmholtz free energy per ion for an alloy may be written, in general [4, 29, 66] as

$$A = A_{vol} + A_{eg} + A_{HS} + A_{Tail}, \tag{3.88}$$

where,

A_{vol} is the volume term;

A_{eg} is the electron gas term;

A_{HS} is the hard sphere (HS) term; and

A_{Tail} is the tail term of potential contributions, respectively.

So, the energy of formation without excess volume correction is expressed as

$$\begin{aligned} \Delta A &= A - \sum_i C_i A^{(i)} \\ &= \Delta A_{vol} + \Delta A_{HS} + \Delta A_{eg} + \Delta A_{Tail}, \end{aligned} \tag{3.89}$$

where, $A^{(i)}$ denotes the free energy of the elemental components. Finally, including the excess volume correction, the total free energy of formation can be written

$$\Delta A' = \Delta A + \Delta A_{EVC}. \tag{3.90}$$

Here, ΔA_{EVC} is excess volume correction.

Volume Dependent Contribution:

In this calculation, we consider local pseudopotential [4, 29, 66] instead of non-local pseudopotential. Now, the electron-ion interaction is written as,

$$
\begin{aligned}
U(N) &= NZu_{el} + \frac{N^2Z^2}{V}\frac{\beta(0)}{Z} \\
&\quad + \frac{1}{2}\sum_{q\neq 0}\frac{8\pi Z^2}{Vq^2}\sum_{i\neq j} e^{iq.(R_i-R_j)} \\
&\quad + \frac{1}{2}\sum_{q\neq 0}\frac{q^2}{8\pi V}\left\{\frac{1}{\varepsilon(0)} - 1\right\}|v_i(q)|^2\sum_{i,j} e^{iq.(R_i-R_j)}. \qquad (3.91)
\end{aligned}
$$

Here, u_{el} is the energy per electron-gas system; the second one is the diagonal term of the electron-ion interaction; the third one is the direct Coulomb interaction between the ions with effective valency, Z and last one is the second order term of the electron-ion interaction.

Here, $V_i(q)$ is the matrix elements of the electron-ion pseudopotential and $\beta(q)$ its non-coulomb part, then $V_i(q)$ is defined as,

$$
V_i(q) = -\frac{8\pi Z}{q^2} + \beta(q), \qquad (3.92)
$$

and $\varepsilon(q)$ is the dielectric function which is defined as

$$
\varepsilon(q) = 1 + \frac{8\pi}{q^2}P(q). \qquad (3.93)
$$

In equation (3.93), P(q) is the polarization and defined as $P = \chi_{el}/\chi_F$ which is taken from [76, 77]. Here, χ_{el}, and χ_F denote the isothermal compressibility of interacting, and non-interacting electrons, respectively.

From equation (3.93) we get,

$$
\begin{aligned}
U(V) &= NZu_{el} + \frac{N^2Z^2}{V}\frac{\beta(0)}{Z} \\
&\quad + \frac{N}{2}\sum_{q\neq 0}\frac{q^2}{8\pi V}\left\{\frac{1}{\varepsilon(q)} - 1\right\}|v_i(q)|^2 \\
&\quad - \frac{N(N-1)}{2V}\lim_{q\to 0}\left[\frac{8\pi Z^2}{q^2} + \frac{q^2}{8\pi}\left\{\frac{1}{\varepsilon(q)} - 1\right\}|v_i(q)|^2\right] \\
&\quad + \frac{1}{2}\left[\frac{8\pi Z^2}{q^2} + \frac{q^2}{8\pi}\left\{\frac{1}{\varepsilon(q)} - 1\right\}|v_i(q)|^2\right]\sum_{i\neq j} e^{iq.(R_i - R_j)}. \qquad (3.94)
\end{aligned}
$$

Hence, the first and the last terms are electron gas term and structure term respectively. The volume terms are rest of terms. So, for the volume term, we can write,

$$
\begin{aligned}
U(V) &= \frac{N^2Z^2}{V}\frac{\beta(0)}{Z} \\
&\quad + \frac{N}{2}\sum_{q\neq 0}\frac{q^2}{8\pi V}\left\{\frac{1}{\varepsilon(q)} - 1\right\}|v_i(q)|^2 \\
&\quad - \frac{N(N-1)}{2V}\lim_{q\to 0}\left[\frac{8\pi Z^2}{q^2} + \frac{q^2}{8\pi}\left\{\frac{1}{\varepsilon(q)} - 1\right\}|v_i(q)|^2\right] \\
&\simeq \frac{N^2Z^2}{V}\frac{\beta(0)}{Z} + \frac{N}{2}\frac{V}{(2\pi)^3}\int\frac{q^2}{8\pi V}\left\{\frac{1}{\varepsilon(q)} - 1\right\}|v_i(q)|^2 d^3q \\
&\quad - \frac{N(N-1)}{2V}\lim_{q\to 0}\left[\frac{8\pi Z^2}{q^2} + \frac{q^2}{8\pi}\{\frac{1}{\varepsilon(q)} - 1\}|v_i(q)|^2\right] \\
&= \frac{N^2Z^2}{V}\frac{\beta(0)}{Z} + \frac{N}{16\pi}\frac{V}{(2\pi)^3}\int_{\phi=0}^{2\pi}\int_{\theta=0}^{\pi}\int_{q=0}^{\infty}\frac{q^2}{V}\{\frac{1}{\varepsilon(q)} - 1\}|v_i(q)|^2 dq\sin\theta d\theta d\phi \\
&\quad - \frac{N^2}{2V}\lim_{q\to 0}[\frac{8\pi Z^2}{q^2} + \frac{q^2}{8\pi}\{\frac{1}{\varepsilon(q)} - 1\}|v_i(q)|^2]. \qquad (3.95)
\end{aligned}
$$

So, the energy per ion is

$$\begin{aligned}\frac{U(V)}{N} &= \frac{NZ^2}{V}\frac{\beta(0)}{Z} \\ &\quad +\frac{1}{32\pi^3}\int q^4\{\frac{1}{\varepsilon(q)}-1\}|v_i(q)|^2dq \\ &\quad -\frac{N}{2V}\lim_{q\to 0}[\frac{8\pi Z^2}{q^2}+\frac{q^2}{8\pi}\{\frac{1}{\varepsilon(q)}-1\}|v_i(q)|^2] \\ &= \rho Z\beta(0)+\frac{1}{32\pi^3}\int_{q=0}^{\infty} q^4\{\frac{1}{\varepsilon(q)}-1\}|v_i(q)|^2dq \\ &\quad -\frac{\rho}{2}\lim_{q\to 0}[\frac{8\pi Z^2}{q^2}+\frac{q^2}{8\pi}\{\frac{1}{\varepsilon(q)}-1\}|v_i(q)|^2]. \qquad (3.96)\end{aligned}$$

Taking the values from equation (3.97) and (3.98), respectively we can write,

$$\lim_{q\to 0}\left[\frac{8\pi Z^2}{q^2}+\frac{q^2}{8\pi}\{\frac{1}{\varepsilon(q)}-1\}|v_i(q)|^2\right] = 2Z\beta(0)+\frac{Z^2}{P(0)}. \qquad (3.97)$$

Putting this value in equation (3.97), we get,

$$A_{vol} = \frac{U(V)}{N}\frac{1}{32\pi^3}\int_{q=0}^{\infty} q^4\{\frac{1}{\varepsilon(q)}-1\}|v_i(q)|^2dq-\frac{\rho Z^2}{2P(0)}. \qquad (3.98)$$

In [4, 29, 57], this value is taken as,

$$A_{vol} = \frac{1}{32\pi^3}\int_{q=0}^{\infty} q^4\{\frac{1}{\varepsilon(q)}-1\}|v_i(q)|^2dq-\frac{ZE_F}{3P}. \qquad (3.99)$$

Here, E_F is the Fermi energy for electrons.

Electron Gas Contribution:

Electron gas term contribution is treated from the Hartree-Fock perturbation [4, 29] approximation for jellium. Jellium is just a collection of electrons, into which ions

are introduced a spatially uniform back ground to maintain overall charge neutrality. Let us consider that, the wave functions of electron in jellium may be presented by plane waves. For N-electrons in a volume, V they are expressed as,

$$\begin{aligned} E_l\Phi_l(\vec{r}) &= -\left[\frac{\hbar^2}{2m}\nabla^2\right]\Phi_l(\vec{r}) - \Phi_l(\vec{r})\left(\frac{N}{V}\right)\int d\vec{r}_2\frac{e^2}{|\vec{r}-\vec{r}_2|} \\ &\quad +\Phi_l(\vec{r})\int d\vec{r}_2\sum_{j=1}^{N} e^2\frac{|\Phi_j(\vec{r})|^2}{|\vec{r}-\vec{r}_j|} \\ &\quad -\delta x_i x_j\sum_{j=1}^{N}\Phi_l(\vec{r})\int d\vec{r}_2\frac{e^2\Phi_j^*(\vec{r})\Phi_l(\vec{r}_2)}{|\vec{r}-\vec{r}_2|}. \end{aligned} \tag{3.100}$$

Total energy

= Kinetic energy + Interaction with ions + Coulomb interaction among electrons + Exchange interaction.

Let us consider, that the normalized plane wave,

$$\Phi_l(\vec{r}) = \frac{e^{i\vec{k}_l.\vec{r}}}{V^{1/2}}. \tag{3.101}$$

In equation (3.100), the kinetic energy term is,

$$-[\frac{\hbar^2}{2m}\nabla^2]\frac{e^{i\vec{k}_l.\vec{r}}}{V^{1/2}} = [\frac{\hbar^2k^2}{2m}]\Phi_l(\vec{r}). \tag{3.102}$$

Since, $|\Phi_j|^2 = \frac{1}{V}$. The interaction with ions, and the Coulomb interaction among electrons cancel each other. So, the exchange interaction is,

$$\begin{aligned} e^2\sum_{j=1}^{N}\frac{e^{i\vec{k}_j.\vec{r}}}{V^{1/2}}\int\frac{d^3\vec{r}_2}{V}\frac{e^{i(\vec{k}_l-\vec{k}_j).\vec{r}_2}}{|\vec{r}-\vec{r}_2|}\delta x_i x_j &= e^2\frac{e^{i\vec{k}_l.\vec{r}}}{V^{1/2}}\sum_{j=1}^{N}\int\frac{d^3\vec{r'}}{V}\frac{e^{-i(\vec{k}_l-\vec{k}_j).\vec{r'}}}{\vec{r'}}\delta x_i x_j \\ &= e^2\Phi_l(\vec{r})\sum_{j=1}^{N}\frac{1}{V}\frac{4\pi}{|k_l-k_j|^2}\delta x_i x_j. \end{aligned} \tag{3.103}$$

Let us consider a ground state. So, states are occupied up-to the Fermi level [4], and the inter-level spacing is very small. Therefore, we can approximate the summation on integration,

$$\sum_k \to \frac{V}{(2\pi)^3}\int_0^{k_F} d^3k.$$

Therefore,

$$\begin{aligned} e^2\Phi_l(\vec{r})\int_0^{k_F}\frac{d^3k}{2\pi_3}\frac{4\pi}{|k_l-k_j|^2}\delta x_i x_j &= \frac{e^2\Phi_l(\vec{r})}{(2\pi)^3}\int_0^{k_F}k^2dk\int_{\theta=0}^{\Pi}\frac{\sin\theta d\theta}{k_l^2+k^2-2kk_l\cos\theta}\int_{\phi=0}^{2\pi}d\phi \\ &= \frac{e^2\Phi_l(\vec{r})}{\pi}\int_0^{k_F}\frac{k^2dk}{2kk_l}\ln\frac{|k+k_l|}{|k-k_l|} \\ &= \frac{e^2\Phi_l(\vec{r})}{\pi}\frac{1}{2k_l}[(k_F^2-k_l^2)\ln(\frac{k_F+k_l}{k_F-k_l})+2k_lk_F] \\ &= \frac{2e^2\Phi_l(\vec{r})}{\pi}k_FF(k_l/k_F). \end{aligned} \tag{3.104}$$

Here, the Linhard dielectric function,

$$\begin{aligned} F(x) &= \frac{1}{2}+\frac{1-x^2}{4x}\ln\frac{1+x}{1-x}, \\ x &= \frac{k_l}{k_F}. \end{aligned}$$

So, the energy of state l is,

$$E_l = \frac{\hbar^2k_l^2}{2m}-\frac{2e^2}{\pi}k_FF(\frac{k_l}{k_F}). \tag{3.105}$$

Thus the total energy,

$$\begin{aligned} E &= \sum_l[\frac{\hbar^2k_l^2}{2m}-\frac{e^2}{\pi}k_FF(\frac{k_l}{k_F})] \\ &= N\left[\frac{3}{5}E_F-\frac{3}{4}\frac{e^2}{\pi}k_F\right]. \end{aligned} \tag{3.106}$$

The free energy per electron can be written

$$\begin{aligned} \frac{E}{N} &= [\frac{2.21}{(r_s/a_0)^2} - \frac{0.916}{(r_s/a_0)}]\text{Rydberg's} \\ or, \frac{E}{Z} &= [\frac{2.21}{{r_s}^2} - \frac{0.916}{r_s}]\text{Rydberg's.} \end{aligned} \tag{3.107}$$

Here, r_s is the dimensionless parameter and can be defined as,

$$r_s = (\frac{3}{4\pi\rho Z})^{\frac{1}{3}}/a_0, \tag{3.108}$$

where a_0 is the first Bohr radius, and the ionic number density,

$$\rho = \frac{\rho_1\rho_2}{(C_1\rho_2 + C_2\rho_1)}. \tag{3.109}$$

Correction term is,

$$\frac{E_{corr}}{Z} = [0.031 \ln r_s - 0.115]\text{Rydberg's.} \tag{3.110}$$

So, the total free energy per electron is,

$$\frac{A_{eg}}{Z} = \frac{E}{Z} + \frac{E_{corr}}{Z}. \tag{3.111}$$

Including, the correction term, it may be written as [45],

$$\frac{A_{eg}}{Z} = \left[\frac{2.21}{{r_s}^2} - \frac{0.916}{r_s} + 0.031 \ln r_s - 0.115\right] \text{Rydberg's.} \tag{3.112}$$

Hard Sphere Contribution:

The hard sphere model for liquid metal, where hard sphere is taken as the reference system for the calculation of structure and thermodynamic properties was proposed by N.W. Ashcroft and J. Lekner [4, 50].

In the hard sphere model, potential is given by,

$$u(R) = \begin{cases} \infty; & \text{if } R < \sigma, \\ 0; & \text{if } R > \sigma. \end{cases} \tag{3.113}$$

In equation (3.113), σ is the hard sphere diameter. Free energy per atom of the reference HS liquid (using C_1 = x and C_2 =1-x) [4, 57] is

$$\begin{aligned} \frac{A_{HS}}{k_B T} &= \sum_i \left[-\ln(\Lambda_i^3 v) + \ln C_i \right] - \frac{3}{2}\left(\frac{5}{3} - y_1 + y_2 + y_3\right) \\ &+ \frac{(3y_2 - 2y_3)}{(1-\eta)} + \frac{3}{2}\frac{(1 - y_1 + y_2 + \frac{y_3}{3})}{(1-\eta)^2} + (y_3 - 1)\ln(1-\eta); \end{aligned} \tag{3.114}$$

From equation (3.114) we can express the individual terms [4] in such a way given below,

$$\Lambda_i = (\frac{2\pi\hbar^2}{{m_1}^{C_1}{m_2}^{C_2} k_B T})^{\frac{1}{2}}, \tag{3.115}$$

m_i is the Ionic mass, and

Packing fraction is,

$$\eta = \sum_i \eta_i; \tag{3.116}$$

$$\eta_i = \frac{C_i \pi \rho_i \sigma_{ii}^3}{6}. \tag{3.117}$$

In equation (3.117) C_i is the atomic concentration of i'th component. From equation (3.114)

$$y_1 = \sum_{j>i} \Delta_{ij}(\sigma_{ii} + \sigma_{jj})/(\sigma_{ii}\sigma_{jj})^{\frac{1}{2}} \tag{3.118}$$

where σ_{ii}, and σ_{jj} are the additive hard sphere diameter (HSD)

$$y_2 = \sum_{j>i} \Delta_{ij} \sum_k (\frac{\eta_k}{\eta})^{\frac{1}{2}} / \sigma_{kk}, \tag{3.119}$$

$$y_3 = [\sum_i (\frac{\eta_i}{\eta})^{\frac{2}{3}} C_i^{\frac{1}{3}}]^3, \tag{3.120}$$

and

$$\Delta_{ij} = [(\eta_i \eta_j)^{\frac{1}{2}} / \eta][(\sigma_{ii} - \sigma_{jj})^2 / \sigma_{ii}\sigma_{jj}](C_i C_j)^{\frac{1}{2}}. \tag{3.121}$$

Tail Potential Contribution:

The contribution of tail part is written in the form given below

$$A_{Tail} = D \sum_{ij} C_i C_j M_{ij}. \tag{3.122}$$

In equation (3.122), C_i, and C_j are the atomic concentrations for i^{th}, and j^{th} components, respectively and

$$D = 2\pi\rho. \tag{3.123}$$

Here, ρ is the ionic number density, and

$$M_{ij} = \int_\sigma^\infty v_{ij}(r) g_{ij}^{HS}(r, \sigma_{ij}, \rho) r^2 dr, \tag{3.124}$$

where v_{ij}(r), and g_{ij}(r) are partial pair potential, and correlation functions, respectively.

3.4.2 Enthalpy of Mixing for Liquid Binary Alloys

A thermodynamic state can be specified by fixing the set of independent thermodynamic variables. A single homogeneous substance has two degrees of freedom with a wide possible choice of pairs for independent variables. For condensed

material [4, 57], it is experimentally convenient to define the temperature, (T), and pressure, (p). The relation between temperature (T), and pressure (p) can be related in terms of enthalpy (H) is

$$H = U + pV. \tag{3.125}$$

Here, U is the internal energy of the system. According to the canonical ensemble theory, we can also relate the enthalpy (H) relation with temperature (T) and pressure (p) as,

$$\begin{aligned} H &= \frac{3}{2}Nk_BT + Nu_g + \frac{N}{2}n\int g_0^{(2)}(R)u(R)d^3R \\ &\quad +pV. \end{aligned} \tag{3.126}$$

In equation (3.126), k_B is the Boltzmann constant, and $g_0^{(2)}$ is the pair distribution function.

The Enthalpy of mixing (ΔH) for liquid binary alloys can be written as in general [4, 45],

$$\Delta H = \Delta H_{vol} + \Delta H_{eg} + \Delta H_{Tail}. \tag{3.127}$$

3.4.3 Entropy of Mixing for Liquid Binary Alloys

After finding the energy of mixing, (ΔA), and the enthalpy of mixing, (ΔH), we can easily get the entropy of mixing (ΔS) for liquid binary alloys at different thermodynamic state using the equation (3.125) after applying some conditions.

$$T\Delta S = \Delta H - \Delta A$$

$$or, \Delta S = \frac{\Delta H - \Delta A}{T} \tag{3.128}$$

3.5 Atomic Transport Theory for Liquid Binary System

Transport properties of condensed matters have been a subject of interest [4] to the metallurgies and physicists from the long past to the present day. Transport properties can be classified into two parts. Firstly, the atomic transport property, and secondly, the electron transport property. In this section, we will discuss the relevant theories involved for studying the transport properties.

We will also discuss, the theories for elemental system study of transport properties at the end of this chapter.

3.5.1 Atomic Transport Property

The concept of Atomic Transport theory is described by the Statistical Mechanics. According to the statistical mechanical theory [4] of atomic or molecular transport properties of simple liquids, it is possible to calculate transport coefficient from the knowledge of atomic or molecular properties, such as mass, and pair potentials and the equation of motion only. The time correlation function and the memory function is used to study the self-diffusion process in liquid metals, which is calculated from the Hard-sphere diameter and the pair-potentials.

The microscopic expression for the hydrodynamic equation of liquids are taken into account, and the time evolution of distribution functions appearing in those

expressions is considered from the point of view of kinetic theories developed by Kirkwood [59], Born and Green [4], Rice and Allnatt [59–64], and others. The viscosity of liquid metals can be achieved using these atomic properties.

The most important forms of atomic transport properties are Viscosity, Thermal conductivity, Electrical conductivity and Diffusion coefficient. The understanding of these properties for liquid metals can be done using the neutron inelastic scattering measurements. Such experiment allows us to determine a scattering law of dynamic structure factor, S(q, ω) which is the Fourier Transformation of the space-time correlation function of Van Hoove G(r,t). The shear viscosity of liquid metals is also calculated using a moment method. Diffusion and Viscous coefficients of liquid alloys are discussed from the same point of view as for pure liquid metals.

3.5.2 Shear Viscosity for Liquid

The transport properties of a liquid, as it is explained by the statistical mechanical equation, we need to determine reduced distribution function. The equation of singlet distribution functions f_1 is

$$\frac{\delta f_1}{\delta t} - \frac{p_1}{M}\nabla_1 f_1 = \Omega_H^1 + \Omega_S^1. \tag{3.129}$$

Here,

$$\Omega_H^1 = -\int \vec{F}_{H,12}\nabla_p f^2 d^3R_2 d^3p_2 \tag{3.130}$$

$$\Omega_S^1 = -\int \vec{F}_{S,12}\nabla_p f^2 d^3R_2 d^3p_2 \tag{3.131}$$

Similar equation can be written for f^2. By solving these equations, we can get both f^1 and f^2.

Substituting the solution of f^1 into equation (3.130) and comparing the equations for f^1 and f^2 one obtains a relation for the kinetic part of the shear viscosity,

$$\sigma_k(R,t) = -M^{-1}\int (P-M)(P-Mu)f^1(R,p), \tag{3.132}$$

and

$$\sigma_v(R,t) = \frac{1}{2}\int \frac{R_0 R}{R}\frac{\delta u(R)}{\delta(R)} f^2(R, R+R_0, P^1, P^2; t) d^3R d^3P_1 d^3P_2. \tag{3.133}$$

Hence we get,

$$\eta_k = \frac{5K_BT}{8g(\sigma)}\frac{1+\frac{4\pi\sigma^3 g(\sigma)}{15v}}{\Omega+\frac{5\zeta_s v}{4Mg(\sigma)}}. \tag{3.134}$$

Using the solution of f^2, Rice & Allant [59–64] found,

$$\eta_v(\sigma) = \eta_v^1 + \eta_v^2(\sigma). \tag{3.135}$$

Here

$$\eta_v^1(\sigma) = \frac{5K_BT}{8g(\sigma)}(\frac{2\pi n\sigma^3}{15})[1+\frac{4\pi n\sigma^3}{15}g(\sigma)]D_\sigma, \tag{3.136}$$

and

$$\eta_v^2 = \frac{8\pi}{15}\frac{n^2\sigma^6 g(\sigma) K_BT}{\Omega}. \tag{3.137}$$

Besides, from equation (3.137)

$$D_\sigma = \left[\Omega + \frac{5\zeta_s}{8Mg(\sigma)}\right]^{-1}\left[1+\frac{4\Omega_0}{\Omega}+\frac{5\zeta_s}{nMg(\sigma)}\right], \tag{3.138}$$

and

$$\Omega = \left(\frac{4\pi K_BT}{M}\right)^{\frac{1}{2}}. \tag{3.139}$$

The contribution of the shear viscosity from the region $R > \sigma$ is obtained by replacing R as r and using small step theory expansion of f^2. According to Rice and Kirkwood [59],

$$\eta_v(r > \sigma) = \frac{4\pi M n^2}{30\zeta_s} \int_0^\infty r^4 \left(\frac{\partial^2 u}{\partial r^2} + \frac{4\partial u}{r\partial r} \right) g(r) dr. \tag{3.140}$$

Thus The total viscosity is

$$\eta = \eta_k + \eta_v(\sigma) + \eta_v(r > \sigma). \tag{3.141}$$

Shear Viscosity for Alloys:

The theory developed for pure metals can be extended for liquid alloys. The starting point of Rice-Allnatt [59–64] theory for atomic transport properties of a fluid, is the general Statistical Mechanical theory of heat flux and Stress Tensor. Considering, the inter-ionic interactions as the pairwise additive, the pair potential is separated into hard and soft parts.

The interaction between the hard cores are treated by the theory of dense rigid sphere [81] fluid, while the soft interaction are handled following Kirkwood, in the Fokker-Plank approximation [80]. Finally, the shear viscosity coefficient appears as a sum of three different contributions (a) the kinetic energy contribution η_k , (b) the hard core interaction contribution, $\eta_v(\sigma)$ and (c) the soft interaction contribution $\eta_v(r > \sigma)$. Symbolically,

$$\eta = \eta_k + \eta_v(\sigma) + \eta_v(r > \sigma). \tag{3.142}$$

where σ denotes the hard sphere diameter. It is worth for noting that, Rice and Allnatt [59–64] originally developed the theory for single component systems. This

theory can be extended to the liquid binary alloys in a straightforward way by [69–72]. Different terms for the alloys can be represented by

$$\eta_k = \sum_i \sum_j \frac{5K_BT}{8g_{0ij}^{HS}(\sigma_{ij})} \frac{1 + 4\pi\rho_j g_{ij}(\sigma_{ij})\sigma_{ij}^3/15}{(4\pi K_BT/M_i)^{\frac{1}{2}}\sigma_{ij}^2 + [5\zeta_{Si}/4M_i\rho_i g_{0ij}^2(\sigma_{ij})]}, \tag{3.143}$$

and

$$\eta_v(\sigma) = \sum_i \sum_j \left[\frac{5K_BT}{36} \frac{M_{ij}\rho_j}{M_i\rho_i} \frac{12\pi\sigma_{ij}^3\rho_j/(5g_{0ij}^{HS}(\sigma_{ij}) + (4\pi\sigma_{ij}^3\rho_i/5)^2)}{(4\pi K_BT/M_i)^{\frac{1}{2}}\sigma_{ij}^2 + (5\zeta_{Si}/4M_i\rho_i g_{0ij}^{HS}(\sigma_{ij}))} \right. \tag{3.144}$$

$$\left. + \frac{8\pi K_BT\rho_i\rho_j\sigma_{ij}^3 g_{0ij}\sigma_{ij}}{15(4piK_BT/M_i)^{\frac{1}{2}}\sigma_{ij}^2} \right].$$

Equation (3.145) can be separated into 4 parts such as,

$$\eta_v(\sigma) = \eta_{11}^H + \eta_{22}^H + \eta_{12}^H + \eta_{21}^H. \tag{3.145}$$

As for the contribution outside the core radius, we get,

$$\eta_v(r > \sigma) = \sum_i \sum_j \frac{M_{ij}}{30} \left(\frac{1}{\zeta_i^S} + \frac{1}{\zeta_j^S} \right) X_{ij}(r) = \eta_{11}^S + \eta_{22}^S + \eta_{12}^S + \eta_{21}^S. \tag{3.146}$$

In equation (3.146) the term integrand X_{ij}(r) can be written as,

$$X_{ij}(r) = \rho_i\rho_j \int_{r>\sigma_{ij}}^{\infty} \left(r^2 \frac{d^2u_{ij}}{dr^2} + 4r\frac{du_{ij}}{dr} \right) g_{0ij}^{HS}(r) d^3r, \tag{3.147}$$

and

$$\zeta_i^S = n_i\zeta_{ii}^S + n_j\zeta_{ij}^S. \tag{3.148}$$

Another fact from equation (3.148),

$$\zeta_{ij}^S = \left(\frac{1}{\zeta_i} + \frac{1}{\zeta_j} \right) C_{ij}, \tag{3.149}$$

and

$$C_{ij} = \frac{M_{ij}}{3} \int (v'' + \frac{2}{r} v') r^2 g_{ij}(r) dr. \tag{3.150}$$

In the above equation, single and double prime over $v(r)$ denote the first and the second derivative, respectively, with respect to r. Now solving (3.150), we get

$$\zeta_1 = \left[\frac{A + B + FB}{2F} + \frac{1}{2F} [(A + D + FB)^2 - 4FBD]^{\frac{1}{2}} \right]^{\frac{1}{2}}, \tag{3.151}$$

and

$$\zeta_2 = \left[\frac{\zeta_1}{n_2 C_1} - \frac{2 n_1 C_{11}}{\zeta_1 n_2 C_)1} - \frac{1}{\zeta_1} \right]^{-1}. \tag{3.152}$$

In equation (3.151), the constant terms can be expressed like below,

$$A = C_{12}^2 n^2, \tag{3.153}$$

$$B = n_1 C_{11} + n_2 C_{12}, \tag{3.154}$$

$$D = 2 n_1^2 C_{11} C_{12} + 4 n_1 n_2 C_{11} C_{22} + 2 n_2^2 C_{12} C_{22}, \tag{3.155}$$

and

$$F = n_1 C_{12} + 2 n_2 C_{22}. \tag{3.156}$$

3.5.3 Diffusion Coefficient for Liquid

The Einstein Relation for Diffusion:

The probability that a particle starting at some position at the initial time t_0 of any liquid will make a displacement ΔR after $\tau = t - t_0$ is governed by the self-diffusion

in mono-atomic liquids. Such a probability satisfy the Ficks law:

$$\frac{\delta G_s}{\delta t} = D\nabla_R^2 G_s. \tag{3.157}$$

Here, D is the self-diffusion coefficient, ∇_R^2 is the Laplace operator. If the origin is considered the initial position of the particle, then we obtain from equation (3.158) that

$$G_s(\vec{R}, t_0) = \delta(\Delta\vec{R}, t_0), \tag{3.158}$$

where $\delta(\Delta\vec{R}, t_0)$ is the delta function. Solution of the equation (3.158) is in the Gaussian form,

$$G_s(\vec{R}, \tau) = (4\pi D_\tau)^{\frac{3}{2}} \exp(-\frac{\Delta\vec{R}}{4D_\tau}). \tag{3.159}$$

There the mean-square value of $\Delta\vec{R}$ is given by,

$$\left\langle (\Delta\vec{R})^2 \right\rangle = \int (\Delta\vec{R})^2 G_s(\vec{R}.\tau) d^3(\Delta\vec{R}) = 6D\tau. \tag{3.160}$$

So the self-diffusion coefficient D is,

$$\lim_{\tau\to 0} \frac{\left\langle (\Delta\vec{R})^2 \right\rangle}{6\tau} = D. \tag{3.161}$$

This expression for D can be rewritten in terms of time correlation function. If $v(t)$ is the velocity of the particle of interest at time t, then,

$$(\Delta\vec{R})(\tau) = \int_0^\tau \vec{v}dt, \tag{3.162}$$

and

$$(\Delta\vec{R})^2 = \int_0^\tau dt' \int_0^\tau dt''\vec{v}(t')\vec{v}(t''). \tag{3.163}$$

The ensemble average $\left\langle (\Delta\vec{R}(\tau))^2 \right\rangle$ is

$$\left\langle (\Delta\vec{R})^2 \right\rangle = \int_0^\tau dt' \int_0^\tau dt'' \left\langle \vec{v}(t')\vec{v}(t'') \right\rangle, \tag{3.164}$$

where $\langle \vec{v}(t')\vec{v}(t'') \rangle$ is the velocity correlation function. Now,

$$\langle \vec{v}(t')\vec{v}(t'') \rangle = \langle \vec{v}(0)\vec{v}(t''-t') \rangle . \tag{3.165}$$

By putting $t = t'' - t'$ and integrating by parts we get,

$$\left\langle (\Delta\vec{R}(\tau))^2 \right\rangle = \int_0^\tau dt(\tau - t) \left\langle \vec{v}(0)\vec{v}(t) \right\rangle . \tag{3.166}$$

Substituting this into the equation of self-diffusion coefficient D, we obtain

$$\frac{1}{3}\lim_{\tau\to 0}\int_0^\tau dt(1-\frac{t}{\tau}) \left\langle \vec{v}(0)\vec{v}(t) \right\rangle = D. \tag{3.167}$$

Since the correlation function tends to be zero in some short interval, the term $\frac{t}{\tau}$ can be ignored. Then,

$$D = \frac{1}{3}\int_0^\infty \left\langle \vec{v}(0)\vec{v}(t) \right\rangle . \tag{3.168}$$

Using the normalized correlation function $\langle \vec{v}(0)\vec{v}(t) \rangle / \left\langle v(0)^2 \right\rangle$, and considering the random collision gives us a solution of the classical Langevin equation (for Brownian

motion) of the following form

$$\langle \vec{v}(0)\vec{v}(t)\rangle = \left\langle v(0)^2 \right\rangle e^{\xi t/m}. \tag{3.169}$$

In equation (3.169), ξ is the friction coefficient. Using the average kinetic energy $\frac{1}{2}m\left\langle |v|^2 \right\rangle = \frac{3}{2}k_BT$ and substituting this in eqn. (3.169) we can find the Einstein relations,

$$D = \frac{k_BT}{\xi}. \tag{3.170}$$

Diffusion Coefficient for Alloys:

If the inter-ionic pair potential is conveniently divided into a hard and soft part $u(r) = u(r)^H + u(r)^S$, the memory function for hard sphere collision leads to

$$\xi_H = \frac{8}{3}\rho\sigma^2(\pi m k_BT)^{\frac{1}{2}}g_0^2(r), \tag{3.171}$$

where σ is the hard sphere diameter, ρ is the ionic number density, m is the mass of the atom and k_B is the Boltzmann constant. The probability function of changing inter-atomic distance between two atoms decays exponentially with time leads

$$\xi_S = \frac{1}{3}m\rho\int_{r>\sigma}\nabla_r^2 u_S(r)g_0^2(r)d^3r. \tag{3.172}$$

The extension to the liquid binary alloys thus become,

$$\xi_i^H = \frac{8}{3}\sum_{j=1}^{2}\rho_j g_{ij}(\sigma_{ij})\sigma_{ij}^2(2\pi m_{ij}KT)^2. \tag{3.173}$$

Here,

$$m_{ij} = \frac{m_i m_j}{m_i + m_j}, \tag{3.174}$$

and

$$\xi_i^S = \rho_i \xi_{ij}^S + \rho_2 \xi_{ij}^S. \tag{3.175}$$

In those formula mentioned earlier can be written,

$$\xi_{ij}^S = \left(\frac{1}{\xi_i^S} + \frac{1}{\xi_j^S} \right) C_{ij}, \tag{3.176}$$

and

$$C_{ij} = \frac{m_{ij}}{3} \int (v_{ij}'' + \frac{2}{r} v_{ij}') r^2 g_{ij} dr. \tag{3.177}$$

Here, v_{ij} denotes the partial inter-ionic pair potentials, single and double prime represent the first and second order derivatives respectively. Therefore, the Diffusion Coefficient of its component in the case of liquid binary alloys reads,

$$D_i = \frac{KT}{\xi_i^H + \xi_i^S}. \tag{3.178}$$

3.6 Electron Transport Theory for Liquid Binary System

We shall first describe the physical principles of Ziman's [9, 15, 65, 67, 68] formula for the electron transport to real liquid metals. Ziman's theory is based on the Nearly Free Electron (NFE) [4] model, predicting reasonable values for the resistivity of liquid metals by the use of adequate pseudopotentials and accurate structure factors. Some corrections proposed for this formula are described which are important for transition or noble liquid metals. Ziman's formula can straightforwardly be extended to liquid alloys, as performed by Faber and Ziman [83] which can formally be employed in resistivity calculation even for liquid metals with strong ionic potentials such as noble metals, transition metals by using pseudopotentials. The concentra-

tion dependence of the resistivity of various liquid alloys is discussed in terms of this formalism.

Weak Scattering Theory of Electrical Resistivity:

The idea behind weak scattering theory is to represent the total potential energy $V(r)$ scattering the conduction electron by a sum of screen potential $v(r)$ at the ionic sites R_i, where one has taken a snapshot of the ion at a particular time,

$$V(r) = \sum_i v(|r - R_i|). \tag{3.179}$$

One can evaluate this force-force correlation function to second order in V by replacing the energy derivative σ of the density matrix by its free electron value. The density matrix ρ for free electrons is readily calculated for plane waves

$$\rho_0(r_1 r_2) = \sum_{|k|<k_F} \gamma^{-1} exp(ik.r_1 - r_2). \tag{3.180}$$

Replacing the summation of K by an integration with the usual constant density of states in K space as

$$\rho_0(r_1 r_2) = \frac{K_F^2}{\pi^2} \frac{j_1(K_F|r_1 - r_2|)}{|r_1 - r_2|}. \tag{3.181}$$

The energy derivative follows by using K_F=$(2E)^{1/2}$. The resistivity ρ is then found by using this result for σ_0; clearly, as only pairs of sites R_i are now corrected, taking the liquid average one obtains a result in terms of the structure factor $S(k)$ and the Fourier transform of the localized $\bar{v}(k)$. The result, when one puts back all the numerical factors, is for weak scattering with a sharp Fermi surface of diameter $2K_F$,

$$\rho = \frac{3\pi}{he^2 v_F^2 \rho_i} \frac{1}{(2k_F)^4} \int_0^{3k_F} S(k)|\bar{v}(k)^2|4k^3 dk. \tag{3.182}$$

This is the basic formula for the electrical resistivity of simple (s-p) nearly metals, ρ_l is the ionic number density, and since S(k) is measurable by diffraction experiments, the only quantity needed to determine ρ is the Fourier transform of the localized atomic-like screened potential energy $\bar{v}(k)$. Some discussion of the way approximations may set up for this quantity has already been given.

It also relevant to note here that real liquid metals have blurred Fermi surface, in accord with the Heisenberg uncertainty principle. The week scattering formula is not self-consistent in the sense that on the right-hand side the integration is out to the Fermi sphere diameter $2k_F$, which clearly implies a perfectly sharp Fermi surface, whereas on the left-hand side, there is a finite electrical resistivity; this, in turn, implies a finite mean free path through the elementary formula,

$$\rho = \frac{hk_f}{ne^2 l}. \tag{3.183}$$

Ferraz and March (1969) make the assumption that the free electron density matrix $\sigma(|r_1 - r_2|)$ can be modified to take into account of Fermi surface blurring by writing

$$\sigma(r_1 r_2) = \sigma_0(|r_1 - r_2|) \exp\left(\frac{-|r_1 - r_2|}{2l}\right). \tag{3.184}$$

the arguments leading to a damping of the off-diagonal matrix being quite analogous to those used to derive the probability of a mean free path of a given length l in classical kinetic theory. These arguments were first applied quantum mechanically be Bardeen (1956), who did not, however, derive a liquid a metal transport theory. The result of electrical resistivity obtained by Ferraz and March [67, 68],

$$\rho = \frac{hk_F}{ne^2 l} = \int_0^{\infty} K^4 S(k)|\bar{v}(k)^2|\Gamma(k, k_F, l)dk. \tag{3.185}$$

3.6.1 Ziman's Formula for the Electrical Resistivity

The Nearly Free Electron model is very useful for describing the behavior of conduction electrons in liquid metals. The conduction electrons are supposed to form a free-electron gas and to be scattered by the ions with appropriate pseudopotentials in a liquid metal. This scattering can be computed by the first-order time-dependent perturbation theory; the transition rate from an initial state $\psi_k^0 = \mid k\rangle$ to final states $\psi_{k+q}^0 = \mid k+q\rangle$ on the Fermi level with the density of states $N_{FE}(E_F)$ is given by the golden rule

$$P(\theta) = \frac{2\pi}{\hbar}(\mid \langle k+q \mid W \mid k\rangle \mid)^2 N_{FE}(E_F). \tag{3.186}$$

Here, θ is the angle between K and K+q, the factor 1/2 arises from the fact that electron spin does not change on scattering, and the factor $(\mid \langle k+q \mid W \mid k\rangle \mid)^2$ is decomposed in the same form. Thus the expression for the electrical conductivity σ_e is,

$$\sigma_e = \frac{1}{3}(\mid e \mid)^2 v_F^2 \tau N_{FE}(E_F). \tag{3.187}$$

Where, v_F is the Fermi velocity or velocity of an electron on the Fermi surface and τ is a relaxation time given by,

$$\frac{1}{\tau} = \int (1-\cos\theta)(P(\theta)4\pi)d\Omega, \tag{3.188}$$

with Ω the solid angle.

Some authors (Szabo, 1972,1973; Rousseau et al., 1973; Evans et al.,1973) have alternatively attempted to derive the resistivity ρ formula with the use of force-

force correlation functions. Ballentine and Heancy (1974) showed that, these force correlation derivations are erroneous unless the random force distinguished from the total force is taken into account; the total force formula was found to be correct only in the lowest order.

The well known Ziman formula [82] for the resistivity of the liquid metal is

$$\rho = \frac{3m^2\pi}{4Ze^2h^3n_{el}k_F^6}\int_0^\infty q^3 S(q)|W(q)^2|\theta(2k_F - q)dq. \tag{3.189}$$

where $S(q)$ is the static structure factor, $W(q)$ is the form factor.η_{el} is the conduction of electron density which is related to Fermi wave vector k_F=$(3\pi^2 n_{el})^{1/3}$, "e" is the electron charge, m is the electron mass, and h is Planck's constant. The unit step function θ is defined as,

$$\theta(2k_F - q) = \begin{cases} 0, & \text{for } q > 2K_F; \\ 1, & \text{for } q \leq 2K_F. \end{cases} \tag{3.190}$$

The extension to a liquid metal binary alloy is done by Faber-Ziman [67] as,

$$\rho = \frac{3m^2\pi}{4Ze^2h^3n_{el}k_F^6}\Bigg[\int_0^\infty q^3[C_iS_{ii}(q)|W_i(q)^2| + C_jS_{jj}(q)|W_j(q)^2|]\theta(2k_F - q)dq \tag{3.191}$$
$$+ \int_0^\infty q^3[2(C_iC_j)^{\frac{1}{2}}S_{ij}(q)W_i(q)W_j(q)]\theta(2k_F - q)dq\Bigg].$$

The finite mean free path corresponds to a finite uncertainty in the electron momentum. Thus the Fermi surface is not perfectly sharp but it is blurred. Some attempts have been made to take into account this blurring. Ferraz-March approach

[67, 68] yields in place of equation.(3.189)

$$\rho = \frac{3m^2\pi}{4Ze^2h^3n_{el}k_F^6}\int_0^\infty q^3 S(q)|W(q)^2|\Gamma(q,k_F,l), \tag{3.192}$$

Here,

$$\Gamma(q,k_F,l) = \frac{2}{\pi}\left[\tan^{-1}(ql) - \frac{1}{2}\tan^{-1}\frac{2ql}{1+4(K_Fl)^2} - \frac{\pi}{2}\Theta\left(q - (\frac{1}{l^2}+4K_F^2)\right)\right]. \tag{3.193}$$

The mean free path l can be determined self consistently. The first step in the self consistently loop is to calculate ρ using l=∞. A new l is then calculated from Drude relation as,

$$\rho = \frac{hk_F}{ne^2l}. \tag{3.194}$$

In which the iterations are continued until ρ_L converges. The extension of the Ferraz-March expression to binary alloys is straight-forward with θ replaced by $\Gamma(q,k_F,l)$ in Eq.(3.193),

$$\rho = \frac{3m^2\pi}{4Ze^2h^3n_{el}k_F^6}\Bigg[\int_0^\infty q^3[C_iS_{ii}(q)|W_i(q)^2| + C_jS_{jj}(q)|W_j(q)^2|]\Gamma(q,k_F,l)dq + \int_0^\infty q^3[2(C_iC_j)^{\frac{1}{2}}S_{ij}(q)W_i(q)W_j(q)]\Bigg]\Gamma(q,k_F,l)dq.$$

Using equation (3.193) and equation (3.194), and taking the consideration that the unit step function $\theta(2k_F - q)$ cuts off the integration at $2K_F$ corresponding to perfect sharp Fermi surface, we get the formula as,

$$\rho = \frac{3m^2\pi}{4Ze^2h^3n_{el}k_F^6}\Bigg[\int_0^{2k_F} q^3[C_iS_{ii}(q)|W_i(q)^2| + C_jS_{jj}(q)|W_j(q)^2|]dq + \int_0^{2k_F} q^3[2(C_iC_j)^{\frac{1}{2}}S_{ij}(q)W_i(q)W_j(q)]dq\Bigg].$$

which is used to calculate the electrical resistivity for Al-based liquid binary alloys in this thesis.

3.6.2 Corrections to Ziman's Expression

The Ziman's formula [9, 15, 65–68], for the resistivity is valid as long as the deviation from the free-electron behavior is small. But the basic assumptions involved implicitly or explicitly in the derivation still remain to be examined. For example, electron inelastic scattering due to the ionic motion would be negligible; high-order correlations of ionic configuration would be unimportant; the Born approximation would be valid. Only these problems are briefly described here. The usual pseudopotential concept employed in deriving Ziman's formula is not always valid for the resistivity calculation in liquid noble metals and transition metals. The use of the static structure factor $S(q)$ implies that the motion of the ions is completely neglected and electron scattering due to the motion of the ions is treated as elastic. However, the effects of ionic density fluctuations strictly yield inelastic scattering of electrons, as in the case of neutron inelastic scattering.

3.6.3 Scaling Laws for Transport Coefficients

Using the universal scaling law proposed by Dzugutov [85], the study of atomic transport coefficients, for the elemental system, has also been completed in this research work for liquid Al and details are given in Appendix B. The transport

coefficients, namely the reduced diffusion coefficient (D_R^*) and reduced shear viscosity (η_R^*) may be written as

$$D_R^* = D\frac{n^{1/3}}{(k_BT/m)^{1/2}}, \tag{3.195}$$

$$\eta_R^* = \eta\frac{n^{-2/3}}{(mk_BT)^{1/2}}. \tag{3.196}$$

where n, and T are the number density and temperature of the systems. These macroscopic reduction parameters (n and T) were chosen for the reduced transport coefficients. Based on the hundreds of simulation results [86–88], the reduced transport coefficients can be written as

$$D_R^* = 0.6e^{0.8S_{ex}}, \tag{3.197}$$

$$\eta_R^* = 0.2e^{-0.8S_{ex}}. \tag{3.198}$$

where, S_{ex} is the excess entropy of the systems. The excess entropy, S_{ex}, can be approximated keeping the two-body contribution as,

$$S_2 = -2\pi n\int_0^\infty \{g(r)\ln[g(r)] - [g(r)-1]\}r^2dr, \tag{3.199}$$

where $g(r)$ is the radial distribution function.

In 1996, the scaling law for diffusion constant is revised by Dzugutov [85] using the microscopic reduction parameters, collision frequency Γ, and inter-particle distance, σ. In 2005, following Dzugutov, Li [87] defined a scaling law relation for viscosity.

Based on, the microscopic reduction parameters, they defined the following reduced diffusion and viscosity coefficients equations are,

$$D_Z^* = D\frac{1}{\Gamma\sigma^2}, \tag{3.200}$$

$$\eta_L^* = \eta\frac{\sigma}{\Gamma m}. \tag{3.201}$$

From equations (3.200) & (3.201), the collision frequency, Γ according to Enskog theory [89] is,

$$\Gamma = 4\sigma^2 g(\sigma) n(\pi k_B T/m)^{1/2}. \tag{3.202}$$

Here $g(\sigma)$ is the radial distribution function evaluated at hard sphere diameter, σ. The hard sphere diameter was chosen at the position of the first principal peak of $g(r)$. Based on the hundreds of simulation results for the reduced transport coefficients, they proposed the following scaling laws,

$$D_R^* = 0.049e^{S_{ex}} \tag{3.203}$$

$$\eta_R^* = 0.035e^{-0.55S_{ex}}. \tag{3.204}$$

Chapter 4

Results, Discussions, & Conclusions

The study of 'Thermodynamic and Transport Properties of Al-based ($Al_{1-x}X_x$, here X=Zn, In, Sn, Bi, Cu, Au) liquid binary alloys', is the main purpose of the present research work. In this chapter, the calculated results for $Al_{1-x}Zn_x$, $Al_{1-x}In_x$, $Al_{1-x}Sn_x$, $Al_{1-x}Bi_x$, $Al_{1-x}Cu_x$ and $Al_{1-x}Au_x$ liquid binary alloys will be discussed gradually. For thermodynamics of mixing, I have gone through the study of Helmholtz free energy (A), the energy of mixing (ΔA), enthalpy of mixing (ΔH), and entropy of mixing (ΔS) for $Al_{1-x}Zn_x$, $Al_{1-x}In_x$, $Al_{1-x}Sn_x$, $Al_{1-x}Bi_x$, $Al_{1-x}Cu_x$ and $Al_{1-x}Au_x$ liquid binary alloys at different thermodynamic states.

Moreover, I have also studied the Atomic Transport Properties (ATP) and Electron Transport Properties (ETP). Firstly, for understanding the behavior of ATP in liquid states, the coefficients of viscosity (η), diffusion coefficients (D), and friction coefficients (ζ) have been calculated. Secondly, for ETP, the theoretical results of electrical resistivity (Ω) and conductivity for those aforementioned liquid binary alloys have been found at different thermodynamic states serially.

The experimental studies of ATP and ETP are not always auspicious and some-

times are very costly. In addition, they are very difficult to manage properly as well. This is why the experimental results for both ATP and ETP are very rare. Consequently, we did not find the sufficient experimental results of liquid binary alloys for the transport properties to compare our results.

Finally, I have submitted all my research works and results with graphical analysis and tables of the corresponding systems.

4.1 Effective Values of Parameters

For, the final calculations, of all the Thermodynamic and Transport properties, we had to determine the two basic ingredients for the binary systems. These two ingredients are, namely:

a) The effective pair potentials (V_{ij}),

and

b) The pair correlation function for the reference hard sphere liquids (g_{ij}).

We have to calculate the effective partial pair potentials (V_{ij}) for understanding the inter-ionic interaction [76–91] in alloys state and then partial pair correlation functions (g_{ij}) for the hard sphere reference liquids for different Al-based alloys for the different set of concentrations, using the Bretonnet-Silbert pseudopotential model [44]. The BS model has three parameters,

(i). The Core Radius, R_c,

(ii). The Softness Parameter, a, and

(iii). The effective electron occupancy number, Z.

These parameters are chosen only to calculate the effective pair potentials. Once it is done, the rest of the calculations (for A, ΔA, ΔH, ΔS, η, D, ζ, and Ω) are completely parameter free. Calculations from the theoretical point of view are also self-consistent and as a result, the accuracy of calculations are much more reliable than the empirical and semi-empirical methods.

Table 4.1: BS Pseudopotential Parameters for Different Liquid Binary Systems.

Elements	Z	R_c	a	*Temperature* (K)
Al	3.0	1.91	0.49	-
Zn	2.0	1.275	0.285	1000
In	3.0	1.37	0.27	1173
Sn	4.0	1.30	0.26	973
Bi	5.0	1.49	0.363	1173
Cu	1.30	1.44	0.30	1373
Au	1.80	2.03	0.49	1338

The values of R_c are generally determined by fitting the physical properties of the system of interest, and the values of the softness parameters, a, are found by fitting the structure factor at low q to the experimental data [29]. We have chosen the three parameters for BS model which listed in the table for Al, Zn, In, Sn, Bi, Cu, and Au.

4.2 Thermodynamic Properties for $Al_{1-x}Zn_x$ Liquid Binary System

In this section, the results for Free energy (A), Energy of mixing (ΔA), Enthalpy of mixing (ΔH), and Entropy of mixing (ΔS) for $Al_{1-x}Zn_x$ liquid binary system at thermodynamic state 1000 K, obtained from the first principles approach, specifically from the perturbation method, and the electronic theory of metals (ETM) are presented.

4.2.1 The Effective Partial Pair Potentials (V_{ij})

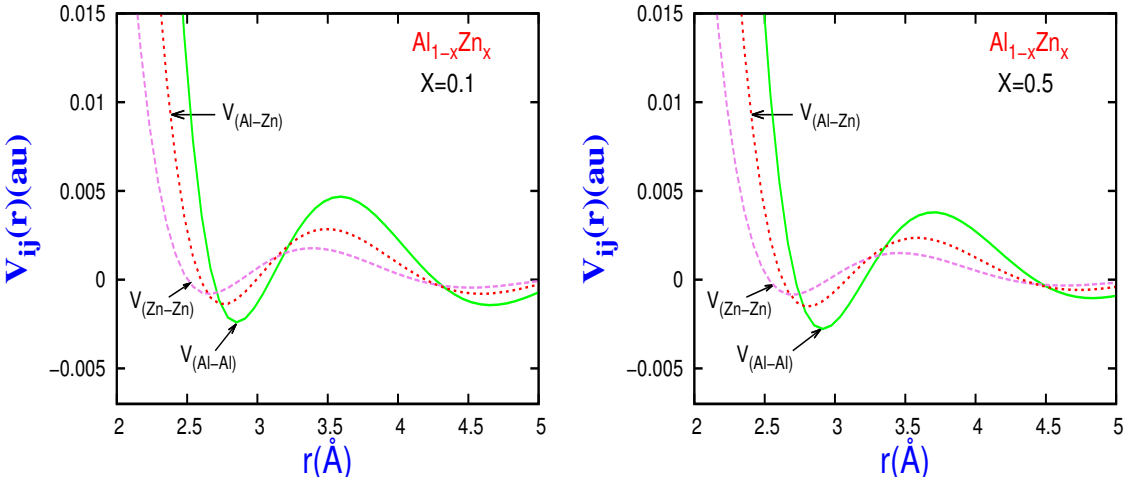

Figure 4.1: Partial pair potential (V_{ij}) for $Al_{1-x}Zn_x$ liquid binary system for concentrations x=0.1 and 0.5.

Figure (4.1-4.2) show the effective partial pair potentials [4, 29, 44] for three different concentrations, x=0.1, 0.5, and 0.9 for $Al_{1-x}Zn_x$ liquid binary system, respectively. From the pseudopotential [16–58] formalism, we can easily say that the direct interactions occurring between the two ion cores and, the interaction [4, 29] between the ion cores are mediated by the conduction electrons. In determining the effective [4, 21] pair potentials, the dielectric function for screening plays an important

role. From the Figure (4.1-4.2), it is seen that the depth of the well of the partial potential is the largest for V_{Al-Al}, and smallest for V_{Zn-Zn}, in all concentrations. We have found that the potential well for V_{Al-Zn} lies between V_{Al-Al} and V_{Zn-Zn} without any exception for the whole range of concentrations.

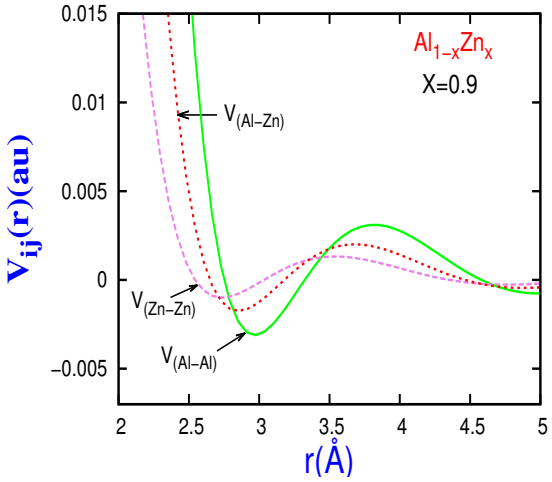

Figure 4.2: Partial pair potential (V_{ij}) for $Al_{1-x}Zn_x$ liquid binary system for concentration x=0.9.

Figure (4.1-4.2) also illustrate the positions of the minimum energy levels for different concentrations of these alloys, and the positions of these alloys vary from concentration range of x=0.1 to 0.9, in the following order, $V_{Zn-Zn} < V_{Al-Zn} < V_{Al-Al}$. Following the same order, the energy levels of this minimum are shifted to large r. Numerically, the values for V_{Al-Al}, V_{Al-Zn}, and V_{Zn-Zn} potential well are found to be -0.0032 eV, -0.0016 eV, -0.001 eV, respectively for concentration x=0.1, and these values slightly increase with the increasing concentration of Zn. But the changing order remains the same for different concentrations in the alloy states.

4.2.2 The Pair Correlation Functions (g_{ij}) for the Reference Hard Sphere Liquids and Hard Sphere Diameters (σ_{ij}):

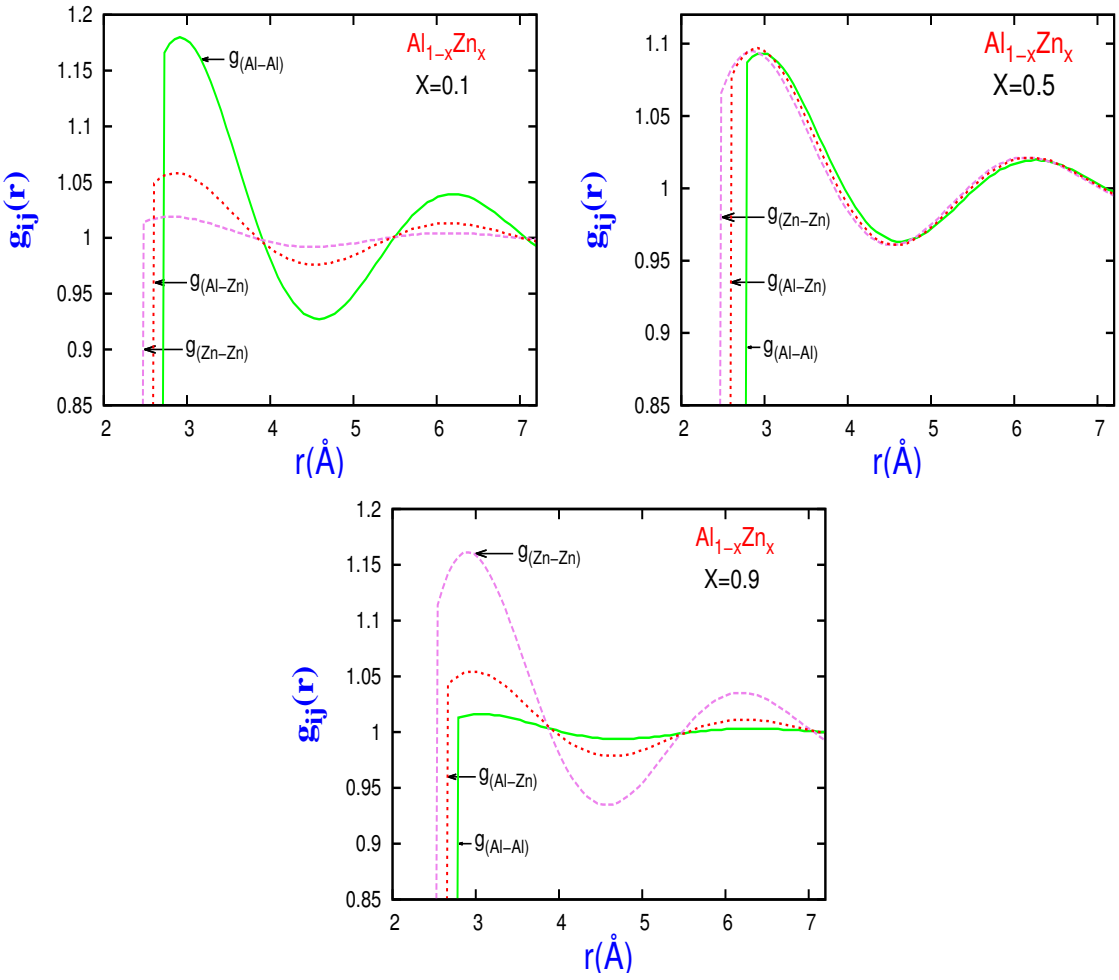

Figure 4.3: Partial pair correlation function for $Al_{1-x}Zn_x$ liquid binary system for concentrations x=0.1, 0.5, and 0.9, respectively.

We evaluated the partial pair correlation function using the Ashcroft-Lagranth [4, 50] theory for the hard sphere. In order to calculate g_{ij}(r), the essential parameter is the effective hard sphere diameter, which we determined by using the thermodynamic perturbation theory known as, linearized WCA (LWCA) [70] theory. In the case of binary alloys, we replace the effective inter-ionic potentials, V(r) with the partial potentials, V_{ij}(r), and follow the same procedure as for the one component systems

[28–31].

Figure 4.3 illustrates the partial pair distribution functions for $Al_{1-x}Zn_x$ liquid binary alloy at thermodynamic state 1000 K for three different concentrations x=0.1, 0.5 and 0.9, respectively. In this figure, we see that the principal peak of g_{Al-Al}(r) is much larger than that of g_{Zn-Zn}(r) for x=0.1 and this trend reverses for x=0.9.

This is due to the fact that, for x=0.1 the alloy is rich in Al. So, the probability of finding another Al ion from the reference one is larger. The situation reverses for x=0.9, because the alloy is rich in Zn. This trend suggests that the peak values of g_{Al-Al}(r) and g_{Zn-Zn}(r) would be comparable for an equiatomic composition *i.e* for x=0.5 concentration. It is exactly reflected in Figure 4.3, for x=0.5 concentration.

Hard Sphere Diameter (σ_{ij}):

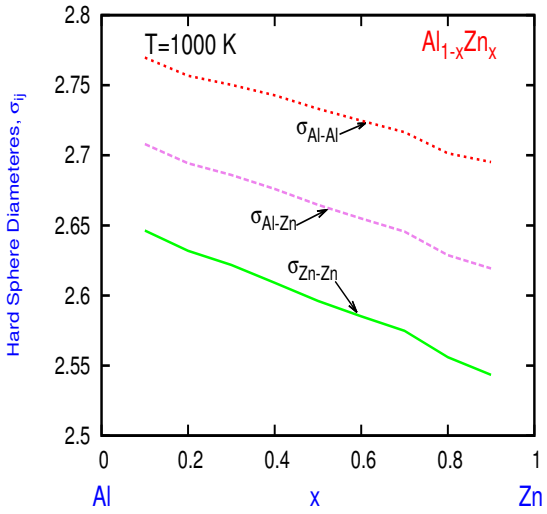

Figure 4.4: Hard sphere diameter for $Al_{1-x}Zn_x$ liquid binary alloys.

Figure 4.4 shows the values of the partial hard sphere diameters (σ_{ij}) as a function of the concentrations for $Al_{1-x}Zn_x$ liquid binary system. Values of HSD decrease with increasing concentrations of Zn but values for σ_{Al-Al} remain larger than σ_{Zn-Zn} for the whole range of concentrations. So, symbolically it can be rearranged as

$\sigma_{Zn-Zn} < \sigma_{Al-Zn} < \sigma_{Al-Al}$. The hard sphere contributions from σ_{Al-Zn} always lies between σ_{Zn-Zn} and σ_{Al-Al} which is consistent as expected.

4.2.3 A, ΔA, ΔH and ΔS for $Al_{1-x}Zn_x$ Liquid Binary System

It is a very challenging task to study the inter-ionic interaction in the liquid state, especially for Al-based alloys, because, Al has some interesting features. Al in the solid phase has a fcc crystalline structure. It is relatively soft, durable, lightweight, ductile and malleable metal. It is a good electrical and thermal conductor, and also a superconductor. It is a polyvalent system with chemical valence 3. Because of its wide application in the industry and it has interesting features; the interest of studying the Al and its alloys is growing.

Inter-ionic interactions of alloys are largely changed from those of individual components. Thermodynamic properties for liquid binary alloys have been studied both experimentally and theoretically for many decades and there are extensive works of literature on this subject [16–58]. At the present section, we have focused our aim to discuss the findings for A, ΔA, ΔH and ΔS for $Al_{1-x}Zn_x$ Liquid Binary System.

Here, it is worth mentioning that, the energy of mixing, ΔA, and the entropy of mixing, ΔS, are not independent of each other. They are related through the equation,

$$\Delta A = \Delta U - T\Delta S \tag{4.1}$$

for a particular temperature, T. Here, ΔU is the internal energy of mixing. It is seen from the equation that, the free energy of formation is lowered when the entropy of formation, ΔS positive, and so the formation of alloys are favored. As a negative value of ΔS increases ΔA; the alloy state becomes more or less unstable from the point of equilibrium condition. So, it is expected that, if ΔS reaches to the

most negative value, a maximum instability of the alloys will occur. The free energy depends directly on the partial pair interaction, $V_{ij}(r)$, and partial pair correlation $g_{ij}(r)$. Besides, the link between the enthalpy of mixing, ΔH and the internal energy, ΔU of a system can be defined as,

$$\Delta H = \Delta U + P\Delta V \tag{4.2}$$

It can also be observed from the equation that, at the very low pressure the enthalpy of mixing and the internal energy of a system are almost equal. After combining these two equations, we can easily get the entropy of mixing, ΔS for any system. The entropy is related directly to the derivative of the free energy with respect to temperature but not directly to the full profile of the inter-ionic potentials, as in the case of energy evaluation [95]. Therefore, the accuracy of the enthalpy, and entropy calculation at a particular concentration mostly relies on the accuracy of the slope of the free energy versus temperature (F-T) curve.

The free energy (A) depends on the inter-ionic interactions and it also depends on the ionic number density, and the number density. Again, these densities change with the change of concentrations in alloy states. Due to this complicated dependence of the free energy on the concentrations, it is difficult to obtain correct slope for all concentrations of the alloys. It possesses a great challenge in calculating numerically the enthalpy of mixing ΔH, and the entropy of mixing ΔS, in correct order from the same inter-ionic potential and partial pair correlation function which were used for the calculation of the energy of mixing.

Free Energy (A):

Free energy, (A) has been illustrated with the detailed breakdown in Figure 4.5 for $Al_{1-x}Zn_x$ system at thermodynamic state 1000 K. We found here that the largest

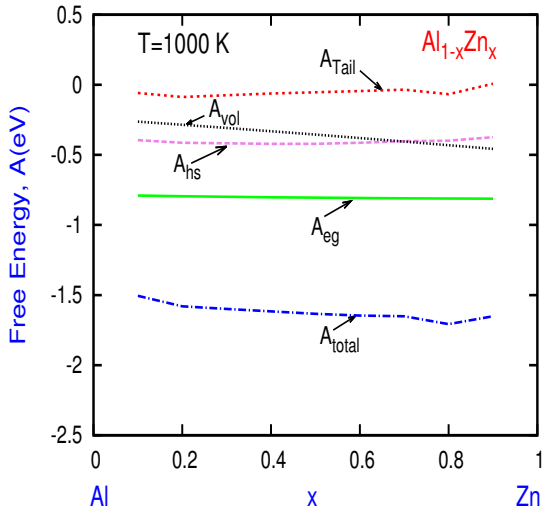

Figure 4.5: Free energy for $Al_{1-x}Zn_x$ liquid binary system.

contribution arises from the electron-gas part, A_{eg}, which is a very strange behavior for the concerned $Al_{1-x}Zn_x$ system. The second contributory part comes from the HS reference system.

To understand this strange behavior of A_{eg}, [4]. we have performed our study in threefold. Firstly, we have chosen the valency, Z as an integral value for the alloy forming elements Al and Zn. We have taken Z=3.0 for Al and 2.0 for Zn respectively. We always found that the largest contribution arises from A_{eg} and the second largest contribution from A_{hs}. Secondly, we have fixed Z=3.0 for Al and took the hybridization effect of Zn and put Z=1.50 [28]. The first and second largest contributions arise from the inter-ionic interactions as A_{eg} and A_{hs}, respectively. Thirdly, we have considered the hybridization effect both for Al and Zn as 1.50. Surprisingly, this time we have found that the largest contribution arises from A_{hs} of the HS reference system of the inter-ionic interactions. This actually manifests that in polyvalent metal with $Z \geqslant 3$ the electron gas, A_{eg} contribution gets larger than the hard sphere term. The third and the fourth largest contributions come from the A_{vol} and A_{tail} part of the inter-ionic interactions. The results of A_{vol} contribution is always negative and

is increased with increasing the concentrations of the system. And, we have always noticed that the A_{tail} is very small compared to the other three contributory parts. The total free energy for $Al_{1-x}Zn_x$ liquid binary system is negative from x=0.1 to 0.9. Symbolically one can present the magnitude of contribution as in the following order $A_{eg} > A_{hs} > A_{vol} > A_{tail}$. Finally, the summation of all four concentrations yields the total free energy A_{total} of the alloy which lies at the bottom in Figure 4.5.

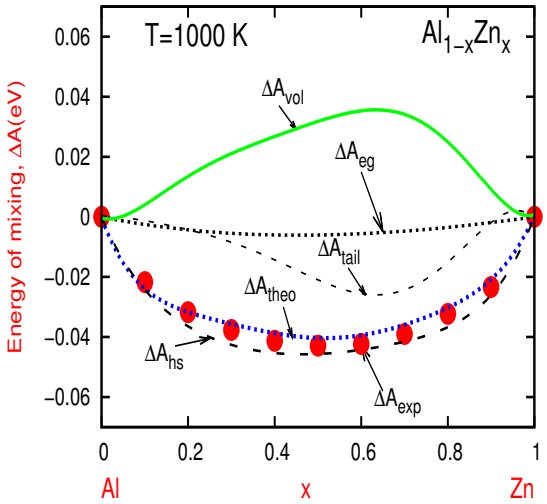

Figure 4.6: Energy of mixing (ΔA) for $Al_{1-x}Zn_x$ liquid binary alloys.

Energy of Mixing (ΔA):

Energy of mixing for $Al_{1-x}Zn_x$ liquid binary alloys at $T = 1000$ K has been illustrated in Figure 4.6. From the Figure (4.6), it is observed that the major contribution comes from the hard sphere (ΔA_{hs}) reference liquid. It is negative across the whole range of concentration, and very close to the experimental values, ΔA_{ex} [92]. The contribution arises from the tail part is large between x=0.4 to 0.8 and a maximum at x=0.7 which is in Zn rich region. The contribution from ΔA_{eg} is very close to zero eV. The ΔA_{vol} part is positive for the whole range of concentrations. The shape of this part is like a parabola.

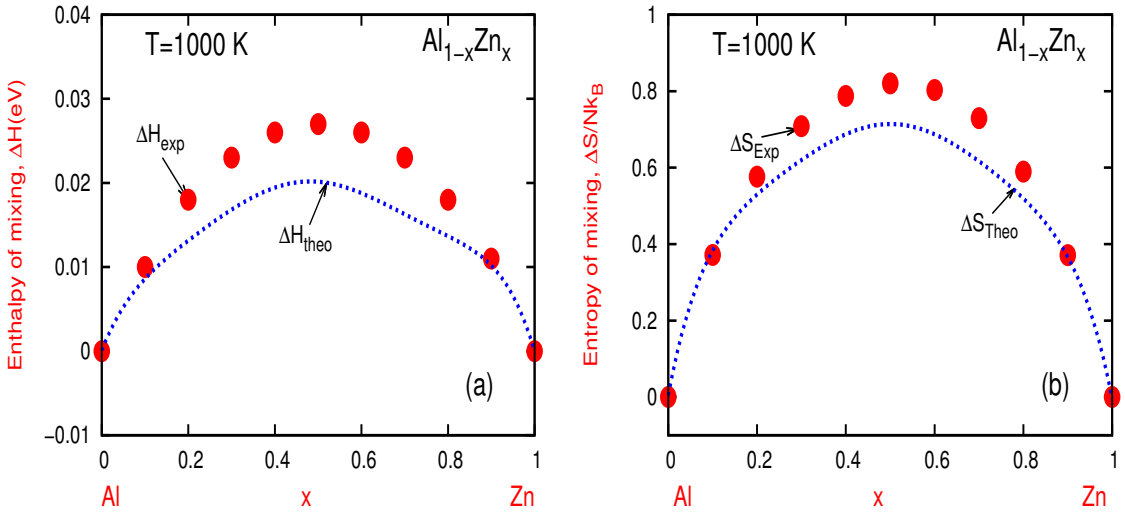

Figure 4.7: Enthalpy of mixing (ΔH) and Entropy of mixing (ΔS) for $Al_{1-x}Zn_x$ liquid binary system.

Enthalpy of Mixing (ΔH) and Entropy of Mixing (ΔS):

Figure 4.7 (a-b) describes enthalpy of mixing, ΔH, and entropy of mixing, ΔS for $Al_{1-x}Zn_x$ liquid binary alloy at T = 1000 K. From the figure it is remarked that the value for both ΔH and ΔS are positive across the whole range of concentrations which are very close to the experimental results [92]. It is noted in Figure 4.7(a) that, the argument is excellent at x=0.1 and 0.9, where the system is rich in Al, and Zn, respectively. In those regions, the theoretical and experimental results are very close to each other. It starts to deviate from the experimental [110] results, and that can be found from concentrations of x=0.2 to 0.8. The maximum deviation is found at x=0.5. Similar trends we have found in Figure 4.7(b) for ΔS.

4.2.4 Conclusion

The results of a systematic investigation for the free energy, energy of formation, enthalpy of formation and entropy of formation for $Al_{1-x}Zn_x$ liquid binary alloy have been presented here. The first order perturbation theory and the microscopic theory

of metals are used to perform the calculations.

An effective hard sphere liquid is considered as a suitable reference system for the perturbation treatment. The results for ΔA, ΔH, and ΔS are found to be good in agreement with the available experimental data [92] for the concerned alloy. From the above results, we can draw the following concluding remarks.

(i) The energy of formation for $Al_{1-x}Zn_x$ liquid binary alloys is almost 10^{-2} an order smaller than the values for the total free energies. This is also much smaller than any possible contribution to the free energy. The available experimental data [92] confirms our findings.

(ii) The volume effect plays an important role in producing a nearly quantitative agreement with the observed data for the energy of formation, although its contribution to the total free energy is relatively insignificant.

(iii) The results for enthalpy of mixing and entropy of mixing are fairly good in agreement when compared with the available experimental data [92].

(iv) The general microscopic theory (GMT) of metals along with a perturbation approach is capable of producing the thermodynamics of formation correctly when adequate care is taken in calculating all different contributions for $Al_{1-x}Zn_x$ liquid binary alloy.

(v) Since the energy of formation for the system is negative for all the studied concentrations range, it indicates that the liquid Zn will be miscible with Al at any concentration.

(vi) Finally, the excellent agreements in the case of $Al_{1-x}Zn_x$ alloy indicate that, the reliability and predictability of the present approach is inherent not accidental. So, this approach may be applied to study other Al-based liquid binary alloys.

4.3 Thermodynamic Properties for $Al_{1-x}In_x$ Liquid Binary System

The results of the calculation for free energy (A), the energy of mixing (ΔA), the enthalpy of mixing (ΔH), and the entropy of mixing (ΔS) are presented in this section for $Al_{1-x}In_x$ liquid binary alloys. First order perturbation theory along with the electronic theory of metal is again applied to perform the calculations. The basic ingredients such as, the effective inter-ionic partial potentials, V_{ij}(r), and the corresponding pair correlation functions, g_{ij} of the reference system are very essential for calculating A, ΔA, ΔH, and ΔS at thermodynamic state T=1173 K, and are evaluated using the same procedure as discussed before for $Al_{1-x}Zn_x$ liquid binary system.

4.3.1 The Effective Partial Pair Potentials (V_{ij})

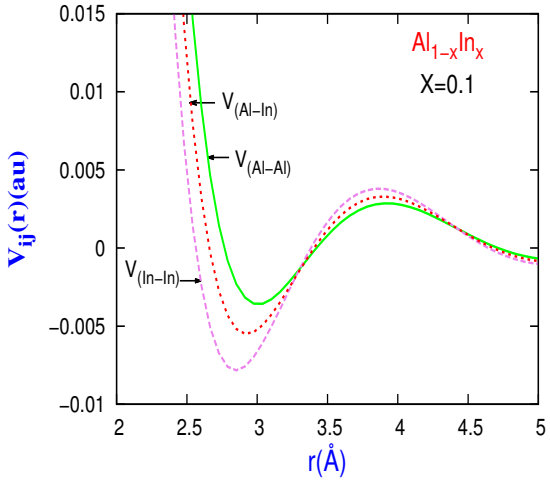

Figure 4.8: Partial pair potential for $Al_{1-x}In_x$ liquid binary alloys.

The study is conducted upon the basis of changing the concentrations of Al_{1-x} from 0.9 to 0.1. Figure (4.8-4.9) showed that, the effective partial pair potentials

for three different concentrations x=0.1, 0.5 and 0.9 for the concerning system, respectively. It is seen in these figures (Figure (4.8-4.9)) that, the depth of the well of the potential is the largest for V_{In-In} and smallest for V_{Al-Al}. The potential well for V_{Al-In} always lies between V_{In-In} and V_{Al-Al}.

The systems, Al and In belong to the same column in the periodic table of elements and they are also from the group IIIB [93]. The group position for Al and In are 2^{nd} and 5^{th}, respectively. Seeing that as the position of In is lower in group IIIB, V_{In-In} gives the larger depth of the potential well. On the other hand, the position of Al is upper in group IIIB. Consequently, V_{Al-Al} shows the smaller depth of the potential well. So apparently, the potential well is directly related to the position of the elements in periodic table.

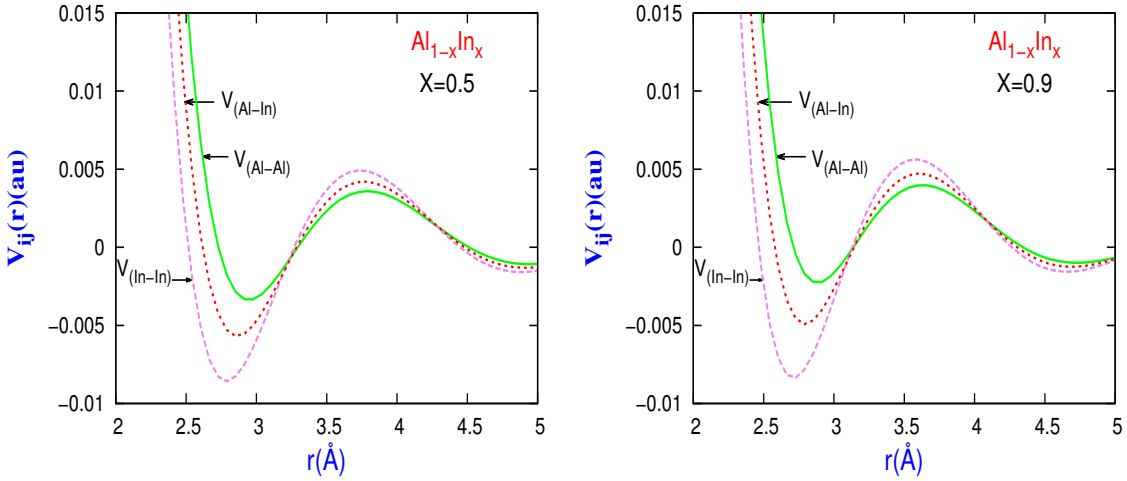

Figure 4.9: Partial pair potentials for $Al_{1-x}In_x$ liquid binary alloys.

4.3.2 The Pair Correlation Functions (g_{ij}) for the Reference Hard Sphere Liquids and Hard Sphere Diameters (σ_{ij}):

Figure 4.10 illustrates the partial pair distribution functions for $Al_{1-x}In_x$ liquid binary alloys at thermodynamic state 1173 K for three different concentrations x=0.1,

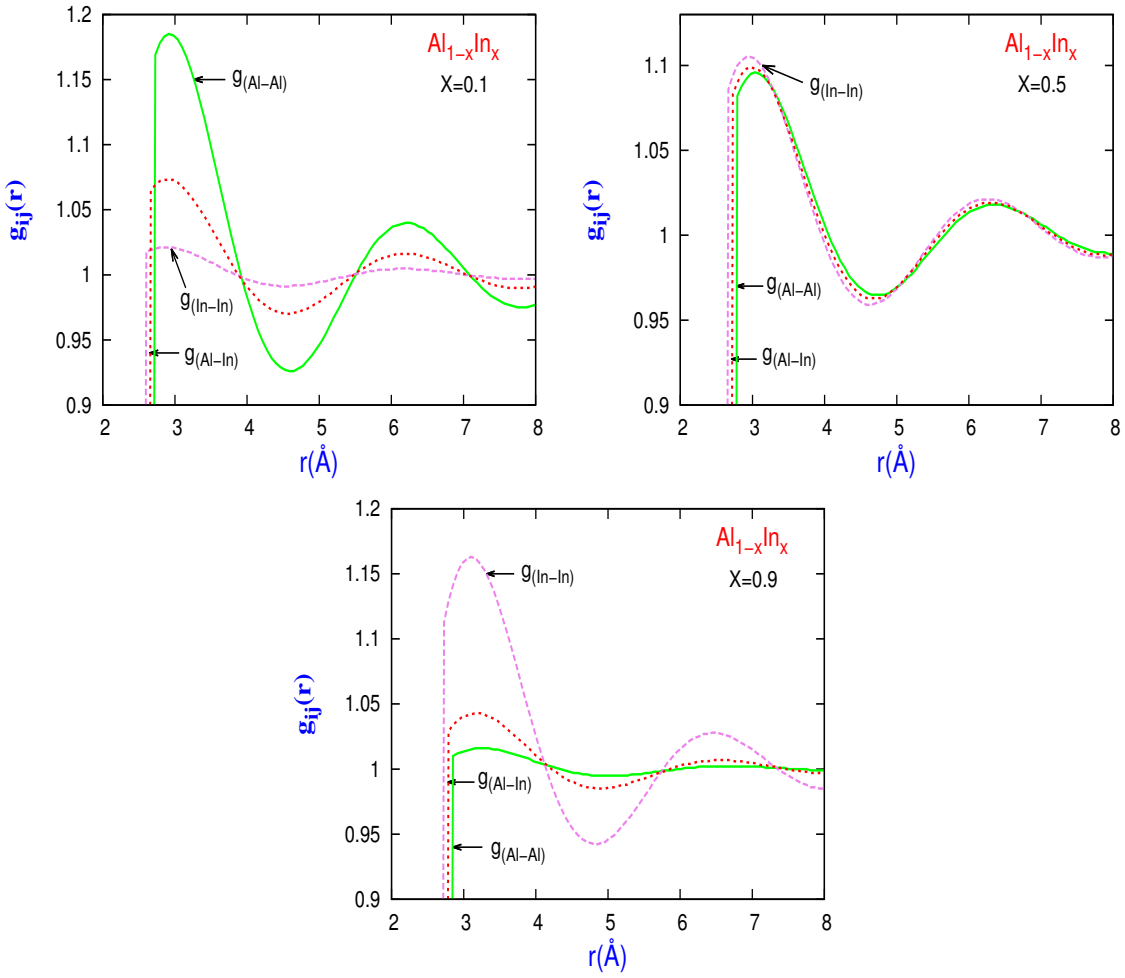

Figure 4.10: Partial pair correlation functions for concentration x=0.1, 0.5, and 0.9, respectively for $Al_{1-x}In_x$ liquid binary alloys.

0.5 and 0.9. The principal peak of g_{Al-Al}(r) is much greater than g_{In-In}(r) for concentration, x=0.1, and this trend reverses for x=0.9. This feature is as same as that of $Al_{1-x}Zn_x$ liquid binary alloys that, we described before.

As we mentioned earlier, this is due to the fact that, for x=0.1, the alloy is rich in Al. So, the probability of finding another Al ion, at a distance r from the reference one is larger. The situation reverses for x=0.9 because the alloy is then rich in In. This trend suggests that the peak values of g_{Al-Al}(r) and g_{In-In}(r) would be comparable for an equiatomic composition *i.e* for x=0.5 concentration. It is exactly reflected in

Figure 4.10, for x=0.5 concentration.

Hard Sphere Diameter (σ_{ij}):

Figure 4.11. illustrates the feature of the partial hard sphere diameters for the corresponding system. It can be rearranged as $\sigma_{In-In} < \sigma_{Al-In} < \sigma_{Al-Al}$. The hard sphere [94] diameters σ_{Al-In} always lie between σ_{In-In} and σ_{Al-Al} which is consistent of our additive hard sphere theory [71].

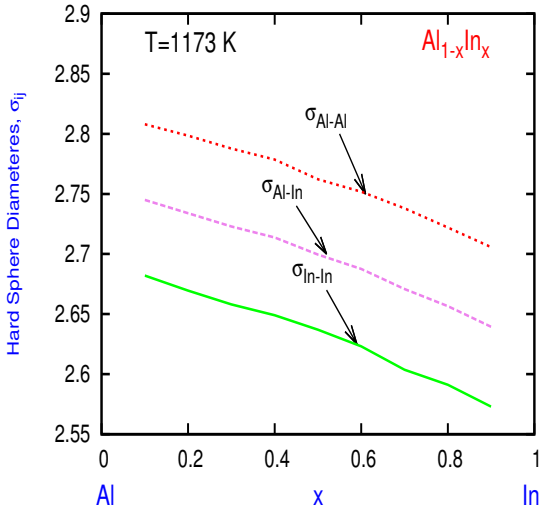

Figure 4.11: Hard sphere diameter for $Al_{1-x}In_x$ liquid binary system.

4.3.3 A, ΔA, ΔH and ΔS for $Al_{1-x}In_x$ liquid Binary System

Free Energy (A):

We now have moved on to the results of free energy, A, for $Al_{1-x}In_x$ liquid binary alloys at T=1173 K. The breakdown details for free energy, A is presented in Figure 4.12 for the concerning system. We get the largest contribution from the electron-gas part, A_{eg} [95] and the second one from the HS reference system.

In order to understand this eccentric behavior [96] of A_{eg}, we have performed our study in twofold again for $Al_{1-x}In_x$ system. We began by choosing the valence, Z as

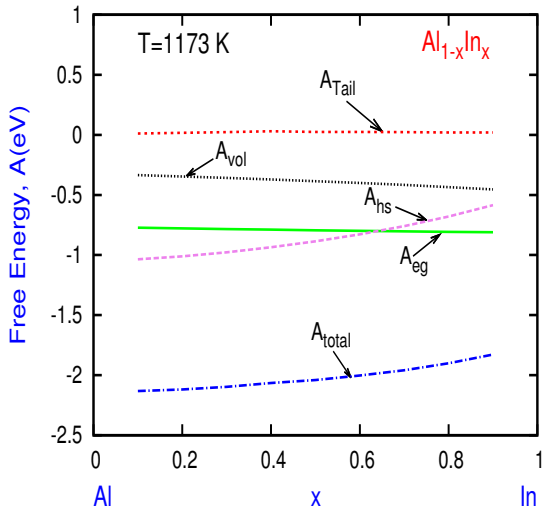

Figure 4.12: Free energy for $Al_{1-x}In_x$ liquid binary alloys.

an integral value for the alloy forming elements Al and In. Since Al, and In are in the same position in periodic table elements. We considered Z=3.0 for both Al, and In, respectively. In every case, we found that the first contribution arises from A_{eg} and the second contribution from A_{hs}. Lastly, we took the hybridization effect for both Al and In as 1.50. Note that, this time we got the different result as expected i.e, the higher contribution came from A_{hs} of the HS reference system. Meaning that in polyvalent metal with $Z \geqslant 3$ the electron gas, A_{eg} contribution gets larger than the hard sphere term. The third and fourth largest contributions come from the volume, A_{vol}, and tail, A_{tail}, part of the inter-ionic interactions. The results of A_{vol} contribution is always negative and increases with increasing the concentrations of the system, from x=0.1 to 0.9.

And, we have audited invariably that the A_{tail} is very small compared to other three contributory parts from concentrations, x=0.1 to 0.9. The total free energy of $Al_{1-x}In_x$ liquid binary system is always negative from x=0.1 to 0.9 which is consistent with expectation. The magnitudes of different contributions can be represented in the following order $A_{eg} > A_{hs} > A_{vol} > A_{tail}$.

In conclusion, the summation of all four concentrations yields the total free energy A_{total} of the alloy which lies at the bottom in the figure 4.12.

Energy of Mixing (ΔA):

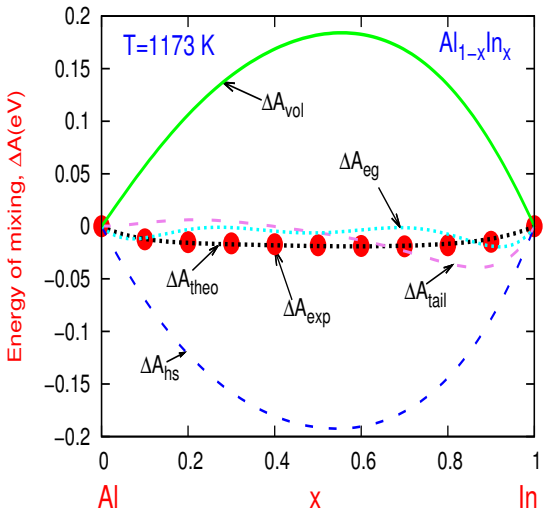

Figure 4.13: Energy of mixing (ΔA) for $Al_{1-x}In_x$ liquid binary alloys.

Figure 4.13 describes the total free energy of mixing, ΔA for the corresponding system. Here, the largest contribution comes from the ΔA_{hs} of the reference system. It is maximum for x=0.5 *i.e* at the equiatomic position. The contribution arising from the tail part possesses both positive and negative values; in the region $x \leq 0.6$ it is positive and in the region $0.6 \leq x < 0.9$ it is negative. It is maximum in negative value at x=0.9 region which is the In rich region. Similarly, the contribution from ΔA_{eg} is very close to zero eV. The ΔA_{vol} part is positive for the whole range of concentrations which is similar to Al_{1-x} based system.

Enthalpy of Mixing (ΔH) and Entropy of Mixing (ΔS):

Figure 4.14(a) represents the enthalpy of mixing, ΔH, as a function of concentration, x, for $Al_{1-x}In_x$ liquid binary alloys at 1173 K. At x=0.1 and 0.9 the results are

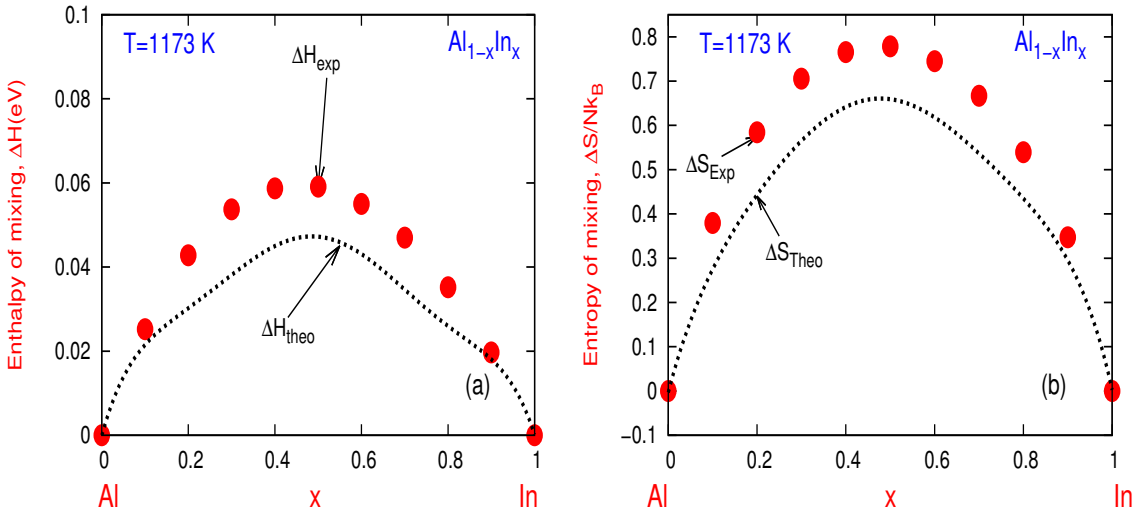

Figure 4.14: Enthalpy of mixing (ΔH) and Entropy of mixing (ΔS) for $Al_{1-x}In_x$ liquid binary system.

good in agreement with the experimental results. This region is rich in Al, and In, respectively. But, the results are found to be deviated in the concentration range $0.2 \leqslant x \leqslant 0.8$ while compared with the experimental data [92]. The qualitative agreement is good as far as the uncertainty of the measurement is concerned. Here, both theory and experiment show the maximum of ΔH at the equiatomic concentration. Figure 4.14(b) represents the entropy of mixing (ΔS). Here, ΔS is symmetric around the equiatomic concentrations as in the case of enthalpy of mixing. The discrepancy between calculated and experimental results [92] is the largest around $x = 0.5$ but it is within the 18% of the experimental data [92]. The discrepancy reduces away from the equiatomic concentration. Therefore, the agreement is qualitatively good as far as the experimental uncertainty is concerned.

4.3.4 Conclusion

The first principle calculation, specifically the application of perturbation method along with the Percus-Yevick [4] HS model as a reference alloy, and electronic theory

of metal is able to describe at least qualitatively the free energy, energy of mixing, enthalpy of mixing and entropy of mixing for $Al_{1-x}In_x$ liquid binary alloys. The local model (BS) for inter-ionic interaction can be a good starting point for studying the heavy polyvalent simple liquid binary alloys, provided that the model parameters are determined appropriately. The volume term plays an important role as far as the agreement with the experiment [92] is concerned. For $Al_{1-x}In_x$ liquid binary alloy, the volume effect is more significant, and consequently, this effect plays a greater role in the present case. Finally, the results of the present calculations imply that our parameter free first principle approach for the study of A, ΔA, ΔH, and ΔS is reliable for the less simple heavy polyvalent liquid binary alloys.

4.4 Thermodynamic Properties for $Al_{1-x}Sn_x$ Liquid Binary System

The system we are interested to discuss in this section which is the $Al_{1-x}Sn_x$ liquid binary alloys at a thermodynamic state T=973 K. The cause of choosing this system is fourfold. Firstly, the alloy forming elements Al and Sn both are heavy polyvalent metals and are sometimes difficult to handle theoretically, particularly in the framework of pseudopotentials. Secondly, $Al_{1-x}Sn_x$ liquid binary alloys have not been studied yet, so our knowledge from any microscopic theory, although some attempts are made from the empirical or semi-empirical models [97–99]. Thirdly, experimental data for static structure factors for the elemental liquid Al and Sn are available in the literature at the thermodynamic state in question [4, 29]. Fourthly, the physical properties that we are interested to investigate theoretically are already measured by different experimentalists [92] from the different experimental approaches.

The microscopic theory, we have applied again in the present research study is the combination of the electronic theory of metals along with perturbation approach and the statistical mechanics. The electronic theory of metals employed in this work is based on a local pseudopotential proposed by Bretonnet and Silbert (BS) [44]. The band structure energy calculated from the pseudopotential theory provides the inter-ionic interaction, which is used to have a static structure factor as well as other physical properties investigated here. It is worth noting that these two parameters of BS pseudopotential (core radius, R_c , and the softness parameters, a) need to be fixed to perform the effective calculations. Here, values of R_c are taken from other published work and values of a are determined following the spirit of original work [57], that is by the best fit of the static structure of the elemental system Al and Sn. Once this is done, the rest of the calculations for thermodynamic proper-

ties of the concerned metals and their alloys is completely parameter free (unlike the self-associated model, SAM). Not only that, the approach we have used is also highly self-consistent from the theoretical point of view. By the term self-consistent, we mean that this approach starts from the electron-ion interaction in metals to derive the inter-ionic interaction, a microscopic property of the condensed state, and then allow us to evaluate static structure factor from it by using thermodynamic perturbation theory and the statistical mechanics. Finally, these results for structure and interactions are applied as inputs to calculate the thermodynamic properties of mixing using the electronic theory of metals. No free parameter or nothing is irrelevant to the inter-ionic interaction which enters in this process laterally. However, the perturbation theory always requires an unperturbed state which is often referred to as reference system. The reference system is also chosen such that it can largely represent the real system in question. In the case of simple metals and their alloys, the hard sphere liquid is a good option as demonstrated in many works [16–58].

4.4.1 The Effective Partial Pair Potentials (V_{ij})

The study is carrying on the basis of changing the concentrations of Al_{1-x} from 0.9 to 0.1 at T=973 K for $Al_{1-x}Sn_x$ liquid binary system, respectively. Figure 4.15 shows the effective inter-ionic partial pair potentials for $Al_{1-x}Sn_x$ liquid binary alloys for three different concentrations (x =0.1, 0.5 and 0.9). Partial pair potential V_{Al-Al} and V_{Sn-Sn} exhibits usual behavior that potential decreases rapidly to a minimum value and then it increases with increasing r, and then performs the so-called Friedel oscillation due to the fluctuation of electronic charge density [27]. But, $V_{Al-Sn}(r)$ exhibits a different feature that a local minimum at small r appears first and then gradually increases and starts oscillation with a minimum value at large r (around 4Å). In order to examine the origin of this unusual feature of the local minimum

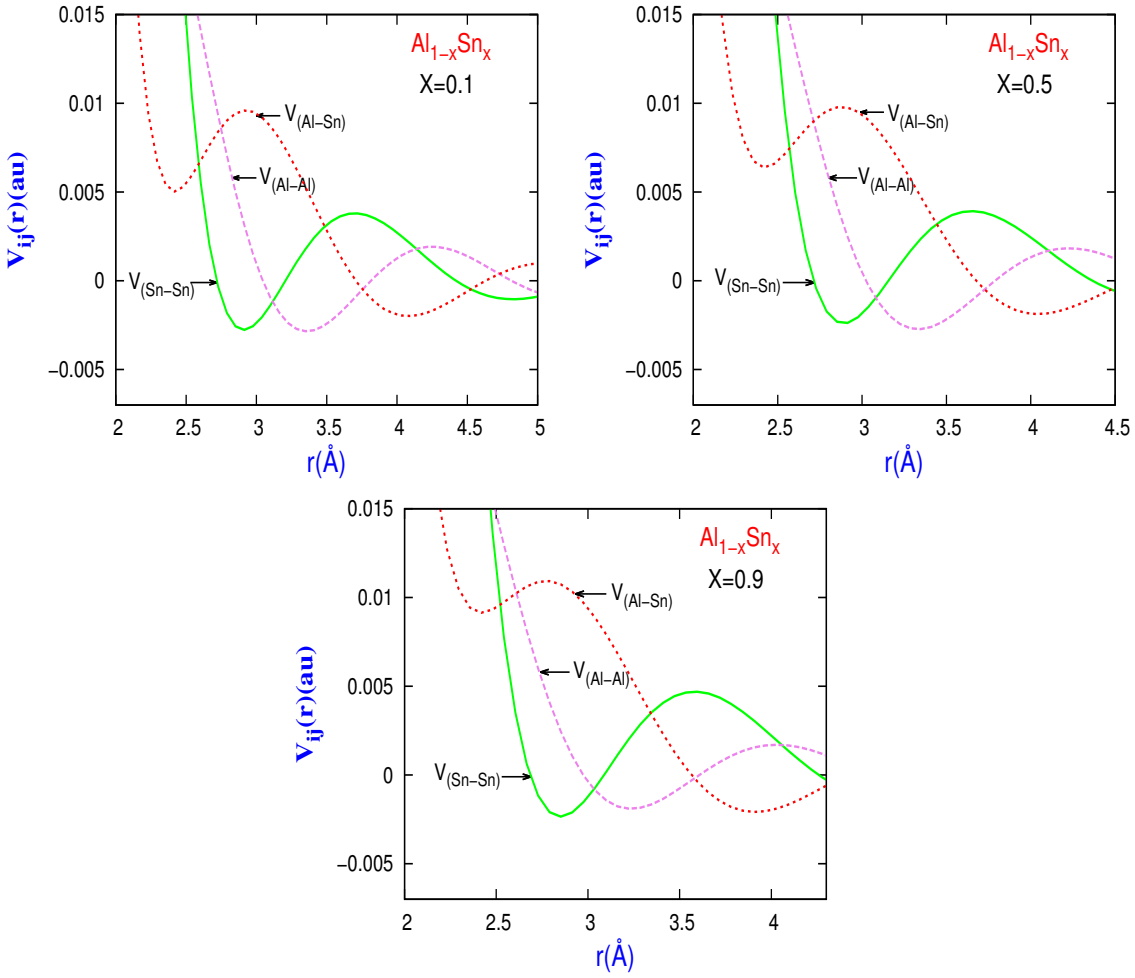

Figure 4.15: Partial pair potential for $Al_{1-x}Sn_x$ liquid binary alloys.

of the partial pair potential, $V_{Al-Sn}(r)$, we have calculated $V(r)$ for pure liquid Al for different values of R_c (see Figure 4.16). It is interesting that for core radius R_c=1.91 a.u, the pair potential does not show a local minimum; rather than exhibits a principal minimum which is followed by Friedel oscillation. Notwithstanding, when the value of R_c is decreased gradually, the depth of the principal minimum reduces and the minimal value shifts from the negative to the positive one.

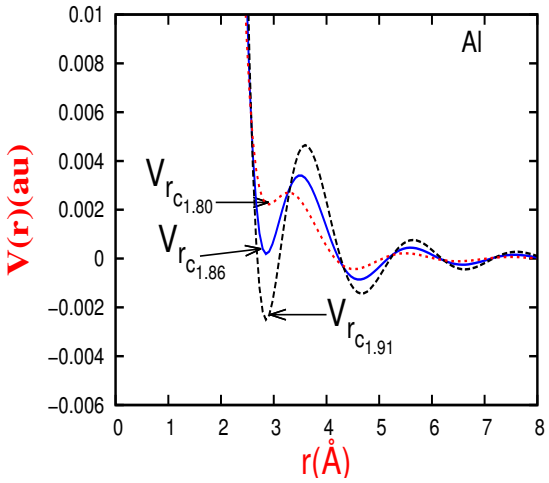

Figure 4.16: Static structure factors for liquid Al element for different core raduis R_c.

Hafner and Jank reported a similar feature for Al with empty core potential for $R_c = 1.12$ a.u. Notwithstanding, they have not performed the calculation with higher values of core radius [57]. In [57, 73–75], it is also reported that even the optimized non-local potentials calculated with relativistic and non-relativistic core orbitals produced similar features. Now, in the present study, the values of R_c for elemental Al and Sn are 1.91 and 1.26 a.u. [57] respectively. The average value of R_c in the alloy state ($= X_1\, R_{C1} + X_2\, R_{C2}$) is 1.58 a.u. which is less than 1.91 a.u. As a result, the local minimum of $V_{Al-Sn}(r)$ potential appears as a characteristic feature due to the influence of Al.

It is worth for noting here, that the BS-model uses the empty core potential from outside the core.

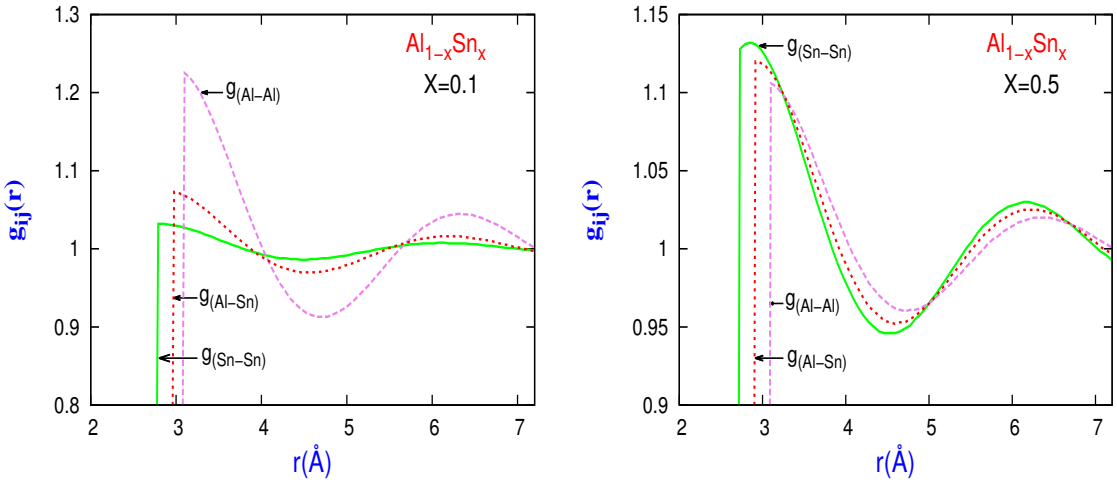

Figure 4.17: Partial pair correlation function.

4.4.2 The Pair Correlation Functions (g_{ij}) for the Reference Hard Sphere Liquids and the Hard Sphere Diameters (σ_{ij}):

Figure (4.17-4.18) illustrate the partial pair correlation functions g_{ij}(r) calculated by using the LWCA [69–72] theory within the HS Percus-Yevick framework for concentrations x =0.1, 0.5, and 0.9, respectively. Figure 4.19 illustrates the partial effective hard sphere diameters, σ_{ij}, for different concentrations of the alloys; this is used in calculating g_{ij}(r). A closer look at the Figure 4.19 reveals that the σ_{Sn-Sn} decreases with increasing concentration of Sn, and σ_{Al-Al} increases with increasing concentration of Al. This is due to the fact that, in the alloy state, the electronic charge is transferred from the atom with higher valence to the atom of lower one [100].

From Figure 4.17 it is also visible that in the Al-rich alloy the height of the principal peak of $g_{Al-Al}(r)$ is maximum whereas the peak of $g_{Sn-Sn}(r)$ is minimum. This scenario reverses for concentration x =0.9, in Figure 4.18 that is, at this concentration, the peak value of $g_{Sn-Sn}(r)$ becomes maximum and that of $g_{Al-Al}(r)$ becomes the minimum value. The pair correlation function, g_{ij}(r) is a measure of

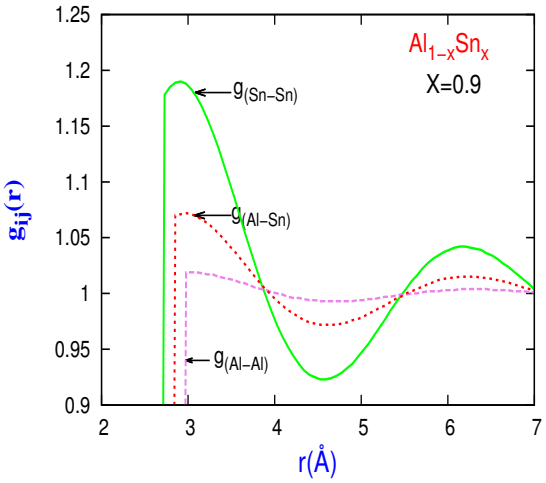

Figure 4.18: Partial pair correlation function.

the probability of finding an ion from another ion located at the origin, so, in Al-rich alloys probability of finding a second Al ion at the nearest neighbor distance will be obviously higher as expected, and vice-versa.

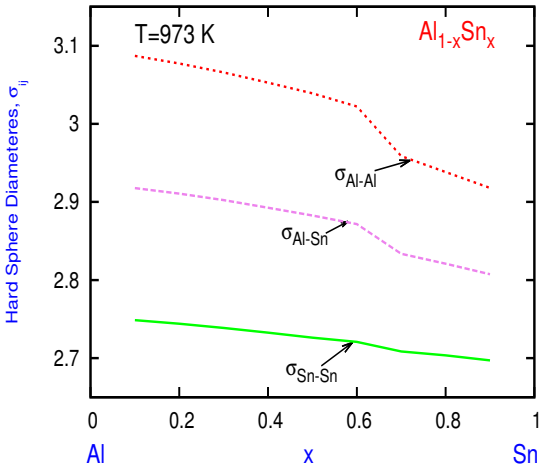

Figure 4.19: Hard sphere diameter for $Al_{1-x}Sn_x$ liquid binary system.

4.4.3 A, ΔA, ΔH and ΔS for $Al_{1-x}Sn_x$ liquid Binary System

Free Energy (A):

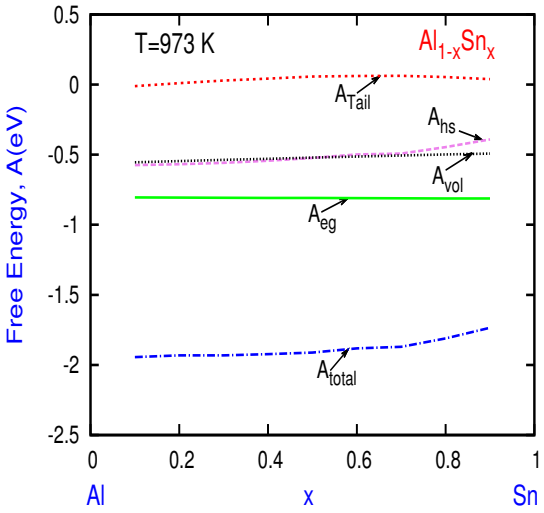

Figure 4.20: Free energy for $Al_{1-x}Sn_x$ liquid binary alloys.

Now we analyze, the results of free energy, (A) for $Al_{1-x}Sn_x$ liquid binary alloys at T=973 K. In this case, we have found almost similar trends as in $Al_{1-x}Zn_x$ and $Al_{1-x}In_x$ for free energy (A). The total features for free energy, (A) has been shown in Figure 4.20 for the concerning system. Similar to the other cases, the largest contribution arises from the electron-gas part, A_{eg}, of the inter-ionic interaction which is a very strange behavior for the concerned $Al_{1-x}Sn_x$ system. The second largest contributory part comes from the HS reference system.

To understand this mystical behavior of A_{eg}, we have to redact our study into twofold. Firstly, we have chosen the valency, Z as an integral value for the alloy forming elements Al and Sn. Regarding, they are heavy polyvalent metals, both of them are from the group IIIB, and IVB, respectively. We have taken Z=3.0 for Al and 4.0 for Sn. As usual, we found that the first contribution arises from A_{eg} and the second contribution from A_{hs}. Lastly, we have considered the hybridization

effect for both Al, Sn and put the value Z=1.50 respectively. As a result, this time we have found that the largest contribution arises from A_{hs} of the HS reference system of the inter-ionic interactions. It actually patents that in polyvalent metal with $Z \geqslant 3, 4$ the electron gas, A_{eg} contribution gets larger than the hard sphere, A_{hs} term. The third and fourth contributions come from the Vol A_{vol} and Tail A_{tail} part of the inter-ionic interactions. The results of the A_{vol} contribution is always negative and is increased with increasing the concentrations of this system. And, it is noticeable that the A_{tail} is very small compared to the other three contributory parts which are similar to our previously studied systems. The total free energy of $Al_{1-x}Sn_x$ liquid binary alloy is negative from x=0.1 to 0.9 which is consistent with our expectations. We can show up the magnitude of the contributions as in the following order, $A_{eg} > A_{hs} > A_{vol} > A_{tail}$. The summation of this four individual contribution yields the total free energy A_{total} of the alloys which lies at the bottom in the figure 4.20.

Energy of Mixing (ΔA):

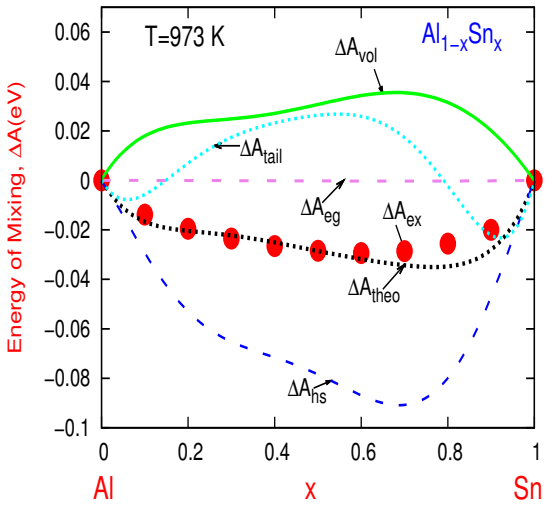

Figure 4.21: Energy of mixing (ΔA) for $Al_{1-x}Sn_x$ liquid binary alloys.

The energy of mixing for liquid binary $Al_{1-x}Sn_x$ alloys at $T = 973$ K is pictorial in Figure 4.21. From the breakdown details of the energy of mixing, it appears that the contribution of the hard sphere reference liquid dominates others and it is negative across the whole range of concentration. The shape of the ΔA profile is asymmetric in nature i.e. its value goes to a minimum in the Sn-rich alloy rather than to be at the equiatomic concentration. On the other hand, the volume contribution of the inter-ionic interaction is positive for the whole span of concentration. The gas term of energy gives a very small contribution, which is almost zero. The contribution of the tail part of the potential shows negative value at a small (up to $x \cong 0.2$) and large ($x \geqslant 0.8$) concentration x and positive magnitudes in between ($0.2 \leqslant x \leqslant 0.8$). However, their combined results yield ΔA, which is negative for all concentrations. When we compare the calculated values with those of experimental ones at 973 K, an excellent agreement is found up to x =0.7. For x >0.7, theoretical values deviate slightly from the experimental ones; if the uncertainty of measurements ($\pm$0.004 eV) is taken into account, the agreement in the region $x = 0.07$ also becomes reasonably good. Recently, Odusute *et al.* [97] studied the energy of mixing for $Al_{1-x}Sn_x$ liquid binary alloys using the self-association model (SAM). In this model, the free energy of mixing is directly related to the free parameters W, known as ordering energy parameter, and η. These parameters are also related to the activity of liquid.

For an arbitrarily chosen parameter value (W/RT=1.97) they (Odusute *et al.*) have found a good agreement for the energy of mixing, but in the case of activity, the agreement is hardly fair for $Al_{1-x}Sn_x$. It is worth for noting that choosing the other value for W and η might yield good agreement for activities but agreement in the case of free energy of mixing could be worse then. In the present study, we have used the microscopic theory involving perturbation scheme and the statistical mechanics. Here, two parameters R_c and a are chosen only to calculate effective pair potentials.

Once it is done, the rest of the calculations (for A ΔA, ΔH, ΔS) are completely parameter free. Not only that, calculations from the theoretical point of view are also self-consistent and as a result, the accuracy of calculations and the predictability of the theory are much more reliable than the empirical and semi-empirical methods.

Enthalpy of Mixing (ΔH) and Entropy of Mixing (ΔS):

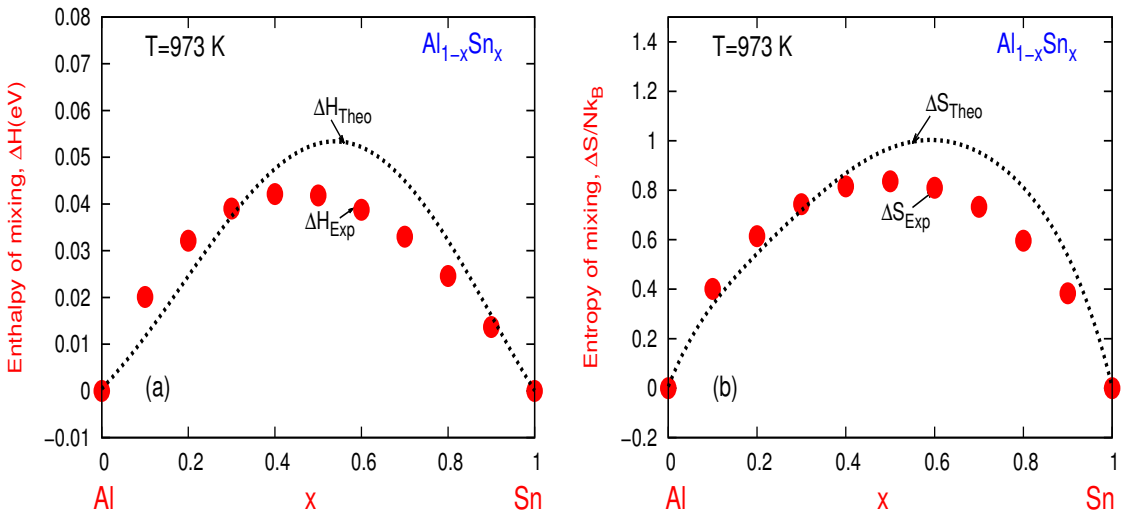

Figure 4.22: Enthalpy of mixing (ΔH) and Entropy of mixing (ΔS) for $Al_{1-x}Sn_x$ liquid binary system.

The calculated results for enthalpy of mixing (ΔH) and entropy of mixing (ΔS) has been presented in Figure 4.22(a-b). ΔS is calculated using equation (8). Here, theoretical values for ΔH and ΔS in different concentrations agree well with experiment [92], at least qualitatively. Theoretical values around the equiatomic concentrations ($0.5 < x < 0.7$) are slightly overestimated. Odusute *et .al* [97] in their work also studied the energy of mixing and the entropy of mixing from the SAM, and the enthalpy is obtained by adding temperature times entropy with the free energy of mixing. But in the entropy calculation, they have used another free parameter, dW/dT, for which they have chosen arbitrarily a value 0.6602, and found a good

agreement with experiment for ΔH as in the case of ΔA.

4.4.4 Conclusion

A systematic study on the thermodynamics of mixing, specifically total free energy [4], energy, enthalpy, and entropy of mixing are presented in this section. Microscopic theories such as the electronic theory of metals treated within the perturbation approach and the statistical mechanics have been employed for numerical calculations. However, from the results of calculations, we can draw the following conclusions.

(i) A combination of pseudopotential theory, first principles perturbation approach and statistical mechanics provides a good starting point for the microscopic description of the thermodynamics of mixing for $Al_{1-x}Sn_x$ liquid binary alloys.

(ii) Agreement between theory and experiment in the case of the energy of mixing (ΔA), is found to be very good within the experimental uncertainty ($\pm$0.004 eV).

(iii) In case of enthalpy of mixing, H, and entropy of mixing, S, the agreement is excellent up to nearly equiatomic concentrations, but in the concentration range $0.5 \leqslant x \leqslant 0.8$ the agreement is not as quantitative as the low concentrations alloys. It is said that the pseudopotential theory has the limited ability in predicting physical properties of the polyvalent metals. Al and Sn both are heavy polyvalent metals with chemical valence 3 and 4, respectively, so, describing Sn-rich alloy will be more difficult, in principle. This is what is reflected through the discrepancy between theory and experiment in Sn-rich alloys. As the entropy of mixing is derived from the energy of mixing and enthalpy of mixing, the agreement between theory and experiment suffers from the backlash of discrepancy in the case of enthalpy.

(iv) However, from the point of view of the good overall qualitative agreement, we can conclude that the present approach could be employed for a microscopic description of other physical properties for $Al_{1-x}Sn_x$ binary alloys as well as to the study of other metallic alloys. We intend to extend the present approach to investigate very interesting segregating properties of $Al_{1-x}Sn_x$ liquid binary alloys, in our next project.

4.5 Thermodynamic Properties for $Al_{1-x}Bi_x$ Liquid Binary System

In this section, the segregating properties of $Al_{1-x}Bi_x$ liquid binary alloys through the thermodynamic route that involves energy of mixing (ΔA), enthalpy of mixing (ΔH) and entropy of mixing (ΔS) will be discussed. In the alloy state, the inter-ionic interactions differ largely from those of individual components that form the alloys. Consequently, a tendency for miscibility or segregation or phase separation increases in some metallic alloys. This mysterious feature of segregation of liquid binary metallic alloys is yet to be completely understood microscopically. This understanding is necessary for the application of segregating materials for technological advancement.

The knowledge of segregation of some liquid metallic binary alloys has been advanced so far by different authors, from the point of the electronic theory of metal in conjunction with the perturbation approach. Bhuiyan *et .al* [53, 54, 101] showed that in their articles, that the origin of the positiveness of the energy of mixing, a characteristic feature of segregation, is strongly related to the volume contribution to the free energy of mixing. This is important to note that, those studies successfully predicted not only the energy of mixing but also some segregating properties such as critical concentrations and critical temperatures of these systems. The present study is also the consecutive series study in which I have studied the thermodynamic mixing properties for $Al_{1-x}Bi_x$ liquid binary system keeping the main focus on the segregation behaviors for verifying the critical temperature and critical concentration [102–107], respectively.

4.5.1 The Effective Partial Pair Potentials (V_{ij})

The alloy, $Al_{1-x}Bi_x$ is formed by two different elements Al and Bi. Al lies in the group IIIB of the periodic table. It has a face-centered-cubic (fcc) structure in the solid phase and its melting point is 933 K. It is a superconducting material. The chemical valency, Z is 3 for Al. On the other hand, Bi is a Basic-metal that lies in the group VB of the periodic table. It has a rhombohedral crystal structure in the solid phase and its melting temperature is 544 K. It becomes a superconductor under high pressure. The chemical valency of Bi is 3 and 5 respectively [4, 29]. There are some shreds of evidence [108–110] from the point of the quasi-lattice theory that the peculiarity in behavior is related to the structural fluctuation. In any way, liquid $Al_{1-x}Bi_x$ is a segregating alloy [102–107]. The study is being carried on the basis of changing the concentrations of Al_{1-x} from 0.9 to 0.1 to study the thermodynamic mixing properties of segregation for ΔA, ΔH, and ΔS of $Al_{1-x}Bi_x$ liquid binary system at different thermodynamic states.

Figure 4.23 shows the effective inter-ionic partial potentials for $Al_{1-x}Bi_x$ liquid binary alloys for three different concentrations (x =0.1, 0.5 and 0.9). Partial pair potentials, V_{Al-Al} and V_{Bi-Bi}, respectively, exhibit the usual behavior that potential decreases rapidly to a minimum value and then increases with increasing r, and then perform the so called Friedel oscillation due to the fluctuation of electronic charge density [4, 27, 29]. But, V_{Al-Bi}(r) exhibits a different feature at concentration x=0.9; a local minimum at small r appears first and then gradually increase and starts oscillation with a minimum value at large r (around 4.5Å). In order to examine the origin of this unusual feature of the local minimum of the partial pair potential, V_{Al-Bi}(r), we have calculated $V(r)$ for pure liquid Al and Bi for different R_c values (see Fig 4.24). It is interesting that for core radius R_c=1.91 a.u., the pair potential does not show a local minimum; it rather exhibits a principal minimum followed

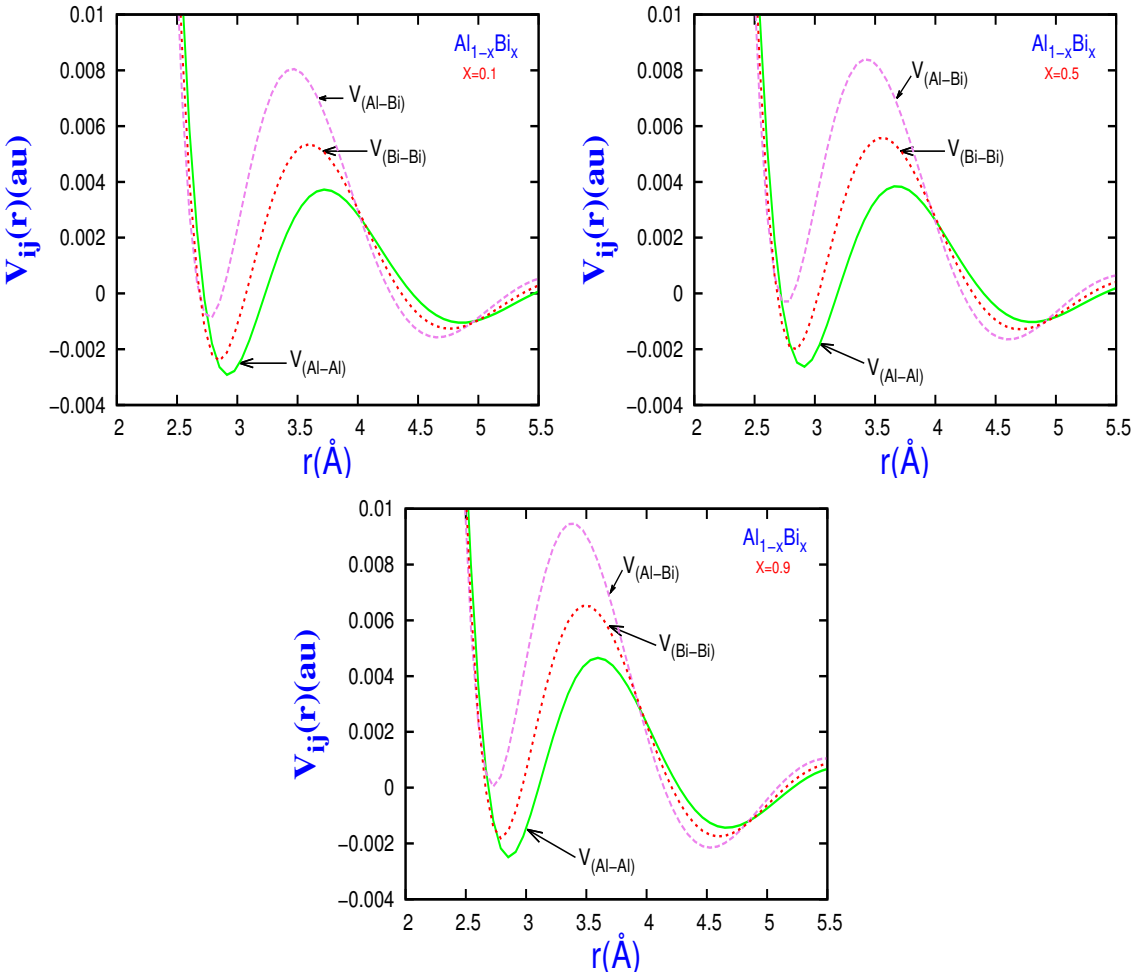

Figure 4.23: Partial pair potential for concentrations x=0.1, 0.5 and 0.9 for $Al_{1-x}Bi_x$ liquid binary alloy at T=1173 K.

by the Friedel oscillation [27]. But, when the value of R_c is decreased gradually, the depth of the principal minimum reduces and the minimal value shifts from the negative to the positive one.

For Bi, R_c=1.49 a.u, the pair potential does not show a local minimum. Hafner and Jank reported [73–75] a similar feature for Al with empty core potential for $R_c = 1.12$ a.u. However, they have not performed the calculation with higher values of core radius [74]. In [73–75] it is also reported that even the optimized non-local potentials calculated with relativistic and non-relativistic core orbitals produced sim-

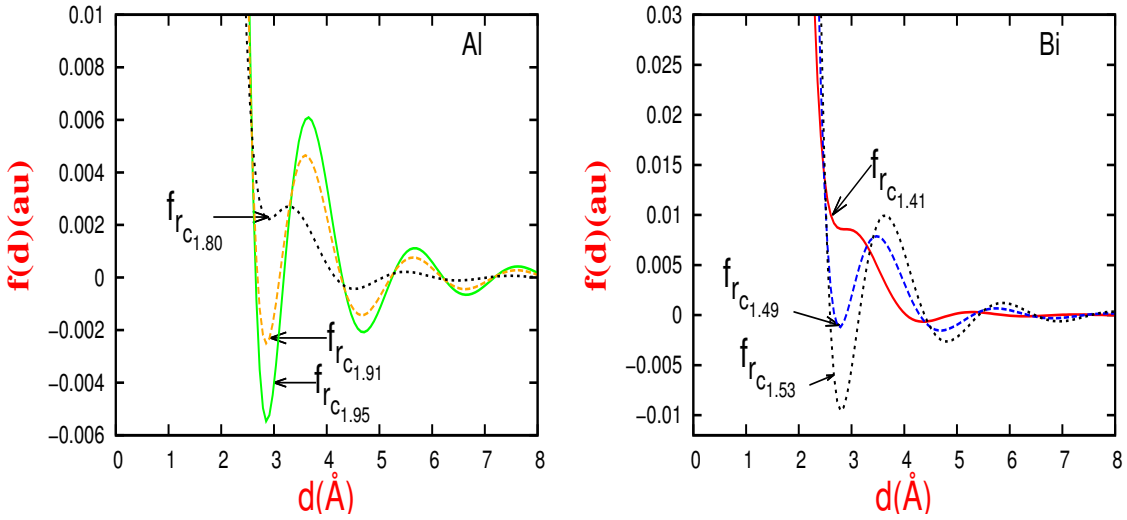

Figure 4.24: Static structure factors for liquid Al and Bi for different core radius R_c.

ilar features. Now, in the present study, the values of R_c for elemental Al and Bi are 1.91 and 1.49 a.u., respectively. The average value of R_c in the alloy state ($= X_1\, R_{C1} + X_2\, R_{C2}$) is 1.70 a.u. which is less than 1.91 a.u. As a result, the local minimum of V_{Al-Bi}(r) potential appears as a characteristic feature due to the influence of Al. It is worth noting here that the BS-model uses the empty core potential outside the core.

4.5.2 The Pair Correlation Functions (g_{ij}) for the Reference Hard Sphere Liquids and the Hard Sphere Diameters (σ_{ij}):

Figure 4.25 illustrates the partial pair correlation functions, g_{ij} calculated by using the LWCA [69–72] theory within the HS Percus-Yevick framework for concentrations x =0.1, 0.5 and 0.9, respectively, at thermodynamic state 1173 K. Figure 4.26 illustrates [4] the partial effective hard sphere diameters (σ_{ij}) for different concentrations of the alloy which are used in calculating g_{ij}. A closer look at the Figure 4.26 unfolds

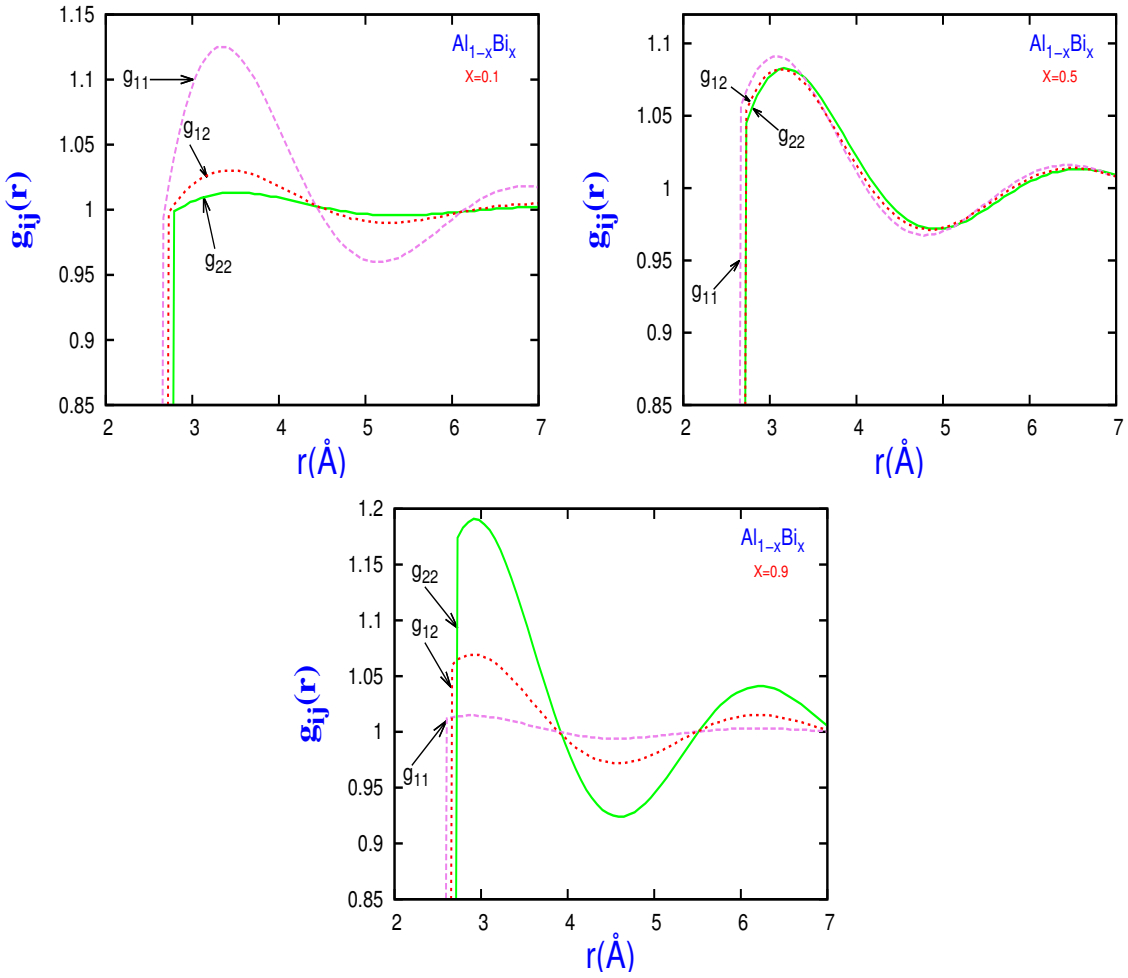

Figure 4.25: Partial pair correlation function for $Al_{1-x}Bi_x$liquid binary alloys.

that the σ_{Bi-Bi} decreases with increasing concentration of Bi, and σ_{Al-Al} increases with increasing concentration of Al. This is due to the fact that, in the alloy state, the electronic charge is transferred from the atom with higher valency to the atom with lower one [111–119]. From Figure 4.25, it is also noticed that in the Al-rich alloy, the height of the principal peak of g_{Al-Al}(r) is maximum whereas the peak of g_{Bi-Bi}(r) is minimum. This scenario reverses for concentration x =0.9, that is, at this concentration the peak value of g_{Bi-Bi}(r) becomes maximum and that of g_{Al-Al}(r) becomes minimum. g_{ij} is a measure of the probability of finding an ion from another ion located at the origin, so, in Al-rich alloys, the probability of finding a second

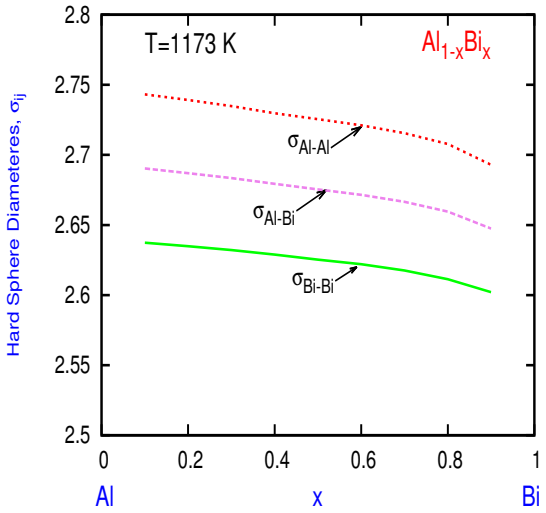

Figure 4.26: Hard sphere diameter for $Al_{1-x}Bi_x$ liquid binary alloys.

Al ion at the nearest neighbor distance will be obviously higher as expected and vice-versa.

4.5.3 Systematic Study of Segregation for $Al_{1-x}Bi_x$ liquid Binary System

The results of segregation for the energy of mixing, enthalpy of mixing and entropy of mixing for $Al_{1-x}Bi_x$ liquid binary system will be discussed here gradually.

Energy of Mixing (ΔA):

Energy of mixing for $Al_{1-x}Bi_x$ liquid binary alloys at $T = 1173$ K is illustrated in Figure 4.27. From the breakdown details of the energy of mixing, it appears that the contribution of the hard sphere reference liquid dominates others and is negative across the whole range of concentration. The shape of the ΔA profile is asymmetric in nature. It goes to a certain region which is in minimum in Bi mixture alloys rather than to be at the equiatomic concentration. On the other hand, both the tail and the volume contribution part of the inter-ionic interaction is positive for the whole range

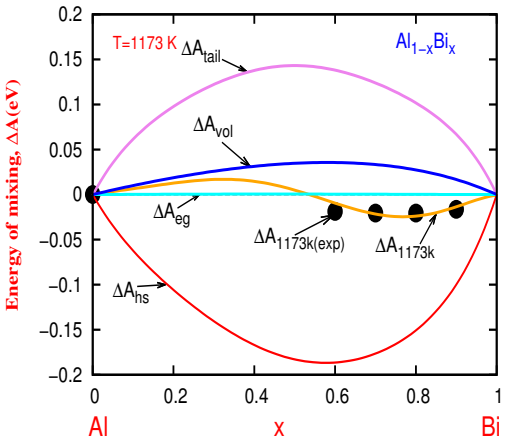

Figure 4.27: Energy of mixing as a function of concentration for $Al_{1-x}Bi_x$ liquid binary alloys at 1173 K.

of concentration. The gas term of energy gives a very small contribution, which is almost zero. We note here that the contribution of the volume part of the potential becomes positive for segregating alloys [100–107].

But it is interesting that, unlike other segregating alloys [53, 101], the tail part of the inter-ionic interaction is positive for the whole range of concentration for $Al_{1-x}Bi_x$ and exhibits positive values up to x=0.1 to 0.9 [54]. However, their combined results yield ΔA, which is negative between $0.5 \leqslant x \leqslant 0.9$ and is positive from $0.1 \leqslant x \leqslant 0.5$ concentrations range. The combination of all contributions, ΔA, agree very well, as far as experimental uncertainty is concerned, with the available experimental data [92]. It is now interesting to examine the reliability of the parameterization [120–124] made for the local pseudopotential by calculating the energy of mixing at another thermodynamic state and comparing them with corresponding experimental and computational work. Figure 4.27 showed that the agreement of ΔA with experimental data is reasonably good for T=1173 K. This result also reflects the suitability of the potentials, those are used in the present study.

Figure 4.28 also demonstrates that the values of ΔA increase and move towards

positive values with decreasing temperature. It appears that at temperature T=1350 K, values of ΔA remain negative across the full concentration range while it becomes partially positive for T=1290 K. Further reduction of temperature increases the concentration width of segregation gap gradually and become positive for complete concentration range at T=1050 K. Positivity of ΔA manifests the segregation to occur. From the above result, one can infer qualitatively that the critical temperature of segregation is 1290 K for $Al_{1-x}Bi_x$ liquid binary alloys.

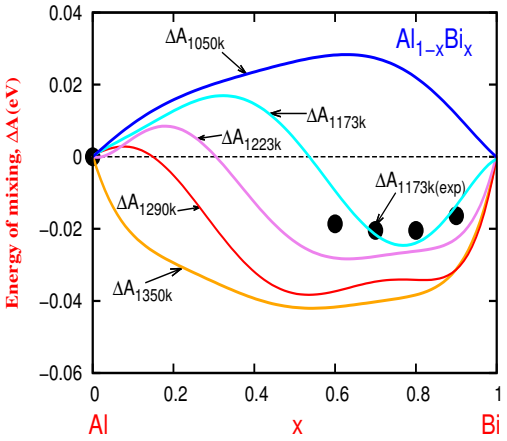

Figure 4.28: Energy of mixing as a function of concentration for $Al_{1-x}Bi_x$ liquid binary alloys at different temperatures.

It is also noticed from the figure (Figure 4.28) that the critical concentration of segregation is at x=0.15. The observed critical concentration reported by A.J. McAlister [102] is 0.1975. This value is very close to our theoretical study. The corresponding critical temperature reported in [100–107] is 1310 K in different journals [4, 29]. So the theoretical value for both critical concentration and critical temperature agree fairly well with the experimental as well as with other theoretical results.

As the positivity of the energy of mixing indicates the segregation for the system whereas the fundamental components namely ΔA_{vol} and ΔA_{Tail} are the main contributor to the energy of mixing, those dictate segregation to happen for $Al_{1-x}Bi_x$

liquid binary alloys.

Enthalpy of Mixing (ΔH) and Entropy of Mixing (ΔS):

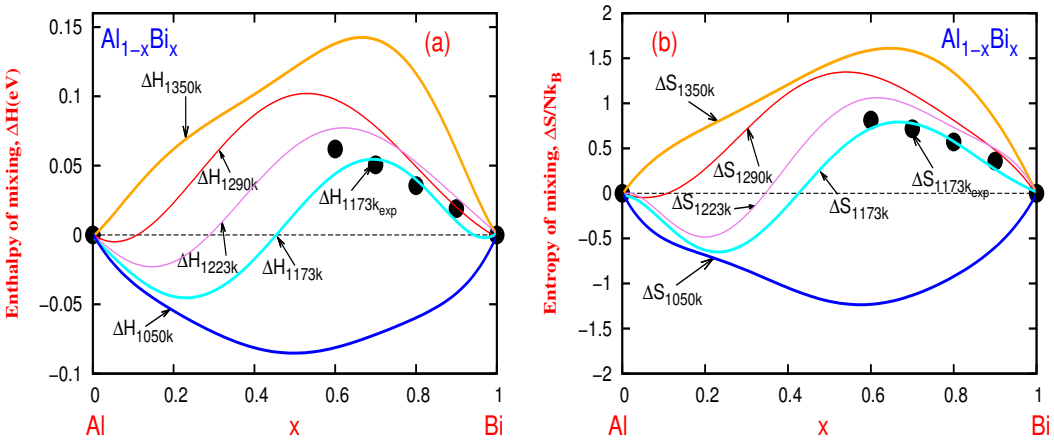

Figure 4.29: Enthalpy of mixing (ΔH) and Entropy of mixing (ΔS) for $Al_{1-x}Bi_x$ liquid binary system.

We have mentioned above that the positiveness of the energy of mixing indicates segregation of $Al_{1-x}Bi_x$ liquid binary alloys. But in the case of enthalpy of mixing (ΔH) and entropy of mixing (ΔS), it is just the opposite, that is, the negativity of ΔH and ΔS manifest segregation of alloys. In order to examine whether the entropy of mixing for the present system of the alloy can predict segregation or not, we have calculated ΔH and ΔS at different thermodynamic states characterized by temperature, T. The calculated results for the enthalpy of mixing (ΔH) and the entropy of mixing (ΔS) as well as segregation are presented in Figure 4.29(a-b) respectively. These are calculated using equation (8) and (10) one after another.

Figure 4.29(a-b) showed that the magnitude of ΔH and ΔS decrease with decreasing temperatures and become partially negative at T=1173 K. For, T<1173 K the concentration gap increase gradually and at T= 1050 K, the gap becomes the largest one. The critical concentration and critical temperature are found for both

the enthalpy of mixing and entropy of mixing are x_c=0.15 and 1290 K, respectively. Most interestingly, these critical values are found to be the same as those obtained from the energy of mixing. Final results from different thermodynamic probes fairly justify the reliability of our approach.

4.5.4 Conclusion

The segregation properties of $Al_{1-x}Bi_x$ liquid binary alloys are systematically investigated through three different thermodynamic quantities, namely, the energy of mixing, the enthalpy of mixing and the entropy of mixing. We have applied for the first time, the enthalpy route to the theoretical study of segregation of liquid binary alloys. The calculated results for ΔA, ΔH, and ΔS are found well in agreement with the corresponding experimental data [92] in the mixed state. However, ΔA_{vol} for $Al_{1-x}Bi_x$ system becomes positive for all concentrations as found in the other segregating alloys [54,101], and thus satisfies the characteristic criteria. But for the present alloy, the ΔA_{tail} also becomes positive for all concentrations and dominates unlike other segregating alloys ($Cu_{1-x}Fe_x$, $Co_{1-x}Cu_x$). Most importantly, ΔA, ΔH, and ΔS are calculated using the same inter-ionic interactions and pair correlation functions, and all these results describe the critical concentration, and critical temperature of segregation for the $Al_{1-x}Bi_x$ alloys with the same level of accuracy. However, ΔA_{tail}, and ΔA_{hs} increase gradually with decreasing temperature. We have observed that a fine balance of all these contributions ultimately turns the segregation of liquid $Al_{1-x}Bi_x$ binary alloys on. The critical concentration for $Al_{1-x}Bi_x$ alloys is found in the Al-rich alloys unlike the other segregating alloys [54, 101] for which the values for x_c is not found to be close to the equiatomic concentration.

4.6 Thermodynamic Properties for $Al_{1-x}Cu_x$ Liquid Binary System

In this section, I will discuss gradually the thermo-physical properties as well as Free energy (A), Energy of mixing (ΔA), Enthalpy of mixing (ΔH) and Entropy of mixing (ΔS) for $Al_{1-x}Cu_x$ liquid binary alloys at temperature 1373 K, within the first principle approach, specifically employing the perturbation method and the electronic theory of metals (ETM). The ingredients of this approach are the effective partial pair potentials (V_{ij}) and partial pair correlation functions (g_{ij}). So, I will start the discussion for the results of the concerning Al-alloys from these ingredients.

The study is carrying on the basis of changing the concentrations of Al_{1-x} from 0.9 to 0.1.

4.6.1 The Effective Partial Pair Potentials (V_{ij})

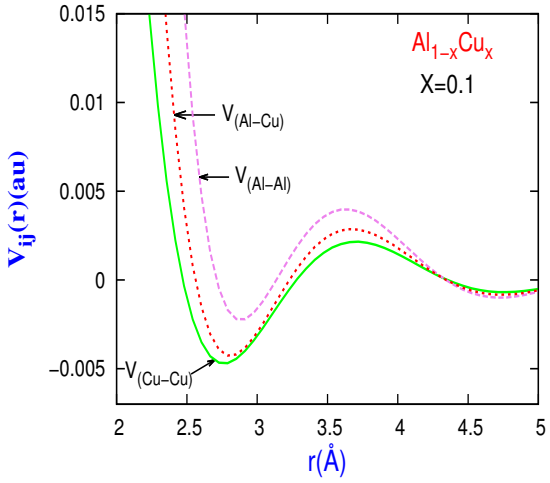

Figure 4.30: Partial pair potential for concentration x=0.1 for $Al_{1-x}Cu_x$ liquid binary alloy.

Figure (4.30-4.31) showed that the effective partial pair potentials for $Al_{1-x}Cu_x$

liquid binary alloys for concentrations x=0.1, 0.5, and 0.9, respectively. The position of the principal potential minimum and the depth of the potential are the results of the exquisite balance between the repulsive and attractive interactions in metals and their corresponding alloys. From our previous study [56] of elemental systems [4, 15, 17, 19, 37, 39, 44, 49], we can claim that this is our second local minima and it appears when after the first local minimum disappear. Here, the second minimum behaves like the principal minimum and is followed by Friedel oscillations [27, 47, 56, 57]. From the pseudopotential formalism, we can easily say that the direct interactions occur between ion cores and the indirect interactions occur also between the ion core and the conduction electrons. In determining the effective pair potentials, the dielectric function for screening plays an important role.

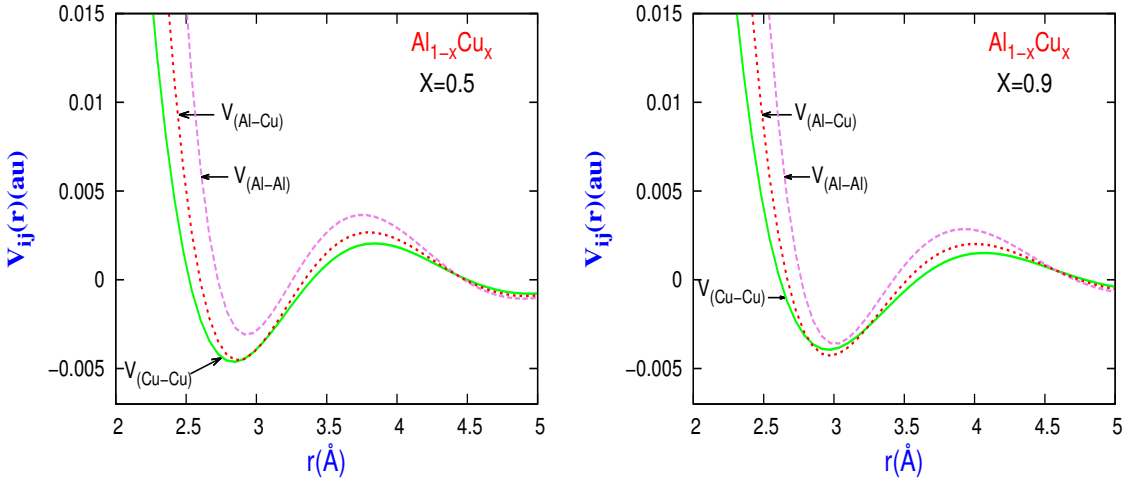

Figure 4.31: Partial pair potential for concentrations x=0.5 and 0.9 for $Al_{1-x}Cu_x$ liquid binary alloy.

From Figure (4.30-4.31), it is also observed that the depth of the well of the potential is the largest for V_{Cu-Cu} and smallest for V_{Al-Al} . The well for V_{Al-Cu} lies in between for concentration x< 0.9. For x=0.9 the potential well for V_{Al-Cu} goes below to that of V_{Cu-Cu}. This feature is very unusual and we have not observed in any alloys which we have studied so far. In all cases, we have found V_{Al-Cu} in between

V_{Al-Al} and V_{Cu-Cu} without any exception. But if the negativity is unusually large as in the present case, one may attribute it to the tendency of compound formation.

4.6.2 The Pair Correlation Functions (g_{ij}) for the Reference Hard Sphere Liquids and the Hard Sphere Diameters (σ_{ij}):

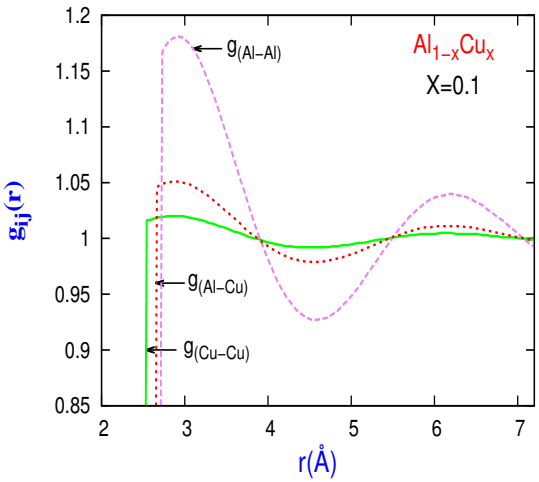

Figure 4.32: Partial pair correlation function for $Al_{1-x}Cu_x$ liquid binary alloys for concentration x=0.1.

We evaluated the partial pair correlation function for our present research work using the Ashcroft-Lagranth [125] theory for the hard sphere. In order to calculate g_{ij}(r), the essential parameter is the effective hard sphere diameter which we determine by using the thermodynamic perturbation theory known as linearized WCA (LWCA) [69–72]. In the case of binary alloys, we replace the effective inter-ionic potentials V(r) with partial potentials V_{ij}(r) and follow the same procedure as for the one component systems.

The partial pair correlation function g_{ij} for $Al_{1-x}Cu_x$ liquid binary alloys calculated from the LWCA theory are shown in Figure (4.32-4.33) for three different

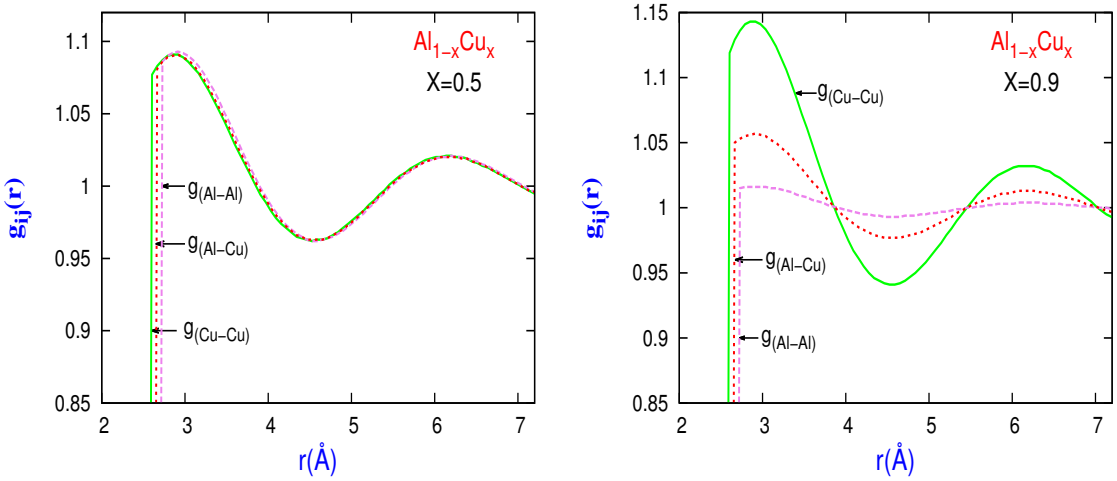

Figure 4.33: Partial pair correlation functions for $Al_{1-x}Cu_x$ liquid binary alloys for concentrations x=0.5 and 0.9, respectively.

concentrations. It is noticed, that for concentration x=0.1, i.e. in the Al-rich alloys the principal peak of g_{Al-Al}(r) is much larger than the g_{Cu-Cu}(r), what is for x=0.1 and this trend reverses for x=0.9, that happens when the alloy becomes rich in Cu concentration. This is due to the fact that, for x=0.1 the alloy is rich in Al.

So, the probability of finding another Al ion from the one at the origin is higher than that of finding a Cu ion and vice versa. This trend, in principle, suggests that for x=0.5 the principal peak value of both g_{Al-Al}(r) and g_{Cu-Cu}(r) should be of equal magnitudes. This is exactly reflected in figure 4.32. We note here that for some alloys, a slight variation of peak values of g_{Al-Al}(r) and g_{Cu-Cu}(r) for concentration x=0.5 might arise due to the size difference of hard spheres.

Hard Sphere Diameter (σ_{ij}):

The hard sphere diameters for the corresponding system has been presented in Figure 4.34. Figure 4.34 illustrates the values of effective hard sphere diameters determined by the LWCA theory [69–72]. The hard sphere contributions from σ_{Al-Cu} always lies between g_{Cu-Cu} and σ_{Al-Al} between concentrations range from x=0.1 to 0.7 which is

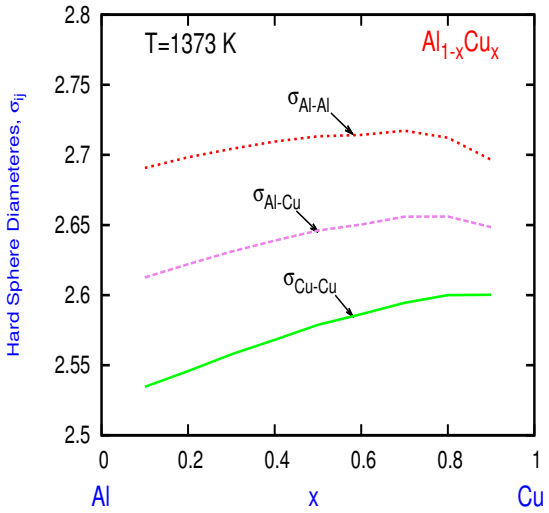

Figure 4.34: Hard sphere diameter for $Al_{1-x}Cu_x$ liquid binary system.

consistent with our theory. In this figure, it is also seen that x=0.1 to 0.7 the values of hard spheres increases with increasing concentrations but at x=0.8 and 0.9 instead of increasing it starts to decrease. At $x \geqslant 0.8$, the alloy is in Cu rich region and due to the hybridization effect, it might have occurred. The values of σ_{ij} can be arranged in order to the hard spheres as $\sigma_{Cu-Cu} \leqslant \sigma_{Al-Cu} \leqslant \sigma_{Al-Al}$.

4.6.3 A, ΔA, ΔH and ΔS for $Al_{1-x}Cu_x$ liquid Binary System

Free Energy (A):

Figure 4.35 interprets the detailed breakdown of the free energy, (A) obtained from general microscopic theory (GMT) for $Al_{1-x}Cu_x$ liquid binary alloys at thermodynamic state 1373 K. We find here that the largest contribution arises from the electron-gas part, A_{eg}, of inter-ionic interactions which is very strange behavior for the concerned Al-based system. The second contributory part comes from the HS reference system.

To understand this obscure behavior of A_{eg}, we have again performed our study in threefold for this system. Firstly, we have chosen the valency, Z as an integral

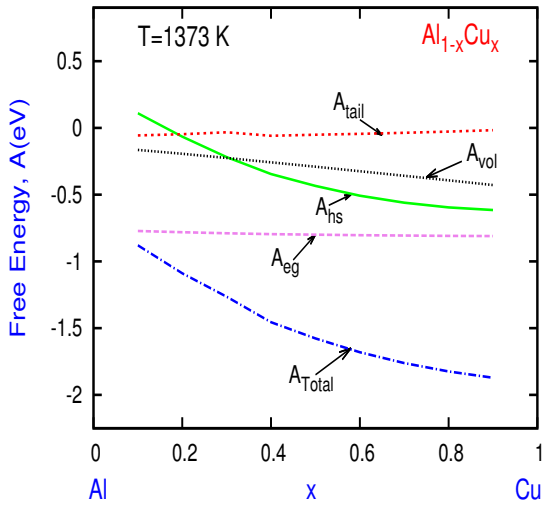

Figure 4.35: Free energy for $Al_{1-x}Cu_x$ liquid binary alloys.

value for the alloy forming elements Al and Cu. We have taken Z=3.0 for Al on the other hand 1.0 and 2.0 for Cu, respectively. We have found that the first contribution arises from A_{eg} and second contribution from A_{hs}. Then, we have fixed Z=3.0 for Al and took the hybridization effect for Cu and put Z=1.30. Similarly, the first and second contribution appeared from the inter-ionic interactions as A_{eg} and A_{hs} respectively. Thirdly, we have taken the hybridization effect both for Al and Cu as 1.50 and 1.30 respectively. As seen in the cases of previous systems this time too we have found the largest contribution comes from A_{hs} of the HS reference system of the inter-ionic interactions. This actually means that in polyvalent metal with $Z \geqslant 3$ the electron gas, A_{eg} contribution gets larger than the hard sphere term. The third and fourth contributions come from the Vol A_{vol} and Tail A_{tail} part of the inter-ionic interactions. The results of A_{vol} contribution is always negative and is increased with increasing the concentrations of the system. And, we have seen always that the A_{tail} is very small comparable to the other three contributory parts. The total free energy of $Al_{1-x}Cu_x$ liquid binary system is alloys negative from x=0.1 to 0.9 which is consistent with our predictions. One can present the magnitude of contribution,

as in the following order $A_{eg} > A_{hs} > A_{vol} > A_{tail}$. Finally, the summation of all four concentrations yields the total free energy A_{total} of the alloy which lies at the bottom in the figure 4.35.

Energy of mixing (ΔA):

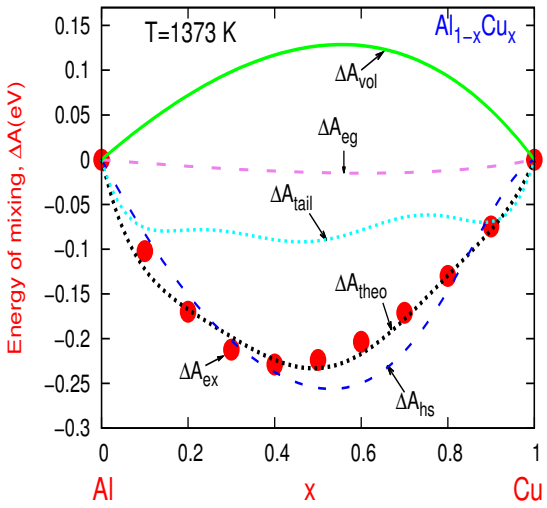

Figure 4.36: Energy of mixing (ΔA) for $Al_{1-x}Cu_x$ liquid binary system.

Figure 4.36 illustrates different parts of Helmholtz free energy of mixing for $Al_{1-x}Cu_x$ liquid binary system obtained using the electronic theory of model (ETM) in conjunction with the perturbation theory. Here it is seen in Figure 4.36 that the largest contribution part comes from the HS reference system which is consistent with our theory and defined as ΔA_{hs}. According to the principle of the first order perturbation method with GMT, this is what we expected. The second largest contribution comes from the tail part and is defined as ΔA_{tail}. The feature of this contributory part is very interesting because it has the oscillatory behavior. From x=0.1 to 0.9, this oscillatory behavior can be easily understood because this is similar to that of Friedel oscillation [27]. Within this range, the ΔA_{tail} is always negative. The third contribution part comes from the electron-gas and is defined as ΔA_{eg}. This is very

small and almost close to zero. The fourth contributory part comes from the volume part and defines as ΔA_{vol}.

The shape of this part as like as parabolic and is positive for the whole range of concentrations which is expected. From x=0.1 to 0.5, it starts to increase and then it starts to decrease from 0.5 to 0.9. However, all four contributions together yield the total energy of forming ΔA_{theo}. We found that, these results agree very well with the available experimental energy of mixing ΔA_{exp} [92] for the full range of concentrations x. And, the experiment [92] suggests that the energy of mixing (ΔA) for the system is 10^{-2} order smaller than the total free energy, A_{total}.

Entropy of mixing (ΔS):

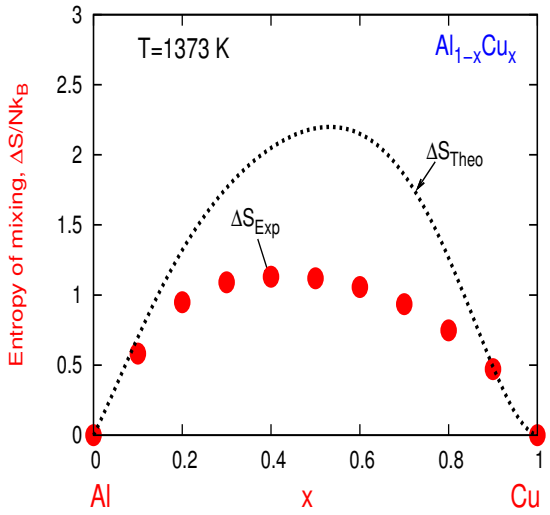

Figure 4.37: Entropy of mixing (ΔS) for $Al_{1-x}Cu_x$ liquid binary system.

Figure 4.37 illustrates the entropy of mixing, ΔS for the concerning system. The results for ΔS of the system is positive for a whole range of concentrations and which is compatible with compare to the experimental results [110]. But our results for ΔS deviated far from the experimental results [110] but shows similar trends.

4.6.4 Conclusion

We, in the present section, have systematically investigated A, ΔA, and ΔS for liquid $Al_{1-x}Cu_x$ binary alloys employing the perturbation method along with the electronic theory of metals. Although the Helmholtz free energy and entropy are closely related to thermodynamically, and the entropy of mixing is much more difficult to calculate as mentioned before. This is because the accuracy of the latter depends on the precise shape of the former one in A versus T curve which is difficult to have in numerical calculation.

From the above results, we can, however, draw the following conclusions. The ETM as described via a local pseudopotential (BS) model in conjunction with the perturbation approach is able to describe the energy of mixing for $Al_{1-x}Cu_x$ binary alloys with a great degree of accuracy. In the case of the entropy of mixing, the calculation is completely free from any adjustable parameter. From this point of view, the result for the entropy of mixing is fairly good qualitatively. The main cause of the discrepancy between theory and experiment in the Cu-rich alloy is in our view, due to the existence of the complicated d-band characteristics including the *sd*- hybridization effect in Cu. In addition, the tendency to form a compound in the Cu rich alloy might also be responsible to widen the discrepancy; in order to establish it, further research is required along with the simulation approach.

So apparently, a quantitative description of thermodynamic properties of $Al_{1-x}Cu_x$ liquid binary alloys from the present approach require a precise account of the *d*-band effects in the inter-ionic interaction with Cu. As our present approach provides total entropy of the elemental and alloy systems, it may be extended to the study of atomic transport properties through the universal scaling laws [85, 86, 126–128]. To conclude, our present approach for free energy calculation may also be applied to the study of temperature dependent on other properties.

4.7 Thermodynamic Properties for $Al_{1-x}Au_x$ Liquid Binary System

The results for the thermodynamic mixing properties for $Al_{1-x}Au_x$ liquid binary system at thermodynamic state 1338 K will be discussed in this section. $Al_{1-x}Au_x$ is the sixth (6^{th}) liquid binary alloys of this series study while the study is carrying on the basis of changing the concentrations of Al_{1-x} from 0.9 to 0.1.

Resembling with $Al_{1-x}Cu_x$ system, the $Al_{1-x}Au_x$ is also a transition alloy. Because Au is a *d*-band transition element and I have taken the hybridization effect for Au in here. In the study of $Al_{1-x}Cu_x$ system, we have found a lot of deviation for the results of enthalpy of mixing (ΔH). But in $Al_{1-x}Au_x$ system, we have found deviation for studied thermodynamical contents like A, ΔA, ΔH, and ΔS. To understand this dislodgement of behavior to compare with experimental results, we need to study the system in different theoretical aspects like simulations and others.

For this system, the results for σ, ΔA, and ΔS [4, 29] will be discussed hereafter to understand the behavior.

Hard Sphere Diameter (σ_{ij}):

The hard sphere diameters (σ_{ij}) for the current system has been presented in figure 4.38. The hard sphere contributions from σ_{Al-Au} always lies between g_{Au-Au} and σ_{Al-Al} with the whole range of concentrations which is consistent with our theory. In this figure, it is also seen that the values of σ_{ij} are decreasing with increasing the concentrations in Au. Surprisingly, at x=0.5, the decrease rate for σ_{ij} is very high to compare the other concentrations. Symbolically, it may be expressed as $\sigma_{Au-Au} < \sigma_{Al-Au} < \sigma_{Al-Al}$.

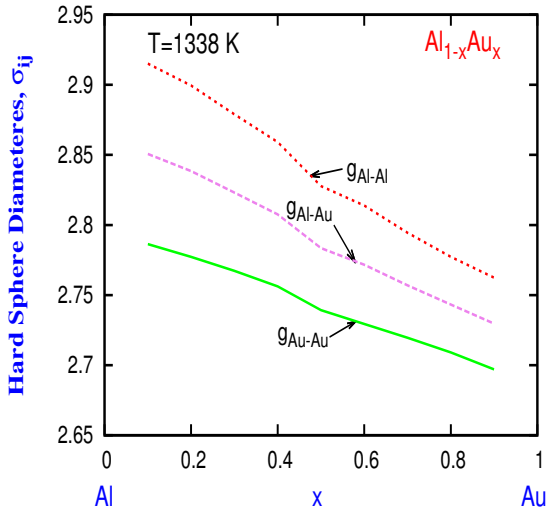

Figure 4.38: Hard sphere diameter for $Al_{1-x}Au_x$ liquid binary system.

Energy of mixing (ΔA) & Entropy of mixing (ΔS):

Figure 4.39 explains the different parts of the free energy of mixing (ΔA) for $Al_{1-x}Au_x$ liquid binary system obtained using the ETM in synchronism with the perturbation theory. It is seen in Figure 4.39, that the largest contribution of the mixing part comes from the HS reference system which is consistent with our theory and defined as ΔA_{hs}. According to the principle of the first order perturbation scheme with GMT, this is what we expected. The tail part is defined as ΔA_{tail} and it gives the second largest contribution of mixing part to ΔA. The feature of this contributory part is very interesting because it has the oscillatory behavior. From x=0.1 to 0.9 range, this oscillatory behavior can easily be comprehended which is similar to Friedel oscillation [4, 27, 29]. Within this range, the ΔA_{tail} is always negative.

The smallest exploiting part of this system is defined as ΔA_{eg} of the inter-ionic interaction and its numerical value is almost very close to zero. The fourth contribution comes for ΔA is Volume part and defined as ΔA_{vol}. The shape of this part is like a parabola and positive for all range of concentrations. From x=0.1 to 0.3, it starts to increase and then it starts to decrease from 0.3 to 0.9. However, all four

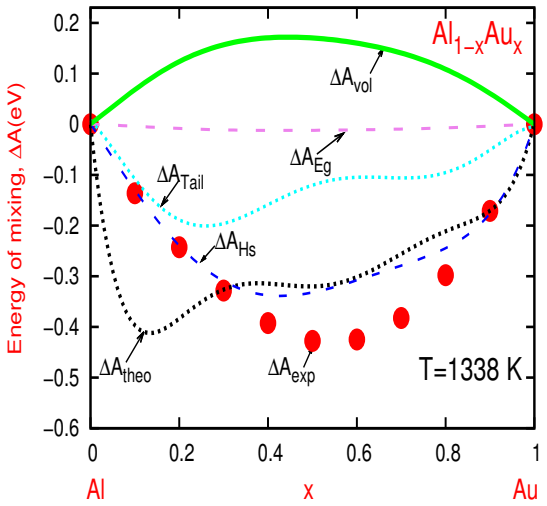

Figure 4.39: Energy of mixing (ΔA) for $Al_{1-x}Au_x$ liquid binary system.

contributions together yield the total energy of forming ΔA_{theo}. We find that these results are deviated more by comparing the available experimental energy of forming ΔA_{exp} [92] for the full range of concentrations x. The greater portion of deviation occurs at the x=0.1 concentration which is the Al rich region also. And, the experiment [92] suggests that the energy of mixing, ΔA for the concerning system that I have found using the ETM model did not pursuit well for the concerning system. But, drawing a concrete conclusion regarding this feature requires further study in detail.

Figure 4.40 illustrates the entropy of mixing, ΔS for the concerning system. The results for ΔS of the system is positive for the whole range of concentrations and which is compatible with compare to the experimental results [92]. But, our results for ΔS deviated far from the experimental results [92], but shows similar trends.

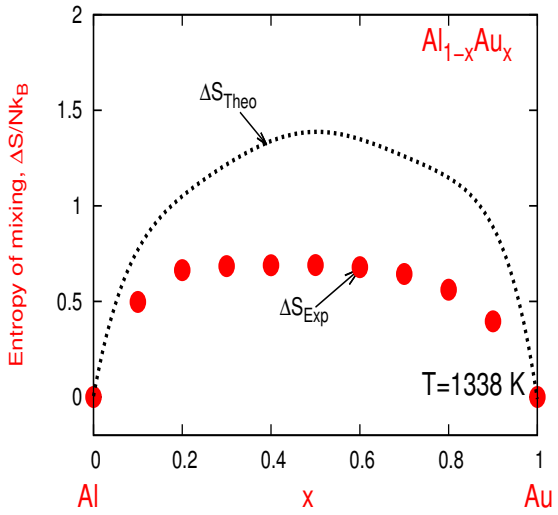

Figure 4.40: Entropy of mixing (ΔS) for $Al_{1-x}Au_x$ liquid binary system.

Although, the approach is quite far from the experimental value in the concentration range from x=0.2 to 0.8, but the shape of theoretical and experimental data are in symmetric in shape which is found in Figure. 4.40. Bhuiyan *et al.* [45] show that, the excess volume correction plays a significant role in the theoretical approach in hybridization effect. But, we do not have the available data for $Al_{1-x}Au_x$ system regarding excess volume correction. Therefore, we could not take it into account in our work. But, we can predict that, the excess volume could play the vital role in the present system.

4.7.1 Conclusion

We have systematically investigated the results for A, ΔA, ΔH, and ΔS for $Al_{1-x}Au_x$ liquid binary alloys employing the perturbation method along with the electronic theory of metals. But, the results that we have found are not good enough to compare with the experimental data [92]. For this, we only present the results for ΔA and ΔS for the liquid binary system. So, further studies are required to understand the thermodynamic mixing behavior in the liquid state for $Al_{1-x}Au_x$ liquid binary alloys.

4.8 Comparative Study for ΔA, ΔH and ΔS for Al-based Alloys

:

Let us compare our results for the energy of mixing (ΔA), the enthalpy of mixing (ΔH), and the entropy of mixing (ΔS) for Al-based liquid binary systems, $Al_{1-x}X_x$; here, X= Zn, In, Sn, and Bi in a common Figures 4.41(a). The results for ΔA of $Al_{1-x}Cu_x$ and $Al_{1-x}Au_x$ systems are very large in scale compare to each other. So it is difficult to adjust to the same figure due to their large range of values. But, the results for these systems can be found in sections 4.6 and 4.7, respectively.

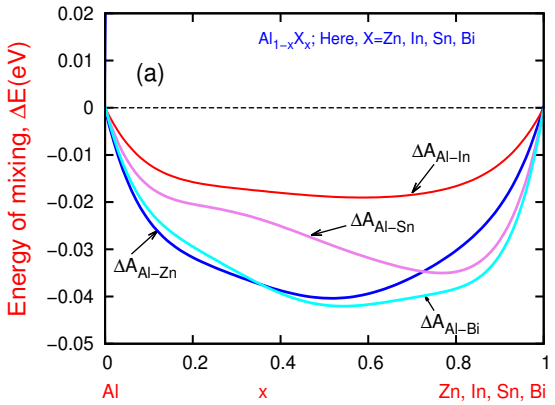

Figure 4.41: Comparing the results of ΔA for Al based liquid binary systems, $Al_{1-x}X_x$; here, X= Zn, In, Sn, and Bi.

Figure 4.41(a) illustrates, the results for ΔA, for $Al_{1-x}Zn_x$, $Al_{1-x}In_x$, $Al_{1-x}Sn_x$ and $Al_{1-x}Bi_x$ liquid binary systems for temperatures 1000 K, 1173 K, 973 K, and 1350 K, respectively. We found that the contribution of the $Al_{1-x}Bi_x$ system is always greater than the other three systems for the whole range of concentrations, except for concentration at x=0.1. Because, in this region, the value of $Al_{1-x}Zn_x$ is greater. At concentrations, x=0.8 and 0.9, the results for ΔA are greater for $Al_{1-x}Sn_x$ system

than $Al_{1-x}Zn_x$ and $Al_{1-x}In_x$ system. Symbolically, the results can be presented for concentration x=0.1, $Al_{1-x}Zn_x > Al_{1-x}Bi_x > Al_{1-x}Sn_x > Al_{1-x}In_x$.

For concentration range x=0.2 to 0.7, $Al_{1-x}Bi_x > Al_{1-x}Zn_x > Al_{1-x}Sn_x > Al_{1-x}In_x$ and finally for concentrations, x=0.8 to 0.9, the results for ΔA of these liquid systems are in order, $Al_{1-x}Bi_x > Al_{1-x}Sn_x > Al_{1-x}Zn_x > Al_{1-x}In_x$.

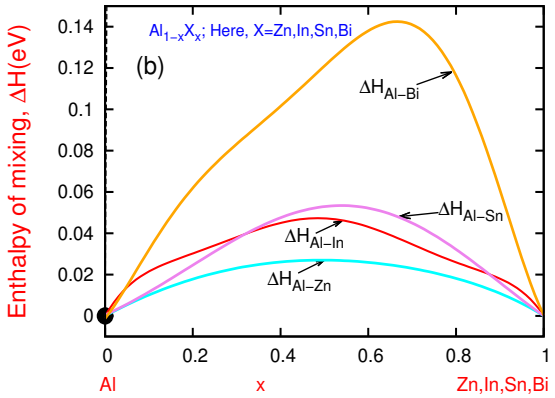

Figure 4.42: Comparing the results of ΔH for Al based liquid binary systems, $Al_{1-x}X_x$; here, X= Zn, In, Sn, and Bi.

Figure 4.42(b) presents, the results for $Al_{1-x}Zn_x$, $Al_{1-x}In_x$, $Al_{1-x}Sn_x$ and $Al_{1-x}Bi_x$ systems for ΔH. We found that, $Al_{1-x}Bi_x$ system gives the largest result for ΔH and is 10 times larger than the others, we have calculated theoretically from concentration range, x=0.1 to 0.9. The results from $Al_{1-x}Zn_x$ system is always smaller for ΔH to compare other systems from x=0.1 to 0.9. Symbolically, one may present the results for ΔH from concentration range x=0.1 to 0.4, as $Al_{1-x}Bi_x > Al_{1-x}In_x > Al_{1-x}Sn_x > Al_{1-x}Zn_x$. From x=0.5 to 0.9 likely to be presented symbolically, $Al_{1-x}Bi_x > Al_{1-x}Sn_x > Al_{1-x}In_x > Al_{1-x}Zn_x$.

The results for ΔS for four different Al-based liquid systems are presented in Figure 4.43(c). We found that, $Al_{1-x}Cu_x$ system gives the largest result for ΔS from

concentration range, x=0.2 to 0.8 (see Figure 4.37). Here, Cu is a transition metal and we have taken the hybridization effect for Cu (Table 4.1). This time the smallest result for ΔS comes from $Al_{1-x}In_x$ liquid system in the concentration range from x=0.1 to 0.9.

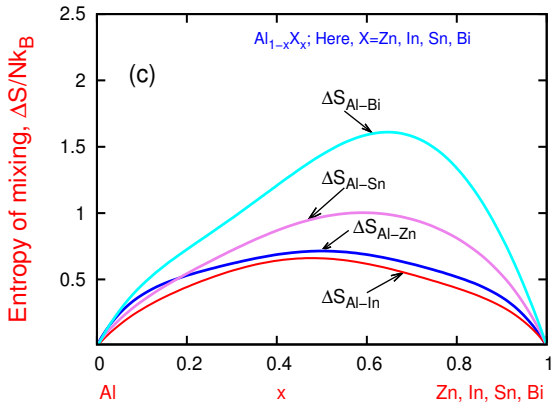

Figure 4.43: Comparing the results of ΔS for Al based liquid binary systems, $Al_{1-x}X_x$; here, X= Zn, In, Sn, and Bi.

Symbolically, one may present the results for ΔS from the concentration range, x=0.1 to 0.5, as $Al_{1-x}Cu_x > Al_{1-x}Au_x > Al_{1-x}Bi_x > Al_{1-x}Sn_x > Al_{1-x}Zn_x > Al_{1-x}In_x$; for concentrations x=0.6 to 0.8, $Al_{1-x}Cu_x > Al_{1-x}Bi_x > Al_{1-x}Au_x > Al_{1-x}Sn_x > Al_{1-x}Zn_x > Al_{1-x}In_x$; for concentration x=0.9, $Al_{1-x}Au_x > Al_{1-x}Bi_x > Al_{1-x}Cu_x > Al_{1-x}Sn_x > Al_{1-x}Zn_x > Al_{1-x}In_x$.

The calculated results employing the perturbation method along with the electronic theory of alloys that we have discussed above for ΔA, ΔH, and ΔS for Al-based liquid binary systems deviate far from experimental results [92], but show the similar trends for all the systems.

4.9 Results & Discussions for Atomic Transport (ATP) Properties

In the present section, theoretically studied results for atomic transport properties (ATP) such as shear viscosity (η), diffusion coefficients (D) and friction coefficients (ζ) for Al-based liquid binary alloys namely $Al_{1-x}Zn_x$, $Al_{1-x}In_x$, $Al_{1-x}Sn_x$, $Al_{1-x}Cu_x$ and $Al_{1-x}Au_x$ will be presented. The essential ingredients for the calculation of ATP are the effective pair potential and the pair distribution function for hard spheres. The Rice-Alnatt theory [59–64] based on the distribution function method is employed here to calculate atomic transport properties as mentioned above.

Necessary ingredients are required to perform the calculations for η, D, ζ, and the ingredients are the inter-ionic interactions and the pair correlation functions of the reference hard sphere systems. We have discussed the ingredients in the study of the thermodynamic of mixings, and used the same functions without any change. In addition, we have employed the BS model [44] for finding the inter-ionic interactions in liquid alloys, used the LWCA [69–72] theory for finding the pair correlation functions, g_{ij}(r) for hard sphere reference liquids, and the Ashcroft-Langreth theory [50] is used for static structure factors for alloys.

The RA theory divides the effective inter-ionic pair potential into a long-range soft part, and a short-range hardcore part. The statistical event due to the short repulsive core of the pair potential at short inter-ionic distances can conveniently be separated from the remaining statistical events considered; this justifies [4] the division of the potential. In the distribution function method, the total viscosity is a sum of three separate contributions. The first one arises from the kinetic theory of dense fluid model through a singlet distribution function [56]. The second contribution arises from the momentum transfer that occurs during the hardcore collisions [63, 64].

This part is derived from using a doublet reduced distribution function. The third contribution for the region $r > \sigma$, σ being the hard sphere diameter, is obtained by deriving the stress tensor for the attractive part of the potential and comparing with the classical Newtonian stress tensor [63,64]. In this process, the friction coefficient is derived by using the small step diffusion theory [4]. Finally, the total shear viscosity reads $\eta = \eta_K + \eta_v(\sigma) + \eta_v(r > \sigma)$. The RA theory for the viscosity involves the pair distribution function of hard spheres and also the first and the second derivatives of the partial pair potential (see below). In a study on viscosity, it is reported [4] that, $\eta_v(r > \sigma)$ evolves as the most dominating term for some liquid metals, while some other studies show that $\eta_v(\sigma)$ dominates more [41–43,58]. Whatever be the situation, the soft part contribution is significant for a quantitative study.

As the first and the second derivatives of the potentials are involved in the RA theory [59–64]. Transport properties are sensitive to the whole potential profile. We need to have appropriate potentials for the concerned liquid systems, as we intend to study the transport properties for both the ATM and ETM of liquid Al-based alloys in which *d*-band plays an important role in determining the physical properties. The transition elements such as Zn, Cu, and Au are involved in $Al_{1-x}Zn_x$, $Al_{1-x}Cu_x$ and $Al_{1-x}Au_x$ systems, have the hybridization effect. However, we have used the same potentials derived from the BS [44] local model to describe the behavior of ATP of liquid Al-based alloys that we have used for studying thermodynamic mixing properties (ΔA, ΔH, ΔS). As this model has already been tested in the study of thermodynamic properties [36–38, 102] that we have recapitulated in the earlier sections, we will employ it again for calculations of η, D, and ζ.

4.9.1 The First and Second Derivatives of the Partial Potential Curve for Different Binary Systems

This study of ATP is dependent on the first and second derivatives of the partial pair potential curves. The effective partial pair potentials v_{ij}(r) for all Al-based alloys under study are obtained from the BS [44] model pseudopotential which is already discussed in earlier sections where the thermodynamic properties are presented. Here, the first and the second derivatives of v_{ij}(r) are shown in Figures (4.44-4.48) for odd values of concentration, x, for different Al-based liquid binary alloys.

These derivatives give a definitive accuracy profile of potential generated by our parameters. The first derivative gives the slope while the second derivative gives the curvature of the potential. These derivatives have the features which explain that, when the slope is negative the curvature becomes positive and vice versa.

This nature is exactly mirrored in these Figures (4.44-4.48). This also provides the level of accuracy of the numerical calculations. It is rather important to say that, the first and the second derivatives converge with increasing r, and also the positions of the minimum in these corresponding Figures (4.44-4.48), change gradually with the increasing values of concentration. These figures are:

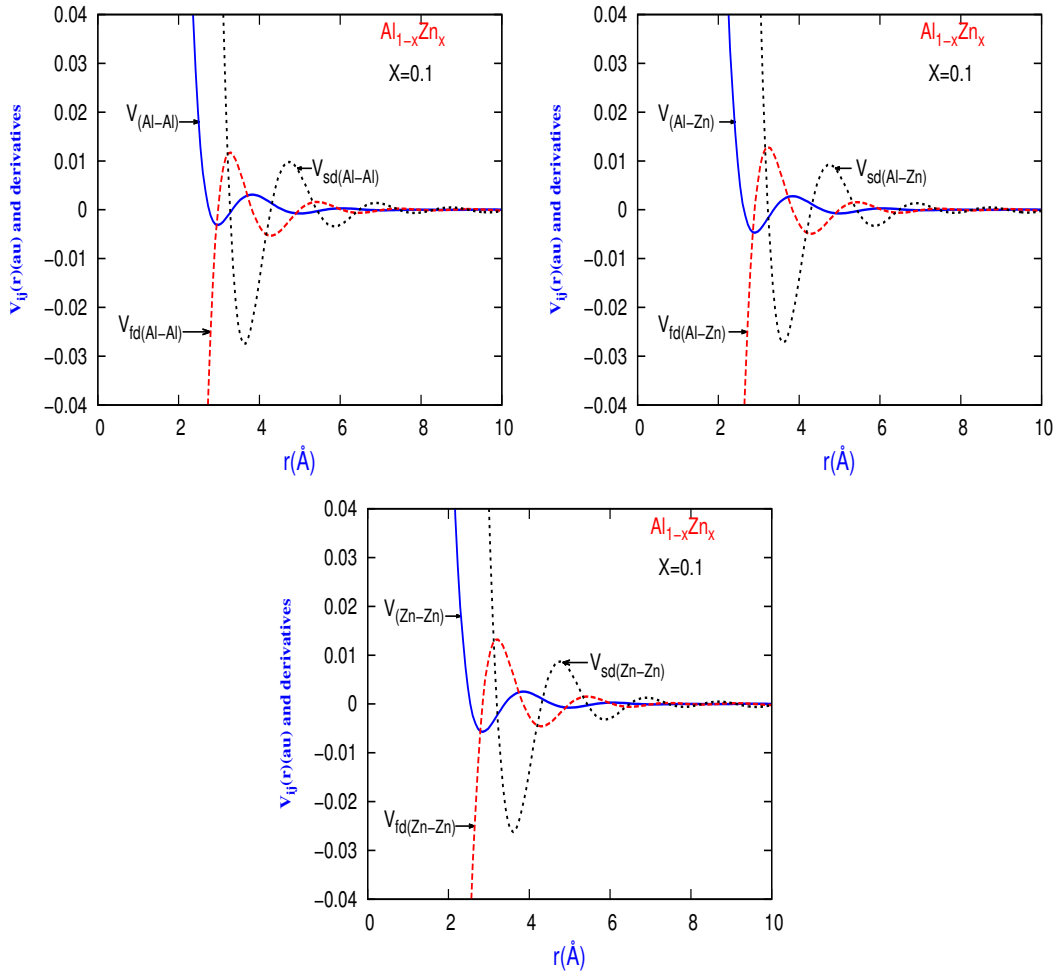

Figure 4.44: Partial pair potential V_{ij} and their derivatives for $Al_{1-x}Zn_x$ liquid binary system for concentration x=0.1 for temperature 1000 K, respectively.

Figures (4.44-4.48) showed that, the first and the second derivatives of the potential profile for $Al_{1-x}Zn_x$, $Al_{1-x}In_x$, $Al_{1-x}Sn_x$, $Al_{1-x}Cu_x$ and $Al_{1-x}Au_x$ liquid binary alloys. It is seen for all the concerning systems mentioned above from Figures (4.44-4.48) that, the oscillations of the first and the second derivatives are 180^0 out of phase with each other. Most importantly, the partial potentials and their derivatives exhibit convergence with increasing r.

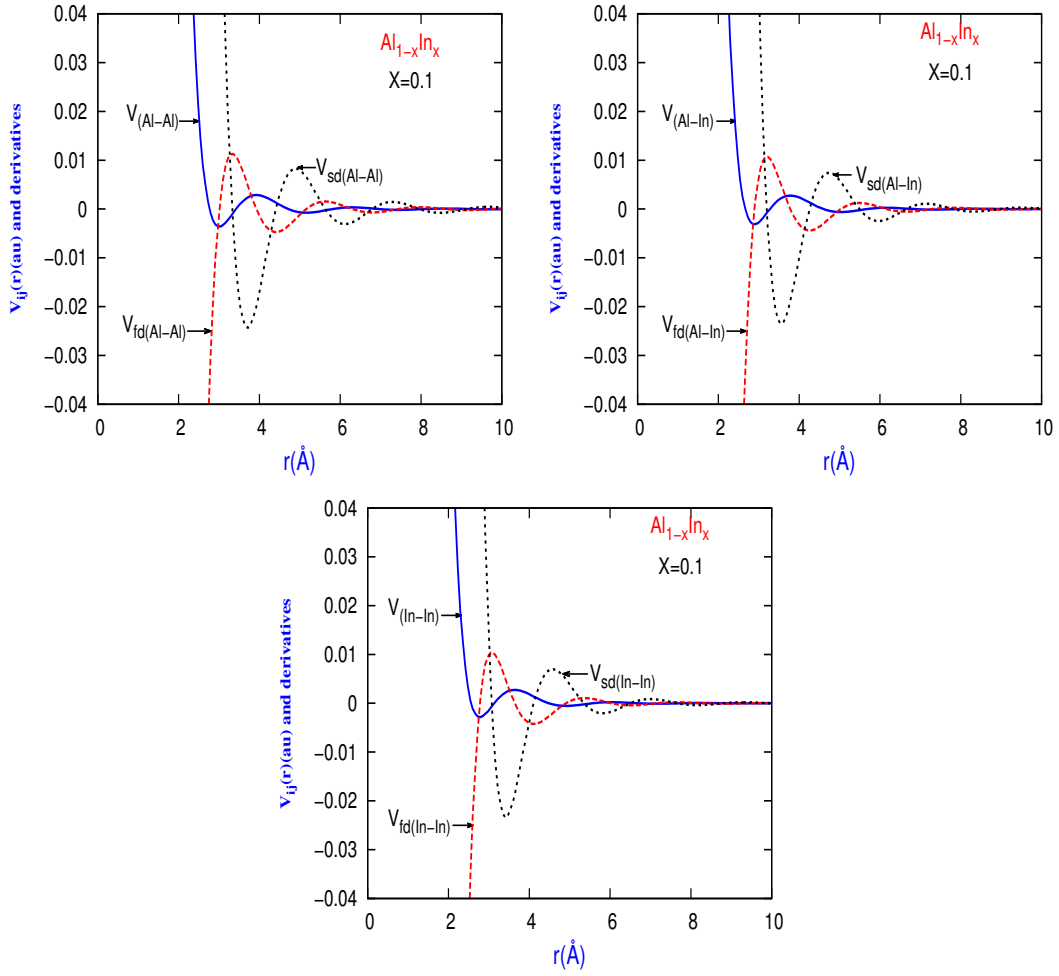

Figure 4.45: Partial pair potential V_{ij} and their derivatives for $Al_{1-x}In_x$ liquid binary system for concentration x=0.1 for temperature 1173 K, respectively.

The major differences observed among these different alloys are that, the depths and positions of the well are larger for $Al_{1-x}Cu_x$ (see Figure 4.47) and $Al_{1-x}Au_x$ (see Figure 4.48). But among these different partial pair potentials, the depth is the smallest in the case of V_{Sn-Sn} for $Al_{1-x}Sn_x$ liquid binary alloy (see Figure 4.46).

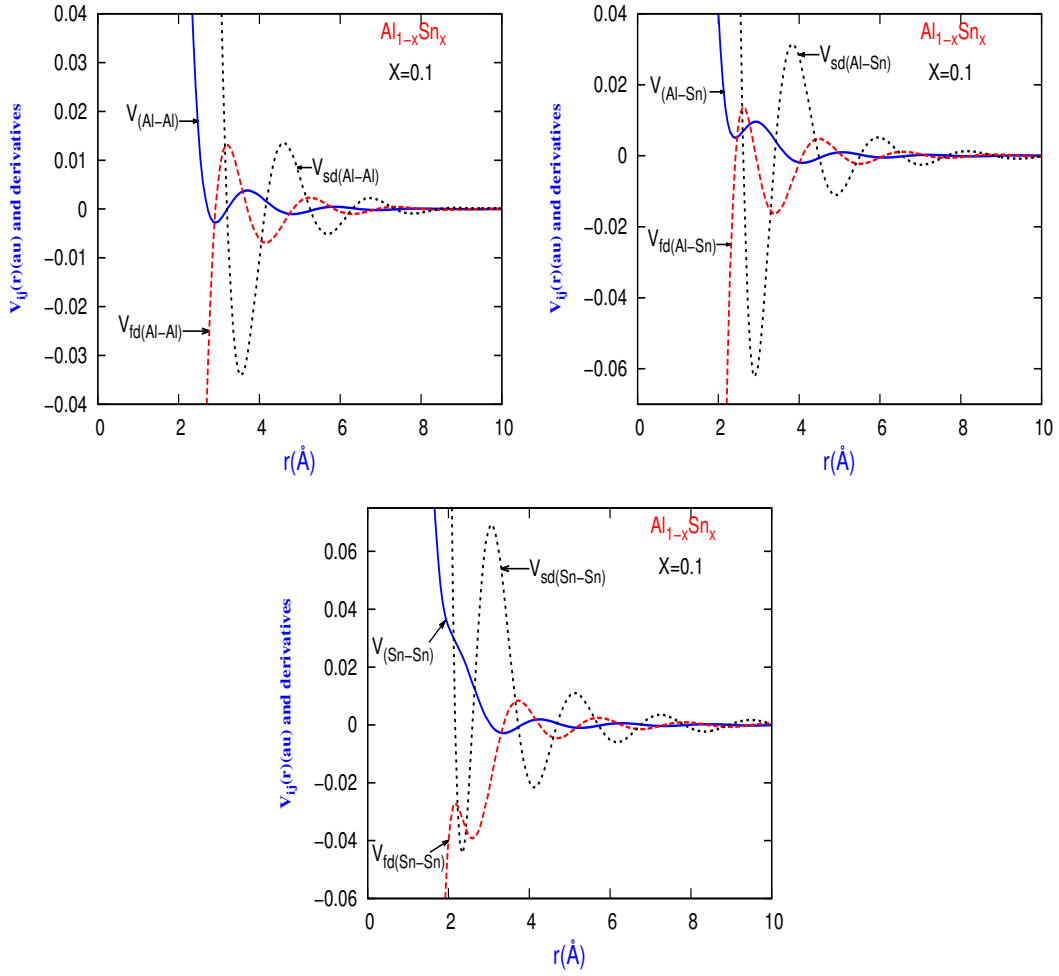

Figure 4.46: Partial pair potential V_{ij} and their derivatives for $Al_{1-x}Sn_x$ liquid binary system for concentration x=0.1 for temperature 973 K, respectively.

The reason is that, Sn largely behaves like simple metals [57], and on the other hand, Cu and Au are transition metals. Besides, I have calculated the partial pair potential for $Al_{1-x}Zn_x$ system without taking any hybridization effect.

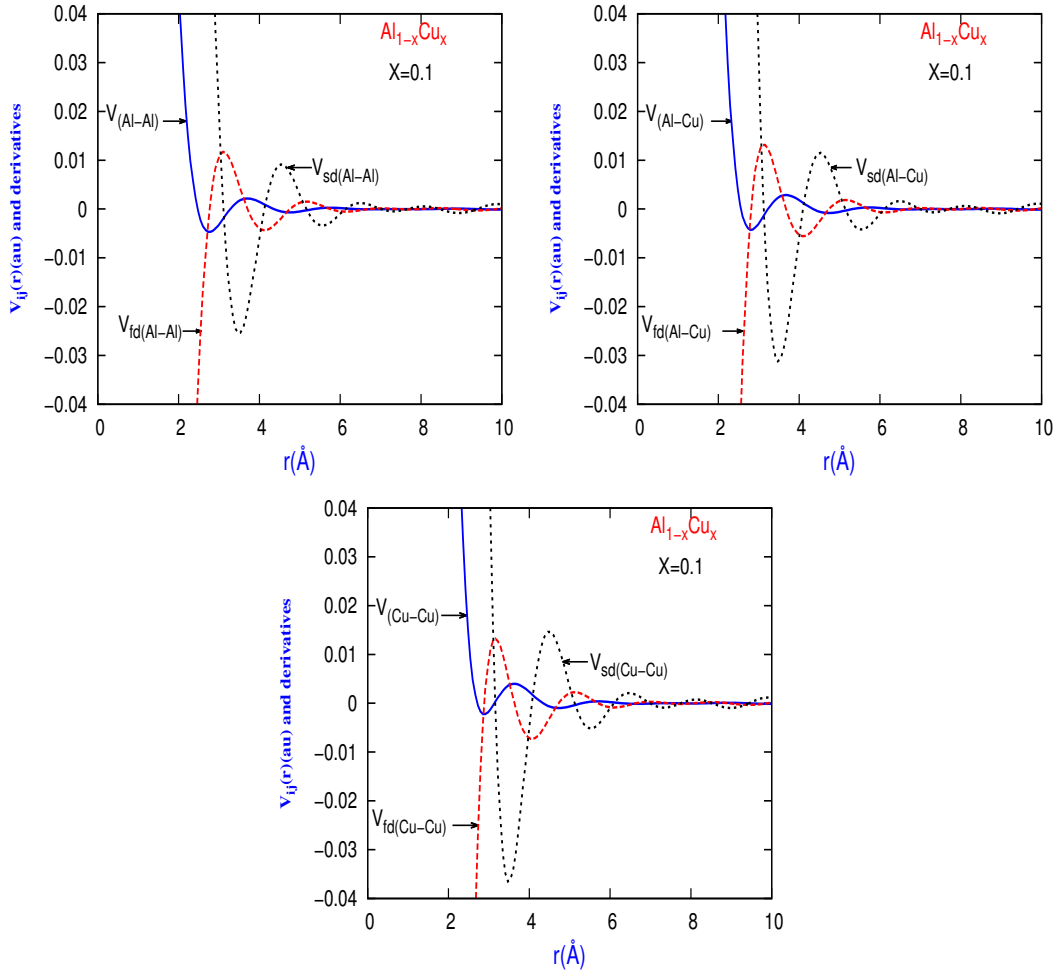

Figure 4.47: Partial pair potential V_{ij} and their derivatives for $Al_{1-x}Cu_x$ liquid binary system for concentration x=0.1 for temperature 1373 K, respectively.

Therefore, one can present the magnitude of the depths, and the positions of the different potential wells for these aforementioned liquid binary alloys in the following order, $Al_{1-x}Au_x > Al_{1-x}Cu_x > Al_{1-x}In_x > Al_{1-x}Zn_x > Al_{1-x}Sn_x$.

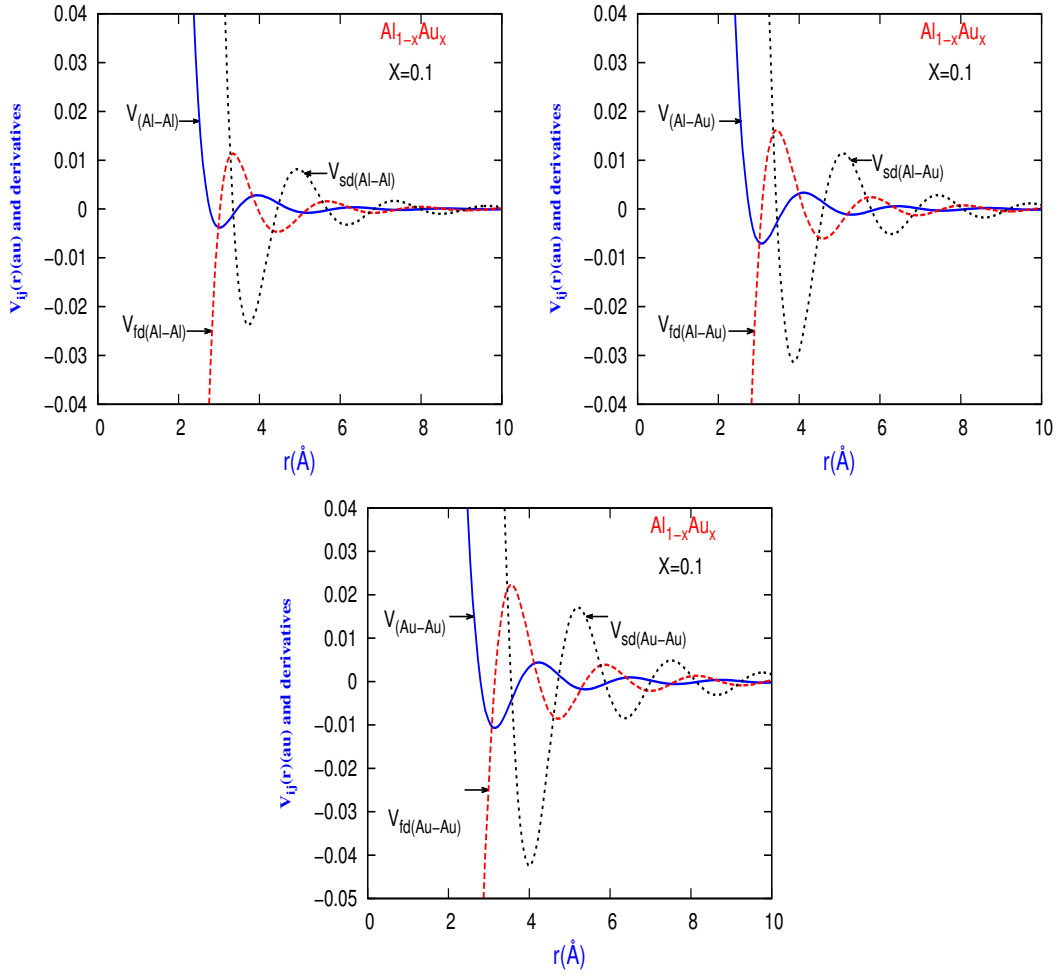

Figure 4.48: Partial pair potential V_{ij} and their derivatives for $Al_{1-x}Au_x$ liquid binary system for concentration x=0.1 for temperature 1338 K, respectively.

4.9.2 The Partial Integrand (X_{ij}) for Different Binary Systems

Using the same values for partial pair potentials, V_{ij}(r), hard sphere diameters, σ_{ij}, and partial pair correlation functions, g_{ij}(r), we have calculated the values for shear viscosities (η), friction coefficients (ζ) and self diffusion coefficients (D) for different concentrations of Al-based alloys. In this calculations, we have to evaluate the partial integrands, χ_{ij}, which are found to diverge for large values of r. The par-

tial integrands, χ_{ij} are shown in Figures (4.49-4.50) for those Al-based alloys for concentration x=0.5.

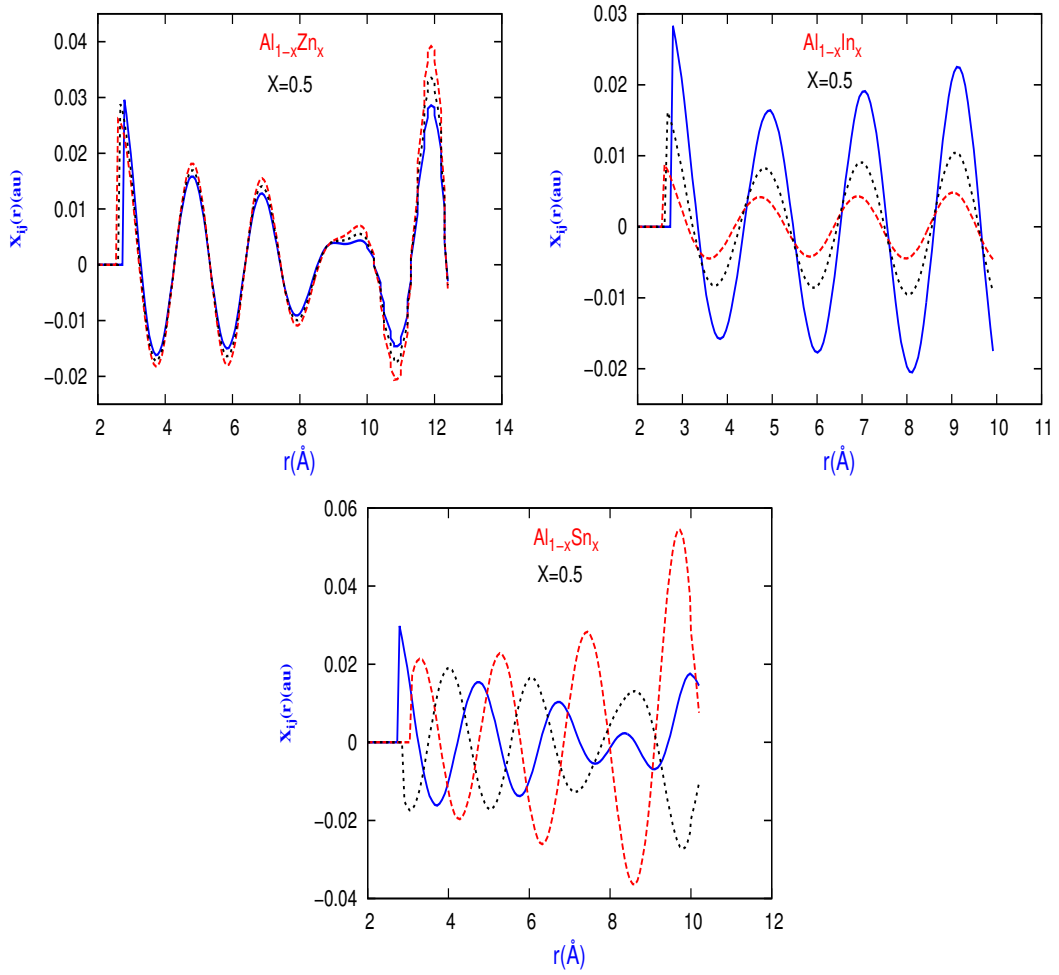

Figure 4.49: Partial integrand X_{ij} as a function of r for $Al_{1-x}X_x$ liquid binary systems for concentration x=0.5; here, X=Zn, In, and Sn respectively.

From the Figures (4.49-4.50), it can easily be understood that the integrand diverges for large values of r where the inter-ionic potentials contain the long range of Friedel oscillations [27]. Despite the first and second derivatives of the partial potentials as well as partial pair correlation functions individually converge, whereas the integrands diverse. The main cause of this phenomena is that, the integrand being directly proportional to r^4. Therefore, the amplitude of oscillation increases

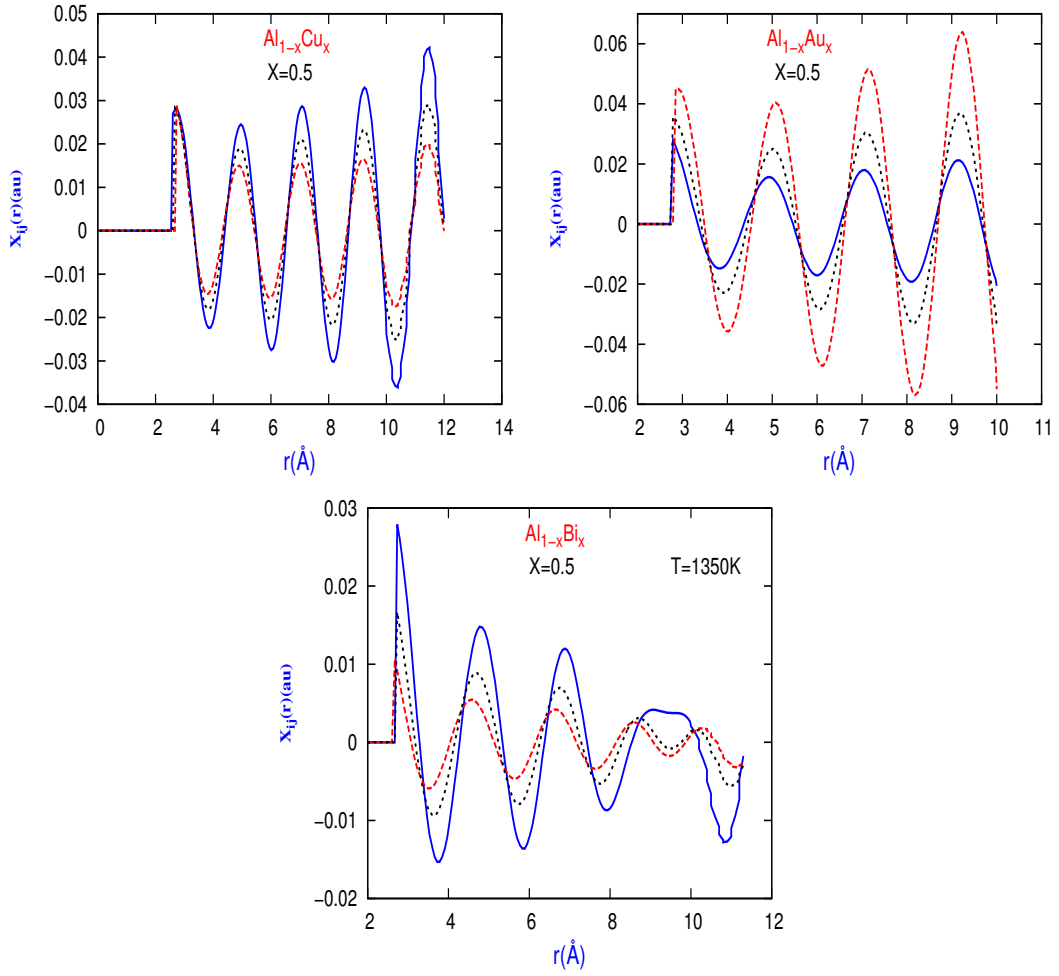

Figure 4.50: Partial integrand X_{ij} as a function of r for $Al_{1-x}X_x$ liquid binary systems for concentration x=0.5; here, X=Cu, Au, and Bi respectively.

with the increasing values of r even when there is no correlation at large r, that is $g_{ij}(r) \approx 1$. So, we need to fix an upper cut off region to truncate the integration at some value of r for all the effective numerical calculations.

In references [41–43], this infinite limit is truncated at a finite value at which the magnitude of the partial pair potential becomes of the order of $10^{-4}eV$. This could have been a good approximation for our present study of shear viscosities (η), friction coefficients (ζ) and self diffusion coefficients (D) for different concentrations. But in the case of shear viscosity, the integrand remains proportional to $1/r$, not r^2.

Bhuiyan *et al.* [41–43] have developed an efficient cutoff procedure for this purpose. In those research works, they showed that the cutoff region can be evaluated with respect to g_{ij}. Their works suggest that one can intend a truncation point based on the minimum value of r for which the correlation effect vanishes, or to say $g_{ij}(r) \sim 1$. This condition is fulfilled around the region where $r \sim 4\sigma$, where σ is the effective hard sphere diameter. For the present study of different Al-based liquid alloys, I have followed the same procedure to tackle the problem of divergence. We note that, the divergence appears not only for BS model [44] but also for all form of pseudopotentials having Friedel oscillations [27] at large values of r [41–43]. With this feature of truncation, we have integrated the partial integrand, X_{ij}, and the results of those are shown in Figures (4.49-4.50).

Three terms of the shear viscosity arise due to three different mechanisms. It is therefore very interesting to see how much each mechanism contributes, and in what way. To this end, we examined the breakdown details of the η in Tables 4.3, 4.5, 4.7, 4.9 and 4.11 for different contributions of $Al_{1-x}Zn_x$, $Al_{1-x}In_x$, $Al_{1-x}Cu_x$, $Al_{1-x}Au_x$, and $Al_{1-x}Bi_x$, systems, respectively.

4.9.3 Table for Atomic Transport Coefficients for Al-based Systems

In the evaluation process for atomic transport properties, we have calculated the hard and soft-core part of the friction and diffusion coefficients. These values are listed below:

As listed in Table 4.2, we can see that the friction coefficients for the first constituent, namely, Al, the hard part (ζ_{Al}^{H}) increases with increasing concentration in the range from x=0.1 to 0.4 and then it starts to decrease from x=0.4 to 0.7. The increasing and decreasing rate, both are very slow for it. For the soft part (ζ_{Al}^{S}), it

Table 4.2: The soft and hard core parts of the friction coefficients, $\zeta(\times 10^{-12} * kgs^{-1})$ and partial diffusion coefficients, $D_{Al,Zn}(\times 10^{-9} * m^2 s^{-1})$ for both constituents and mutual diffusion coefficients, $D_{Al-Zn}(\times 10^{-9} * m^2 s^{-1})$ are listed for $Al_{1-x}Zn_x$ alloys.

x	ζ_{Al}^{H}	ζ_{Al}^{S}	ζ_{Zn}^{H}	ζ_{Zn}^{S}	D_{Al}	D_{Zn}	D_{Al-Zn}
0.1	0.858	1.33	1.10	1.78	6.31	4.78	4.93
0.2	0.864	1.15	1.09	1.49	6.85	5.35	5.65
0.3	0.872	1.05	1.08	1.31	7.16	5.77	6.19
0.4	0.875	0.93	1.06	1.08	7.64	6.43	6.92
0.5	0.874	0.83	1.04	1.26	8.08	5.99	7.04
0.6	0.873	0.94	1.02	1.01	7.60	6.81	7.29
0.7	0.871	0.83	1.00	0.78	8.09	7.75	7.98
0.8	0.864	1.13	0.97	0.64	6.92	5.96	6.73

decreases from x=0.1 to 0.5. At x=0.6, it increases and at x=0.7, it shows the same value as it was on x=0.5. At x=0.8 the value increases again.

The friction coefficients for second constituent Zn; the hard part ζ_{Zn}^{H} decreases with increasing concentration x on Zn and for soft part ζ_{Zn}^{S}, it decreases from x=0.1 to 0.4. At x=0.5, for ζ_{Zn}^{S} it increases and then again decreases to x=0.8.

But it is noticeable in Figure 4.4, that Zn has a smaller hard sphere diameter than Al. It is obvious, that the HS with smaller diameter plays the important role for the frictions in the alloy states. The consequence of this effect is reflected in ρ. We know that the diffusion coefficient is less for a system with larger friction coefficients. This effect is observed with the results in the table above. As the friction coefficient increases for Zn and then the diffusion coefficient tends to decrease in each step of increment for concentration x. On the other hand, the diffusion coefficient for liquid Al increases with the concentration, x. We did not find any

experimental data of diffusion coefficients for $Al_{1-x}Zn_x$ liquid binary alloy to compare our calculated results. But theoretical values are of the same order of magnitudes as the experimental data for elemental systems [4, 29].

It is obvious that, if the diffusion were more then the friction would be less. This effect is exactly reflected by the result of the diffusion for both the cases of partial diffusion coefficients and the mutual diffusion coefficients. The partial diffusion coefficients for Al increases with the increasing concentrations of x. Consequently, the partial diffusion coefficients for Zn increases from x=0.1 to 0.4 and at x=0.5 it decreases to 5.99 cP, then it again increases till x=0.7 and at x=0.8 it decreases.

In all cases, the mutual diffusion coefficient, D_{Al-Zn} lies between D_{Al} and D_{Zn} which is explained in details in [8]. The weighted average of two individual component of self-diffusion coefficients are taken as the mutual diffusion coefficient, $D_{Al-Zn} = (1-x)D_{Al} + xD_{Zn}$. This relation is valid for Lennard-Zones liquids but not for the strongly ordering systems [4, 29]. For mutual diffusion coefficients, D_{Al-Zn}, it starts to increase from concentration range x=0.1 to 0.7 and then starts to decrease from x=0.8.

Now we present the values of shear viscosity for $Al_{1-x}Zn_x$, obtained from our theoretical calculation. The results are presented in Table 4.3.

Here η_K is the kinetic contribution to the viscosity while $\eta_v(\sigma)$ and $\eta_v(r > \sigma)$ are the hard-core and the soft-core contributions, respectively. We can see that, the hard-core part plays the most significant role in determining the shear viscosity (η). The most important feature to notice here is that the soft core part mostly varies with the increment of concentration, x.

It shows a linear trend of increment for most of the parts. For the slight discrepancy in theoretical and experimental results, we conclude that many body potentials instead of pseudopotential may improve the agreement. We further note that, the

Table 4.3: Different contributions to the viscosity (η) for $Al_{1-x}Zn_x$ liquid binary alloys. Units are in cP.

x	η_K	$\eta_v(\sigma)$	$\eta_v(r > \sigma)$	η	η_{expt}
0.1	0.0723	0.869	0.256	1.20	-
0.2	0.0827	0.868	0.345	1.30	0.90 [129]
0.3	0.0902	0.868	0.416	1.37	-
0.4	0.1020	0.868	0.440	1.41	-
0.5	0.0974	0.850	0.610	1.56	-
0.6	0.1050	0.839	0.727	1.67	-
0.7	0.1220	0.839	0.799	1.76	-
0.8	0.0851	0.785	0.767	1.64	1.28 [129]

different size ratio of HS might be a factor. For further studies of transport properties, we intend to apply the molecular dynamics approach for $Al_{1-x}Zn_x$ system to get more informative information.

Table 4.4 describes the features of friction coefficients (ζ) and diffusion coefficients (D) for $Al_{1-x}In_x$ liquid binary alloys at thermodynamic state T=1173 K. We see that the friction coefficients for Al, for hard part (ζ^H_{Al}) increases with the increasing concentrations from the range x=0.1 to 0.7.

For the soft part (ζ^S_{Al}), at concentrations x=0.1, 0.2 and 0.3, 0.4, the values of ζ^S_{Al} are same as 1.03 and 1.11 ($\times 10^{-12} * kgs^{-1}$), respectively. Then it decreases from x=0.5 to 0.7.

The friction coefficients, for the second constituent, In, for hard part (ζ^H_{In}) increases in the range from x=0.1 to 0.4 and then it decreases in the range from x=0.5 to 0.7. But, for the soft part (ζ^S_{In}), it remains the same at x=0.1 & 0.2, then it decreases from the concentration range x=0.1 to 0.6, but at 0.7 it again increases

very slowly.

Table 4.4: The soft and hard core parts of the friction coefficients, $\zeta(\times 10^{-12} * kgs^{-1})$ and partial diffusion coefficients, $D_{Al,In}(\times 10^{-9} * m^2 s^{-1})$ for both constituents and mutual diffusion coefficients, $D_{Al-In}(\times 10^{-9} * m^2 s^{-1})$ are listed for $Al_{1-x}In_x$ liquid binary alloys.

x	ζ_{Al}^{H}	ζ_{Al}^{S}	ζ_{In}^{H}	ζ_{In}^{S}	D_{Al}	D_{In}	D_{Al-In}
0.1	0.722	1.03	0.973	1.65	9.24	6.16	6.47
0.2	0.727	1.03	0.983	1.65	9.21	6.14	6.75
0.3	0.732	1.11	0.989	1.63	8.80	6.18	6.97
0.4	0.740	1.11	0.992	1.62	8.73	6.19	7.21
0.5	0.744	1.05	0.984	1.61	9.03	6.24	7.64
0.6	0.752	0.96	0.978	1.50	9.42	6.53	8.26
0.7	0.757	0.82	0.962	1.52	10.02	6.53	9.13

If the diffusion coefficients are less for any liquid binary alloys then it will produce the higher friction coefficients for that system. This effect is observed with the results in Table 4.4 for $Al_{1-x}In_x$ liquid binary alloys. As the friction coefficient increases for In, the diffusion coefficient tends to decrease in each step of increment for concentration x.

On the other hand, the diffusion coefficient for liquid Al decreases from x=0.1 to x=0.4 and again it increases with the concentration, x. In all concentrations, up to x=0.1 to 0.7 the mutual diffusion coefficient, D_{Al-In} lies between D_{Al} and D_{In} which is stated in [8]. We did not find any experimental data of diffusion coefficients for $Al_{1-x}In_x$ liquid binary alloy to compare our results. But, theoretical values are of the same order of magnitudes as the experimental data for elemental systems [4, 29].

Now we present the values of shear viscosity, obtained from our theoretical calculation. The results are given as a tabular form (Table 4.5) right below:

Table 4.5: Different contributions to the viscosity (η) for $Al_{1-x}In_x$ liquid binary alloys. Units are in cP.

x	η_K	$\eta_v(\sigma)$	$\eta_v(r > \sigma)$	η	η_{expt}
0.1	0.0866	0.694	0.095	0.876	-
0.2	0.0866	0.696	0.144	0.927	-
0.3	0.0855	0.692	0.159	0.937	0.68 [130]
0.4	0.0856	0.692	0.177	0.955	0.78 [130]
0.5	0.0873	0.687	0.214	0.988	0.98 [130]
0.6	0.0927	0.687	0.237	1.020	-
0.7	0.0964	0.683	0.238	1.020	-

The breakdown details of the shear viscosity are shown in Table 4.5 for $Al_{1-x}In_x$ liquid binary alloys at 1173 K. η_K is the kinetic contribution to the viscosity while $\eta_v(\sigma)$ and $\eta_v(r > \sigma)$ are the hard-core and the soft-core contributions, respectively. It is seen from the Table 4.5, that the largest contribution which comes from the hard part, $\eta_v(\sigma)$, of the potential, is more than 89% of the total value in the concentration range x=0.1 to 0.4, but from x=0.5 to 0.7 is 80%.

The second largest contribution comes from the soft part which is up to 18%. At concentration x=0.1, this is more than 1% in the concentration range x=0.2 to 0.4, this is more than 8% and for the concentration range x=0.5 to 0.7, this is up to 18%. The rest of the contribution comes from the kinetic part, η_K.

We observed that the hard-core part plays the most significant role in the measurement of the shear viscosity (η). Another important feature to notice here is that the soft-core part, $\eta_v(\sigma)$, mostly varies with the increment of concentrations from

x=0.1 to 0.8. It shows a linear trend of increment for the most part. Symbolically, one can present the magnitude of the breakdown details of the shear viscosity as in the following order, $\eta > \eta_v(\sigma) > \eta_v(r > \sigma) > \eta_K$. Table 4.6 illustrates the friction coefficients (ζ) and diffusion coefficients (D) for $Al_{1-x}Cu_x$ liquid binary alloys at thermodynamic state T=1373 K. It is seen that, the hard part (ζ^H_{Al}) of friction coefficients for Al, increases with the increasing concentrations from x=0.1 to 0.7. We have also found, the similar trends for soft part (ζ^S_{Al}). But at x=0.8, it decreases and remains the same at concentration x=0.9.

At concentration x=0.1 the values of ζ^S_{Al} is $0.85\times10^{-12}kgs^{-1}$ and at x=0.7 the values for ζ^S_{Al} is 1.92 $\times10^{-12}kgs^{-1}$. The friction coefficients, ζ^H_{Cu}, for the second constituent, Cu show the same value from concentrations x=0.1 to 0.7 and its numerical value is around 1.14$\sim$1.16 $\times10^{-12}kgs^{-1}$.

But for ζ^S_{Cu}, it increases from x=0.1 to 0.7, and for these range the numerical values are found in the order 0.77 $\sim$ 1.60 $\times10^{-12}kgs^{-1}$. We have seen that, the contributions for ζ^H_{Al}, ζ^S_{Al}, and ζ^S_{Cu} increase from x=0.1 to 0.7. However, the results at concentrations x=0.8 & 0.9 remain same for ζ^H_{Al}, ζ^S_{Al}, respectively; but it decreases for ζ^S_{Cu}.

The diffusion coefficient tends to decrease in each step of increment for concentration x. We have not found any experimental data of diffusion coefficients for $Al_{1-x}Cu_x$ liquid binary alloy to compare our calculated results. But theoretical values are of the same order of magnitudes as the experimental data for the elemental systems [4, 29]. The partial diffusion coefficients, D_{Al}, starts to decrease from the concentration x=0.1 to 0.8 and for D_{Cu} it decreases from the concentration range x=0.1 to 0.8, but at x=0.9 both starts to increase.

In all concentrations, the mutual diffusion coefficient, D_{Al-Cu} lies between D_{Al} and D_{Cu} which is explained in details in [8]. The results for D_{Al-Cu} decreases con-

Table 4.6: The soft and hard core parts of the friction coefficients, $\zeta(\times 10^{-12} * kgs^{-1})$ and partial diffusion coefficients, $D_{Al,Cu}(\times 10^{-9} * m^2 s^{-1})$ for both constituents and mutual diffusion coefficients, $D_{Al-Cu}(\times 10^{-9} * m^2 s^{-1})$ are listed for $Al_{1-x}Cu_x$ alloys.

x	ζ_{Al}^{H}	ζ_{Al}^{S}	ζ_{Cu}^{H}	ζ_{Cu}^{S}	D_{Al}	D_{Cu}	D_{Al-Cu}
0.1	1.27	0.85	1.14	0.77	8.95	9.90	9.81
0.2	1.30	0.93	1.15	0.99	8.90	9.19	9.14
0.3	1.33	1.04	1.15	1.03	8.01	8.67	8.47
0.4	1.35	1.27	1.16	1.18	7.22	8.12	7.76
0.5	1.37	1.50	1.16	1.32	6.60	7.65	7.13
0.6	1.39	1.66	1.15	1.43	6.21	7.35	6.67
0.7	1.40	1.92	1.14	1.60	5.69	6.89	6.05
0.8	1.41	1.91	1.13	1.59	5.70	6.96	5.95
0.9	1.41	1.91	1.10	1.58	5.71	7.05	5.85

tinuously up to the concentration range x=0.1 to 0.9.

Now we present the values of shear viscosity, obtained from our theoretical calculation. The results are given as a tabular form (Table 4.7) right below:

The detailed part of the shear viscosity are given in Table 4.7 for $Al_{1-x}Cu_x$ liquid binary alloys at thermodynamic state 1373 K, where Cu is a *d*-band transition element. It is seen in Table 4.7 that, the contribution comes from the hard part, $\eta_v(\sigma)$, is almost same from concentration range x=0.1 to 0.8 which shows almost the similar trend of our previously studied results for $Al_{1-x}Zn_x$ and $Al_{1-x}In_x$ and its numerical values vary from $1.33 \sim 1.35, 1.37$ in cP range.

η_K is the kinetic contribution to the viscosity and its numerical values vary from $0.181 \sim 0.104$ cP from concentration, x=0.1 to 0.9. The largest contribution coming

Table 4.7: Different contributions to the viscosity (η) for $Al_{1-x}Cu_x$ liquid binary alloys. Units are in cP.

x	η_K	$\eta_v(\sigma)$	$\eta_v(r > \sigma)$	η	η_{expt} [131]
0.1	0.181	1.33	3.12	4.64	3.963
0.2	0.177	1.37	2.33	3.87	4.868
0.3	0.156	1.37	1.45	2.97	4.740
0.4	0.138	1.37	0.893	2.40	5.075
0.5	0.124	1.37	0.738	2.23	2.560
0.6	0.115	1.37	0.692	2.18	-
0.7	0.104	1.37	0.642	2.12	1.484
0.8	0.104	1.37	0.408	1.88	1.032
0.9	0.104	1.35	0.474	1.93	1.331

from the soft part, $\eta_v(r > \sigma)$, of the potential; which is more than 80% of the total value in the concentration range x=0.1 to 0.3, but from concentration, x=0.4 to 0.9 this trends is totally different from previous.

So, we can say from the Table 4.7, we have found the largest contribution from the two different parts of the total viscosity. For $\eta_v(r > \sigma)$, the largest contribution comes from concentration range, x=0.1 to 0.3 and on the other hand, the largest contribution comes for $\eta_v(\sigma)$, from the concentration range x=0.4 to 0.9. It is reported [4] that, for some elemental simple and less simple liquid metals, the major contribution comes from the soft part for some potentials [4]. In the present case, the situation is different.

As we can say, that the hard-core part plays the most significant role in the measurement of shear viscosity (η). Another important feature to notice here is that the soft-core part, $\eta_v(\sigma)$, varies very rapidly at the concentrations range from x=0.4 to

0.8. We have found that, the experimental data [131] of shear viscosity for $Al_{1-x}Cu_x$ liquid binary alloys, where it is seen that, our calculated shear viscosity results are very close to the experimental results at every concentration. Symbolically, one can present the magnitude of the breakdown details of the shear viscosity as in the following order for concentration range, x=0.1 to 0.3, are $\eta > \eta_v(r > \sigma) > \eta_v(\sigma) > \eta_K$. From concentration range, x=0.4 to 0.8 it can be written as, $\eta > \eta_v(\sigma) > \eta_v(r > \sigma) > \eta_K$.

Table 4.8: The soft and hard core parts of the friction coefficients, $\zeta(\times 10^{-12} * kgs^{-1})$ and partial diffusion coefficients, $D_{Al,Au}(\times 10^{-9} * m^2 s^{-1})$ for both constituents and mutual diffusion coefficients, $D_{Al-Au}(\times 10^{-9} * m^2 s^{-1})$ are listed for $Al_{1-x}Au_x$ liquid binary alloys.

x	ζ_{Al}^{H}	ζ_{Al}^{S}	ζ_{Au}^{H}	ζ_{Au}^{S}	D_{Al}	D_{Au}	D_{Al-Au}
0.1	1.07	1.40	2.15	3.35	7.47	3.36	3.77
0.2	1.08	1.42	2.11	3.61	7.39	3.22	4.06
0.3	1.09	1.42	2.06	3.56	7.37	3.28	4.51
0.4	1.09	1.42	2.01	3.56	7.35	3.32	4.93
0.5	1.08	1.27	1.94	3.14	7.87	3.63	5.75
0.6	1.08	1.12	1.90	2.58	8.41	4.12	6.70
0.7	1.07	1.10	1.84	1.54	8.53	5.45	7.61

Table 4.8 shows, the features of the friction coefficients (ζ) and the diffusion coefficients (D) for $Al_{1-x}Au_x$ liquid binary alloys at thermodynamic state, T=1338 K. We can see that, the friction coefficients for Al, for hard part (ζ_{Al}^{H}) are almost the same from x= 0.1 to 0.7 and its values around $(1.07 \sim 1.09) \times 10^{-12} kgs^{-1}$. Moreover, the values for ζ_{Al}^{S}, increases at x=0.2 and remains 1.42 $\times 10^{-12} kgs^{-1}$ till x=0.4, then again decreases till x=0.7.

But the values for ζ^H_{Au}, and ζ^S_{Au} are decreasing with the increasing values of x. In Table 4.8, the 6^{th}, 7^{th} and 8^{th} column from left side present the partial diffusion coefficients and mutual diffusion coefficients for $Al_{1-x}Au_x$ liquid binary alloys and defined as D_{Al}, D_{Au}, and D_{Al-Au}, respectively. The value for D_{Al} decreases from concentration x=0.1 to 0.4 and then it starts to increase from x=0.5 to 0.7. We have seen the similar pattern for D_{Au}.

It starts to decrease from x=0.1 to 0.3 and then it starts to increase up to x=0.7 Similarly, from our previous studied results, the mutual diffusion coefficient, D_{Al-Au} lies between D_{Al} and D_{Au} which are expected [8]. We don't have any experimental data for diffusion coefficients, so, we couldn't compare our theoretical results for $Al_{1-x}Au_x$ liquid binary alloys with the experimental results.

But theoretical values are of the same order of magnitude as the experimental data for elemental systems [4, 29].

Now we present the values of shear viscosity, obtained from our theoretical calculation. The results are given in a table below:

Table 4.9: Different contributions to the viscosity for $Al_{1-x}Au_x$ liquid binary alloys. Units are in cP.

x	η_K	$\eta_v(\sigma)$	$\eta_v(r > \sigma)$	η	η_{expt} [132]
0.1	0.131	1.71	0.663	2.50	3.25
0.2	0.124	1.68	0.430	2.24	-
0.3	0.124	1.65	0.147	1.92	-
0.4	0.123	1.60	-0.229	1.50	-
0.5	0.134	1.55	-0.271	1.41	2.47
0.6	0.154	1.53	-0.329	1.36	2.25
0.7	0.205	1.53	-0.447	1.29	1.78

The breakdown detailed of the results for shear viscosity for $Al_{1-x}Au_x$ liquid binary alloys at thermodynamic state 1338 K where Au is a *d*-band transition element are shown in Table 4.9. It is seen in the table that, the contribution comes from the hard part, $\eta_v(\sigma)$, decreases from concentration range x=0.1 to 0.7, which shows the different trend from our previous studied results for $Al_{1-x}Zn_x$, $Al_{1-x}In_x$ and $Al_{1-x}Cu_x$ and its numerical values vary from $1.71 \sim 1.53$ cP range.

η_K is the kinetic contribution to the viscosity and its numerical values vary from $0.123 \sim 0.205$ cP from concentration, x=0.1 to 0.7. The largest contribution comes from the hard part, $\eta_v(\sigma)$, of the potential, which is more than 78% of the total value in the concentration range x=0.1 to 0.3, but from concentration, x=0.4 to 0.7 this trends is totally different from the previous.

On the other hand, the contribution comes from $\eta_v(r > \sigma)$, is negative from x=0.4 to 0.7 which is very unusual. It is also reported that for some simple element and less simple liquid metals the contribution comes from $\eta_v(r > \sigma)$ may be negative and detailed can be found in [4, 29]. Thus we can say that the hard-core part plays the most significant role in the measurement of shear viscosity (η). Another important feature to notice here is that the soft-core part, $\eta_v(r > \sigma)$, varies very rapidly at the concentrations range from x=0.4 to 0.7. We have found the experimental data [132] of shear viscosity for $Al_{1-x}Au_x$ liquid binary alloys, and it is seen that our calculated shear viscosity results are very close to the experimental results at those concentrations. Symbolically, one can present the magnitude of the breakdown details of the shear viscosity as in the following order for concentration range, x=0.1 to 0.3, are $\eta > \eta_v(\sigma) > \eta_v(r > \sigma) > \eta_K$. From concentration range, x=0.4 to 0.7 it can be written as, $\eta > \eta_v(\sigma) > \eta_K > \eta_v(r > \sigma)$.

Table 4.10 illustrates the results for mutual diffusion coefficients, D_{Al-Bi}, for $Al_{1-x}Bi_x$ segregating liquid binary alloys at different temperatures to understand the

Table 4.10: Mutual diffusion coefficients, $D_{Al-Bi}(\times 10^{-9} * m^2 s^{-1})$ for $Al_{1-x}Bi_x$ liquid binary segregating alloys at different temperatures.

x	D_{1350k}	D_{1290k}	D_{1223k}	D_{1173K}	D_{1050K}
0.1	11.4	9.64	9.16	8.85	8.17
0.2	10.7	10.4	10.1	9.79	8.68
0.3	10.1	9.78	9.48	9.89	9.30
0.4	10.0	9.78	9.53	9.28	8.72
0.5	9.38	9.16	8.93	8.70	8.69
0.6	8.72	8.54	9.01	8.83	8.43
0.7	8.42	8.27	8.16	8.00	7.62
0.8	7.68	7.50	7.34	7.23	6.88
0.9	7.02	6.83	6.65	6.50	6.21

behavior in segregating states. It is reported in [102–106] that, the critical temperature and concentration are 1310 K, and 0.195 moles in Bi for $Al_{1-x}Bi_x$ system, respectively. But we have found in our study that, T_c, and x_c are 1290 K and 0.20 moles in Bi, respectively. The second column in Table 4.10 presents the results of D_{Al-Bi} for 1350 K. It is found that the value of D_{Al-Bi} decreases from concentration x=0.1 to 0.9. Third to sixth column present the results for temperatures 1290 K, 1223 K, 1173 K, and 1050 K, respectively.

It is seen at concentration x=0.1, the mutual diffusion coefficients, D_{Al-Bi} for different studied temperatures are always less than for D_{Al-Bi}, at x=0.2. From concentrations x=0.1 to 0.2, it always increases and then it starts to gradually decrease from x=0.2 to 0.9 concentrations range.

But for temperature 1223 K the value constantly goes up and down from x=0.2 to 0.6 and then starts to decrease.

Table 4.11: Different contributions to the total viscosity for $Al_{1-x}Bi_x$ liquid binary segregating alloys at different temperatures. Units are in cP.

x	η_{1350k}	η_{1290k}	η_{1223k}	η_{1173K}	η_{1050K}
0.1	0.367	0.991	0.991	1.00	1.04
0.2	0.483	0.415	0.322	0.239	0.998
0.3	0.593	0.542	0.474	0.381	0.166
0.4	0.658	0.614	0.553	0.504	0.346
0.5	0.703	0.668	0.620	0.581	0.455
0.6	0.725	0.702	0.634	0.595	0.465
0.7	0.718	0.697	0.670	0.641	0.536
0.8	0.737	0.712	0.684	0.669	0.587
0.9	0.756	0.731	0.701	0.680	0.623

Table 4.11 presents the breakdown details for the total viscosity, η, of $Al_{1-x}Bi_x$ segregating liquid binary alloys at different temperatures. The first column presents the concentration in Bi from 0.1 to 0.9 range. The second column presents the results of η_{1350} for 1350 K. It is found that, the value of η_{1350} increases from concentration x=0.1 to 0.6, and decreases at x=0.7 and again increases to x=0.9. Third to the sixth column presents the results for temperatures 1290 K, 1223 K, 1173 K, and 1050 K, respectively.

At T=1290 K, the value for η_{1290} maximum at concentration x=0.1. At x=0.2, the value for η_{1290}, drops very fast and again it starts to increase from x=0.3 to 0.6. We found at x=0.7, η_{1290} slightly drops and its numerical value is 0.697 cP and it starts increasing from x=0.8 to 0.9 concentrations. η at temperatures 1223 k and 1173 K at x=0.1 is maximum. At x=0.2, it drops very fast and starts to increase from x=0.3 to 0.9. At temperature 1050 K, the value is maximum for η at concentration x=0.1.

It decreases slightly at x=0.2 and drops very fast at x=0.3 and again increases from x=0.4 to 0.9.

4.9.4 Conclusion

The present study on atomic transport properties is summarized in this section with some concluding remarks. We, in this study, have presented results of an intensive study of ATP, namely shear viscosity, diffusion coefficient and friction coefficient for the Al-based liquid binary alloys ($Al_{1-x}X_x$, here X=Zn, In, Cu, Au, Bi). Here, the distribution function method theory has been employed for the study of viscosity. The BS model has been employed to describe the effective inter-ionic interactions of the alloys. The effective HSDs essential for the calculations are obtained from the LWCA theory [69–72]. The results of the calculations are found to be satisfactory, in particular, the results for the shear viscosity are found to be in good in agreement with available experimental data [129–131] for $Al_{1-x}Zn_x$, $Al_{1-x}In_x$, and $Al_{1-x}Cu_x$ systems, respectively.

From the studied results, and discussions we can conclude that, the BS model [44] for the inter-ionic interaction is a good starting point for the concerned metallic Al-based liquid binary alloys. The integrand, χ_{ij}, related to the soft part contribution is oscillatory, and it diverges with increasing r. Regarding the cutoff of the upper limit of integration, the even node positions give the maximal cancellation, and thus it is required for the good agreement of the viscosity results. To take more care about the small variations in the values of viscosity for different even positions one should take the cutoff at a distance $r \sim 4\sigma$ for all systems where $g_{ab} \sim 1$. The ATP of the $Al_{1-x}X_x$ (here, X= Zn, In, Cu, Au, Bi) liquid binary alloys may be well described by using the additive HS reference systems. The contribution of the repulsive part of the potential to the viscosity dominates for the concerned systems. Shear viscosity for $Al_{1-x}X_x$

(here, X= Zn, In, Cu, Au, Bi) liquid binary alloys increase almost linearly with increasing Al_{1-x} concentrations. Finally, the level of agreement with experimental data [129–131] for $Al_{1-x}X_x$ (here, X= Zn, In, Cu) liquid binary alloys confirms the validity and effectiveness of the truncation approach proposed in [41–43].

4.10 Comparative Study for Viscosity and Diffusion Coefficients for Al-based Alloys

:

In this section, the results for viscosity, η, and mutual diffusion coefficients, D, will be discussed for Al-based liquid binary systems, $Al_{1-x}X_x$. Here, X= Zn, In, Au, and Bi in Figures (4.51-4.54). The results for η, and D of $Al_{1-x}Cu_x$ system are not presented in those figures but can be found in the earlier mentioned table in the result section.

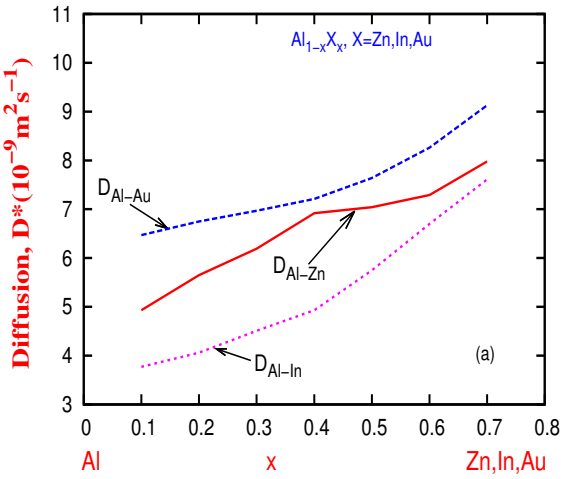

Figure 4.51: Comparison of Mutual Diffusion Coefficients for Al-based alloys at different thermodynamic states

Figure 4.51 illustrates the results for D, for $Al_{1-x}Zn_x$, $Al_{1-x}In_x$, and $Al_{1-x}Au_x$

liquid binary systems for temperatures 1000 K, 1173 K, and 1338 K, respectively. We found that the contribution comes from the $Al_{1-x}Au_x$ system is always greater than the other systems for the whole range of concentrations. Besides, the contribution arises from $Al_{1-x}In_x$ system is the smallest from the concentration range x=0.1 to 0.7.

Symbolically, the results for mutual diffusion coefficients, D, can be presented from concentrations, x=0.1 to 0.7, $Al_{1-x}Au_x > Al_{1-x}Zn_x > Al_{1-x}In_x$.

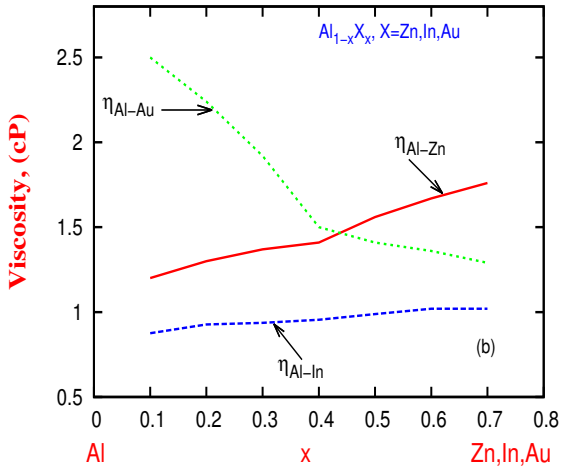

Figure 4.52: Comparison of total Viscosity for Al-based liquid binary alloys at different thermodynamic states

Figure 4.52 presents, the results for viscosity, η for $Al_{1-x}Zn_x$, $Al_{1-x}In_x$ and $Al_{1-x}Au_x$ systems. We found that $Al_{1-x}Au_x$ system gives the largest result for η from concentration range, x=0.1 to 0.4. After that, from concentration range, x=0.4 to 0.7, the largest value for η comes from $Al_{1-x}Zn_x$ system.

We have seen a rapid decrease in results for the $Al_{1-x}Au_x$ system in those concentration ranges. Similarly, with comparing to the feature of D, $Al_{1-x}In_x$ system gives the smaller results for η from the concentration range, x=0.1 to 0.7. Symbolically, the

results for η from concentration range, x=0.1 to 0.4 can be presented as $Al_{1-x}Au_x > Al_{1-x}Zn_x > Al_{1-x}In_x$; from x=0.4 to 0.7 range, $Al_{1-x}Zn_x > Al_{1-x}Au_x > Al_{1-x}In_x$. The result for η of $Al_{1-x}Cu_x$ system is not plotted in this figure and can be found in Table 4.7.

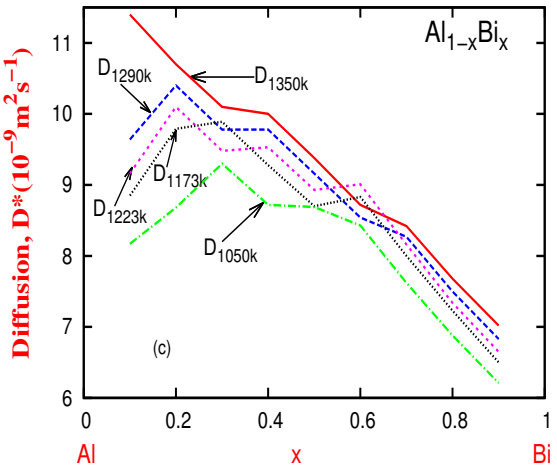

Figure 4.53: Comparison of Mutual Diffusion Coefficients for $Al_{1-x}Bi_x$ liquid binary alloys at different thermodynamic states

The results for mutual diffusion coefficients, D for $Al_{1-x}Bi_x$ system are presented in Figure 4.53 for five different temperatures. $Al_{1-x}Bi_x$ is a segregating system. To understand this segregating behavior in ATP, we have studied both D, and η for different temperatures.

The critical temperature, T_c, and critical concentration, x_c for this system are reported in [102–106], 1310 K, and 0.195 moles in Bi, respectively. But in our study, we have found that the results for T_c, and x_c are 1290 K, and 0.15 mole in Bi, respectively; and discussed in detail in thermodynamic section (Section 4.5).

But from Figure 4.53, we found that, at concentration x=0.2, the behaviors of D are very strange from temperature range 1290 K to 1050 K. So we could predict that, the critical concentration region might be around this point which is consistent with

the experimental value [102]. The numerical values for D, below 1350 K temperature also show some unpredictable results.

It is seen in Figure 4.53, that the value for D of temperature 1350 K gradually decreases from concentrations x=0.1 to 0.9 and which is very normal behavior. But for other below temperatures with respect to 1350 K, the values for D sometimes increase or decrease of our different studying concentrations. So we could also predict from our ATP study for $Al_{1-x}Bi_x$ system, that the critical temperature might be exist below 1350 K. Symbolically, it can be presented according to the magnitude of D for $Al_{1-x}Bi_x$ system at different temperatures for concentrations, x=0.1 to 0.2 and 0.7 to 0.9, $D_{1350} > D_{1290} > D_{1223} > D_{1173} > D_{1050}$.

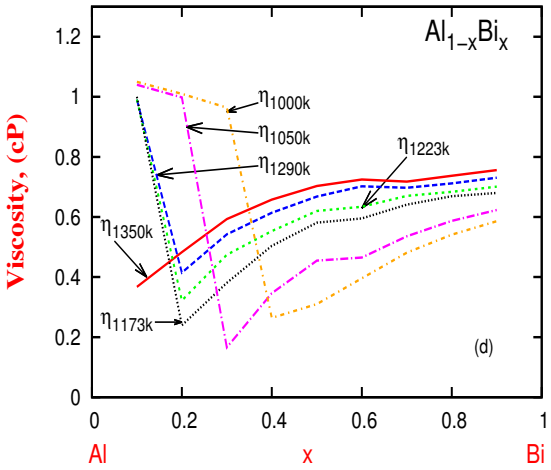

Figure 4.54: Comparison of the total Viscosity for $Al_{1-x}Bi_x$ liquid binary alloys at different thermodynamic states

Figure 4.54 illustrates the results for viscosity, η for $Al_{1-x}Bi_x$ liquid binary alloys for different thermodynamic temperatures. It can easily be understood from this figure that $Al_{1-x}Bi_x$ has some strange behavior again, around concentration x=0.2 mole in Bi, and in our study for η we can claim that it is our critical concentration. This behavior starts with T=1290 K which is the critical temperature that we have

claimed in our thermodynamic section, and similar strange results we found for the concerning system. The continuation of this strange behavior observed till 1000 K.

At concentration x=0.1, we have found that the value of η is the largest for all the studied high temperatures except for 1350 K of $Al_{1-x}Bi_x$ system. For x=0.2, we have found the minimum value of η, again except for 1350 K. It is shown in Figure 4.54 that, the certain rapid decrease of η is very surprising for $Al_{1-x}Bi_x$ liquid binary alloy below 1350 K. Then, it starts increasing up to x=0.9 concentration for all studied thermodynamic temperatures, T. So we could again predict from the analysis of η at ATP that the critical temperature might exist is below at 1350 K.

Another interesting behavior is that, at T=1050 K, we have found the total segregating nature for the studied system, and discussed all the facts in our thermodynamic section for $Al_{1-x}Bi_x$ liquid binary alloys, but below this temperature, at T=1000 K, the critical concentration position shifts from x=0.2 towards an increasing range of Bi which is a very interesting nature of this segregating system. To understand this segregating nature in liquid state further studies is required.

Therefore, the numerical value for η from the study of ATP for the $Al_{1-x}Bi_x$ liquid binary alloys can be written according to the range of concentrations from x=0.2 to 0.9, $\eta_{1350} > \eta_{1290} > \eta_{1223} > \eta_{1173} > \eta_{1050} > \eta_{1000}$.

4.11 Results, Discussion, & Conclusions for Electron Transport Properties for Al-based Liquid Binary Systems

Electron transport properties such as the electrical resistivity (Ω), the thermoelectric power, and thermal conductivity (β) of materials play a major role in metallurgy, technology and industry. In alloys, electron transport is an important concept for interpreting various physical quantities of alloys.

Mankind is now experiencing its fifth and most intense technological revolution [133–147] which is mainly relying on electric power. Electricity works like a driving force in the field of medicine, transport, communication, entertainment, manufacture, industry, home appliance, and even art. Without exaggerating we can safely say that everything depends on electricity. Here, obviously conductor plays a vital role to conduct electricity to every-where, and it is well known that the Aluminium and Aluminium based different alloys behave like a good conductor, and has the lowest resistivity as far as our knowledge [133–147]. If we can reduce the resistivity of conductor then the waste of electricity would be minimized, and this minimization certainly will help us to provide more electricity in the aforementioned fields.

The melting temperatures for basic metals are very high, and it is very difficult to do experiment due to convection effects. Besides, the experiments are very expensive, and time consuming also. On the other hand, computer simulation also takes a lot of time to study this properties [120, 121]. From the theoretical point of view, Harrison [4, 43] applied pseudopotential methods to the transition metals for the first time. Moriarty [42] modified these pseudopotential methods to study the basic metals like Al, In, Sn, Bi, the alkaline earth metals, Ca, Sr, and Ba; and transition metals namely Zn, Cu, Au etc. Some fundamental reasons also inspire us to conduct

the study on resistivity of Al-based liquid binary alloys.

Firstly, working in this method is totally cost effective. Secondly, studying about transport properties at high temperature is very precise, and accurate, and most importantly, it's firmly a time saving process. And hence, the study of electrical transport properties of liquid metals and their alloys remain one of the favorite quantities theoretically [6].

Theoretical results for the electrical transport properties mainly electrical resistivity (Ω) of Al-based liquid binary alloys namely $Al_{1-x}Zn_x$, $Al_{1-x}In_x$, $Al_{1-x}Cu_x$ and $Al_{1-x}Au_x$ are presented in the section. The study is carried out by changing the concentrations of Al_{1-x} from 0.9 to 0.1. Previously, Faber and Ziman [9] and Dreirach *et al*. [147] had investigated the resistivity of noble liquid metal alloys by using pseudopotential, and a simple muffin tin model.

Difficulties arise, when the study involves simple and heavy polyvalent metals like Al, In, Sn, Bi; transition metals as Zn, Cu, Au, and rare-earth metals. In noble metals, Zn, Cu, and Au, narrow *d*-bands are filled, and lied below the Fermi energy. Since, the d-bands are not seriously affected by melting, as suggested by experimental studies, pseudopotenial for noble metals have to be energy dependent. For simple Electronic Transport Properties (ETP) such as for electrical resistivity, the local energy is independent of pseudopotentials, and it seems to give results reasonably good in agreement with the experimental results [133–147]. But for our studied Al-based liquid binary alloys, we do not have the experimental results to compare our theoretical results, but the calculated results are in the same order with comparing their results with the elemental system. So, we could predict that our theoretical results are consistent.

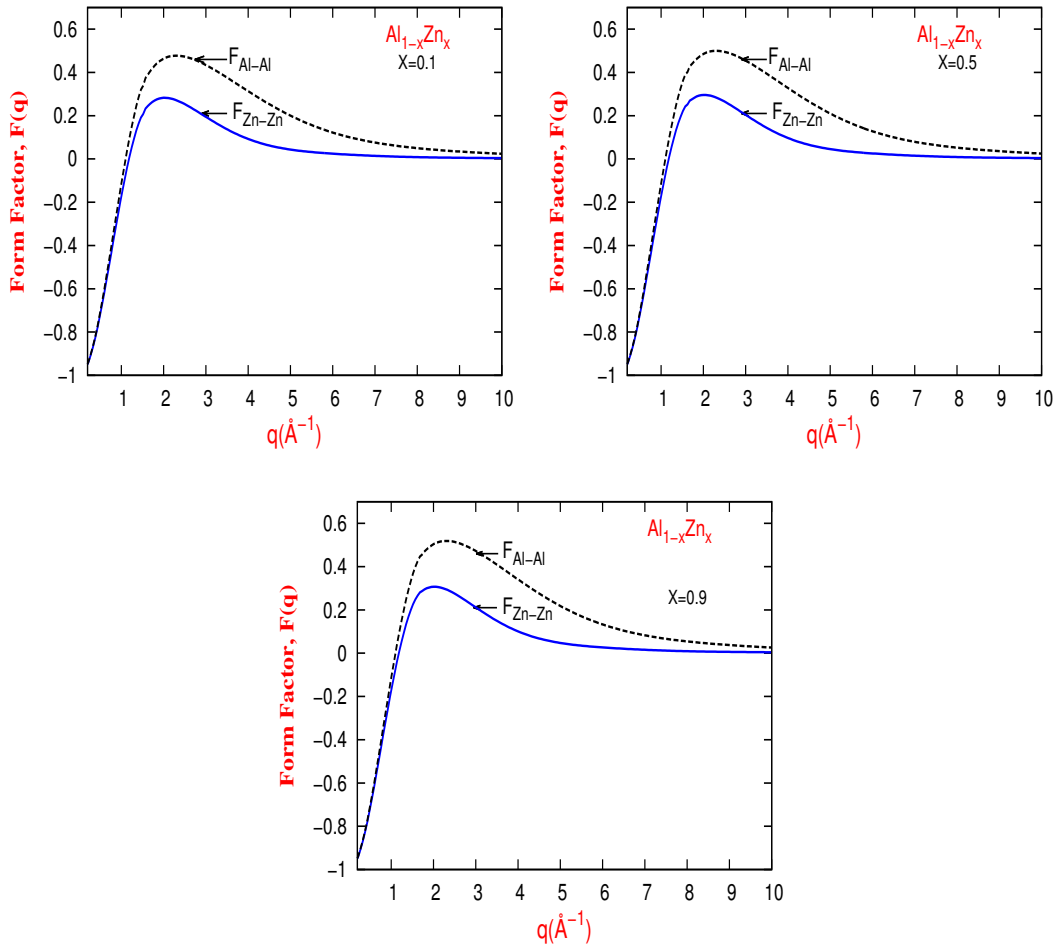

Figure 4.55: Variation of Form-factor, $F(q)$ as a function of q for $Al_{1-x}Zn_x$ liquid binary system for concentration, x=0.1, 0.5, and 0.9, respectively.

4.11.1 Form-factor for Different Al-Based Binary Systems

Figures (4.55-4.58) present, the different Form-factor, $F(q)$, for $Al_{1-x}Zn_x$, $Al_{1-x}In_x$, $Al_{1-x}Cu_x$ and $Al_{1-x}Au_x$ systems, respectively. As far as Faber and Ziman [9] or, Ziman [65] formulas are concerned, then the Form-factor, $F(q)$, of electron-ion interaction is essential to perform the calculations. Necessary inputs for evaluating the form factors and the effective inter-ionic pair potentials are taken from the previous study for the energy of mixing for different Al-based alloys because we use the same potentials.

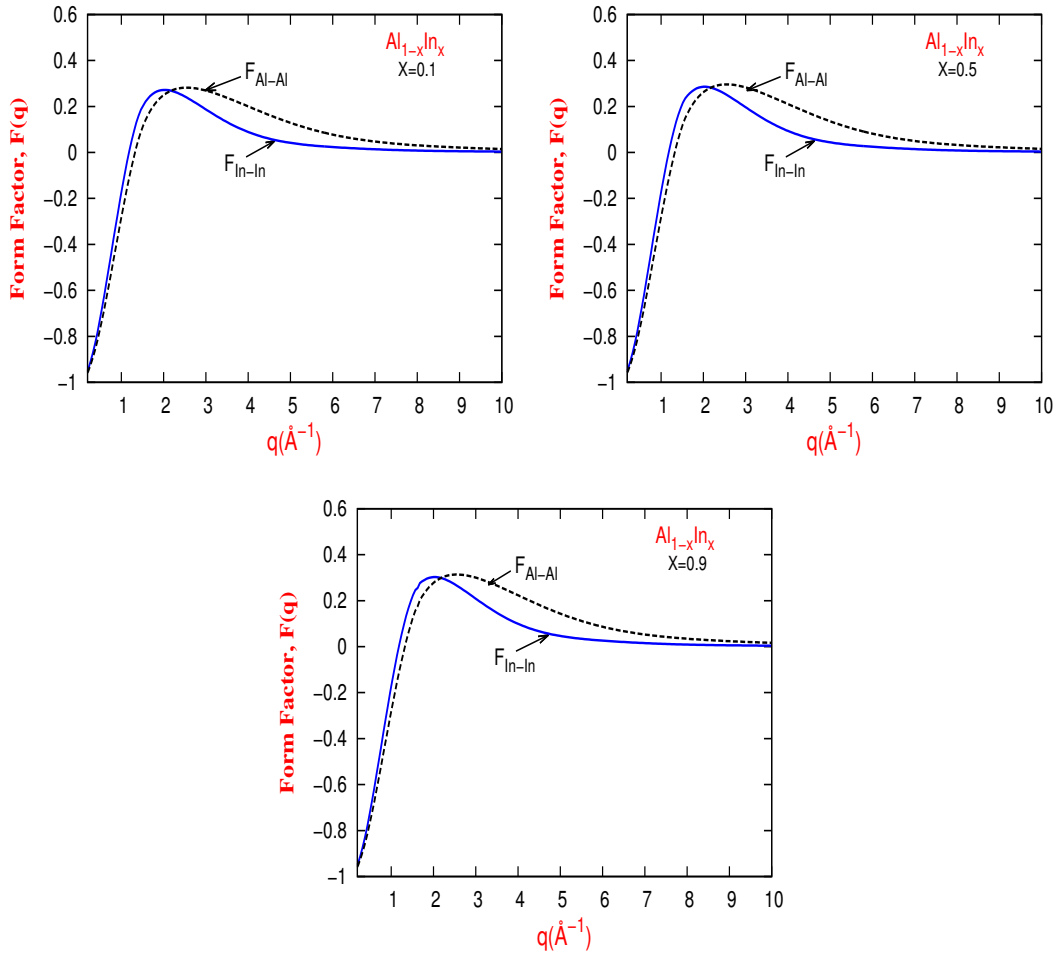

Figure 4.56: Variation of Form-factor, $F(q)$ as a function of q for $Al_{1-x}In_x$ liquid binary system for concentration, x=0.1, 0.5, and 0.9, respectively.

In Figure (4.54-4.55), the peak positions and the height of the peaks for F_{Al-Al} are always changing for different alloys with the changing of concentrations, x. The height of the peaks for F_{Al-Al} are always greater than the height of the peaks for F_{Zn-Zn}, F_{In-In}, F_{Cu-Cu} and F_{Au-Au}, in different systems, respectively.

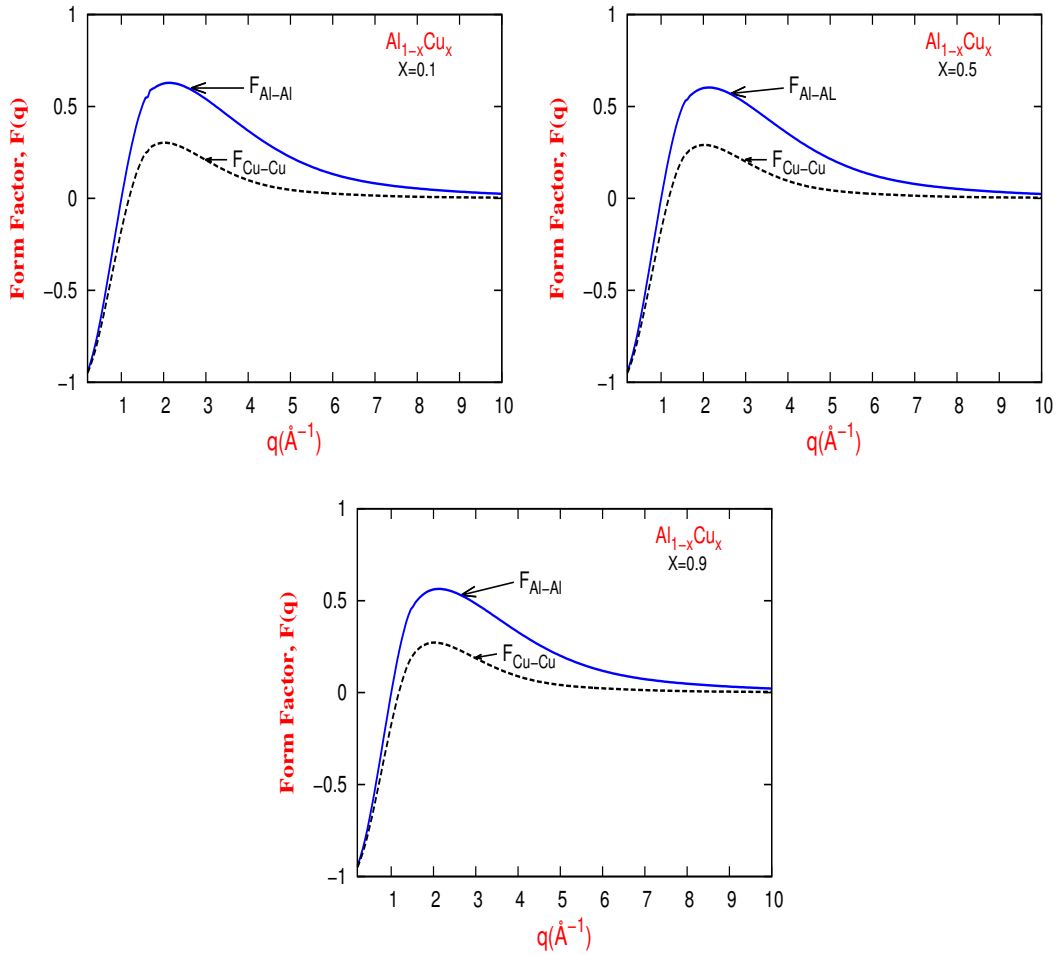

Figure 4.57: Variation of Form-factor, $F(q)$ as a function of q for $Al_{1-x}Cu_x$ liquid binary system for concentration, x=0.1, 0.5, and 0.9, respectively.

The consequence of these discrepancies is nicely reflected in the corresponding profiles for the effective inter-ionic pair potentials. That is the position of minimum of the potential for (Al-Al) alloys has shifted toward the large r relative to the others in the alloys state. The depth of the potential well is a result of delicate balance among the different contributions of the input parameters, and is found to be largest for Al. The difference between depths for the other systems are small.

The similar explanation is also applicable for the other alloys.

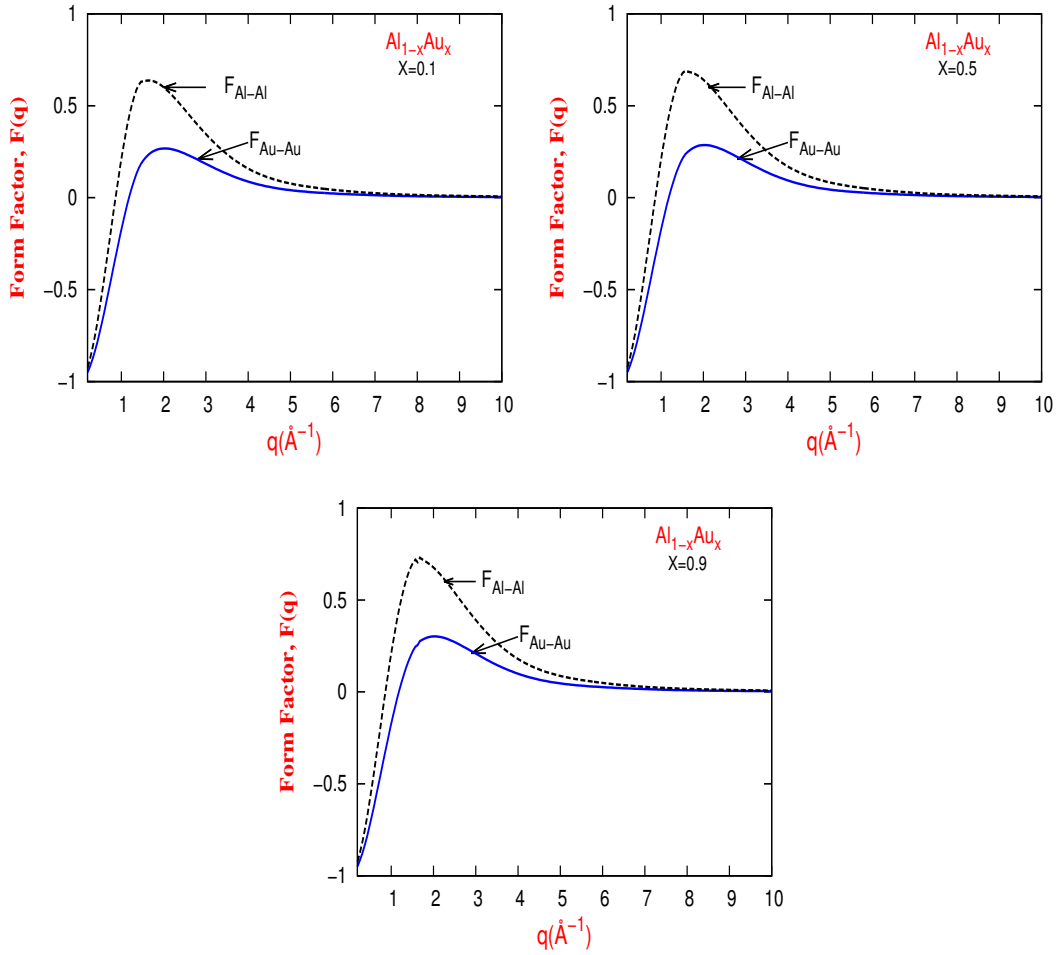

Figure 4.58: Variation of Form-factor, $F(q)$ as a function of q for $Al_{1-x}Au_x$ liquid binary system for concentration, x=0.1, 0.5, and 0.9, respectively.

4.11.2 Table for Electrical Resistivity (Ω)

Table 4.12 shows the calculated resistivity for different Al-based systems. From this phenomenon, we can conclude that the reasonably good results are found at cut off region $2k_F$, and our consideration is very justifiable.

Besides, with Figure 4.56, we have also compared our calculated resistivity (Ω) results for Al-based systems. The results for Ω, of $Al_{1-x}Cu_x$ liquid binary alloys at thermodynamic state 1373 K is presented in the second column in Table 4.12. It is seen in the Table (4.12), that the value for Ω starts to increase from concentration, x=0.1 to 0.7 and then it starts to decrease from x=0.7 to 0.9. So, the maximum value for Ω reaches at concentration, x=0.7 and its numerical value is 25.4806 Ω-m. The results for Ω, of $Al_{1-x}Zn_x$ liquid binary alloys at thermodynamic state 1000 K

Table 4.12: Comparison among the calculated resistivity at different concentrations for Al-based liquid binary alloys. Units are in Ω-m

	Ω			
Al_{1-x}	Cu_x	Zn_x	In_x	Au_x
0.1	5.44815	7.28650	8.96227	22.2576
0.2	10.5241	11.2542	11.6722	34.9515
0.3	15.3050	13.0051	12.5520	41.2972
0.4	19.5599	13.2197	12.1000	42.5141
0.5	23.0660	12.2809	10.7803	40.4613
0.6	25.3222	10.5715	8.84485	35.0706
0.7	25.4806	8.33404	6.62418	27.8769
0.8	22.7600	5.75257	4.34063	19.3445
0.9	15.2250	2.98830	2.14730	9.99879

is presented in the third column in Table 4.12. It is seen in the Table (4.12) that the value for Ω starts to increase from concentration, x=0.1 to 0.4 and then it starts to decrease from x=0.4 to 0.9. The maximum value for Ω, of $Al_{1-x}Zn_x$ is found at concentration, x=0.4 and its numerical value is 13.2197 Ω-m.

The fourth column in Table 4.12 presents the calculated results of Ω, for $Al_{1-x}In_x$

liquid binary alloys. We have found the maximum result for this alloys at concentration, x=0.3 and its numerical value is 12.5520 Ω-m. Its minimum result is found at concentration, x=0.9.

The results for Ω, of $Al_{1-x}Au_x$ liquid binary alloys at thermodynamic state 1338 K is presented in the fifth column in Table 4.12. It is seen in the Table (4.12) that the value of Ω starts to increase from concentration, x=0.1 to 0.4 and then it starts to decrease from x=0.4 to 0.9. So, the maximum value for Ω, of $Al_{1-x}Au_x$ liquid binary alloys is found at x=0.4 and its numerical values is 42.5141 Ω-m.

Symbolically, one can present the magnitude of the calculated resistivity, Ω for the studied Al-based liquid binary alloys according to its maximum values as in the following order $Al_{1-x}Au_x > Al_{1-x}Cu_x > Al_{1-x}Zn_x > Al_{1-x}In_x$

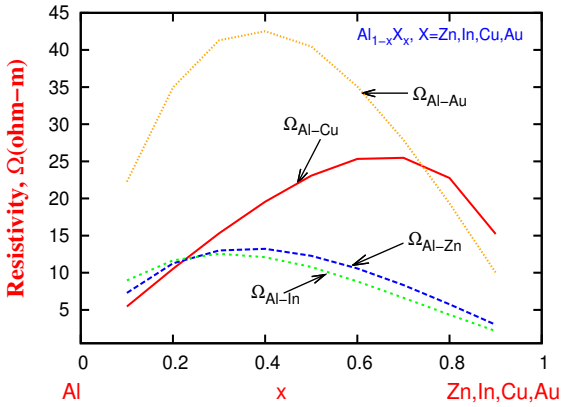

Figure 4.59: Comparison of resistivity, Ω, for $Al_{1-x}Zn_x$, $Al_{1-x}In_x$, $Al_{1-x}Cu_x$, and $Al_{1-x}Au_x$ liquid binary alloys.

4.11.3 Conclusion

We have investigated the electronic transport properties of Al-based liquid binary alloys, $Al_{1-x}Zn_x$, $Al_{1-x}In_x$, $Al_{1-x}Cu_x$ and $Al_{1-x}Au_x$ respectively. The essential ingredients in the calculations are the BS [44] model potentials, the LWCA [50] theory of liquids and extended Zimans original theory [68] for the electrical resistivity.

The analysis of the results of the present work allows us to draw the following concluding remarks:

(i). The BS pseudopotential may be a good starting point for studying structural, thermodynamics, atomic and electronic transport properties of liquid less-simple metals and their alloys.

(ii). We did not find any experimental data of electrical resistivity for $Al_{1-x}Zn_x$, $Al_{1-x}In_x$, $Al_{1-x}Cu_x$, and $Al_{1-x}Au_x$ liquid binary alloys to compare our calculated results. But the theoretical values are the same in order of magnitudes as the experimental data for the elemental systems [4].

(iii). Finally, we would like to say that, our present approach provides the GMT theory along with the extended Ziman's theory of alloys and, it may be extended to the study of simulation through the molecular dynamics.

Appendix A

Origin of Local Minimum in Potentials of Polyvalent Metals

A.1 Introduction

Local minimum appearing in the inter-ionic pair potentials, when derived from local model pseudo-potential, for Al (and some other polyvalent metals) remains as a long standing problem of clear understanding of it's origin, although some attempts have been made by a few researchers. The origin of this feature of local minimum is systematically investigated for the first time in this research work, considering both the core size and the conduction electron density as variables. "Ashcroft's empty core model" [4] is used to describe the inter-ionic pair-potential, because it depends on these two variables only. Results of this investigation showed that, the monovalent metals do not exhibit a local minimum at all.

However, trivalent Al and some other polyvalent metals do exhibit. Here, the combined effect of the core size and the conduction electron density plays the role. More interestingly, for smaller core size conduction electron density plays major role and for larger core size the core radius plays the major role of ion determining the

local minimum.

Knowledge of inter-ionic interactions is vital for microscopic description of many physical and chemical properties of condensed matters [87–90]. In order to evaluate the inter-ionic interactions, many theories, semi-empirical [4] and empirical models have been proposed so far. Among them "The Pseudopotential theory" is being widely used with a high degree of reliability. In the pseudopotential theory, which effectively started in the sixties of the last century, the electron-ion pair pseudopotentials are treated in two different ways [125]. One is the ab-initio type, which derived by employing the first principles right from the atomic level description [133, 134] and the second types are the model pseudopotentials, proposed by many authors [4–6, 44, 48, 49], which are generally parameter dependent. Among the model of pseudopotentials, the Ashcroft's empty core model [137, 138], and its kin [35] are widely used, and hundreds of articles studying physical properties of simple metals and their alloys have been published so far.

However, Hafner and coworkers [139–141] studied structural and electronic properties of many polyvalent metals using EMC and optimized pseudo-potentials. The inter-ionic interactions derived by them from these pseudopotentials with Vashista and Singwi [142], or Ichimaru and Utshumi [67] for dielectric function including relativistic, or non-relativistic core orbitals. In all cases, they found a positive local minimum at small r near the first nearest neighbor distance in solid [140] and in liquid phase for Al. Similar trends were also found for some other polyvalent metals such as Zn, In, Sn etc. Abbas et al. also found the existence of local minimum for Al in their study on $Al_{1-x}Sn_x$ liquid binary alloys [102]. According to Jank and Hafner [140], the strong electron-ion interaction leads to high electron density around the ion core and as a result, the first attractive minimum closed to rnb distances becomes quite shallow, and the minimum is practically coverd by the repulsive core.

Now question remains, if the repulsive core be much stranger, would the attractive minimum go up to yield a local minimum in the positive energy region of potential as in the clear case of Al?. This question is not addressed in [140], but an explanation of shifting the position of the first minimum is given by Jank and Hafner [139–141] that "As the electron density increases the core radius, r_c decreases and the minimum is shifted relative to the nearest distance and gets flattened". Jank and Hafner [139–141] also suggested that, the essential trend may be parameterized in terms of r_c/R_s (R_s being the also electron density parameter also sometimes refereed to as Wegner-Seitz radius) ratio. But any such theory explaining local minimum is yet to be seen. In this Appendix section, we have rather observed a different trend, that is, when the core radius increases, potential well gets shallow, relatively flattened and the same time the position of the minimum shifts of large r (see the figures).

It is surprising why no one, until now attempted systematically to explain the origin of the characteristic feature of local minimum in the positive energy region of potential, particularly for Al, during the last couple of decades after encountering the local minimum. theoretically for the first time. In the present research work, we intend to address the root cause of the characteristic feature. Specially, we shall investigate the role of the core size r_c and the conduction electron density mediated by chemical valence, and how do they effect the local minimum of the effective pair interactions.

A.2 Result

We are interested to investigate the origin of forming local minimum in the effective pair potentials of polyvalent metals, in particularly, for Al, at small r. In order to examine this feature systematically, we have started calculations for monovalent metals such as Na and K. Then we gradually advance toward the divalent (Zn),

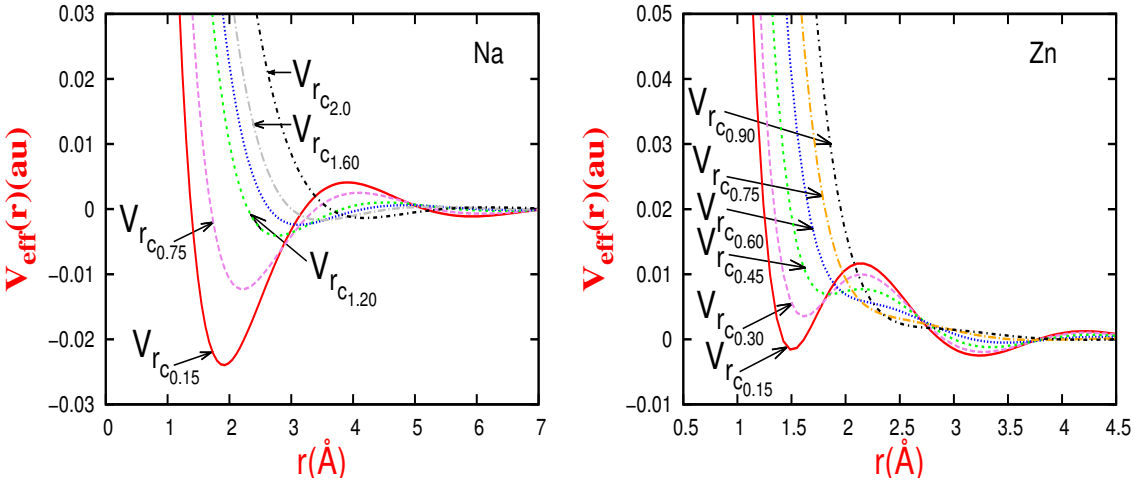

Figure A.1: Effective partial pair potential for liquid Na and Zn from core radius r_c=0.15 a.u to 2.0 and 0.90 a.u respectively.

trivalent (Al, In), tetravalent (Sn) and pentavalent (Bi) metals.

Figure A.1 shows the effective pair potentials, V_{eff}(r), for monovalent Na and divalent Zn as a function of r for different values of R_c. It is noticed that, the potential well for Na is the deepest for the smallest core size that is for the smallest value of core radius, R_c (=0.015 Å). As core radius increases the depth of the well reduces gradually and at the same time the position of the minimum shifts toward large r. However, the value of the minimum remains always negative and no local minimum appears for any value of R_c. Hafner and Jank [139–141] argued that, as the core radius decreases the electron density increases and the parameter defined as r_c/R_s (R_s being the also electron density parameter also sometimes refereed to as Wegner-Seitz radius) can easily explain the essential trend of the pseudopotential. We note that, the average conduction electron density, in this study, is assumed to remain constant during variation of core size.

It is worth for nothing that, we have also observed similar feature in V_{eff}(r) for monovalent metal, K. So, we have not presented potentials for K. Figure A.1 also shows how the depth of the well reduces with increasing value of R_c for diatomic

metal, Zn. It is noticed that, the depth of the potential well reduces and the position of the well shifts with increasing R_c as in the case of mono atomic metals.

But, in this case, a difference is noticed; the first minimum crosses the zero energy level and goes up to the positive energy region to yield a local minimum for a certain value of R_c. Farther, increase of R_c value causes the local minimum to be gradually shallow and flattened and finally to disappear from the scene completely. Consequently, the second minimum turns to be as the principal minimum of the effective potential.

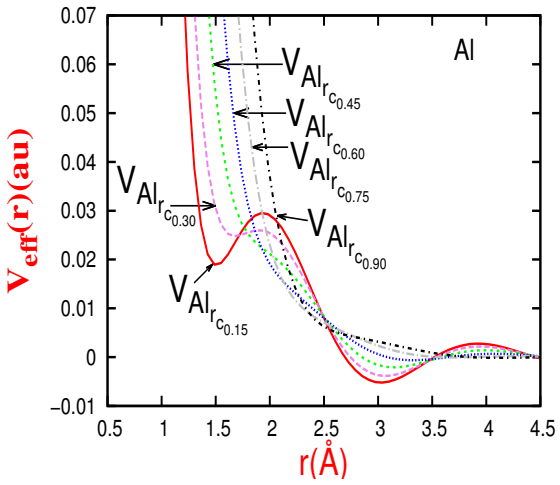

Figure A.2: Effective partial pair potential for liquid Al from core radius r_c=0.15 a.u to 0.90 a.u.

Figure A.2 shows the V_{eff}(r) as a function of r for the trivalent metal Al. Here, it is seen that the first minimum lies in the positive energy region of V_{eff}(r) even seen for the smallest core size used in the calculation and it behaves like a local minimum. The energy level of this local minimum moves upward and at the same time position of the minimum shifts to large r as R_c value increases. After certain value of R_c, which may be referred to as critical core radius R_c^c, this local minimum disappears from the scene completely, and then second minimum, then becomes the principal minimum as shown by Zn.

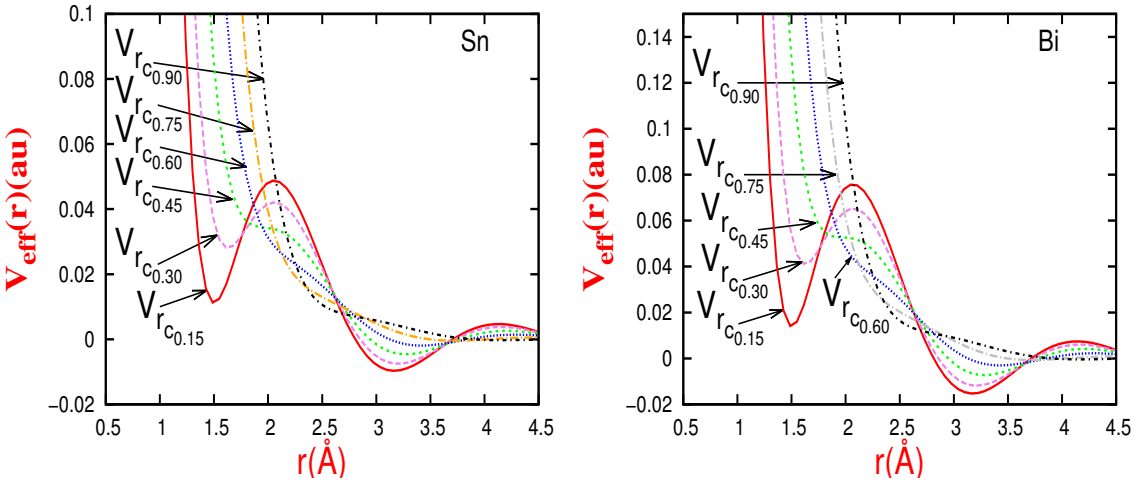

Figure A.3: Effective partial pair potential for liquid Sn and Bi from core radius r_c=0.15 a.u to 0.90 a.u respectively.

Similar trends of changing in the local minimum are also found in the case of tetravalent (Sn) and pentavalent (Bi) metals (see Figure A.3). But, in the latter cases, the level of the well of the local minimum goes to higher and higher energy positions with increment of R_c^c. Other minor differences in the behavior of local minimum, between different monovalent and polyvalent metals are also discussed in Figure A.4.

Let us now look at, what is the underlying physics involved in forming the local minimum in the effective pair potentials of some polyvalent metals. From the global perspective of the metallic sample, increment of the core size increases the distance r, from the center of the core to the nearest conduction electron in metals, and thus reduces the strength of the electron-ion interaction due to the fact of the Coulomb potential energy is inversely proportional to r.

As a result, magnitude of the form factor $F(q)$ diminishes, because R_c lies in the argument of the cosine function (see eqn (3.59)). On the other hand, the attractive indirect interaction is proportional to $|F(q)|^2$ (see eqn (3.60) and (3.61)). Consequently, attractive indirect interaction term gets weaker with increasing R_c, and the repulsive

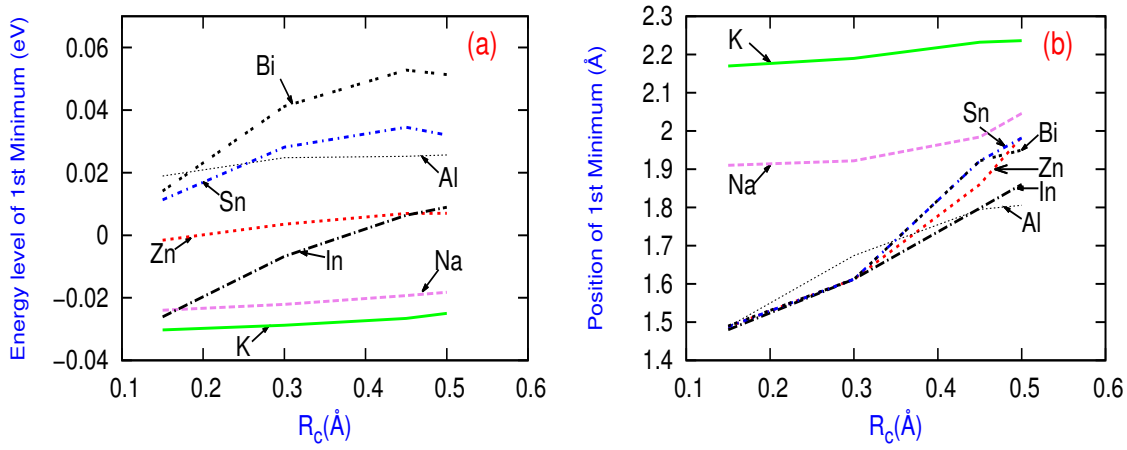

Figure A.4: (a) Position of minimum of the 1^{st} well of V_{eff}(r) as a function of R_c. (b) Energy level of the 1^{st} well of V_{eff}(r) as a function of R_c.

direct term becomes relatively stronger and dominates to reduce the depth of the well. It is informative that the conduction electron density (ρ=nZ; n being ionic number density) of Na, K, Zn, Al, Sn and Bi at T= 300 K are 0.025, 0.013, 0.0136, 0.180, 0.0140 and 0.140 $\mathring{A}^{-3}$ respectively. So. ρ is the largest for Al the smallest for K, for the rest density lies in following order, $\rho_{Al} > \rho_{Bi} > \rho_{Sn} > \rho_{Zn} > \rho_{Na} > \rho_{K}$. Now it is clear that, the depth of the well of V_{eff}(r) reduces due to the interplay between the repulsive direct and attractive indirect interactions of equation (3.60). The interesting thing is that, as the core size (R_c) increases the principal well gradually rises keeping the well in the memory [139–141] and, it continuous until a critical core radius R_c^c, is reached for each metal.

For, $R_c = R_c^c$, the form factor $F(q)$ becomes such a weak that the local minimum of V_{eff}(r) in the memory is then totally lost, it means, the local minimum disappears completely. It is interesting to note here, that the values of R_c^c are found to be $\sim 90\mathring{A}$ for all polyvalent systems. Figure A.4(a) shows the amount of shifting of the first minimum of the V_{eff}(r) for different values of R_c and for different metals. In a general point of view, it appears that the slope of shifting of minimum versus R_c curve is

the smallest for mono-atomic metals Na and K, respectively, and it is much larger for polyvalent metals. That is, increase of R_c value cause polyvalent metals to shift position of minimum of V_{eff}(r) to large r much than monovalent ones.

It is also noticed from Figure A.4(a), that the position of the first minimum for the smallest R_c value lies at the larger r for mono-atomic metals than polyvalent ones. Interestingly, for the smallest value of R_c, positions of first minima are almost same for all polyvalent metals irrespective of their valence Z. But the lines indicating shifting of position of minima differ from each other with increasing R_c, and cross each other at large R_c.

Figure A.4(b) illustrates how the energy level of the first minimum of the effective inter-ionic potential varies with the change of R_c values. In this case, it appears that Na, K, Zn and Al show one kind of trends and, Sn and Bi showed that a different one. Metals belong to the former group are monovalent, divalent and trivalent, and and in the later group are tetravalent and pentavalent. From Figure A.4(b) it is also noticed that, for the smallest value of R_c(=0.015 Å) energy level of the first minimum is positive for Al, Sn and Bi., whereas it is negative for others (i.e for Na, K, Zn).

That is, polyvalent metals Al,Sn and Bi exhibit local minima even from the smallest core size chosen and the divalent Zn shows at larger values of R_c; but Na and K never show. Figure A.4(b) illustrates another very interesting feature that, the energy levels of the first minimum at the smallest value of R_c are different for different metals and varies in the following order, $V_{eff}^{Al} > V_{eff}^{Bi} > V_{eff}^{Sn} > V_{eff}^{Zn} > V_{eff}^{Na} > V_{eff}^{K}$. Interestingly enough that, the conduction electron density of the envisaged systems varies exactly in the same order as V_{eff}(r). This obviously raises a question that, is the energy level of the first minimum at the smallest possible core size strongly related to the conduction electron density of the corresponding metals?

In order to address the above question, and to find any possible relation between

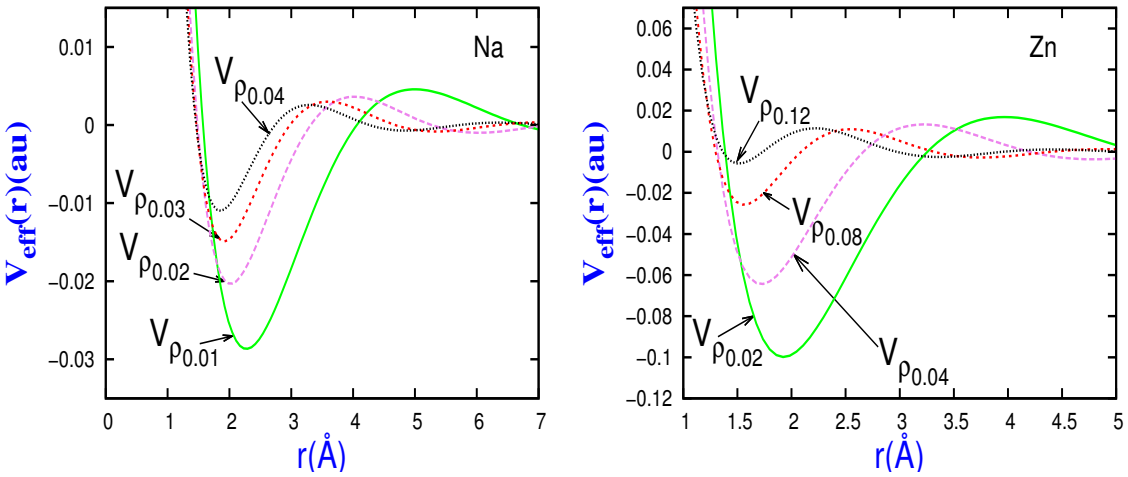

Figure A.5: Efective partial pair potential for liquid Na and Zn for fixed core radius r_c=0.15 a.u, but for different electron number density, ρ(=nZ).

the energy level of the local minimum and the conduction electron density we have calculated V_{eff}(r) for different conduction electron densities keeping R_c constant. These calculated results are presented in Figure A.5 and Figure A.6. Here, it is worth for nothing that, as the direct interaction depends on chemical valence Z, we kept Z fixed for each system and varied ionic number density, n, in calculating conduction electron densities ρ(=nZ) for different metals. Figure A.5 and Figure A.6 showed that, the energy level of the first minimum *i.e.* the depth of the potential well reduces with increasing ρ and at the same time the position of the minimum shifts towards small r; the later trend is just opposite to that found for increasing R_c. The indirect interaction term of equation (3.59) depends on both Z and conduction electron density through the dielectric function. It is therefore obvious that, with the increase of ρ dielectric function increase and consequently indirect attractive term will get weaker. This will cause reduction of the potential well of V_{eff}(r). This is what exactly displayed in Figure A.5 and Figure A.6. From Figure A.5, and Figure A.6, it is also noticed that, at metallic density of the individual element, the minimum energy level and position of local minimum for R_c=0.15 Å matches exactly with

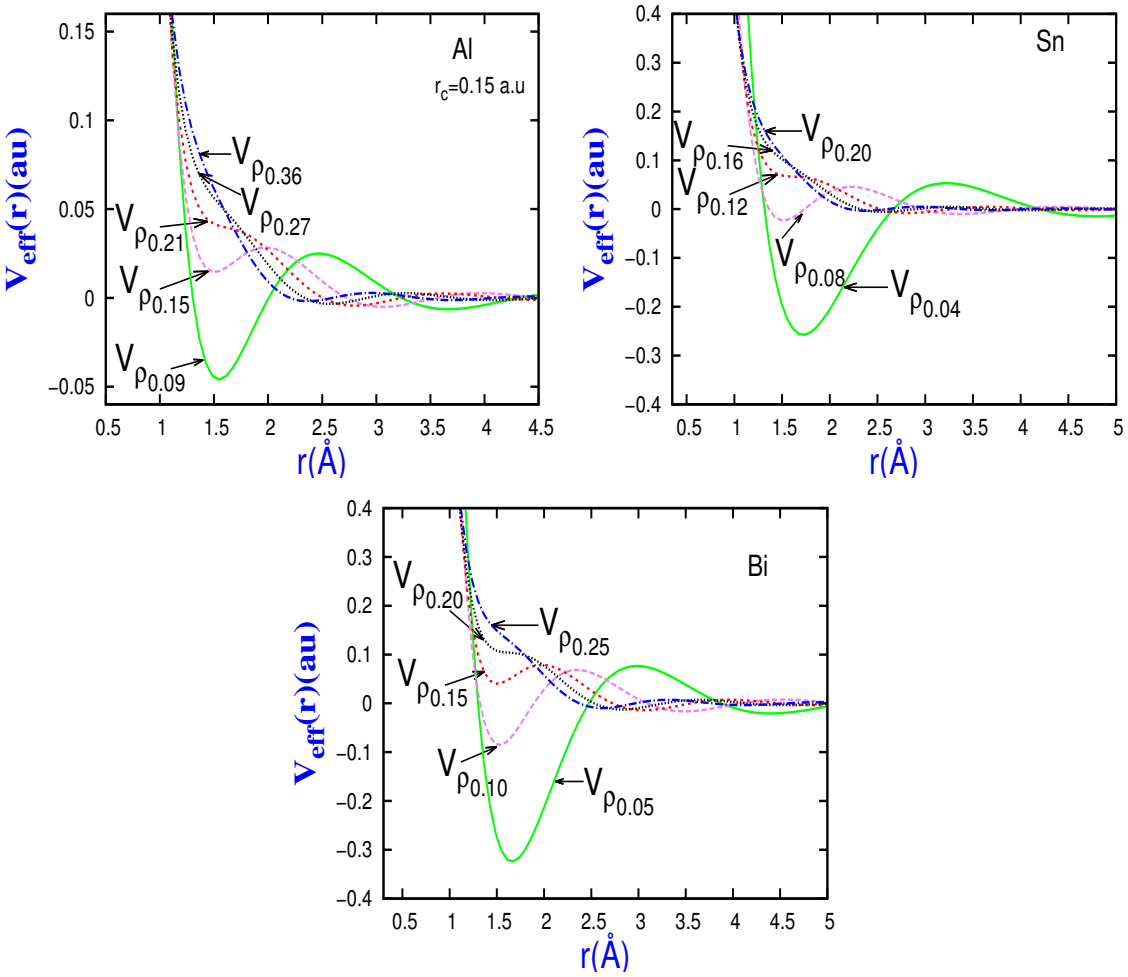

Figure A.6: Efective partial pair potential for liquid Al, Sn and Bi for fixed core radius r_c=0.15 a.u, but for different electron number density, $\rho(=nZ)$.

those in Figure A.1, Figure A.2 and Figure A.3. Here, it is relevant to note that the local minimum disappears again when $\rho \sim 0.36$ Å^{-3} for all polyvalent metals. The knowledge of variation of V_{eff}(r) with change of electron density might be useful in the study of physical properties at high pressures, because the density will increase with increasing the pressure.

A.3 Conclusion

We have systematically investigated for the first time that, the effect of core size of the ion, and the role of conduction electron density on the inter-ionic pair interactions of monovalent and polyvalent metals. The effective inter-ionic interaction is described by the Ashcroft empty core model [15] and Ichimaru- Utsumi theory for dielectric function [67]. From the analysis of the core radius R_c and the conduction electron density ρ, we can draw the following conclusions:

(i) The depth and position of the first minimum of V_{eff}(r) are results of delicate valence between the repulsive direct and attractive indirect interactions.

(ii) The depth of the first minimum of V_{eff}(r) reduces and at the same time its position shifts towards large r with increasing values of R_c, and an opposite trend of shifting towards small r happens with increasing electron density ρ. But any local minimum has not not been found at all for monovalent metals. Only polyvalent metals are exhibiting the local minimum.

(iii) The local minimum and its position are results of combined effects of the core size and the conduction electron density. Effects of core size dominate at large R_c and that of ρ, dominates R_c.

(iv) Among polyvalent metals divalent Zn does not exhibit a local minimum initially but it does for large values of R_c, whereas all other polyvalent systems with $Z > 2$ show local minimum right from the smallest value of R_c chosen.

(v) For $R_c > R_c^c$ form factor, $F(q)$, becomes negligibly small. The critical values of core radius are almost same (0.90 Å) for different metals.

(vi) At the smallest possible of core size, the energy level of the first minimum of V_{eff}(r) is mostly determined by conduction electron density of metals, that is,

the level of the minimum is higher with larger value of ρ. But, for large values of R_c, energy levels are affected by the core size. Then the initial relative order of magnitudes of minimum energy level for different metals understudy is not strictly followed; they may cross each other.

Appendix B

Effects of Local Minimum appeared in Inter-atomic Potential on Atomic Transport of Liquid Aluminium

B.1 Introduction

The study of the relationship between the structural and the thermodynamic properties of metallic liquids has been attracted to scientists and metallurgists because of its importance in both academic and industrial researches. Universal Scaling Laws (USLs) proposed by Dzugutov [85] and Rosenfeld [121] showed how the structure and thermodynamics are connected to the transport coefficients, for example, the diffusion and the shear viscosity coefficients. Diffusion and shear viscosity coefficients are usually known to play a important role for a detailed understanding of the solidification process including crystal growth [135–137], vitrification [138] and in the casting industry as well [139–141].

Very recently, the authors in ref. [57] performed a study on thermodynamic mixing behaviors for liquid binary segregating alloys, namely $Al_{1-x}Sn_x$ at near the melting temperature (973 K) of Al where they had seen some interesting features in the potential of the liquid binary alloys [56]. The interesting feature is that, a local minimum is appeared near the principal potential well and it is shifted from its negative region to the upper positive region [56, 73–75] with increasing core radius, r_c of liquid Al, which motivated us to study in the mentioned topics.

Atomic transport properties can be studied either using theoretical approaches [148–151], or experimental techniques [151–153] or computer simulation methods [85,121,149,151,154]. Recently, USLs [155] have been widely used to calculate transport coefficients theoretically, especially for high temperature melts, we should note here that, in ref. [148], the author used 3 body excess entropy for the calculation of diffusion coefficient. In ref. [149], Ju Yuan *et .al* have observed the the effects of variation of temperature to calculate diffusion coefficients from molecular dynamics where the chosen potential is obtained from the Embedded atom method (EAM). In addition, shear-viscosity using the Stokes-Einstein relation have been studied and then compared their MD results with experimental data [149]. Differently from the above consideration, Iida *et .al* [150], Iida *et .al* introduced a new parameter indicating the hardness and softness of the interaction to calculate transport properties. Still the problem was that, this considered model is dependent on experimental data. In ref. [151], temperature dependent self diffusion coefficients of liquid Al has been studied experimentally by using incoherent quasi elastic scattering theory. Besides they also compare the self diffusion coefficients results with calculated results using the Sutherland-Einstein relation instead of Stokes-Einstein relation. The calculated and experimental results agree surprisingly well.

Apart from the theoretical study, these properties can be studied experimentally,

for example, Demmel *et .al* [153] has been performed the coherent quasi-elastic neutron scattering for the study the diffusion coefficients of liquid Al. They also compare their experimental results with theoretical results obtained from Stokes-Einstein relation and some MD results obtained from different potential like pseudo-potentials and first-principles molecular dynamics. In ref. [151], the authors used highly pure Aluminium (99.99) as Hydro-Aluminium. In ref. [152], the oscillating vessel viscometer has been performed to measure experimentally viscosity for liquid metals such as Al at various temperatures.

Recently, simulation studies come forward to explain diffusion and viscous behavior of liquid metals, such as, Kargil *et al*. did MD simulation with different model potential like LOARH, MKBA1, LEA and MDSL and then compare them to their experimental results. In ref. [154] had chosen ab initio molecular dynamics for the study of diffusion and viscosity of liquid Al. In their article, they compared the results obtain from MD with experimental data and different MD results obtain from different potentials. Dzugutov *et .al* [85] introduced a Universal scaling law based on the microscopic origin for diffusion coefficients for liquid metals and combined it with MD simulations. Before that, in Ref [121], Rosenfeld studied the transport properties using USL described from the macroscopic parameters. For finding the transport coefficients using USLs, temperature dependent excess entropy is the main ingredient. Besides al this articles discussed above some other articles for Pasturel *et .al* [155–157], where they studied about the MD simulations with different potentials and combined it with Stokes-Einstein formula and excess entropy used as for basic ingredient.

In those studies [148–158], we have observed that for calculations of atomic transport properties, the prescribed theories are revised from different point of views, but the effect of local minimum or local structures appeared at low r_c for liquids Al, Bi,

Sb. etc. on the transport properties has not been considered with the combination of USLs and empty core model(EMC) potential.

Therefore, we, in the present article, intend to study for the first time to investigate the atomic transport coefficients for liquid Al at near its melting temperatures using the EMC model [4] for inter-ionic interaction along with VMHNC theory. The principle reason for applying the EMC model in the present study is to understand the behavior of interaction in valence level with change of its core radius, r_c. Essentially, the EMC model potential is a local potential which makes an effective complete cancellation in the region $r < r_c$ [4]. Actually it consists of both repulsive and attractive interaction between ions. The repulsive inter-ionic interaction in the model is manifested by just Coulomb interaction, where as the attractive inter-ionic interaction is mediated by conduction electron density [56]. Considering all the facts mentioned above, we have studied the transport coefficients of liquid Al with EMC of various core radius with VMHNC theory to see either this combination can explain the transport properties or not.

The layout of the Appendix is as follows: In section 2, we describe theory in brief related with the study. In section 3, we will present our obtained results and then discuss with arguments. Finally, in section 4, we conclude the study with future plan.

B.2 Theory

The theory we have used in this study are given below,

B.2.1 Scaling Laws for Transport Coefficients

The relation between the transport coefficients and structural properties, the USLs are proposed by several authors [85,86,121,122]. Among them, Rosenfeld [82] consid-

ered macroscopic reduction parameters, temperature and density whereas Dzugutov and Li [85, 122] considered microscopic reduction parameter, collision frequency and hard sphere diameter (HSD) to calculate transport coefficients. Hoyt *et al.* [121] applied scaling law provided by Dzugutov *et al.* [85] to calculate transport coefficients numerically for various systems with different potentials. Following Dzugutov, recently, Li *et al.* [122] proposed a similar scaling relationship for viscosity. These are as follows.

Atomic transport coefficients, namely the reduced diffusion coefficient (D_R^*), and the reduced shear viscosity (η_R^*) proposed by Rosenfeld *et al.* [121] may be written as,

$$D_R^* = D\frac{n^{1/3}}{(k_BT/m)^{1/2}} \tag{B.1}$$

$$\eta_R^* = \eta\frac{n^{-2/3}}{(mk_BT)^{1/2}} \tag{B.2}$$

where, n, and T are the number density and temperature of the systems respectively. These macroscopic reduction parameters (n and T) were chosen for the reduced transport coefficients. Based on the hundreds of simulation results [121, 122, 158], the reduced transport coefficients can be written as,

$$D_R^* = 0.6e^{0.8S_{ex}} \tag{B.3}$$

$$\eta_R^* = 0.2e^{-0.8S_{ex}} \tag{B.4}$$

where, S_{ex} is the excess entropy of the sytems. The excess entropy, S_{ex}, can be approximated using the two-body contribution as,

$$S_2 = -2\pi n\int_0^\infty \{g_2(r)\ln[g(r)] - [g_2(r)-1]\}r^2dr \tag{B.5}$$

where, $g_2(r)$ is the pair distribution function.

In 1996, the scaling law for diffusion coefficients is revised by Dzugutov [85] using the microscopic reduction parameters, collision frequency Γ, and HSD, σ. In 2005, following Dzugutov, Li [122] defined a scaling law relation for viscosity. Based on the microscopic reduction parameters, they defined the following reduced diffusion and viscosity coefficients,

$$D_Z^* = D\frac{1}{\Gamma\sigma^2} \tag{B.6}$$

$$\eta_L^* = \eta\frac{\sigma}{\Gamma m} \tag{B.7}$$

where collision frequency Γ according to Enskog theory is,

$$\Gamma = 4\sigma^2 g_2(\sigma) n(\pi k_B T/m)^{1/2}. \tag{B.8}$$

where, $g_2(\sigma)$ is the pair distribution function evaluated at hard sphere diameter, σ. The hard sphere diameter was chosen at the position of first principal peak of $g_2(r)$. Based on the hundreds of simulation results for the reduced transport coefficients, they proposed the following scaling laws,

$$D_R^* = 0.049e^{S_{ex}} \tag{B.9}$$

$$\eta_R^* = 0.035e^{-0.55S_{ex}}. \tag{B.10}$$

B.2.2 The Empty Core Model Potential(EMC)

The Empty core potential (EMC) for one component metallic systems may be expressed as [4, 125],

$$W_b(r) = \begin{cases} 0; & \text{if } r < r_c, \\ \\ -Ze^2/r; & \text{if } r > r_c. \end{cases} \tag{B.11}$$

Where, r_c, Z, and e are the core radius, the effective s-electron effective valence and the electronic charge respectively. The unscreened form factor of equation (B.11) is [4, 73–75],

$$v_{ij}(r) = -\frac{4\pi Z\rho}{q^2}\cos(qr_c) \tag{B.12}$$

where, ρ is the ionic number of density, q the momentum transfer. If we observe the equation (12) then we can noticed that the core radius r_c, enters into the form factor of the interaction through the scattering matrix. This form factor finally carries the r_c into the inter-ionic interaction.

Within the pseudo-potential formalism, the effective inter-ionic pair interaction can be written as,

$$v_{eff}(r) = \frac{Z^2}{r}\left[1 - \frac{2}{\pi}\int dq I^N \frac{\sin(qr)}{q}\right] \tag{B.13}$$

Here, the energy wave number characteristic can be defined as,

$$I^N = [\frac{q^2}{\pi n Z}]^2 |V(q)|^2 \left[1 - \frac{1}{\varepsilon(q)}\right]\left[\frac{1}{1 - G(q)}\right] \tag{B.14}$$

Where, $V(q)$ denotes the local pseudo-potential of the component and n the number density of ions. Besides $\varepsilon(q)$, and $G(q)$ the dielectric screening function and the local field factor, respectively. Here, the dielectric function,

$$\varepsilon(q) = 1 - \left[\frac{\frac{4\pi e^2}{q^2}\chi(q)}{1 + \frac{4\pi e^2}{q^2}G(q)\chi(q)}\right] \tag{B.15}$$

Where, $\chi(q)$ is Lindhard function,

$$\chi(q) = -\frac{mk_F}{\pi^2\hbar^2}\left[\frac{1}{2} + \frac{4k_F^2 - q^2}{8qk_F}\ln\left|\frac{2k_F + q}{2k_F - q}\right|\right] \tag{B.16}$$

B.2.3 VMHNC Integral Equation Theory

The VMHNC theory, originally proposed by Rosenfeld [121], belongs to a new generation of integral equation theory of liquid. Like most other integral equation theories, the VMHNC solves the Ornstein-Zernike (OZ) equation with a closure relation

$$g_2(r) = \exp\left[h(r) - c(r) - \beta u_{eff}(r) - B(r)\right] \tag{B.17}$$

Table B.1: Temperature dependent number density (ρ), hard sphere diameters (σ) and excess entropy (S_E) for our concerned liquid.

T(K)	ρ	$\sigma_{rc_{0.90}}$	$\sigma_{rc_{1.092}}$	$\sigma_{rc_{1.20}}$	$S_{E_{rc_{0.90}}}$	$S_{E_{rc_{1.092}}}$	$S_{E_{rc_{1.20}}}$	$S_{E_{Expt.}}$
950	0.05314	2.4814	2.6100	2.6785	-1.5396	-2.9101	-4.5281	-3.55
975	0.05298	2.4772	2.6057	2.6740	-1.5219	-2.8594	-4.4208	
1000	0.05282	2.4732	2.6014	2.6696	-1.5047	-2.8118	-4.4073	
1025	0.05267	2.4691	2.5971	2.6653	-1.4883	-2.7658	-4.3094	-3.40
1050	0.05251	2.4651	2.5930	2.6610	-1.4719	-2.7218	-4.2133	
1075	0.05236	2.4612	2.5888	2.6567	-1.4552	-2.7114	-4.1232	
1100	0.05220	2.4573	2.5847	2.6525	-1.4408	-2.6633	-4.0348	
1125	0.05204	2.4535	2.5807	2.6484	-1.4245	-2.6263	-3.9499	
1150	0.05189	2.4497	2.5767	2.6443	-1.4104	-2.5868	-3.8706	

where $g_2(r)$, $h(r)$, $c(r)$, $B(r)$ and β denote pair correlation function, total correlation function, direct correlation function, bridge function and inverse of tempera-

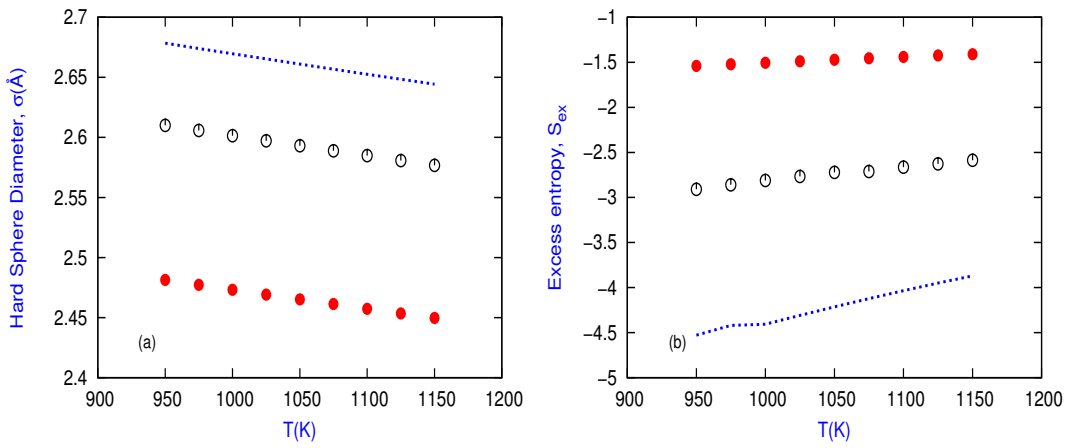

Figure B.1: (a) Hard sphere diameter for core radius, r_c= 0.90 a.u, 1.092 a.u and 1.20 a.u respectively for liquid Al. (b) Excess entropy for core radius, r_c= 0.90 a.u, 1.092 a.u and 1.20 a.u respectively for liquid Al.

ture times Boltzmann constant, respectively. The bridge function $B(r)$ is approximated by using the analytic solution of the Percus-Yevick equation for HS namely $B(r) = B^{HS}_{PY}(r, \zeta)$. ζ is the variation parameter which is determined by minimizing the free energy.

B.3 Results and Discussion

We have presented the effects of local minimum on the calculation of temperature dependent atomic transport co-efficients, namely the shear viscosity and the diffusion coefficient of liquid Al using USLs. As we said earlier, the essential ingredients of the study are the temperature dependent effective HS diameter σ(T) and excess entropy, S_{ex} in USLs. To calculate S_{ex}, we have used equation (5), where $g_2(r)$ is obtained using VMHNC [121] with EMC model potential of various core radii.

EMC model [4, 125] has been developed from the combination of a perturbation scheme and the statistical mechanics approach. It has two parameters, namely core radius, r_c and valency Z. Before the numerical calculation, one has to fix them. In

this study, the parameter, r_c, has been chosen from the fitting of the experimental data [29] of $g_2(r)$. The fitting values of r_c=0.90 a.u, 1.092 a.u, and 1.20 a.u have been plotted in Figure B.2 and potential full profiles plotted in Figure B.3 (a-f). The valency Z=3.0 [57], has been chosen for liquid Al. Once the parameterization is done, the rest of the calculations for the transport coefficients are parameter free and theoretically much consistent and sound. Consequently accuracy is much more reliable.

The results for the transport coefficient namely the shear viscosities, η has been calculated using core radius r_c=0.90 a.u, 1.092 a.u, and 1.20 a.u for EMC model, respectively. On the other hand, the diffusion coefficients, D have been calculated by using the EMC model only for understanding the core interactions very deeply [17, 28, 29, 37]. Valency Z=3.0 has been taken for this model. Values of atomic transport coefficients are very sensitive to the profile of the potentials and their corresponding pair correlation functions.

Figure B.1 represents the profile of (a) the hard sphere diameter (σ) and (b) excess entropy (S_{ex}) of liquid Al at three different r_c=0.90 a.u, 1.092 a.u and 1.20 a.u. In each r_c, we have studied the transport coefficients from T=950 K to 1150 K, and we observe that, the value of σ is maximum at low temperature and it starts to decrease with increasing the temperatures. It is observed that, the value of S_{ex} is negative from whole range of temperature from three different r_c, which is consistent with our theory. At T=950 K, the negative value is minimum and at T=1150 K negative value is maximum which is also consistent with our theory. Table B.1 represent the numerical value of number density (ρ), σ, and S_{ex}.

The pair correlation function $g(r)$ for liquid Al at different core radius r_c=0.90 a.u, 1.092 a.u and 1.20 a.u have been presented at T=1323 K for fitting the parameters and compare them with available experimental data [29] in Figure.2. The peak value is

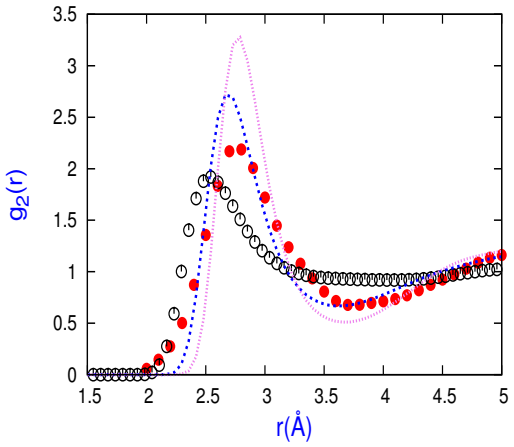

Figure B.2: Pair correlation function for liquid Al with EMC model for core radius, r_c= 0.90 a.u, 1.092 a.u and 1.20 a.u respectively. The red circles are corresponding experimental data [29].

maximum for r_c=1.20 a.u and minimum for r_c=0.90 a.u. It is also observed that, the peak value is shifted slightly right side for increasing r_c. It directly indicate that, the empty core size is also increasing. But if we see the value of η and D in Table B.2 and Table B.3, it can be easily said that, it causes the effect for this transport coefficients and which are not consistent with theoretical [148–151], experimental [151–153] and simulated data [85, 121, 149, 151, 154].

Figure B. 3(a-f) represent the effective partial pair potentials u(r) for Al with three different core radius r_c for finding the interaction with EMC model at different thermodynamic temperatures. In Figure B. 3(a-f), it can be seen that, the well depth of the first minima is maximum for r_c=1.20 a.u, and if we start to decrease the value of r_c then the first minima value also decrease in Figure B. 3(e-d)) and after certain value of r_c the first minima is just disappeared Figure B. 3(a-b) which is very interesting features of liquid Al in interaction level.

It means that after certain value of r_c, the interaction is very low and sometimes there might be no interaction [57, 73–75] and we have found the similar pattern on

our study. At high r_c, the values of η and D are maximum and far deviate from the results of theoretical, experimental and simulation. Figure B. 3(b,d,f) provide the informations that, the position of first minima also slightly shifted from left side to right side. The depth of the potential well also related with temperature. It is seen in Figure B. 3(b,d,f) that, the potential well depth also increase with the increasing temperatures [151, 154]. This behavior still remains where there is no interaction in ion.

Table B.2: Presents viscosities of liquid polyvalent Al metal. Calc.1 present calculated viscosities by Empty Core model with core radius r_c=0.90 a.u, 1.092 a.u and 1.20 a.u respectively. Similarly, Calc.2 present calculated viscosities by Rosenfeld model with core radius r_c=0.90 a.u, 1.092 a.u and 1.20 a.u respectively. Calculated viscosities are compared with Experimental, Theoretical and Simulated results.

T(K)	η(mPa s)										
	Expt.	Calc.1			Calc.2			Theory	Sim		
	[152]	$r_{c_{0.90}}$	$r_{c_{1.092}}$	$r_{c_{1.20}}$	$r_{c_{0.90}}$	$r_{c_{1.092}}$	$r_{c_{1.20}}$	[148–150]	[154]	[85]	[121]
950	1.298	0.452	1.292	3.917	0.2358	0.706	2.576	1.125	-	1.36	1.21
975	1.235	0.444	1.226	3.538	0.2351	0.685	2.390	1.05-1.237	-	-	-
1000	1.178	0.440	1.178	3.397	0.2343	0.666	2.390	-	1.05-1.51	1.25	1.15
1025	1.126	0.439	1.144	3.150	0.2337	0.649	2.233	1.10	-	-	-
1050	1.079	0.446	1.119	2.954	0.2330	0.633	2.088	1.035	1.15	1.17	1.01
1075	1.035	0.470	1.118	2.803	0.2322	0.634	1.962	0.935	-	1.155	-
1100	0.996	0.484	1.091	2.756	0.2317	0.616	1.846	0.95	1.0	1.13	0.92
1125	0.959	0.489	1.074	2.817	0.2308	0.603	1.740	-	0.98-1.21	1.07	-
1150	0.925	0.486	1.048	2.811	0.2303	0.590	1.648	-	0.88	1.05	0.85

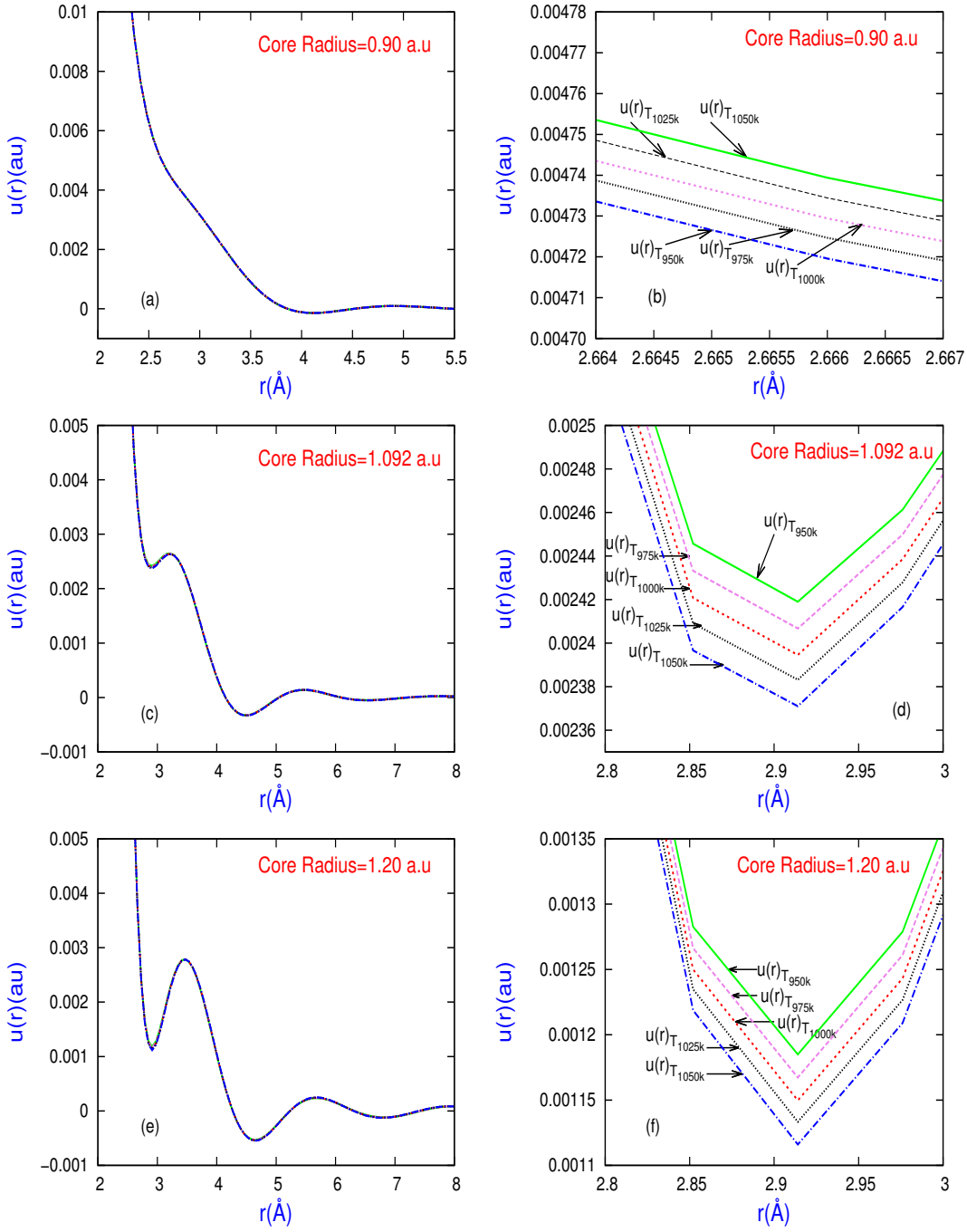

Figure B.3: Figure: (a) and (b) representing the potential well for r_c=0.90 a.u. for two different range. Similarly, Figure: (c) and (d), Figure: (e) and (f) representing the potential well for r_c=1.092 a.u. and 1.20 a.u, respectively.

Table B.3: Diffusion coefficients of liquid polyvalent Al metal. Calc.1 present calculated diffusion coefficients by Empty Core model with core radius r_c=0.90 a.u, 1.092 a.u and 1.20 a.u respectively. Similarly, Calc.2 present calculated diffusion coefficients by Rosenfeld model with core radius r_c=0.90 a.u, 1.092 a.u and 1.20 a.u respectively. Calculated diffusion coefficients are compared with Experimental, Theoretical and Simulated results.

	$D(10^{-9}\mathrm{m}^2\mathrm{s}^{-1})$									
T(K)	Expt.		Calc.1			Calc.2			Theory	Sim.
	[153]	[151]	$r_{c_{0.92}}$	$r_{c_{1.092}}$	$r_{c_{1.20}}$	$r_{c_{0.90}}$	$r_{c_{1.092}}$	$r_{c_{1.20}}$	[151]	[149, 151]
950	6.097	-	19.744	7.845	2.094	25.092	8.383	2.297	6.20-6.50	-
975	7.060	7.14-7.26	19.841	8.015	2.167	25.809	8.853	2.538	-	-
1000	7.311	-	20.085	8.250	2.222	26.528	9.323	2.601	7.80-7.82	4.39-6.42
1025	-	7.20-8.60	20.435	8.560	2.328	27.239	9.802	2.851	-	5.05
1050	8.776	8.10-9.50	21.211	8.918	2.521	27.961	10.287	3.119	9.10-9.25	4.11
1075	-	-	22.809	9.014	2.738	28.699	10.506	3.395	-	5.47-5.81
1100	9.696	-	23.914	9.433	3.074	29.396	11.055	3.690	10.20-10.40	-
1125	-	-	24.645	9.783	3.566	30.151	11.528	3.998	-	6.17-8.75
1150	11.1201	-	24.949	10.11	4.005	30.858	12.041	4.311	11.30-12.02	7.17-9.97

The pair correlation function ($g(r)$) of Al with different r_c has been presented in Figure B. 4(a,b) with different temperature. Figure B. 4(a) represents the characteristics of g_2 for r_c=0.90 a.u, 1.092 a.u and 1.20 a.u at temperature 950 K. The peak value is maximum for r_c=1.20 a.u and minimum for r_c=0.90 a.u, where there is very low interaction in core. On the other hand, Figure B. 4(b) presents $g(r)$ for r_c=1.092 a.u at temperature T=950 K and 1150 K. But, the change of $g(r)$ is very negligible.

Figure B.5 represents the verification of stokes-Einstein law. From the Figure, we can easily claim that, the multiplication of transport coefficients of liquid Al violates the stokes-Einstein law.

Table B.2 represents the shear viscosities, η for liquid Al at different temperatures with core radius r_c=0.90 a.u, 1.092 a.u, and 1.20 a.u, respectively using the USLs for both Dzugutov [85] and Rosenfeld [121] approach. Here, Cal.1 and Cal.2 denote the results for shear viscosity using the method of Dzugutov [85] and Rosenfeld [121], respectively. It is seen that, the conjunction of EMT model with VMHNC approximation does not work very well to predict results of η near the core region, and also far distance of core. Moreover, the combination can predict the results for η within Dzugutov [121] approach works nicely. At r_c=1.092 a.u, the calculated results are very close to experimental, simulated and some other theoretical results. For r_c=1.20 a.u, the calculated results are larger than our reference and r_c=0.90 a.u obtained results very low to compare with them.

Similarly, the atomic diffusion coefficients, D for liquid Al has been presented in Table B.3, for three difference core radius. The trends are very common for D. The calculated results obtain from Dzugutov [85] are more physical than the results from Rosenfeld [121]. With increasing the temperature the diffusion coefficients also increase, but the increase rate are very slow. But the results are found to be very close to the experimental data's [151, 153], and some other simulated and calculated data's.

Table B.4 represent the stokes-Einstein law verification data. From the table, we can easily claim that, the multiplication of this two transport coefficients is almost same. So, the results we have obtained is good enough for liquid Al.

We have observed that, the Universal Scaling Laws proposed by Dzugutov [85] work very well to investigate the transport coefficients for liquid Al than Rosenfeld

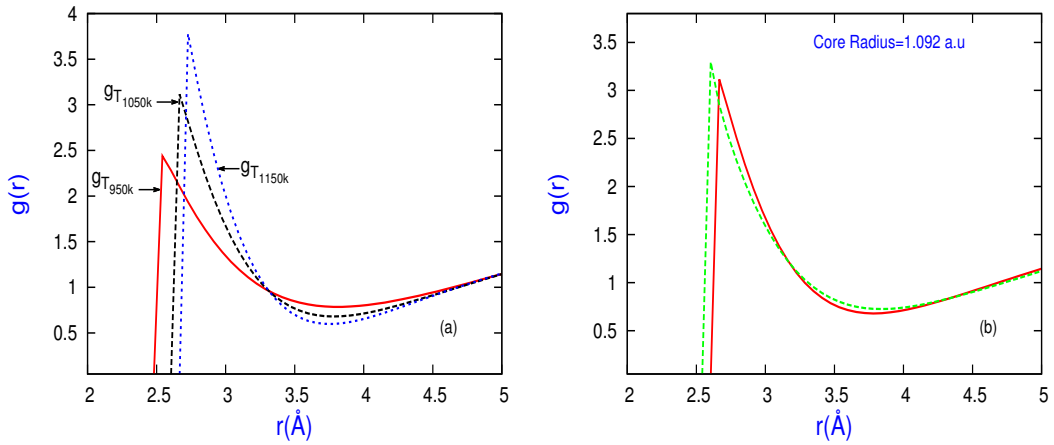

Figure B.4: (a) Black circle, dashed line and black-white circle representing the pair correlation function with temperature 950 K for core radius r_c=1.20 a.u, 1.092 a.u and 0.90 a.u respectively (b) Triangle and dashed line representing the pair correlation function with different temperatures for T= 950 K and 1150 K respectively with core radius, r_c= 1.092 a.u.

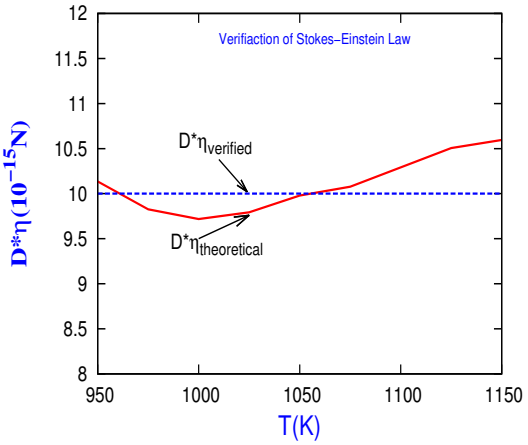

Figure B.5: Verification of Stokes-Einstein Law.

Table B.4: Verification of Stokes-Einstein Law.

T(K)	η(mPa s)	$D(10^{-9}\mathrm{m^2s^{-1}})$	η^*D
950	1.292	7.845	10.135
975	1.226	8.015	9.8263
1000	1.178	8.250	9.7185
1025	1.144	8.560	9.7926
1050	1.119	8.918	9.9792
1075	1.118	9.014	10.077
1100	1.091	9.433	10.291
1125	1.074	9.783	10.506
1150	1.048	10.110	10.5952

[121] approach. Among the three core radius, r_c=0.90 a.u, 1.092 a.u, and 1.20 a.u, we have observed that, at nearest core region r_c=1.092 a.u the transport coefficients results are found to be very close with experimental [148–151], simulation [85, 121, 149, 151, 154] and other theoretical [148–151] results.

In the inter-ionic interaction, the depth of the first minimum of Empty Core (EMC) potential profile also increases with the increasing of r_c value. The reverse trend is found, that if we decrease the value of r_c the well depth also decrease and at certain value of r_c, the mimimum is just disappeared which is very interesting. A further study is required to understand this behavior.

Another interesting feature at r_c=0.90 a.u, the calculated results for η are very low for both Dzugutov [85], and Rosenfeld [121] to compare with other results. Similarly, for D the results are very high. This behavior suggests us that, the interaction is very low or interaction empty in that core region within the ion.

B.4 Conclusion

A combination of EMC and VMHNC can give a good starting point for the study of the atomic transport coefficients for polyvalent simple elements. From the point of view for USLs, it can work very nicely for polyvalent simple elements. Finally, we would like to extend our study for different polyvalent systems, for understanding the potential well behavior in core level as well as how the transport coefficients change with changing its core radius.

Appendix C

Some Relevant Theories for Liquids

C.1 Pair Distribution Function for Liquids

For a canonical ensemble or $N\Omega T$ ensemble the normalized equilibrium probability density $f_0^{(N)}$ for a system of homo-nuclear atoms of the number, N is given by

$$f_0^{(N)}(\bar{r}_1, ..., \bar{r}_N, \bar{p}_1, ..., \bar{p}_N) = \frac{\exp\left[-\beta\mathcal{H}(\bar{r}_1, ..., \bar{r}_N, \bar{p}_1, ..., \bar{p}_N)\right]}{N!h^{3N}Z_N(\Omega, T)} \tag{C.1}$$

where the number $N!$ comes from indistinguishably of particles, $\beta = (k_B T)^{-1}$, k_B denotes Boltzmann constant, T is the temperature and h is the Plank's constant and normalizing factor $Z_N(\Omega, T)$ is the configuration partition function which can be expressed as,

$$Z_N(\Omega, T) = \mathrm{Tr}\exp(-\beta\mathcal{H}) \tag{C.2}$$

The trace runs over both electronic and ionic states of the system. By using

adiabatic approximation we may separate electronic and ionic states as [15] in the total partition function

$$Q_N = \frac{1}{N!h^{3N}} \int d\bar{r}_1, ..., d\bar{r}_N \int d\bar{p}_1, ..., d\bar{p}_N \mathrm{Tr}_e \exp(-\beta\mathcal{H}) \tag{C.3}$$

where $\mathrm{Tr_e}$ refers to a complete set of electronic states corresponding to particular ionic configuration. In the case of classical statistics for ions the integration over the momentum in trivial. Then the total partition function comes:

$$\begin{aligned} Q_N &= \frac{1}{N!}\Big[\frac{2\pi M}{h^2\beta}\Big]^{3N/2} Z_N(\Omega, T) \\ &= \frac{1}{N!}\Lambda^{3N} Z_N(\Omega, T) \end{aligned} \tag{C.4}$$

where, $\Lambda = \left(Mk_BT/2\pi\hbar^2\right)^{\frac{1}{2}}$ is the partition function for the kinetic energy in one dimensional motion* and Z_N is the confrontational partition function and is defined as

$$Z_N(\Omega, T) = \int d\bar{r}_1, ..., d\bar{r}_N \exp(-\beta H_{ii}) \left\{\mathrm{Tr}_e \exp\left[-\beta(H_e + H_{ee} + H_{ei})\right]\right\} \tag{C.5}$$

since H_{ii} is independent of electronic coordinates in equation (C.5) the term inside the curly brackets is just $\exp\big[-\beta F'(\bar{r}_1, ..., \bar{r}_N)\big]$ where $F'(\bar{r}_1, ..., \bar{r}_N)$ is the Helmholtz free energy of an electron system interacting in the presence of an external potential describe by H_{ii}. The latter corresponding to the fixed ionic configuration $(\bar{r}_1, ..., \bar{r}_N)$. Within the same approximation approach F' can be evaluated which we discuss in Chapter 3. Once F' is evaluated the electronic degrees of freedoms disappear and the problem is reduced to that of a classical fluid in which the ions move in an effective interaction potential given by

$$U_N = H_{ii} + F' \tag{C.6}$$

*Λ^{-1} is the de Broglie thermal wavelength

Equation (C.5) can now be written as

$$Z_N(\Omega, T) = \int d\bar{r}_1, ..., d\bar{r}_N \exp(-\beta U_N) \tag{C.7}$$

From the above, we see that the direct evaluation of the configuration partition function Z_N of a liquid is very difficult because of the complicated positional dependence of the potential energy U_N in the liquid. We know that [4], potential energy of a metal consists of volume dependent part $U_\Omega = NE(\Omega)$ which is independent of the relative positions of the particles and the structure dependent part which can be approximately (neglecting many-body interactions) taken in to account as a sum of pairwise additive potentials of central force type $u(r_{ij})$, where r_{ij} is the separation distance between atoms i and j. So the total potential energy turns in the form

$$U_N\left(\bar{r}_1, ..., \bar{r}_N\right) = NE(\Omega) + \frac{1}{2}\sum_{i \neq j}^{N} u(r_{ij}). \tag{C.8}$$

We should note here that, the configuration partition function Z_N for liquids is mathematically intractable because of the presence of the pair potentials. So the concept of distribution function or correlation function is conveniently adopted in the theory of liquids. In this approach, the probability of configuration grouping of two or more particles are introduced so that the use of such a function may give the same information on the properties of liquids as is obtained from the direct calculation of the configuration partition function [15].

Consider a small volume d^3r in a system of uniform density. Now the probability of finding a particle in such an element is nd^3r, where n is the number density defined as N/Ω. n is also regarded as the one body distribution function $n^{(1)}$. The subsequent case in the hierarchy of the groups of particles is concerned with the two body or pair distribution function $n^{(2)}$. If d^3r_1 and d^3r_2 be the two volume elements separated

by a distance $r = |\bar{r}_2 - \bar{r}_1|$ the probability of finding particles in these two elements is given by $n^{(2)}(r)d^3r_1d^3r_2$. Similarly, we may define the higher order distribution function $n_N^{(L)}(\bar{r}_1, ..., \bar{r}_N)$ for the group of L particles as,

$$n_N^{(L)} = \frac{N!}{(N-L)!} \frac{\int ..... \int d\bar{r}_{L+1}.....d\bar{r}_N \exp(-\beta U_N)}{Z_N} \tag{C.9}$$

which is related to the L-particle distribution function $g^{(L)}(\bar{r})$,

$$g_0^{(L)}(\bar{r}_1, ..., \bar{r}_L) = \frac{n_N^{(L)}}{n^L} = \frac{N!}{n^L(N-L)!} \frac{\int ..... \int d\bar{r}_{L+1}.....d\bar{r}_N \exp(-\beta U_N)}{Z_N} \tag{C.10}$$

putting $L = 2$ in equation (C.10) we get pair distribution function (PDF) [15]

$$g_0^{(2)}(\bar{r}_1, \bar{r}_2) = \frac{N(N-1)}{n^2} \frac{\int ..... \int \exp(-\beta U_N) d\bar{r}_3 ..... d\bar{r}_N}{Z_N} \tag{C.11}$$

The inter-ionic interaction in simple liquid is spherically symmetric. Therefore, $g(\bar{r}_1, \bar{r}_2)$ depends only upon the relative distance $\bar{r}_2 - \bar{r}_1 = \bar{r}$ between particle 1 and 2. Hence, in such case PDF is $g(\bar{r}_1 - \bar{r}_2) = g(|\bar{r}_1 - \bar{r}_2|) = g(r)$. It is very important to note that PDF $g_0^{(2)}$ is of central importance in the theory of liquid. Experimentally this function can be determined from the X-ray or neutron diffraction experiments.

In grand canonical ensemble, we define the densities as,

$$\begin{aligned} n^{(n)}(\bar{r}^n) &= \frac{1}{\Xi} \sum_{N \geq n}^{\infty} \frac{Z^n}{(N-n)!} \int ..... \int \exp\left(-\beta U_N(\bar{r}^N)\right) \bar{d}r_{n+1} ..... \bar{d}r_N \\ &= \frac{1}{\Xi} \sum_{N \geq n}^{\infty} \frac{Z^N}{N!} Z_N n_N^{(n)}(\bar{r}^n) \end{aligned} \tag{C.12}$$

where the partition function of the grand canonical ensemble is given as,

$$\Xi = \sum_{N\geq n}^{\infty} \frac{\exp(-\beta\mu N)}{N!h^{3N}} \int\int \exp\left[-\beta\mathcal{H}\left(\bar{r}^N, \bar{p}^N\right)\right] \bar{dr}^N \bar{dp}^N \tag{C.13}$$

μ is the chemical potential. Equation (C.12) has the normalization condition

$$\int n^{(n)}(\bar{r}^n)\bar{dr}^n = \left\langle \frac{N!}{(N-n)!} \right\rangle \tag{C.14}$$

Applying two particle density in the above normalization condition we get

$$\int\int n^{(2)}\left(\bar{r}_1, \bar{r}_2\right) \bar{dr}_1 \bar{dr}_2 = \left\langle N \right\rangle^2 - \left\langle N \right\rangle \tag{C.15}$$

Now subtracting from $n^{(2)}\left(\bar{r}_1, \bar{r}_2\right)$ its asymptotic form $n^{(1)}(\bar{r}_1)n^{(2)}(\bar{r}_2)$ we get from equation (C.15)

$$\int\int \left[n^{(2)}\left(\bar{r}_1, \bar{r}_2\right) - n^{(1)}\left(\bar{r}_1\right)n^{(1)}\left(\bar{r}_2\right)\right] \bar{dr}_1 \bar{dr}_2 = \left\langle N^2 \right\rangle - \left\langle N \right\rangle - \left\langle N \right\rangle^2 \tag{C.16}$$

Replacing $n^{(2)}\left(\bar{r}_1, \bar{r}_2\right)$ for a homogeneous system by $n^2 g^{(2)}(\bar{r}_1 - \bar{r}_2)$ and $n^{(1)}(\bar{r})$ by $n = \left\langle N \right\rangle / V$ we get

$$1 + n \int \left[g^{(2)}(\bar{r}) - 1\right] \bar{dr} = \frac{\left\langle N^2 \right\rangle - \left\langle N \right\rangle^2}{\left\langle N \right\rangle} = k_B T \chi_T \tag{C.17}$$

This is known as compressibility equation [4]. We write equation (C.30) as

$$1 + n \int h(\bar{r})\bar{dr} = k_B T \chi_T \tag{C.18}$$

where total correlation function $h(\bar{r})$ is defined as

$$h(\bar{r}) = g_0^{(2)}(\bar{r}) - 1 \tag{C.19}$$

Practically equation (C.11) cannot be solved analytically for real effective [4,29,57] inter-ionic pair potential for liquids. Eventually, different approximation methods are used to evaluate $g(r)$. We may classify these approximations in three major groups: (a) The perturbation and variational theories, (b) The integral equation theories and (c) Computer simulations. Some of these theories concerning our present studies are discussed below.

C.2 Gibbs-Bogoliubov Variational Scheme

The statistical-mechanical variational principle is based on the minimizing of free energy. The Gibbs-Bogoliubov method becomes the most popular although there are several other variational techniques [15]. This variational method gives a rigorous lower bound to the exact partition function, namely an upper bound to the free energy. In this method Helmholtz free energy of a real system is expressed in terms of the free energy of the reference system along with the perturbation energy as an additive or averaged over the reference system.

Now we may recall the partition function $Q_N(\Omega, T)$ from equation (C.4) as

$$Q_N = \frac{1}{N!}\Big[\frac{2\pi m}{\hbar^2\beta}\Big]^{\frac{3N}{2}} Z_N(\Omega, T) \tag{C.20}$$

where Z_N is the configuration partition function.

Now we may express the Helmholtz free energy in terms of the logarithm of the partition function for an ion at temperature T as follows:

$$F = -k_B T \ln Q_N(\Omega, T). \tag{C.21}$$

The effective potential involved in the configuration partition function can be rewritten as

$$U_N = NE(\Omega) + U'(r) \tag{C.22}$$

and

$$U'(r) = U_{ref} + U_{pert} \tag{C.23}$$

where $NE(\Omega)$ is the structure independent term of the total energy, U_{ref} is the contribution of the reference fluid and U_{pert} is assumed to be pairwise additive interaction, which can be given as

$$U_{pert} = \frac{1}{2}\sum_{i\neq j}^{N} u_{pert}(r_{ij}). \tag{C.24}$$

If F be the Helmholtz free energy of a system with Hamiltonian H and F_0 be the Helmholtz free energy of a system with a Hamiltonian H_0, then it is found that [15]

$$F \leq F_0 + \left\langle H - H_0 \right\rangle_0 \tag{C.25}$$

Here in equation (C.25) the symbol $\left\langle .....\right\rangle_0$ means average over the system of Hamiltonian H_0 *i.e.*

$$\left\langle X \right\rangle_0 = \begin{cases} \dfrac{Tr\{X\exp(-\beta H_0)\}}{Tr\{\exp(-\beta H_0)\}} & \text{quantal case} \\ \dfrac{\int X\exp(-\beta H_0)d^N p d^N q}{\int \exp(-\beta H_0)d^N p d^N q} & \text{classical case} \end{cases} \tag{C.26}$$

where X represents any dynamical variable.

Equation (C.25) is known as Gibbs-Bogoluibov inequality which gives the upper bound of the exact free energy [15]. Now if we take the system with subscript 0 as a reference system we may write the equation (C.25) by using equation (C.22) as

$$F_H \leq F_{ref} + E(\Omega) + \left\langle U_{pert} \right\rangle_{ref} \tag{C.27}$$

where,

$$\left\langle U_{pert} \right\rangle_{ref} = \frac{n}{2} \int U_{pert}(r) g_{ref}(r) d\bar{r} \tag{C.28}$$

F_H in equation (C.27) denotes the free energy per atom.

In this method, any free parameter is determined by minimization of Helmholtz free energy and this method is consistent with thermodynamics. The real system is described by g_{ref} and F. This method works well for a wide range of temperature and metallic densities [15] and holds for quantum and classical statistics [15] as well.

C.3 Derivative form for Entropy

The concept of Atomic Transport theory is described by the Statistical Mechanics. According to the statistical mechanical theory of atomic or molecular [4] transport properties of simple liquids, it is possible to calculate transport coefficient from the knowledge of atomic or molecular properties, such as mass, and pair potentials and the equation of motion only. The time correlation function and the memory function is used to study the self-diffusion process in liquid metals, which is calculated from the Hard-sphere diameter and the pair-potentials.

The microscopic expression for the hydrodynamic equation of liquids are taken into account, and the time evolution of distribution functions appearing in those expressions is considered from the point of view of kinetic theories developed by

Kirkwood [59], Born and Green [4], Rice and Allnatt [59–64], and others. The viscosity of liquid metals can be achieved using these atomic properties.

The most important forms of atomic transport properties are Viscosity, Thermal conductivity, Electrical conductivity and Diffusion coefficient. The understanding of these properties for liquid metals can be done using the neutron inelastic scattering measurements. Such experiment allows us to determine a scattering law of dynamic structure factor, S(q, ω) which is the Fourier Transformation of the space-time correlation function of Van Hoove G(r, t). The shear viscosity of liquid metals is also calculated using a moment method. Diffusion and Viscous coefficients of liquid alloys are discussed from the same point of view as for pure liquid metals.

$$\int\int \left[n^{(2)}\left(\bar{r}_1,\bar{r}_2\right) - n^{(1)}\left(\bar{r}_1\right)n^{(1)}\left(\bar{r}_2\right)\right]\bar{d}r_1\bar{d}r_2 = \left\langle N^2\right\rangle - \left\langle N\right\rangle - \left\langle N\right\rangle^2 \tag{C.29}$$

Replacing $n^{(2)}\left(\bar{r}_1,\bar{r}_2\right)$ for a homogeneous system by $n^2 g^{(2)}(\bar{r}_1-\bar{r}_2)$ and $n^{(1)}(\bar{r})$ by $n = \left\langle N\right\rangle/V$ we get

$$1 + n\int \left[g^{(2)}(\bar{r}) - 1\right]\bar{d}r = \frac{\left\langle N^2\right\rangle - \left\langle N\right\rangle^2}{\left\langle N\right\rangle} = k_B T\chi_T \tag{C.30}$$

This is known as compressibility equation [15]. We write equation (C.30) as

$$1 + n\int h(\bar{r})\bar{d}r = k_B T\chi_T \tag{C.31}$$

where total correlation function $h(\bar{r})$ is defined as

$$h(\bar{r}) = g_0^{(2)}(\bar{r}) - 1 \tag{C.32}$$

Practically equation (C.11) cannot be solved analytically for real effective interionic pair potential for liquids. Eventually, different approximation methods are used

to evaluate $g(r)$. We may classify these approximations in three major groups: (a) The perturbation and variational theories, (b) The integral equation theories and (c) Computer simulations. Some of these theories concerning our present studies are discussed in Chapter 3.

Appendix D

Phase Diagram

Phase diagram for $Al_{1-x}Zn_x$ System:

Figure D.1 presents the phase diagram for $Al_{1-x}Zn_x$ system for thermodynamic state at 1000 K.

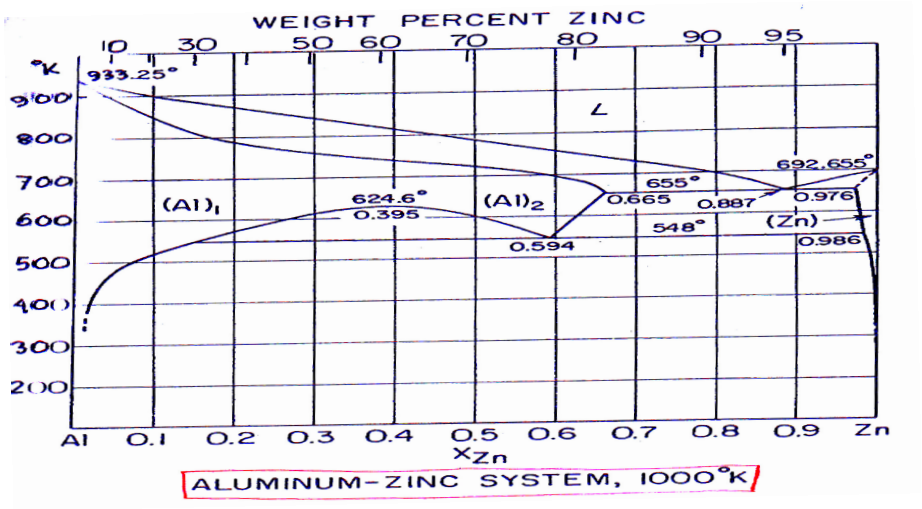

Figure D.1: Phase diagram for $Al_{1-x}Zn_x$ liquid binary system.

Phase diagram for $Al_{1-x}In_x$ liquid Binary System:

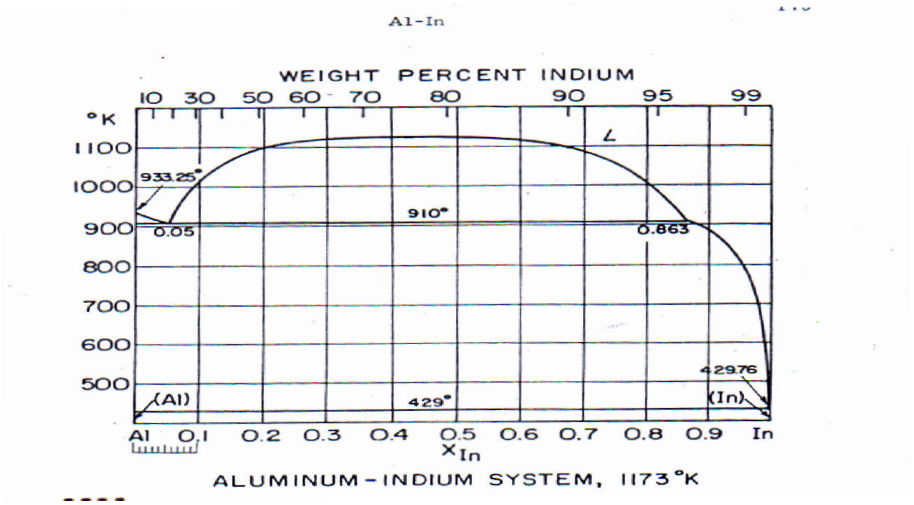

Figure D.2: Phase diagram for $Al_{1-x}In_x$ system for liquid state at 1173 K.

Phase diagram for $Al_{1-x}Sn_x$ liquid Binary System:

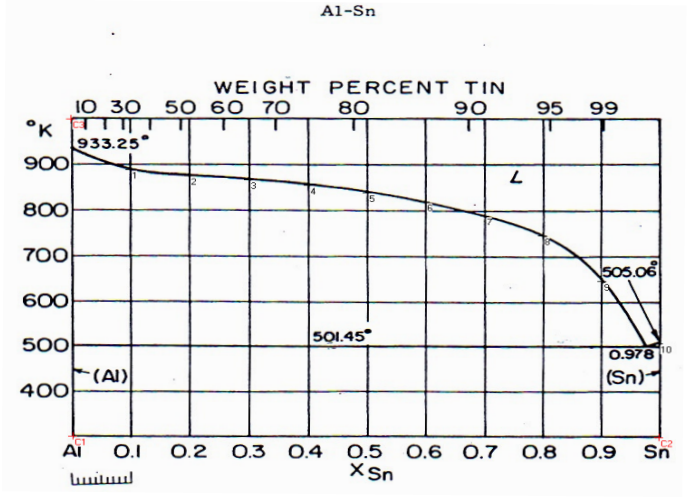

Figure D.3: Phase diagram for $Al_{1-x}Sn_x$ system for liquid state at 1173 K.

Phase diagram for $Al_{1-x}Cu_x$ liquid Binary System:

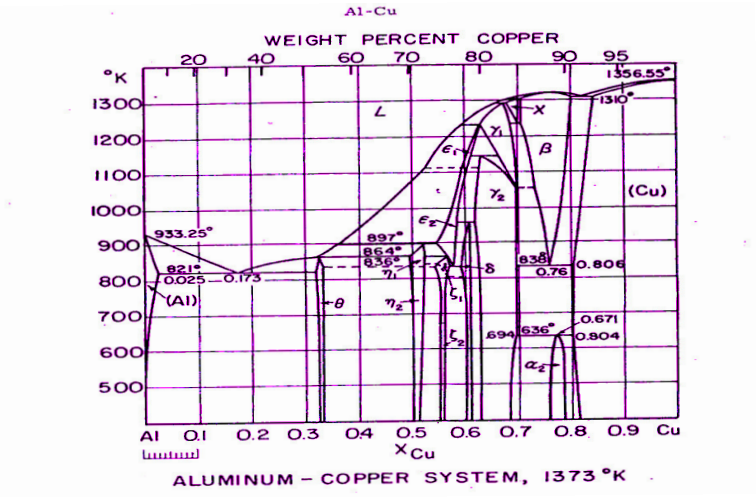

Figure D.4: Phase diagram for $Al_{1-x}Bi_x$ system for liquid state at 1373 K.

Phase diagram for $Al_{1-x}Au_x$ liquid Binary System:

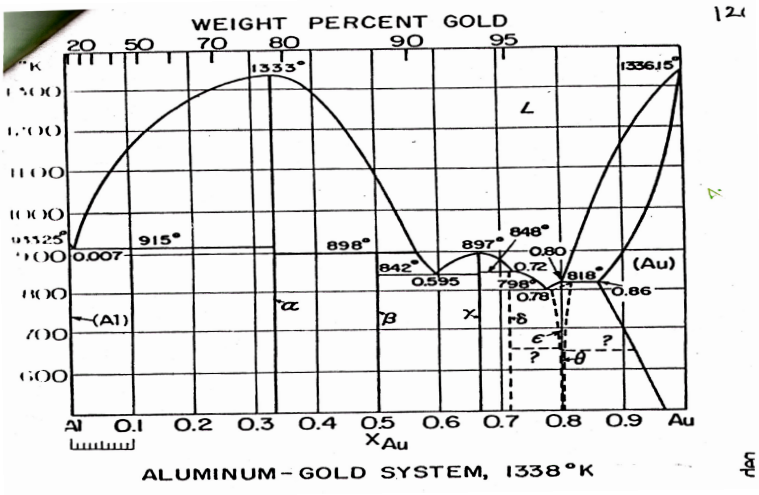

Figure D.5: Phase diagram for $Al_{1-x}Bi_x$ system for liquid state at 1338 K.

Bibliography

[1] D. J. Gonzalez, L. E. Gonzalez, J. M. Lopez, M. J. Stott. "Collective modes in liquid binary alloys. An ab initio molecular dynamics study of the LiMg and LiBa alloys". Journal of Physics: Condensed Matter, Vol. **17**, No. 10, (2005).

[2] X. J. Han, B. Wei. "Thermophysical properties of undercooled liquid CoMo alloys". Philosophical Magazine, Vol. **83**, No. 13, pp. 1511-1532 , (2003).

[3] R. N. Singh, F. Sommer. "Segregation and immiscibility in liquid binary alloys". Reports on Progress in Physics. Vol. **60**, No. 01, (1997).

[4] M. Shimoji. "**Liquid Metals**, An Introduction to the Physics and Chemistry of Metals in the Liquid States". Academic Press, London, pp. 96, (1977).

[5] W. A. Harrison. "Pseudopotential in the theory of metals". Benjamin, New York, (1966).

[6] V. Heine, I. Abarenkov. "A new method for the electronic structure of metals". Philosophical Magazine, Vol. **9**, No. 99, pp. 451-46, (1964).

[7] F. Y. Xie, T. Kraft, Y. Zuo, C. H. Moon, and Y. A. Chang. "Microstructure and microsegregation in Al-rich Al-Cu-Mg alloys". Acta Materialia, Vol. **47**, No. 2, pp. 489500, (1999).

[8] J. P. hansen and I. R. Mcdonald. "Theory of Simple Liquids. Academic press, London UK, 3rd Edition, 2006".

[9] T. E. Faber, J.M. Ziman. "A theory of the electrical properties of liquid metals". Philosophical Magazine. Vol. **11**, pp. 153-173, (1964).

[10] Y. Arai, Shirakawa, S. Tamaki, M. Sato, Y. Waseda. "Structural Properties of Liquid Ag-In System". Physics and Chemistry of Liquids. Vol. **35**, Issue 4, pp. 253-268, (1998).

[11] P. Chieux and H. Ruppersberg. "The Observation of Chemical Short-Range Order in Liquid and Amorphous Metallic Systems by Diffraction Methods". Le Journal de Physique Colloques (J. Phys. Colloques). Vol. **41**, pp. C8-145-C8-152, (1980). doi: 10.1051/jphyscol:1980838.

[12] R*ü*diger Kniep, Peter Lamparter, Siegfried Steeb. "Structure of Anodic Oxide Coatings on Aluminum".
Wiley Online Library, (1989). doi.org/10.1002/anie.198909511

[13] Everett Thiele. "Equation of State for Hard Spheres".
The Journal of Chemical Physics. Vol. **39**, pp. 474 (1963). doi.org/10.1063/1.1734272.

[14] J. L. Lebowitz. "Exact Solution of Generalized Percus-Yevick Equation for a Mixture of Hard Spheres". Phys. Rev., **133**, A895, (1964).

[15] T. E. Faber. "Introduction to the theory of liquid metals". Cambridge Univ. Press, Cambridge, (1972).

[16] Carlos Fiolhais, John P Perdew, Sean Q Armster, James M MacLaren, Marta Brajczewska. "Dominant density parameters and local pseudopotentials for simple metals." Physical Review B, Vol **51**, Issue 20, pp. 14001, (1995).

[17] Carlos Fiolhais, John P Perdew. "Energies of curved metallic surfaces from the stabilized-jellium model." Physical Review B, Vol **45**, Issue 11, pp. 6207, (1992).

[18] Alim B Alchagirov, John P Perdew, Jonathan C Boettger, RC Albers, Carlos Fiolhais. "Energy and pressure versus volume: Equations of state motivated by the stabilized jellium model." Physical Review B, Vol **63**, Issue 22, pp. 224115, (1992).

[19] Fernando Nogueira, Carlos Fiolhais, Jingsong He, John P Perdew, Angel Rubio. "Transferability of a local pseudopotential based on solid-state electron density." Journal of Physics: Condensed Matter, Vol. **8**, Issue 3, pp. 287, (1996).

[20] LM Almeida, John P Perdew, Carlos Fiolhais. "Surface and curvature energies from jellium spheres: Density functional hierarchy and quantum Monte Carlo." Physical Review B, Vol **66**, Issue 7, pp. 075115, (2002).

[21] M. W. Finnis and J. E. Sinclair. "A Simple Empirical N-Body Potential for Transition Metals." Philosophical Magazine A, Vol. **50**, pp. 45-49, (1984).

[22] Murray S. Daw and M. I. Baskes. "Embedded-atom method: Derivation and application to impurities, surfaces, and other defects in metals."
Physical Review B, Vol. **29**, pp. 6443-6469, (1984).

[23] C. Regnaut. "Analysis of the liquid structure of $3d$ transition metals from the Wills-Harrison model." Zeitschrift f*ü*r Physik B Condensed Matter, Vol **76**, Issue 2, pp. 179-184, (1989).

[24] P. Hohenberg and W. Kohn. "Inhomogeneous Electron Gas."
Physical Review B, Vol. **136**, pp. 864, (1984).

[25] W. Kohn and J. L. Sham. "Self-Consistent Equations Including Exchange and Correlation Effects." Physical Review A, Vol. **140**, 1153, (1965).

[26] N. David Mermin. "Thermal Properties of the Inhomogeneous Electron Gas." Physical Review A, Vol. **137**, pp. 1441, (1965).

[27] J. Fridel. "The Physics of Metals 1, in: J. M. Ziman (Ed.), Electrons, Cambridge University, pp. 340, (1971)".

[28] S. D. Korkmaz, S. Korkmaz. "Electronic transport properties of liquid $Na_{1-x}K_x$ alloys." Journal of Molecular Liquids, Vol. **186**, pp. 85-89, (2013).

[29] Y. Waseda. "The structure of Non-crystaline Materials, McGraw Hill, Newyork, (1980)."

[30] A. B. Bhatia, R. N. Singh. "A Quasi-lattice Theory for Compound Forming Molten Alloys." Phys. Chem. Liq. **13**, Issue 3, pp. 177, (1984). doi.org/10.1080/00319108408080778.

[31] Ram Nadan Singh, Ferdinand Sommer. "Simple model for demixing binary liquid alloys. Zeitschrift fuer Metallkunde (Materials Research and Advanced Techniques)." Vol. **83**, issue 7, pp. 533-540, (1992).

[32] I. H. Umar, A. Mayer, M. Watabe, W.H. Young. J. Phys. F: Metal Phys. **4**, pp. 1691, (1974).

[33] J. J. Hoyt, M. Asta. "Atomistic computation of liquid diffusivity, solid-liquid interfacial free energy, and kinetic coefficient in Au and Ag." Phys. Rev. **B**, Vol. **65**, pp. 214106, (2002).

[34] Dimitri A. Sverjensky & P. A. Molling. "A linear free energy relationship for crystalline solids and aqueous ions." Nature. Vol. **356**, pp. 231-234, (1992). doi:10.1038/356231a0.

[35] G. M. Bhuiyan, J. L. Bretonnet, M. Silbert. "Liquid structures of the 3d transition metals." Journal of Non-Crystalline Solids, Vol. **145**, pp. 156-158, (1993).

[36] G. M. Bhuiyan, M. Silbert, M. J. Stott. "Structure and thermodynamic properties of liquid transition metals: An embedded-atom-method approach." Physical Review B, Vol. **53**, pp. 636, (1996).

[37] S. Sharmin, G. M. Bhuiyan, M. A. Khaleque, R. I. M. A. Rashid and S. M. Mujibur Rahman. "Electronic Transport Properties of Liquid Less-Simple Metals." Phys. Status Solidi B, Vol. **232**, pp. 243-253, (2002).

[38] R. C. Gosh, A.Z. Ziauddin Ahmed and G.M. Bhuiyan. "Investigation of surface entropy for liquid less simple metals." The European Physical Journal B, Vol. **56**, Issue 3, pp. 177-181, (2007).

[39] R. C. Gosh, Ramprosad Das, Sumon C. Sen, G.M. Bhuiyan. "Surface entropy of liquid transition and noble metals." Surface Science, Vol. **637**, pp. 63-68, (2015).

[40] R. C. Gosh, M.R. Amin, A.Z.Z. Ahmed, I.M. Syed, G.M.Bhuiyan. "Calculation of surface entropy of liquid transition and noble metals." Applied Surface Science. Vol. **258**, pp. 5527-5532, (2012).

[41] G. M. Bhuiyan, I. Ali and S. M. M. Rahman. "Atomic transport properties of Ag-In liquid binary alloys." Physica B, Vol. **334**, pp. 147-159, (2003).

[42] E. H. Bhuiyan, A. Z. Ziauddin Ahmed, G. M. Bhuiyan, M. Shahjahan. "Atomic transport properties of Ag_xSn_{1-x} liquid binary alloys." Physica B, Vol. **403**, pp. 1695-1703, (2008).

[43] Shuvomoy Chanda, A. Z. Ziauddin Ahmed, G. M. Bhuiyan, S.K. Barman and Shiplu Sarker. "A test of distribution function method in the case of liquid transition metals alloys." Journal of Non-Crystalline Solids, Vol. **357**, pp. 3774-3780, (2011).

[44] J. L. Bretonnet, M. Silbert. "Interionic Interactions in Transition Metals. Application to Vanadium Phys." Chem. Liq **24**, pp. 169, (1992).

[45] G. M. Bhuiyan, A. Z. Ziauddin Ahmed. "Energy of formation for Ag_xIn_{1-x} and Ag_xSn_{1-x} liquid binary alloys." Physica B, Vol. **390**, Issue 1, (2007).

[46] G. M. Bhuiyan, Md. Saiful Alam, A. Z. Ziauddin Ahmed, Istiaque M. Syed and R. I. M. A. Rashid, "Entropy of mixing for Ag_xIn_{1-x} and Ag_xSn_{1-x} liquid binary alloys." The Journal of chemical physics, Vol. **131**, pp. 034501, (2009).

[47] Fysol Ibna Abbas, G. M. Bhuiyan, A. Z. Ziauddin Ahmed. "Energy of mixing and entropy of mixing for Cu_xAl_{1-x} liquid binary alloys." arXiv:1607.05827v1 [cond.mtrl-sci] (2016).

[48] J. A. Moriarty. "Analytic representation of multi-ion interatomic potentials in transition metals." Physical Review B, Vol. **42**, pp. 1609, (1990).

[49] J. M. Wills , W. A. "Harrison. Interionic interactions in transition metals." Phys. Rev. lett. **B**, Vol. **28**, pp. 4363, (1983).

[50] I. N. W. Ashcroft, D. C. Langreth "Structure of Binary Liquid Mixtures. I." Physical Review B, Vol. **156**, pp. 685, (1967).

[51] A. Mayer, M. Silvert, W. H. Young. "Soft Core Description of the Structure of Liquid Rare Earth Metals." Chem. Phys. Vol. **49**, pp. 47, (1980).

[52] G. M. Bhuiyan, J. L. Bretonnet, L. E. González and M. Silbert. "Liquid structure of titanium and vanadium; VMHNC calculations." Journal of Physics: Condensed Matter, Vol. **4**, pp. 7651, (1992).

[53] Mir Mehedi Faruk, G. M. Bhuiyan. "Investigation of segregation for Al_xIn_{1-x} liquid binary alloys." Physica B, Vol. **422**, pp. 156, (2013).

[54] Md. Riad Kasem, G. M. Bhuiyan and Md. Helal Uddin Maruf. "A systematic study of segregation for Zn_xBi_{1-x} liquid binary alloys." The Journal of Chemical Physics, Vol. **143**, pp. 034503, (2015).

[55] G. M. Bhuiyan, M. A. Khaleque. "Structure and thermodynamic properties of liquid rare earth metals: an embedded atom method approach." Journal of Non-Crystalline Solids, Vol. **226**, pp. 175-181, (1998).

[56] G. M. Bhuiyan, Fysol Ibna Abbas. "Local minimum in effective pairpotentials: Pseudopotential theory revisited." arXiv:1710.07931v1 [cond.mtrl-sci] (2017).

[57] Fysol Ibna Abbas, G. M. Bhuiyan , Md. Riad Kasem. "A study of thermodynamics of mixing for $Al_{1-x}Sn_x$ liquid binary alloy". Journal of Non-Crystalline Solids, Vol. **481**, pp. 391396, (2018).

[58] F. Zahid, G. M. Bhuiyan, S. Sultana, M. A. Khalaque, R. I. M. A. Rashid and S. M. M. Rahaman. "Investigations of the static and dynamic properties of liquid less simple metals." physica status solidi (b), Vol. **215**, pp. 987-998, (1999).

[59] S. A. Rice, J. G. Kirkwood, J. Ross and R. W. Zwanzig. "Statistical mechanical theory of transport processes. XII. Dense rigid sphere fluids." The Journal of Chemical Physics, Vol. **31**, pp. 575, (1959).

[60] Stuart A. Rice and Alan R. Allnatt. "Approximate Theory of Transport in Simple Dense Fluid Mixtures." The Journal of Chemical Physics. Vol. **34**, pp. 409, (1961). doi.org/10.1063/1.1700966.

[61] Stuart A. Rice and Alan R. Allnatt. "On the Kinetic Theory of Dense Fluids. VI. Singlet Distribution Function for Rigid Spheres with an Attractive Potential." The Journal of Chemical Physics. Vol. **34**, pp. 2144, (1961). doi.org/10.1063/1.1731836.

[62] Stuart A. Rice and Alan R. Allnatt. "On the Dynamical Theory of Diffusion in Crystals. V. RandomWalk Treatment of the Heat of Transport." The Journal of Chemical Physics. Vol. **33**, pp. 573, (1960). doi.org/10.1063/1.1731187.

[63] Stuart A. Rice and Alan R. Allnatt. 85,121,149, "On the Kinetic Theory of Dense Fluids. VII. The Doublet Distribution Function for Rigid Spheres with an Attractive Potential." The Journal of Chemical Physics. Vol. **34**, pp. 2156, (1961). doi.org/10.1063/1.1731837.

[64] Stuart A. Rice and Alan R. Allnatt. "On the Kinetic Theory of Dense Fluids. VI. Singlet Distribution Function for Rigid Spheres with an Attractive Potential." The Journal of Chemical Physics, Vol. **34**, pp. 2144, (1961).

[65] J. M. Ziman. "A theory of the electrical properties of liquid metals. I: The monovalent metals." Philosophical Magazine, Vol. **6**, pp. 1013-1034, (1961).

[66] "An Introduction to the Theory of Liquid Metals by Faber and Ziman, Cambridge University Press, (2010)."

[67] A. Ferraz and N. H. March. "Electrical Resistivity of Liquid Metals in Regime of Short Mean Free Path." Physics and Chemistry of Liquids. Vol. **8**, pp. 271-278, (1979). doi.org/10.1080/00319107908084758.

[68] T. E. Faber, J. M. Ziman. "A theory of the electrical properties of liquid metals." Philosophical Magazine. Vol. **11**, pp. 153-173 (1965).

[69] Hans C. Andersen and David Chandler. "Optimized Cluster Expansions for Classical Fluids. I. General Theory and Variational Formulation of the Mean Spherical Model and Hard Sphere PercusYevick Equations." The Journal of Chemical Physics, Vol. **57**, pp. 1918, (1972). doi.org/10.1063/1.1678512.

[70] H. C. Andersen and D. Chandler. "Optimized Cluster Expansions for Classical Fluids. II. Theory of Molecular Liquids." The Journal of Chemical Physics, Vol. **57**, pp. 1930, (1972). doi.org/10.1063/1.1678513.

[71] Hans C Andersen, John D Weeks, David Chandler. "Relationship between the hard-sphere fluid and fluids with realistic repulsive forces." Phys. Rev. A, Vol. **4**, Issue 4, No. 12, pp. 1597-1602, (1971).

[72] H. C. Andersen and D. Chandler. "Role of Repulsive Forces in Determining the Equilibrium Structure of Simple Liquids." The Journal of Chemical Physics, Vol. **54**, pp. 5237, (1971). doi.org/10.1063/1.1678513.

[73] W. Jank and J. Hafner, "Structural and electronic properties of the liquid polyvalent elements II. The divalent elements." Phys Rev. B, Vol. **42**, No.11, pp. 6926, (1990).

[74] J. Hafner and W. Jank, "Structural and electronic properties of the liquid polyvalent elements. III. The trivalent elements." Phys Rev. B, Vol. **42**, No. 18, pp. 11530, (1990).

[75] W. Jank and J. Hafner, "Structural and electronic properties of the liquid polyvalent elements: The group-IV elements Si, Ge, Sn, and Pb." Phys Rev. B, Vol. **41**, No. 03, pp. 1497, (1990).

[76] P. Vashishta and K. S. Singwi, "Electron Correlations at Metallic Densities. V." Phys Rev. B, Vol. **6**, No. 03, pp. 875, (1972).

[77] S. Ichimaru and K. Utsumi. "Analytic expression for the dielectric screening function of strongly coupled electron liquids at metallic and lower densities." Phys. Rev. B, Vol. **24**, No. 12, pp. 7385, (1981).

[78] C. R. Leavens, A. H. Mackdonald, R. Taylor, A. Ferraz and N.H.March. "Finite Mean-Free-Paths and the Electrical Resistivity of Liquid Simple Metals." Physics and Chemistry of Liquids. Vol. **11**, pp. 115-136, (1981).

[79] E. Nardi. "Plasma and liquid-metal resistivity calculations using the Ziman theory." Physical Review E, Vol. **54**, pp. 1899, (1996).

[80] Y. Rosenfeld. "Comments on the Variational Modified Hypernetted Chain Theory for Simple Fluids." J.Stat. Phys. Vol. **42**, pp. 437-457, (1986).

[81] Dieter Forster, Paul C. Martin, and Sidney Yip. "Moments of the Momentum Density Correlation Functions in Simple Liquids." Physical Review Journals Archive. Vol. **170**, pp. 155, (1968).

[82] Y. Rosenfeld. "Quasi-universal scaling law for atomic transport in simple fluids." Journal De Physique IV. France. Vol. **10**, Issue P5, pp. 129-134, (2000).

[83] Yaakov Rosenfeld. "A quasi-universal scaling law for atomic transport in simple fluids." Journal of Physics: Condensed Matter. Vol. **11**, No. 28, (1999).

[84] R. N. Singh and F. Sommer. "Thermodynamic investigation of viscosity and diffusion in binary liquid alloys." Phys. Chem. Liq., Vol **36**, pp. 17, (1998).

[85] M. Dzugutov. "A universal scaling law for atomic diffusion in condensed matter." Nature (London), **381**, 137, (1996).

[86] J. J. Hoyt, Mark Asta, and Babak Sadigh. "Test of the Universal Scaling Law for the Diffusion Coefficient in Liquid Metals." Phys. Rev. Lett. Vol **85**, pp. 594, (2000).

[87] Masahiro Kitajima, K. Saito and Mitsuo Shimoji. "Shear Viscosity of Liquid Na-K Alloys." Transactions of the Japan Institute of Metals, Vol. **17**, No. 9, pp. 582-587, (1976).

[88] Masahiro Kitajima, Toshio Itami and Mitsuo Shimoji. "Viscosity of liquid K-Hg alloys." The Philosophical Magazine: A Journal of Theoretical Experimental and Applied Physics. Vol. **30**, No. 8, pp. 285-291, (1974). doi.org/10.1080/14786439808206555.

[89] Toshio Itami and Mitsuo Shimoji. "Thermoelectric powers of liquid K-Hg, K-T1, and K-Pb alloys." The Philosophical Magazine: A Journal of Theoretical Experimental and Applied Physics. Vol. **28**, No. 8, pp. 85-90, (1973). doi.org/10.1080/14786437308217435.

[90] Masahiro Kitajima, Toshio Itami and Mitsuo Shimoji. "The Volume of Liquid Hg-Tl and Hg-Cs Alloys." Journal of the Physical Society of Japan, Vol. **51**, No. 8, pp. 2493-2500, (1982).

[91] J. F. Wax, R. Albaki, and J. L. Bretonnet. "Structural and dynamical properties of liquid alkaline-earth metals near the melting point." Phys. Rev. B, Vol. **62**, pp. 14818, (2000).

[92] R. Hultgren, R. D. Hawking, M. Gleiser, K. K. Keluey. "Selected values of the Thermodynamics properties of Binary Alloys. American Society of Metals (1973)."

[93] H. C. Longuet-Higgins, "The statistical thermodynamics of multicomponent systems." Proceedings of The Royal Society Royal A, Vol. **205**, pp. 247-269, (1951). doi: 10.1098/rspa.1951.0028.

[94] A. B. Bhatia, W. H. Hargrove and N. H. March. "Concentration fluctuations in conformal solutions and partial structure factor in alloys." Journal of Physics C: Solid State Physics, , Vol. **6**, No. 4, pp. 621, (1973).

[95] J. A. Alonso, and N. H. March, "Concentration fluctuations in metallic liquid alloys." Physica B. Vol. **114**, Issue 1, pp. 67-70, (1982).

[96] B. Bernu, J. P. Hansen, Y. Hiwatari and G. Pastore. "Soft-sphere model for the glass transition in binary alloys: Pair structure and self-diffusion." Phys. Rev. A, Vol. **36**, pp. 4891, (1987). doi.org/10.1103/PhysRevA.36.4891.

[97] Y. A. Odusote, A. I. Popola, S. S. Oluyamo. "Bulk and surface properties of demixing liquid Al-Sn and Sn-Ti alloys." Applied Physics A, Vol. **122**, pp. 80, (2016).

[98] C. A. Popescu, D. Taloi. "UPB Sci. Bull.Thermodynamic calculations in liquid Al-Sn alloys system." Ser. B, Vol. **69(1)**, pp. 78-83, (2007).

[99] L. C. Prasad, A. Mikula. "Concentration fluctuations and interfacial adhesion at the solidliquid interface between Al_2O_3 and Al-Sn liquid alloys." High Temp. Mater. Process. Vol. **19(1)**, pp. 61-69, (2000).

[100] W. Li and M. P. Tosi. "Electron theory of long-wavelength concentration fluctuations in liquid metal alloys." Il Nuovo Cimento D, Vol. **11**, Issue 12, pp. 1863-1863, (1989). doi.org/10.1007/BF02459127.

[101] Mir Mehedi Faruk, G. M. Bhuiyan, Amitabh Biswas, and Md. Sazzad Hossain. "Study of microscopic origin of segregation for Fe_xCu_{1-x} and Cu_xCo_{1-x} liquid binary alloys." The Journal of Chemical Physics. Vol. **140**, pp. 134505, (2014).

[102] A. J. McAlister. "National Bureau of Standards. Bulletin of Alloy Phase Diagrams, Vol. **5**, No. 3 (247), (1984).

[103] Z. Fan, S. Ji, and J. Zhang. "Processing of immiscible metallic alloys by rheomixing process. Materials Science and Technology. Vol. **17**, pp. 837, (2001).

[104] Ivan G. Kaban and Walter Hoyer. "Characteristics of liquid-liquid immiscibility in Al-Bi-Cu, Al-Bi-Si, and Al-Bi-Sn monotectic alloys: Differential scanning calorimetry, interfacial tension, and density difference measurements. Physical Review B, Vol. **55**, pp. 47-56, (1997).

[105] V. Raghavan. Journal of Phase Equilibria and Diffusion, Vol. **32**, No. **5**, (2011).

[106] V. Raghavan. Journal of Phase Equilibria and Diffusion, Vol. **29**, No. **2**, (2008).

[107] I. N. W. Ashcroft. "Electron-ion pseudopotentials in metals." Physics Letters. Vol. **23**, Issue 1, p. 48-50, (1966). doi:10.1016/0031-9163(66)90251-4.

[108] B. A. Oli. "An inverse-scattering approach to the physics of transition metals." Il Nuovo Cimento D, Vol. **10**, Issue 08, pp. 891-900, (1988).

[109] Peter Swan. "Deduction of non-singular potentials from scattering phase shifts (II). Charged particles." Nuclear Physics A, Vol. **90**, Issue 2, pp. 436-448, (1967).

[110] Ferdinand Sommer, Ram Nandan Singh and Victor Witusiewicz. "On the entropy of mixing." Journal of Alloys and Compounds. Vol. **325**, Issues 1-2, pp. 118-128, (2001).

[111] C. Zener, In Phase Stability in Metals and Alloys. "Edited by P. S. Rudman, J. Stringer, and R. I. Jaffee." pp. 25, (McGraw Hill, New York, 1967).

[112] Walter Kauzmann. "The Nature of the Glassy State and the Behavior of Liquids at Low Temperatures." Chem. Rev.(Washington, D.C.) Vol. **43**, Issues 2, pp. 219256, (1948). doi: 10.1021/cr60135a002.

[113] C. Detavernier, R. L. Van Meirhaeghe, F. Cardon, and K. Maex. "Influence of mixing entropy on the nucleation of $CoSi_2$." Phys. Rev. B, Vol. **62**, pp. 12045, (2000). doi.org/10.1103/PhysRevB.62.12045.

[114] D. A. McQuarrie, Harper, Row. "Statistical Mechanics, New York, 261, (1974)."

[115] J. Hafner. "Hamiltonoians to phase Diagrams, Springer, Berlin, pp. 56, (1987)."

[116] G. D. Mahan. "Many-Particle Physics, Plenum Press, New York, London, pp. 459, (1987)."

[117] John G. Kirkwood. "The statistical mechanical theory of transport processes i. general theory." J. Chem. Phys., Vol. **14**, 180, (1946).

[118] M. Born and H. S. Green. "A general kinetic theory of liquids i. the molecular distribution functions." Proc. Roy. Soc. A, Vol. **188**, pp. 10-18, (1946).

[119] R Evans and T J Sluckin. "The role of attractive forces in the structure of simple liquids: a theory for small-angle scattering." Journal of Physics C: Solid State Physics. Vol. **14**, No. 19, (1981).

[120] P. Protopapas, Hans C. Andersen and N. A. D. Parlee. "Theory of transport in liquid metals. I. Calculation of selfdiffusion coefficients." Phys. Rev. A **15**, 2545, (1973).

[121] Rosenfeld, Y. "A quasi-universal scaling law for atomic transport in simple fluids." J. Phys. Condens. Matter, Vol. **11**, pp. 5415-5427, (1999).

[122] G.X. Li, C.S. Liu, Z.G. Zhu. "Excess entropy scaling for transport coefficients: diffusion and viscosity in liquid metals." J. Non-Cryst. Solids, Vol. **351**, pp. 946-950, (2005).

[123] I. Yokoyama. "A relationship between excess entropy and diffusion coefficient for liquid metals near the melting point." Physica B, Vol. **254**, pp. 172-177, (1998).

[124] S. Chapman and T. G. Cowling. "The Mathematical Theory of Non-uniform Gases." J. Phys. Chem., Vol. **45**, Issue. 5, pp. 876-877, (1941).
doi: 10.1021/j150410a017.

[125] N. W. Ashcroft. "Electron-ion pseudopotentials in metals." Physics Letters. Vol. **23**, pp. 48-50, (1966). doi.org/10.1016/0031-9163(66)90251-4.

[126] P. L. Roster. "The Electrical Resistivity of Metalsand Alloys, Cambridge University Press, Cambridge (1991)."

[127] W Jank, Ch Hausleitner and J Hafner. "Electronic structure of the liquid 3d and 4d transition metals." Journal of Physics: Condensed Matter. Vol. **3**, No. 24, (1991).

[128] C Hausleitner, G Kahl and J Hafner. "Liquid structure of transition metals:investigations using molecular dynamics and perturbation and integral-equation techniques." Journal of Physics: Condensed Matter. Vol. **3**, No. 11, (1991).

[129] Y. H. Liu. "Density and Viscosity of Molten Zn-Al Alloys, Metallurgical and Materials Transactions." Vol. **37A**, pp. 2767, (2006).

[130] LIU Guang-Rong, BIAN Xiu-Fang, Sun Min-Hua. "Experimental Studies of Liquid Viscosity in Immiscible Al-In Alloys." Chin Phys Lett. Vol. **20**, No. 8, pp. 1326, (2003).

[131] Michael Schick, Jurgen Brillo, Ivan Egry, Bengt Hallstedt. "Viscosity of AlCu liquid alloys: measurement and thermodynamic description." J Mater Sci. Vol. **47**, pp. 81458152, (2012). doi.10.1007/s10853-012-6710-x.

[132] H. L. Peng, Th. Voigtmann, G. Kolland, H. Kobatake, and J. Brillo. "Structural and dynamical properties of liquid Al-Au alloys." Phys. Rev. B, Vol. **92**, pp. 184201, (2015).

[133] R. Car and M. Parninello. "Unified Approach for Molecular Dynamics and Density-Functional Theory." Phys Rev Lett. Vol. **55**, pp. 2471-2474, (1966). doi.org/10.1103/PhysRevLett.55.2471.

[134] Martin Fuchs and Matthias Scheffler. "Ab initio pseudopotentials for electronic structure calculations of poly-atomic systems using density-functional

theory." Computer Physics Communications. Vol. **119**, Issue 1, pp. 67-98, (1999).

[135] John Campbell. "Castings, (2^{nd} Edition), Oxford, United Kingdom: Butterworth Heinemann, (2003)."

[136] Cheng Y. Q., Ma E. "Atomic−level structure and structure−property relationship in metallic glasses." Progress in Materials Science, Vol. **56**, pp. 379, (2011).

[137] Hajime Tanaka. "Bond orientational order in liquids: Towards a unified description of water-like anomalies, liquid-liquid transition, glass transition, and crystallization." The European Physical Journal E, Vol. **35**, pp. 113, (2012).

[138] Inooue, A. "Stabilization of metallic supercooled liquid and bulk amorphous alloys." Acta mater. Vol. **48**, pp. 279-306, (2000).

[139] Bogicevic A, hansen L B and Lundqvist B I. "Simulations of atomic structure, dynamics, and self-diffusion in liquid Au." Phys. Rev. E, Vol. **55**, pp. 5535, (1997).

[140] Chauhan A S, Ravi R and Chhabra R P. "Self-diffusion in liquid metals." Chem. Phys. Rev. **252**, pp. 227, (2000).

[141] M. Mantina, Y. Wang, R. Arroyave, L. Q. Chen, Z. K. Liu, and C. Wolverton. "First-Principles Calculation of Self-Diffusion Coefficients." Phys. Rev. Lett. **100**, pp. 215901, (2008).

[142] Ran Li, Yihua Zhong, Chao Huang, Xiaoma Tao, Yifang Ouyang. "Surface energy and surface self-diffusion of Al calculated by embedded atom method." Physica B, Vol.**422**, pp. 51-55, (2013).

[143] M. Shimoji, I. Itami. "Atomic Transport in Liquid Metals, Trans Tech Publications Ltd. 4711 Aedermannsdorft, Switzerland, (1986)."

[144] D. J. Gonzlez, L. E. Gonzlez, J. M. Lpez, M. J. Stott. "Microscopic dynamics in the liquid Li-Na alloy: An ab initio molecular dynamics study." Phys. Rev. E, Vol. **69**, pp. 031205, (2004).

[145] L. Calderin, D. J. Gonzlez, L. E. Gonzlez, J. M. Lpez. "Structural, dynamic, and electronic properties of liquid tin: An ab initio molecular dynamics study." J. Chem. Phys. Vol. **129**, Issue 19, pp. 194506, (2008). doi.org/10.1063/1.3020304.

[146] R. A. Matula. "Electrical resistivity of copper, gold, palladium, and silver." Journal of Physical and Chemical Reference Data 8. pp. 1147-1298, (1979). doi.org/10.1063/1.555614.

[147] O. Dreirach, R. Evans, H. J. Guntherodt, H. U. Kunzi. "A simple muffin tin model for the electrical resistivity of liquid noble and transition metals and their alloys." Journal of Physics F: Metal Physics. Vol. **02**, Issue 4, pp. 709-725, (1972).

[148] Isao Yokoyama and Shusaku Tsuchiya. "Excess Entropy, Diffusion Coefficient, Viscosity Coefficient and Surface Tension of Liquid Simple Metals from Diffraction Data." Materials Transactions, Vol **43**, No. 01, pp. 67-72, (2002).

[149] Ju Yuan-Yuan, Zhang Qing-Ming, Gong Zi-Zheng, and Ji Guang-Fu. "Molecular dynamics simulation of self-diffusion coefficients for liquid metals." Chin. Phys **B**, Vol. **22**, No. 22, (2013).

[150] T. Iida, N. Tripathi, M. Isac and R. I. L. Guthrie. "Models and Equations for Atomic Transport Coefficients of Liquid Metals: Viscosity and

Self-Diffusivity." Materials Science Forum Vols. **(539-543)**, pp 2509-2517, (2007).

[151] F Kargl, H Weis, T Unruh and A Meyer. "Self diffusion in liquid aluminium." Journal of Physics: Conference Series **340**, 012077, (2012).

[152] Marc J.Assael, Konstantinos kakosimos, R.Michael Banish, Jurgen Brillo, Ivan Egry, Robert Brooks, Peter N.quested, Kenneth C. Mills, Akira nagashima, Yuzuru sato, William A.Wakeham.
"Reference Data for the Density and Viscosity of Liquid Aluminum and Liquid Iron." J. Phys. Chem. Ref. Data. Vol. **35**, No. 01, (2006).

[153] F. Demmel, D. Szubrin, W. C. Pilgrim, and C. Morkel. "Diffusion in liquid aluminium probed by quasielastic neutron scattering." Phys Rev. B, Vol. **84**, pp. 014307, (2011). Doi: 10.1103/PhysRevB.84.014307.

[154] N. Jakse and A. Pasturel. "Liquid Aluminum: Atomic diffusion and viscosity from ab initio molecular dynamics." Scientific Reports: Vol. **3**, pp. 3135, (2013).

[155] N. Jakse and A. Pasturel. "Excess Entropy Scaling Law for Diffusivity in Liquid Metals." Nature, **6**, Article number : 20689, (2016).

[156] N. Jakse and A. Pasturel. "Transport properties and Stokes-Einstein relation in Al-rich liquid alloys." The Journal of Chemical Physics, Vol. **144**, pp. 244502, (2016).

[157] N. Jakse and A. Pasturel. "Validity of the Stokes-Einstein relation in liquids: simple rules from the excess entropy." J. Physics: Condens. Matter **28**, pp. 485101, (2016).

[158] S. D. Korkmaz, S. Korkmaz. "Investigation of surface properties of liquid transition metals:Surface tension and surface entropy." Applied Surface Science **257**, pp. 261, (2010).